UNSW SYDNEY

Reconstructing El Nino-southern oscillation

Author:
Gergis, Joëlle L.

Publication Date:
2006

DOI:
https://doi.org/10.26190/unsworks/23622

License:
https://creativecommons.org/licenses/by-nc-nd/3.0/au/
Link to license to see what you are allowed to do with this resource.

Downloaded from http://hdl.handle.net/1959.4/24222 in https://unsworks.unsw.edu.au on 2024-04-20

RECONSTRUCTING EL NIÑO-SOUTHERN OSCILLATION

EVIDENCE FROM TREE-RING, CORAL, ICE AND DOCUMENTARY PALAEOARCHIVES, A.D. 1525-2002.

Joëlle L. Gergis

A thesis submitted under the requirements for the degree of
Doctor of Philosophy,
School of Biological, Earth and Environmental Sciences,
University of New South Wales,
Sydney, Australia.

April, 2006.

EXECUTIVE SUMMARY

El Niño-Southern Oscillation (ENSO) is the most important coupled ocean-atmospheric phenomenon to cause global climate variability on interannual time scales. Efforts to understand recent, apparently anomalous ENSO behaviour are hampered by the lack of long, high-quality climate records. While instrumental data generally covers the past 150 years, record length is insufficient for the assessment of past changes in the frequency, magnitude, and duration of ENSO. Here, multiproxy networks of high-resolution tree-ring, coral, ice and documentary records derived from eastern and western Pacific ENSO 'centres of action' are analysed (A.D. 1525-2002). Considerable improvements in ENSO reconstruction are achieved from expanding the use of records from the western Pacific. In particular, ~500 years of a continuous 3,722 year ENSO sensitive tree-ring record from New Zealand is introduced.

Although extreme ENSO events are seen throughout a 478-year discrete event analysis, 43% of extreme, 20% of very strong and 28% of all protracted ENSO events occur within the 20th century. Principal component analysis was used to extend instrumental records of the Southern Oscillation Index (SOI) Niño 3.4 Sea Surface Temperature (Niño 3.4 SST) and a newly developed coupled ocean-atmospheric ENSO index (CEI) by 347 years. Significantly, of the three indices reconstructed here, CEI reconstructions were largely found to be the best predictors of ENSO. The results suggest that ENSO may be more effectively characterised using a coupled ocean-atmosphere index, particularly for December-May periods.

Compared to the pre-instrumental period, the late 19th and early 20th centuries indicate a clear trend toward increased ENSO variability over the past 150 years. Significantly, spectral analysis of reconstructed indices reveals a marked change in the frequency and intensity of ENSO beginning ~A.D. 1850, coinciding with the end of the Little Ice Age and the boom in global industrialisation. This suggests that ENSO may operate differently under natural (pre-industrial) and anthropogenically influenced background states. This study asserts that recent ENSO variability appears anomalous in the context of the past five centuries. Given the considerable socio-economic impacts of ENSO events, future investigation into the implications an increasingly anthropogenically-warmed world may have on ENSO is vital.

ACKNOWLEDGEMENTS

First and foremost, thanks must go to 'Team Dendro' from the Tree-Ring Laboratory, and the School of Geography and Environmental Science at the University of Auckland, New Zealand, for hosting me in 2003 & 2004. This project would not have been possible without the training and support I gained from working with the 'fellowship of the rings'; Anthony Fowler, Gretel Boswijk, Peter Crossley, Jonathan Palmer, Andrew Lorrey, Jenny Lux and Tim Martin. Thank you for all your efforts in making the 'Aussie sheila' feel welcome in NZ. I am particularly grateful to you all for participating in the community consultation required for my fieldwork and sharing the hours of 'forest madness' spent out there. Thanks for introducing me to the life of professional research.

In particular, I am indebted to (Lord) Anthony Fowler for taking on the challenges involved with this project and mentoring me. I am most thankful for all your time, patience and good humour during those "NIÑO NIÑA NIÑO" conversations on both sides of the Tasman. I am appreciative of all those meticulous 'spanners in the works' that trained me in the rigors of good science. Many thanks for developing the tree-ring master chronologies (AGAU05a and AGAU05b) used in Chapter 4. It was a privilege working with you and outstanding Team Dendro on the landmark Kauri project.

Sincere thanks to Richard Gilles and Janeen Collings (New Zealand Department of Conservation), Stephen King (Waipoua Forest Trust), Davey Paniora (Te Iwi O Te Roroa), Jeff Marsden (Panguru Development Trust), Rongo Bentson and Bobby Proctor (Te Iwi o Te Rarawa) for overseeing the collection Kauri tree-ring sampling process.

On the sunny side of the ditch, particular thanks to Scott Mooney (UNSW), for his inspired introduction to the world of palaeoclimatology. I am grateful for your foresight, careful editing, financial assistance and guidance over the years. Thank you for taking a stand for geography existing at UNSW under such trying circumstances. I have appreciated all your time, patience and encouragement in pursuing my vision with this project.

I am fortunate to have crossed paths with Karl Braganza (National Climate Centre, Bureau of Meteorology, Melbourne) at CLIVAR in 2004. I have really appreciated all your time, online support and good humour in the final year of this project. I have learned much from your sharp insight into ENSO and the vision you have brought to interface of palaeoclimatology and dynamical studies. I gratefully acknowledge the scrupulous PCA reconstructions and advice on the material presented in Chapter 6. Many thanks to James Risbey (CSIRO, Hobart) for your interest and willingness to be involved in this cross-disciplinary project. I am very thankful for your support of my research and some of the spectral results presented in Chapter 6.

Thank you to Penny Whetton (CSIRO, Melbourne) and Ian Rutherfurd (University of Melbourne) for access to the Nile Flood Record, Berlage Teak Chronology, North China Rainfall data, Erica Hendy (Lamont Doherty Earth Observatory, New York) for the Great Barrier Reef coral luminescence master chronology, Pavla Fenwick (Lincoln University, New Zealand) for Pink Pine tree-ring data, and Bruce Bauer (World Data Centre for Palaeoclimatology/National Climatic Data Centre Palaeoclimatology Branch) for data acquisition and assistance. I would also like to thank a number of academics who have provided me with advice and feedback during the course of my PhD; Mike Gagan, John Chappell, Erica Hendy, Simon Haberle, Michael Mann, Connie Woodhouse, Raj Kane, Takanori Horii, David Edwards, Gary Meyers, Anita Drumond, Manu Black, Jim Renwick, David Enfield, and David Meko.

Above all I would like to acknowledge the friends and family that provided me with the personal support to get this one 'over the line'. Endless thanks to my soul family; Emma Walter, Rebecca Schofield, Katy Alexander, Petra Lane, Charlie Honner and Juliette Di Moro for the unique support you have provided me on this journey. Thanks to all for making it over to New Zealand (and China!) to share precious time-out with me. I appreciate all the time spent bringing me back from my "I'm not a scientist" days. I am so fortunate to have such extraordinary people in my life; this PhD would not have been possible without you. Special thanks must go to Jennifer Ezzy for neighbourly support in the final stages of this project; always at the ready to drag me away from my desk for a reality check. Every thanks for your eleventh hour proof of the final manuscript and reassuring me that "I'm not having an ugly baby"!

I would especially like to thank my family; Mum, Dad and Chris for all your moral support during this time. Particular thanks to my Mum for all your love and

encouragement on the 'PhD-crisis hotline', and my Dad for instilling 'education is the key' from an early age. Thanks to Chris for, ah…being Chris! Thank you all for putting up with my unavailability over the past few years. I look forward to making up for lost time.

This project acknowledges financial assistance from a UNSW Faculty Research Grant 'Late 20th Century El Niño-Southern Oscillation in the Context of Holocene Climate Change' and the Royal Society of New Zealand's Marsden Project 'Reconstructing ENSO history from Kauri tree-rings' (UOA Contract 108). I would also like to acknowledge generous funding from;

i. The University of New South Wales for supporting my research with an Australian Postgraduate Award, 2002-2005.

ii. CLIVAR for full financial assistance to participate in the *1st International CLIVAR Science Conference: Understanding and Predicting Our Climate System,* Baltimore, USA, June 2004.

iii. The European Geophysical Union and the International Research Center on El Niño (CIFFEN) for financial assistance to participate in the *1st International Alexander Von Humboldt Conference on the El Niño phenomenon and its global impact,* Guayaquil, Ecuador, May 2005.

iv. PAGES full finanical assistance to participate in the *PAGES 2nd Open Science Meeting: Palaeoclimate, Environmental Sustainability and Our Future*, Beijing, China, August 2005.

v. The Australian Research Council, Monash University and the Bureau of Meteorology Research Centre for full financial assistance to participate in *A Workshop on Earth System Models of Intermediate Complexity*, Melbourne Australia, February 2006.

Finally, I would like to thank my partner Josh Bassett for his steadfast love, patience and support through every stage of this task, including the move to New Zealand. I am eternally grateful for all your technical wizardry, heart-starter coffees and gentle reminders of life 'outside of the PhD'. Thank you for providing me the great freedom and luxury of being fully consumed in the process of realising this project.

PUBLICATION INFORMATION

Chapter 2 appeared in full as:

Gergis, J. and Fowler (2005), Classification of synchronous oceanic and atmospheric El Niño-Southern Oscillation (ENSO) events for palaeoclimate reconstruction, *International Journal of Climatology* **25***:* 1541–1565.

I was the primary investigator and lead author of this paper and conducted all of the analyses presented therein.

Material contained in Chapter 4 has appeared as:

Gergis, J., Boswijk, G. and Fowler, A. (2005). An update of modern Northland Kauri (*Agathis australis*) tree-ring chronologies 1: Puketi State Forest. New Zealand tree-ring Site Report No.19, School of Geography and Environmental Science Working Paper 29, University of Auckland, New Zealand.

Gergis, J., Boswijk, G. and Fowler, A. (2005). An update of modern Northland Kauri (*Agathis australis*) tree-ring chronologies 2: Trounson Kauri Park. New Zealand tree-ring Site Report No.20, School of Geography and Environmental Science Working Paper 30, University of Auckland, New Zealand.

Fowler, A., Boswijk, G., Gergis, J. and Lorrey, A. (2006). ENSO history recorded in *Agathis australis* (Kauri) tree-rings, Part A: Kauri's potential as an ENSO proxy. *International Journal of Climatology*: *in review*.

Sections of Chapter 5 have appeared as:

Gergis, J. and Fowler, A. (2005). How unusual was late Twentieth Century El Niño-Southern Oscillation (ENSO)? Assessing evidence from tree-ring, coral, ice and documentary archives, A.D. 1525-2002. *Advances in Geoscience* **6**: 173-179.

The majority of Chapter 5 is being prepared for submission as:

Gergis, J. and Fowler, A. A History of El Niño-Southern Oscillation (ENSO) events since A.D. 1525; implications for future climate change to *Climatic Change*.

I was the primary investigator and lead author of both papers and conducted all of the analyses presented therein.

Much of Chapter 6 is being prepared for submission as:

Braganza, K., Gergis, J., Risbey, J., and Fowler, A. El Niño-Southern Oscillation (ENSO) since A.D. 1525 to *Climate Dynamics* or *Science*.

I am the second author of this paper. I contributed all primary data, some analytical work and the majority of the intellectual interpretation of the results presented therein. I acknowledge assistance from Karl Braganza and James Risbey for providing the PCA reconstructions and spectral analyses presented in Chapter 6.

Elements of Chapters 5, 6 and 7 were submitted as an invited paper entitled:

Gergis, J., Braganza, K., Fowler, A., Risbey, J. and Mooney, S. Reconstructing El Niño-Southern Oscillation (ENSO) using high-resolution palaeoarchives to *Journal of Quaternary Science, in review.*

I am the primary investigator and lead author of this paper and conducted all of the analyses and interpretation of the material presented therein, aside from those explicitly acknowledged above.

Dedicated to Josh…

for love, light and laughter…

CONTENTS

LIST OF FIGURES

LIST OF TABLES

LIST OF ELECTRONIC APPENDICIES

It is not the strongest of the species that survives, nor the most intelligent,

but rather the one most responsive to change.

Charles Darwin

(A.D. 1809-1882)

CHAPTER 1. INTRODUCTION

1.1 Overview

1.1.1 Introduction

El Niño-Southern Oscillation (ENSO) is a complex interaction of oceanic and atmospheric processes that result in the global redistribution of weather phenomena. ENSO events initially generated in the tropical Pacific create a far-reaching system of climate anomalies, termed 'teleconnections' that operate on a range of time scales important to society. This happens through the modulation of climatic extremes including drought, flooding, bushfires and tropical cyclone activity across vast areas of the Earth. As seen through Table 1.1, ENSO events are associated with large-scale socio-economic adversity for the millions of people living in areas where agricultural productivity is influenced by the Asian, African, and American monsoons (Bouma *et al.*, 1997; Dunbar and Cole, 1999; Caviedes, 2001; Chen *et al.*, 2001).

Table 1.1. Persons affected by disaster (PAD) per 1000 population, 1963-1993 by region. Average and Maximum (max) PAD values quoted for selected geographical regions. El Niño and post-Niño years compared with pre-Niño years based on defining El Niño as equatorial Pacific SST anomalies (20°N-20°S, 170°E-80°W). **Source:** Modified from Bouma *et al.*, (1997).

Persons Affected by Disaster (PAD)/1000 population	*World*	*Caribbean*	*South America*	*East Asia*	*South Asia*	*Sub-Saharan Africa*
Average PAD rates (all years)						
	22.90	12.0	14.20	15.30	67.00	*22.00*
Average total per year (millions)						
	106.90	0.36	3.29	20.50	67.90	9.09
Average (max) PAD rates						
Pre-El Niño	8.06 (*20.24*)	3.07 (*8.60*)	5.89 (*14.50*)	11.10 (*50.60*)	13.44 (*30.50*)	10.87 (*28.02*)
El Niño	34.66 (*74.48*)	3.21 (*7.00*)	5.99 (*17.20*)	31.60 (*181.40*)	101.15 (*303.50*)	20.94 (*41.20*)
Post-El Niño	35.19 (*61.23*)	27.94 (*90.40*)	32.55 (*132.50*)	12.80 (*57.50*)	117.08 (*242.60*)	33.58 (*76.10*)

Despite being the dominant source of global inter-annual climate variability, how the frequency, duration and magnitude of ENSO events has varied through time is still poorly understood (Crowley, 2000; Grove and Chappell, 2000). Significantly, the late 20th century contained a number of extreme and prolonged ENSO episodes, (Folland *et al.*, 2001). Since the mid-1970s, ENSO has apparently changed in character to a dominance of El Niño conditions, the extreme phase of which appears coincidental with recognised 20th century global warming (Trenberth and Hoar, 1997; Fedorov and Philander, 2000; Folland *et al.*, 2001; Tsonis *et al.*, 2003; Jones and Mann, 2004) and changes in the Inter-decadal Pacific Oscillation (IPO/PDO) (Mantua *et al.*, 1997; Zhang *et al.*, 1998; Power *et al.*, 1999; Salinger *et al.*, 2001; Trenberth and Stepaniak, 2001; Mantua and Hare, 2002).

The two most intense El Niños (1982-83 and 1997-98) and La Niñas (1988-89, 1973-74) and the longest event in the instrumental record (1990-1995) occurred over the past three decades (Trenberth and Hoar, 1996; Allan and D'Arrigo, 1999; Folland *et al.*, 2001; Allan *et al.*, 2003). However, the long-term context of these apparently anomalous events is still being debated (Crowley, 2000; Folland *et al.*, 2001; Mann, 2003b; Soon and Baliunas, 2003).

In particular, recent research has sought to clarify whether the modern behaviour of ENSO is a manifestation of human-induced global warming (Folland *et al.*, 2001; Timmermann, 2001; Tsonis *et al.*, 2003; Collins, 2005), or simply an expression of natural decadal or multi-centennial climate variability (Wang, 1995; Folland *et al.*, 2001; Jones and Mann, 2004).

Although significant advances in the reconstruction of mean hemispheric and global temperatures of the past millennium have been made (Figure 1.1) (Mann *et al.*, 1998; Crowley, 2000; Folland *et al.*, 2001; Jones and Mann, 2004; Moberg *et al.*, 2005), relatively little attention has focused on the apparently anomalous ENSO behaviour witnessed in recent decades (Trenberth and Hoar, 1996; Trenberth and Hoar, 1997; Crowley, 2000; Folland *et al.*, 2001; Mann, 2003b).

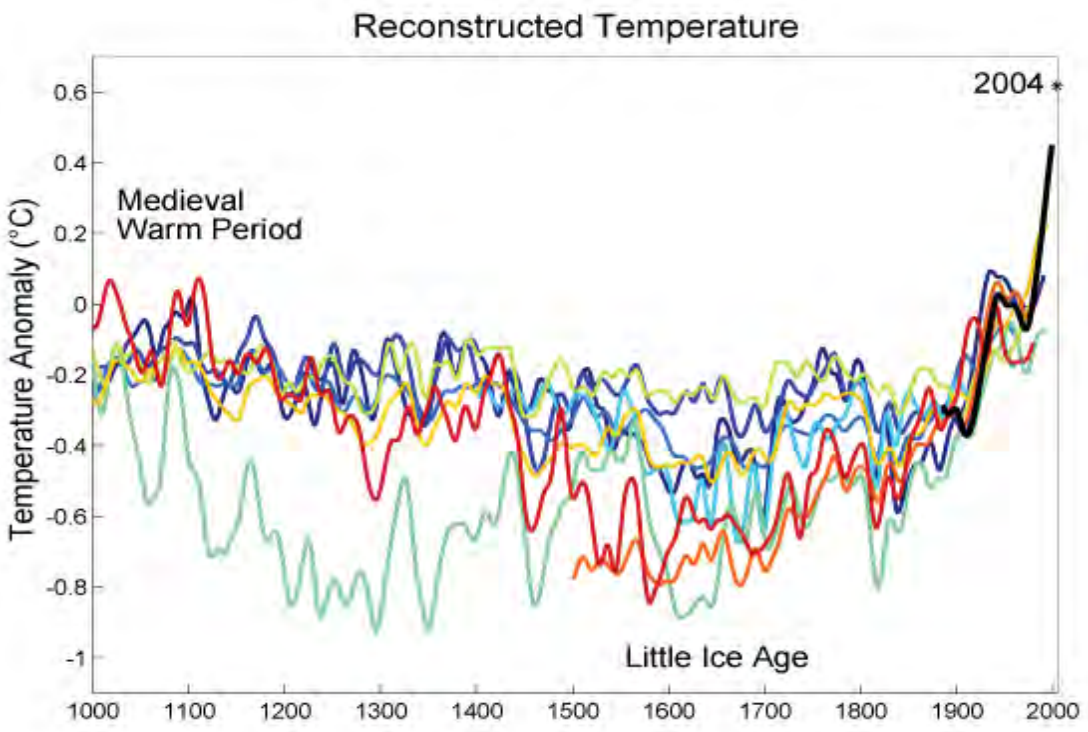

Figure 1.1. A comparison of ten different published reconstructions of mean temperature changes during the last 1000 years. The Medieval Warm Period and Little Ice Age are labelled at roughly the times when they are historically believed to occur, though it is still disputed whether these were truly global or only regional events. The reconstructions used, in order from oldest to most recent publication are: 1.dark blue- A.D. 1000-1991: Jones *et al.* (1998), 2. blue- A.D. 1000-1980: Mann *et al.*: (1999), 3. light blue- A.D. 1000-1965: Crowley (2000), 4. lightest blue- A.D. 1402-1960: Briffa *et al.* (2001), 5. green- A.D. 831-1992: Esper *et al.*, (2002), 6. light green- A.D. 1000-1980: Mann (2003a), 7. orange- A.D. 200-1995: Jones and Mann (2004), 8. red-orange- A.D. 1500-1980: Huang (2004), 9. red- A.D. 1-1979: Moberg *et al.*, (2005), 10. dark red- A.D. 1600-1990: Oerlemans (2005), **black**- A.D. 1856-2004: instrumental data was jointly compiled by the Climatic Research Unit and the UK Meteorological Office Hadley Centre. Global Annual Average data (TaveGL2v2). See Jones and Moberg (2003). **Source:** http://en.wikipedia.org/wiki/Image: 1000_Year_Temperature_Comparison.png

Instrumental time series are generally less than 150 years, and are therefore too short to assess whether 20th century ENSO behaviour was atypical (Allan and D'Arrigo, 1999; Dunbar and Cole, 1999; Fedorov and Philander, 2000). Consequently, multi-century palaeoclimate reconstructions derived from proxy records, such as annually resolved tree ring, coral, ice or documentary records are sought to provide the long-term background against which recent ENSO variability can be assessed (Jones and Mann, 2004).

A lack of sensitive proxies for key ENSO locations of the Southern Hemisphere and differences in regional teleconnection signatures make it necessary to include proxy

indicators from a variety of regions to adequately capture the spatial variability of ENSO through time (Fairbanks *et al.*, 1997). Data used for previous reconstructions have predominately come from East Pacific teleconnection regions (Stahle *et al.*, 1998; D'Arrigo *et al.*, 2005), with no or little representation of sites influenced by the west Pacific warm pool, a key area of ENSO influence (Allan *et al.*, 1996). Clearly, reconstructions of ENSO derived from a number of widely-spaced regional proxies, with sufficient east and west Pacific representation, is more likely to be representative of large-scale ocean-atmosphere processes than any of the spatially restricted networks necessitated by single site reconstruction (Baumgartner *et al.*, 1989; D'Arrigo *et al.*, 1994; Diaz and Pulwarty, 1994; Gedalof and Mantua, 2002).

Further hampering efforts aimed at reconstructing past ENSO behaviour is the fact that palaeo-ENSO research rarely incorporates instrumental indices from both components of ENSO. The result is that the calibration process may fail to represent large-scale dynamics of the coupled ocean-atmosphere system. To date, reconstructive efforts have tended to focus on only one aspect of the ENSO phenomenon, commonly the Southern Oscillation Index (SOI) (Stahle *et al.*, 1998) or oceanic Niño 3 SST region (Mann *et al.*, 1998; 2000; D'Arrigo *et al.*, 2005). However, it is not clear if reconstructions based on calibrating proxy indicators using such indices fully characterise the magnitude and timing of ENSO perturbations.

Thus, utilising a variety of instrumental indices and proxy records provides an opportunity to characterise regional signals (tropics versus extra tropics, terrestrial versus marine environments) allowing complementary information on the large-scale nature of ENSO to be investigated (Jones and Mann, 2004). This study documents a 'multiproxy' approach to ENSO reconstruction, aimed at taking advantage of the complementary strengths of a selected number of ENSO-sensitive data sources to provide insight into ENSO since A.D. 1525.

1.1.2 Global research frameworks; CLIVAR, PAGES and ARTS

Palaeoclimate reconstructions offer the only source of information on the long-term changes in past climate variability. There is a vital need for long, continuous records of inter-annual to centennial variability from the tropics and key teleconnections areas to extend indices of large-scale climate systems into pre-instrumental periods (Dunbar and Cole, 1999). Well-calibrated, multi-century reconstructions derive even broader utility

when interfaced with numerical simulations to drive or test general circulation model simulations (Dunbar and Cole, 1999).

The principal coordinating organisation for climate research throughout the world is the World Climate Research Programme (WCRP) (CLIVAR Scientific Steering Group, 1995). The objectives of the WCRP are to develop a fundamental scientific understanding of the physical climatic system and processes, including determination of the extent anthropogenic climate change and overall climate predictability (CLIVAR Scientific Steering Group, 1995).

CLIVAR (Climate Variability and Predictability) is the largest interdisciplinary program of the WCRP which focuses on the variability and predictability of seasonally to centennially varying components of the climate system (CLIVAR Scientific Steering Group, 1995). In particular, the phenomenon of interest for the seasonal-to-inter-annual variability component of CLIVAR is ENSO and its global influence, along with the Australasian, American and African monsoon systems (CLIVAR Scientific Steering Group, 1995).

The WCRP also emphasises the need for the Earth's physical climate system to be integrated with the research involved in the International Geosphere-Biosphere Programme (IGBP), which focuses on the biological and chemical processes involved in global environmental change (CLIVAR Scientific Steering Group, 1995).

PAGES (Past Global Changes) is the IGBP's core project responsible for providing a quantitative understanding of the Earth's past environment and defining the framework of natural variability within which anthropogenic impact on the Earth system can be evaluated (Dunbar and Cole, 1999). One of PAGES principal objectives aims to obtain and interpret a variety of palaeoclimatic records and to provide the data essential for the evaluation of predictive climatic models (Dunbar and Cole, 1999).

A joint initiative, the PAGES/CLIVAR Intersection, further aims to improve the understanding of decadal to century scale climate variability, especially in regard to improving predictability, through the use of high-resolution palaeoarchives, such as corals, tree-rings, laminated sediments and ice cores.

The principal objectives are to:

i. extend the instrumental climate record back in time with quantitative proxy data that can be accurately calibrated against instrumental records;

ii. document rapid climate change, natural climate variability during the Holocene and other interglacial periods, and;

iii. test the ability of climate models to capture known past climate variability.

In 1996, the Annual Records of Tropical Systems (ARTS) initiative was conceived as a joint CLIVAR/PAGES Intersection endeavour aimed at promoting the synthesis of palaeoclimatic data with instrumental and modeling to address key uncertainties in the understanding of tropical climate variability and its impacts (Dunbar and Cole, 1999). The main objectives of the ARTS program are to document and understand the behaviour of the tropical ocean-atmosphere and its teleconnections, with seasonal to annual resolution, over the past several centuries; and assess the stability of tropical climate systems and their teleconnections as background climate and associated forcing phenomena change over longer periods.

1.1.3 Research objectives

In response to the global research priorities outlined above, the primary intention of this study is to develop long-term multiproxy reconstructions of ENSO back to A.D. 1525 to provide context for the assessment of recent ENSO variability. A lack of long-term coral data from tropical regions makes it difficult to establish evidence of global teleconnections associated with ENSO events beyond a few centuries. Accordingly, the analysis is limited to the A.D. 1525-2002 period.

To target some of the key uncertainties associated with the nature and long-term history of ENSO, the following research objectives were defined;

- **Objective 1.** Investigate the use of appropriate ENSO definitions and indices used for proxy calibration for ENSO reconstruction.

- **Objective 2.** Contribute to the development of a regional West Pacific ENSO proxy using the New Zealand Kauri tree-ring record.

- **Objective 3.** Develop a chronology of discrete ENSO events using tree-ring, coral, ice core and documentary records spanning both east and west Pacific 'centres of action', and to examine trends in the frequency and magnitude of pre-instrumental ENSO episodes on decadal-centennial timescales.

- **Objective 4.** Analyse past changes in (i) the frequency and amplitude in oceanic, atmospheric and coupled elements of ENSO, and (ii) the relative stability of regional teleconnections using spectral analysis and principal component regression techniques.

1.2 The Role of El Niño-Southern Oscillation (ENSO)

1.2.1 What is ENSO?

El Niño-Southern Oscillation (ENSO) is recognised as the strongest natural inter-annual climate fluctuation operating on the planet aside from the seasonal cycle and monsoon systems (Allan *et al.*, 1996; Wang *et al.*, 1999). As such, studies on the ENSO cycle and related climate variability are considered to rank among the most important frontiers in the atmospheric and oceanic sciences (Wang *et al.*, 1999).

The ENSO phenomenon is a coupled cycle in the atmosphere-oceanic system (Bjerknes, 1966; 1969). It is an irregular phenomenon that tends to reoccur every 2-7 years and alternates between its two phases or extremes, termed El Niño and La Niña events (Allan *et al.*, 1996; Diaz and Markgraf, 2000). Generally, during an El Niño (La Niña) event, warming (cooling) of tropical regions of the Pacific and Indian Oceans leads to massive redistributions of major rainfall-producing systems (Figure 1.2) (Rasmusson and Carpenter, 1983; Allan, 2000).

A 'typical' ENSO event tends to last for 18-24 months with peaks in amplitude generally occurring in the austral summer (December-February) (Rasmusson and Carpenter, 1982; Allan, 2000; Horii and Hanawa, 2004). Although ENSO is phase-locked to the annual cycle, episodes can differ in terms of their relative strengths, season of onset and maturity, overall duration, and the spatial extent of maximum Sea Surface Temperature (SST) anomalies in the tropical Pacific (Rasmusson and Carpenter, 1982; Allan *et al.*, 1996; Trenberth, 1997; Trenberth and Stepaniak, 2001; Horii and Hanawa,

2004; Lyon and Barnston, 2005). Along with SSTs, rainfall and wind field anomalies associated with ENSO events differ considerably from event to event, as tropical 'centres of action' shift (Ropelewski and Halpert, 1987; 1989; Allan *et al.*, 1996; Fedorov and Philander, 2000).

Extra-tropical climate variability associated with ENSO episodes are commonly referred to as teleconnections (Figure 1.3) (Wang *et al.*, 1999; Allan, 2000; Clark *et al.*, 2000). As tropical regions are linked to higher latitudes in both hemispheres, for example through the Hadley Cell, any major variations in mass, energy and momentum due to redistributed equatorial rainfall are communicated to more temperate regions of the globe (Allan, 2000). This effect extends ENSO's influence beyond the tropics and causes near-global modulations of climate. Indeed, much remains to be revealed about relationships between climatic features such as the North Atlantic Oscillation (NAO), the Antarctic Circumpolar Wave (ACW), the Artic Oscillation (AO), and North Pacific Oscillation (NPO) in relation to ENSO cycles (Allan, 2000; Cook *et al.*, 2002; Keskin and Olmez, 2004; Turner, 2004). A better understanding of ENSO links to these features may to shed light on the nature of teleconnections and the phenomenon's evolution.

The strength of ENSO teleconnection patterns during the instrumental record have responded to fluctuations in mean state characteristics such as changes in 'centre of action' locations, seasonal timing, and intensity of anomalies (Troup, 1965; Chen, 1982; Allan *et al.*, 1996; Allan, 2000; Mann *et al.*, 2000). For example, ENSO appears to have weakened during the 1920–1950s and existed in a more amplified state from the 1970s onwards (Allan *et al.*, 1996; Allan, 2000). Clearly, characterising the frequency and strength shifts associated with the non-stationarity of ENSO has considerable implications for the accurate modeling of future climate change scenarios and their regional socio-economic impacts (Hoerling *et al.*, 1997; Karl, 1999; Easterling *et al.*, 2000; Chen *et al.*, 2001; Folland *et al.*, 2001).

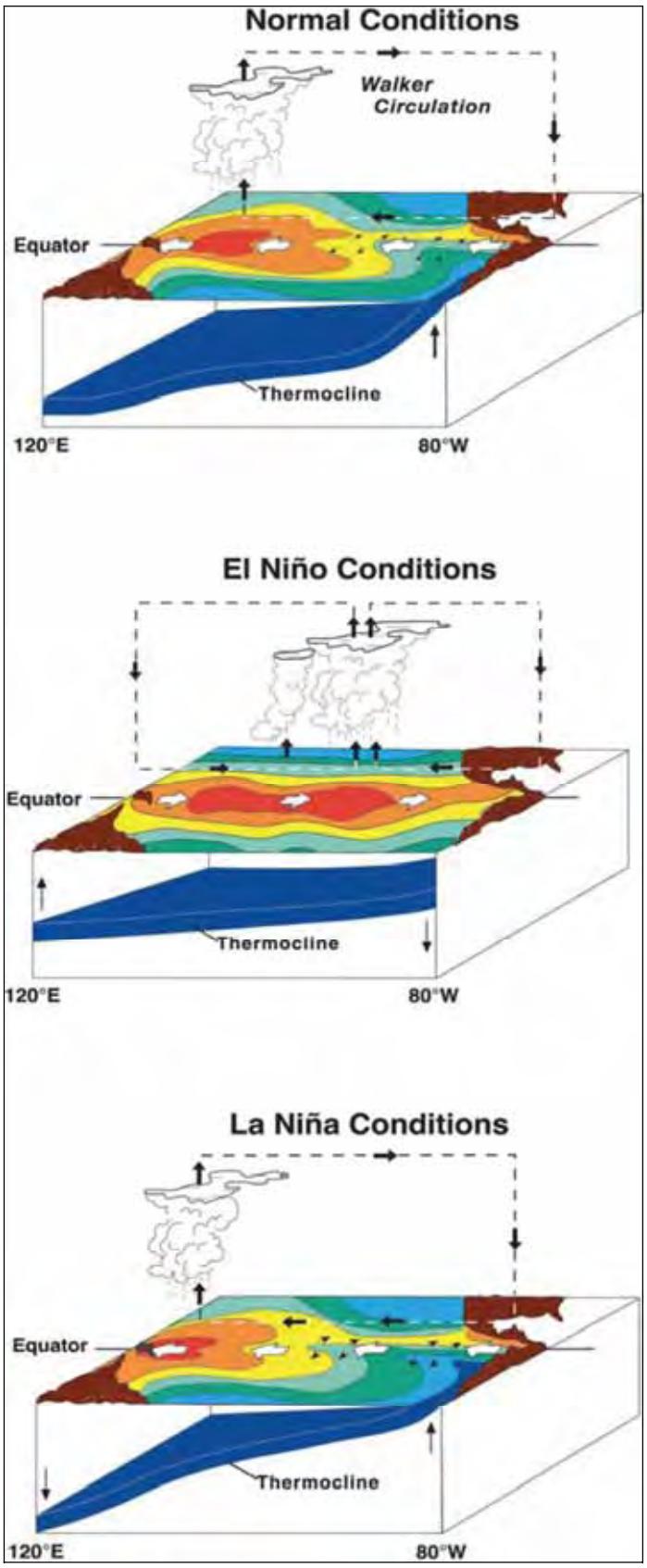

Figure 1.2. Schematic of coupled atmospheric and oceanic interactions in the equatorial Pacific during normal (top), El Niño (middle) and La Niña (bottom) conditions. **Source:** Mc Phaden (2004).

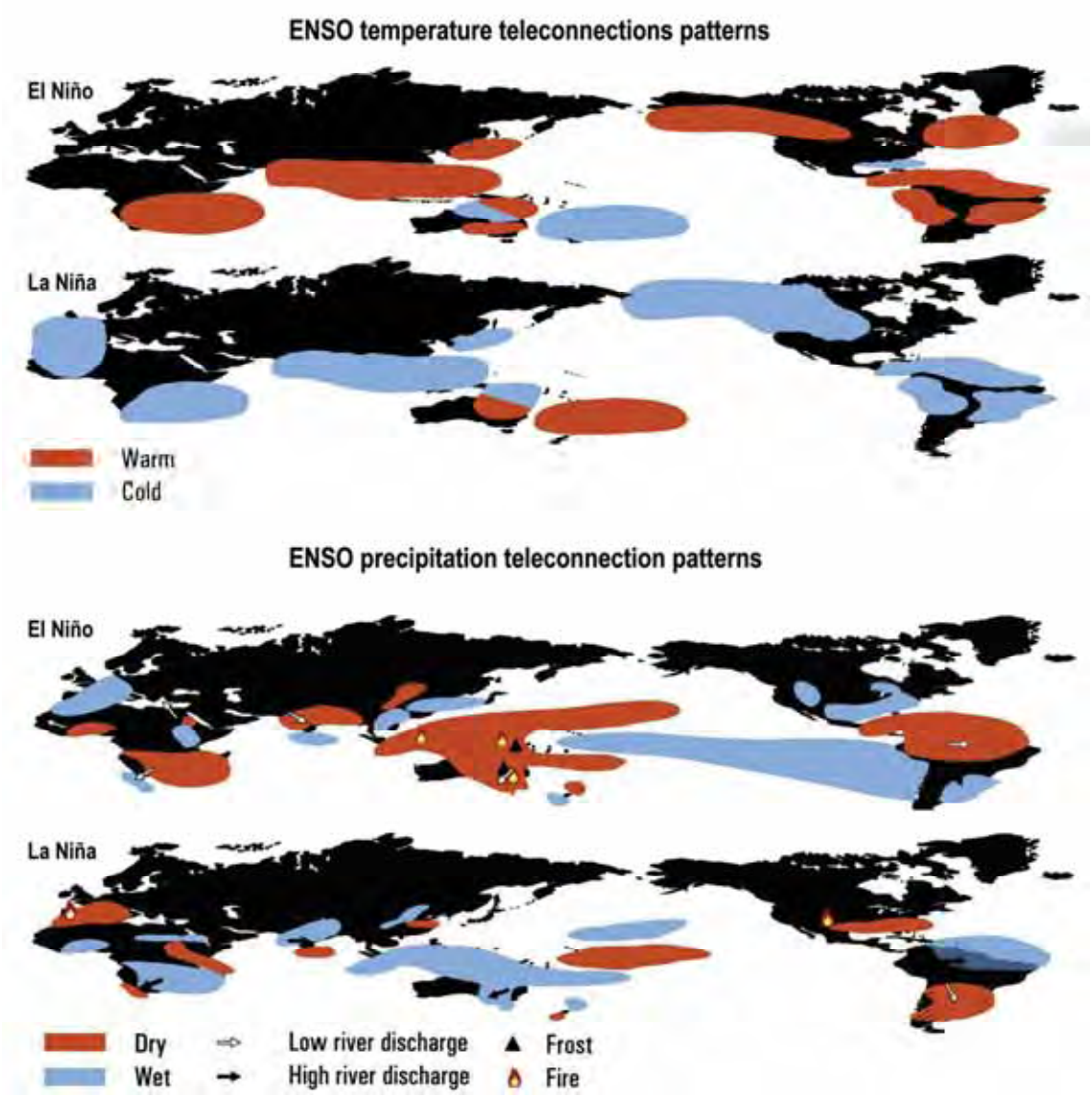

Figure 1.3. ENSO teleconnections patterns associated with (i) precipitation anomalies and (ii) temperature anomalies during El Niño (top panel) and La Niña (lower panel) episodes. **Source:** Modified from Allan (1996).

1.2.2 Oceanic component of ENSO; El Niño

Instrumental measurements of the equatorial Pacific Sea Surface Temperature (SST) signatures of ENSO events have provided the basis for simple indices of the phenomenon (Allan *et al.*, 1996). The temperature based indices are defined with a mean SST from different regions of the equatorial Pacific (Allan *et al.*, 1996; Hanley *et al.*, 2003). The most widely used ENSO indices of Pacific SST fluctuations are characterised by the Niño SST anomaly regions, shown in Figure 1.4.

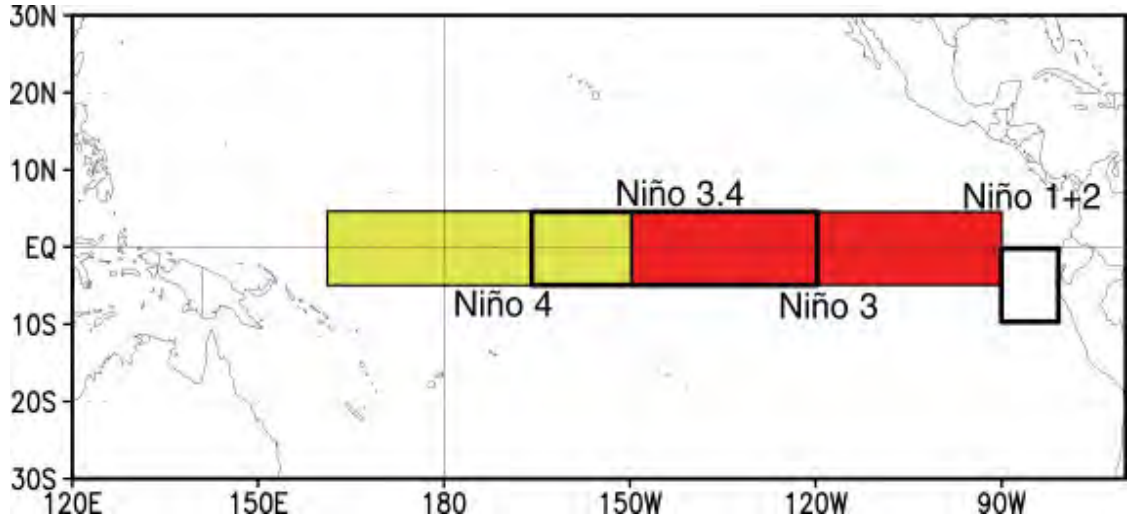

Figure 1.4. The Niño Sea Surface Temperature (SST) regions used to characterise ENSO conditions in the Pacific Ocean. Niño 1+2 (0-10°South, 90°West-80°West), Niño 3 (5°North-5°South, 150°West-90°West) Niño 4 (5°North-5°South,160°East-150°West) Niño 3.4 (5°North-5°South, 170-120°West). **Source:** NOAA Climate Prediction Centre (http://www.cpc.ncep.noaa.gov/).

The Niño 1 region is located off the coast of Peru and Ecuador, while the Niño 2 region is located near the Galapagos Islands (Hanley *et al.*, 2003). The combined Niño 1+2 region is considered the classical 'El Niño' region highly responsive to seasonal El Niño induced changes in the eastern Pacific (Hanley *et al.*, 2003). This refers to the anomalous warming traditionally experienced off the South American coastline around Christmas time, traditionally associated with collapses in fisheries and marine bird populations in coastal Peru and Ecuador (Quinn *et al.*, 1978; Trenberth, 1997; Caviedes, 2001).

The location of the Niño 3 region straddles two distinct ENSO-affected regions (Allan *et al.*, 1996; Hanley *et al.*, 2003). The beginning of an ENSO warm event has commonly been defined by SST warming in the eastern part of the Niño 3 region, adjacent to South America (Allan *et al.*, 1996; Hanley *et al.*, 2003). The mature phase of ENSO, several months later, brings maximum SST anomalies to the western portion of the region (Cane, 1983; Fairbanks *et al.*, 1997). Consequently, a considerable focus of ENSO-related research is based on the Niño 3 SST region (Mann *et al.*, 1998; Evans *et al.*, 2002; D'Arrigo *et al.*, 2005), and it remains the primary area of ENSO anomalies predicted by climate models (Trenberth, 1997;Timmermann *et al.*, 1999; Latif *et al.*, 2001; Cane, 2004; Mann *et al.*, 2005).

The Niño 4 region encompasses part of the western equatorial Pacific where the sea surface temperatures are typically warmest during ENSO events (Hanley *et al.*, 2003). Changes in SSTs in this region are related to longitudinal shifts of the strong east-west temperature gradients along the equator (Hanley *et al.*, 2003). The Niño 4 region has a deeper mixed layer compared to the other ENSO regions, which suppresses the amount of warming recorded in the sea surface temperatures (Figure 1.5) (Hanley *et al.*, 2003). Hanley *et al.* (2003) noted that the Niño 4 index responds weakly to warm phase events and downgrades the magnitude of moderate-strong events, when compared to the Southern Oscillation Index (SOI). Like Niño 3, the Niño 4 index is commonly used in model simulations of past ENSO behaviour (Latif *et al.*, 2001), highlighting the potential implications of unsuitable representation of ENSO in state-of-the-art climate prediction.

From the 1990s, it has become apparent that the key region for coupled atmospheric ocean interactions involved in ENSO is located further west than traditionally defined by the eastern Pacific ENSO zones (Wang, 1995; Trenberth and Hoar, 1996; Trenberth, 1997; Trenberth and Hoar, 1997). SST anomalies have fluctuated in the traditional El Niño region along the South American coastline in contrast to the central equatorial Pacific where a greater stability of oceanic anomalies have been noted (Trenberth, 1997). The understanding of the importance of SST variability in this area lead to the introduction of the Niño 3.4 region in 1996, combining the overlapping portions of the Niño 3 and Niño 4 regions covering an area from 5°N-5°S to 120°-170°W (Trenberth and Hoar, 1996; Trenberth, 1997).

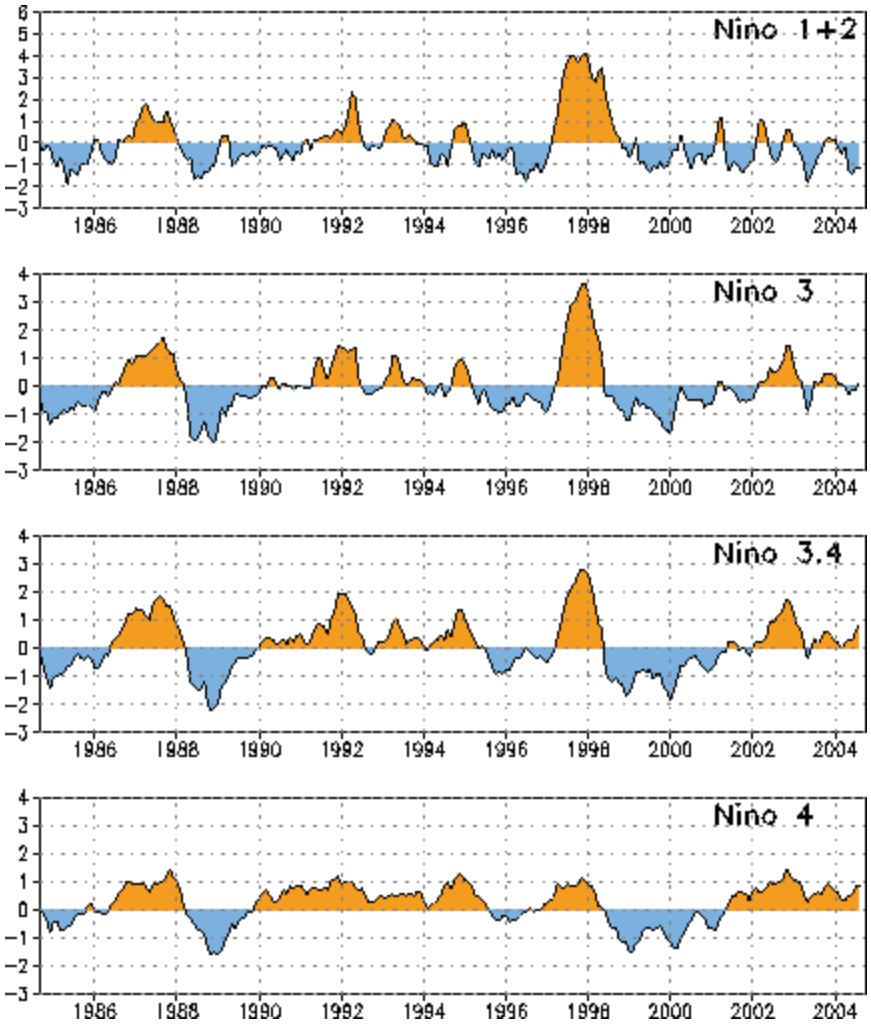

Figure 1.5. Monthly Niño Region Sea Surface Temperature (SST) anomalies, 1985-2005. A base period of 1971-2000 used to calculate the mean and standard deviations of anomalies. Vertical scale indicates SST anomalies in °C. The Niño 1+2 region represents SST anomalies from the far eastern Pacific near South America spanning to the far western Pacific represented by Niño 4 adjacent to the Papua New Guinean coast. Note the considerable differences in the amplitude of SST anomalies for each region during the 1997-98 El Niño event. **Source:** National Oceanic and Atmospheric Administration (NOAA) Climate Prediction Centre (http://www.cpc.ncep.noaa.gov/data/indices)

Higher mean temperatures than the often-quoted Niño 3 zone, and its proximity to the west Pacific warm pool and main centres of ocean convection, account for the physical importance of the Niño 3.4 region (Trenberth, 1997). Thus, Niño 3.4 SST anomalies may be thought of as departures from average equatorial SST conditions across the Pacific from the western to central Pacific, that have a more robust correlation with the SOI than the Niño 3 index (Trenberth and Stepaniak, 2001; Hanley *et al.*, 2003). Most recently, the significance of this SST region was acknowledged by its selection as the

geographical basis for the USA's National Oceanic and Atmospheric Administration's operational Oceanic Niño Index (ONI) (Elsey, 2004; Mc Phaden, 2004). In fact, the recent successful prediction of all prominent ENSO events since 1857 reported by Chen *et al.* (2004) made use of SST data from the Niño 3.4 region, highlighting the improved accuracy attainable through the appropriate use of SST indices of ENSO.

1.2.3 Atmospheric component of ENSO; Southern Oscillation

The atmospheric component of ENSO, first termed the Southern Oscillation (SO) by Sir Gilbert Walker, represents a seesaw in atmospheric mass between the Indonesian equatorial low and the South Pacific subtropical high (Walker and Bliss, 1932; Rasmusson and Wallace, 1983; Allan *et al.*, 1996; Trenberth, 1997). It is a measure of the pressure difference between eastern and western hemispheres (Figure 1.6) (Walker and Bliss, 1932; Troup, 1965; Bjerknes, 1966; Chen, 1982; Trenberth and Caron, 2000). Meteorological and oceanographic variables such as the equatorial zonal east-west Walker circulation, rainfall, sea surface temperatures, air temperature, winds and sea level in the equatorial Pacific are closely related fluctuations in the SO (Bjerknes, 1966; Chen, 1982; Rasmusson and Carpenter, 1982).

Comparing a number of meteorological stations in the Pacific, Chen (1982) showed that combining Port Darwin with Tahiti Mean Sea Level Pressure (MSLP) is homogeneous and relatively unbiased, and as such was recommended for diagnostic studies of the SO, referred to as the Southern Oscillation Index (SOI) (Figure 1.7). The SOI is calculated using monthly average pressure anomalies at each station, normalised by the respective standard deviation, and combined by the subtraction of Darwin anomalies from Tahiti pressure anomalies to give an index of the atmospheric pressure gradient between the eastern and western Pacific (Allan *et al.*, 1996). The SOI is a dimensionless parameter since the anomaly of each factor is divided by its standard deviation (Troup, 1965).

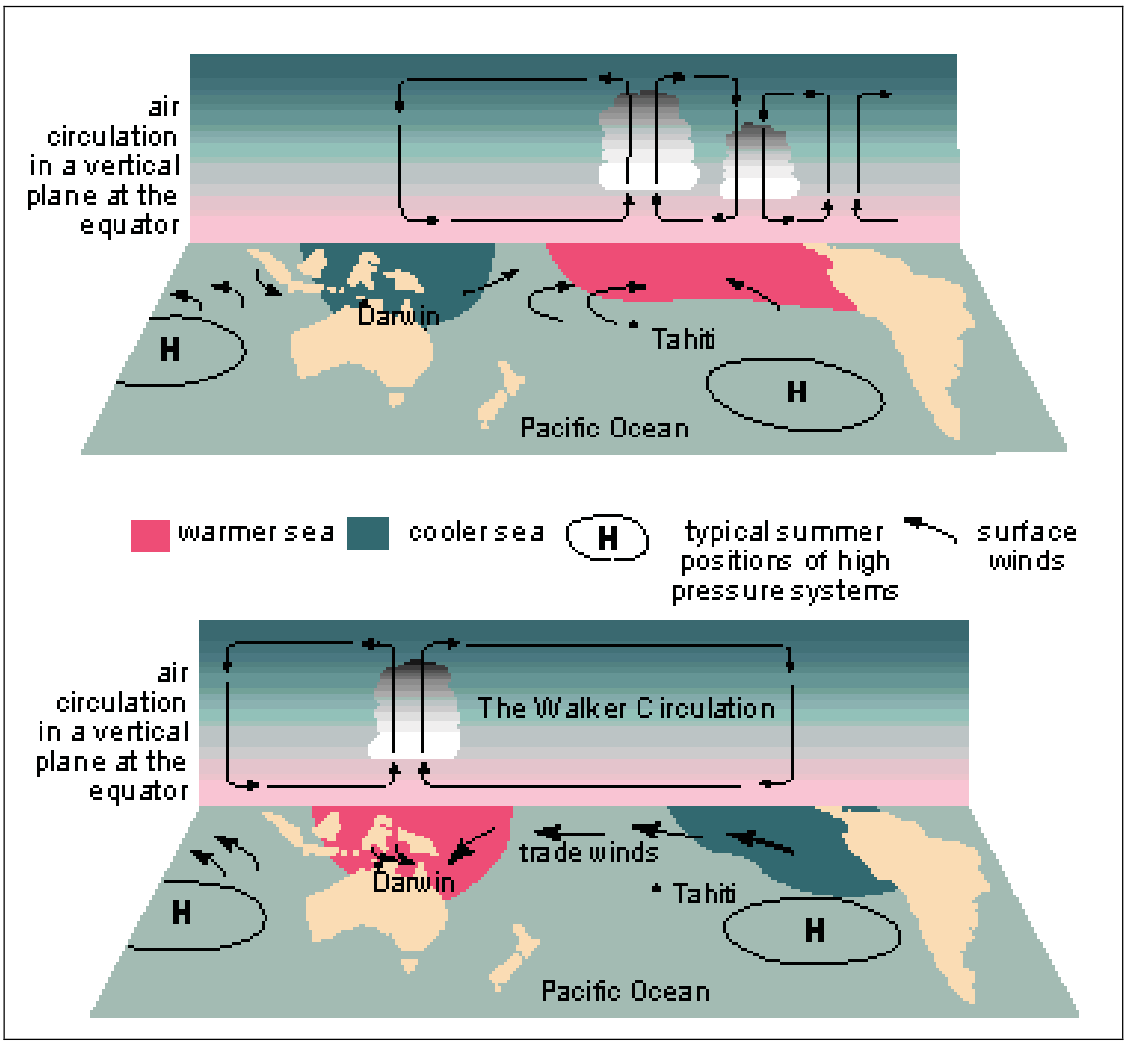

Figure 1.6. Walker circulation associated with the Southern Oscillation Index (SOI). During El Niño conditions (top panel), there is an eastward displacement of the Walker circulation, resulting in high atmospheric pressure and cooler SST conditions over the western Pacific. During La Niña conditions (bottom), there is an intensification of normal Walker circulation conditions, producing low atmospheric pressure and warmed SSTs in the western Pacific. **Source:** Commonwealth Scientific and Industrial Research Organisation (CSIRO) (http://www.bom.gov.au/lam/climate/levelthree/analclim/elnino.htm).

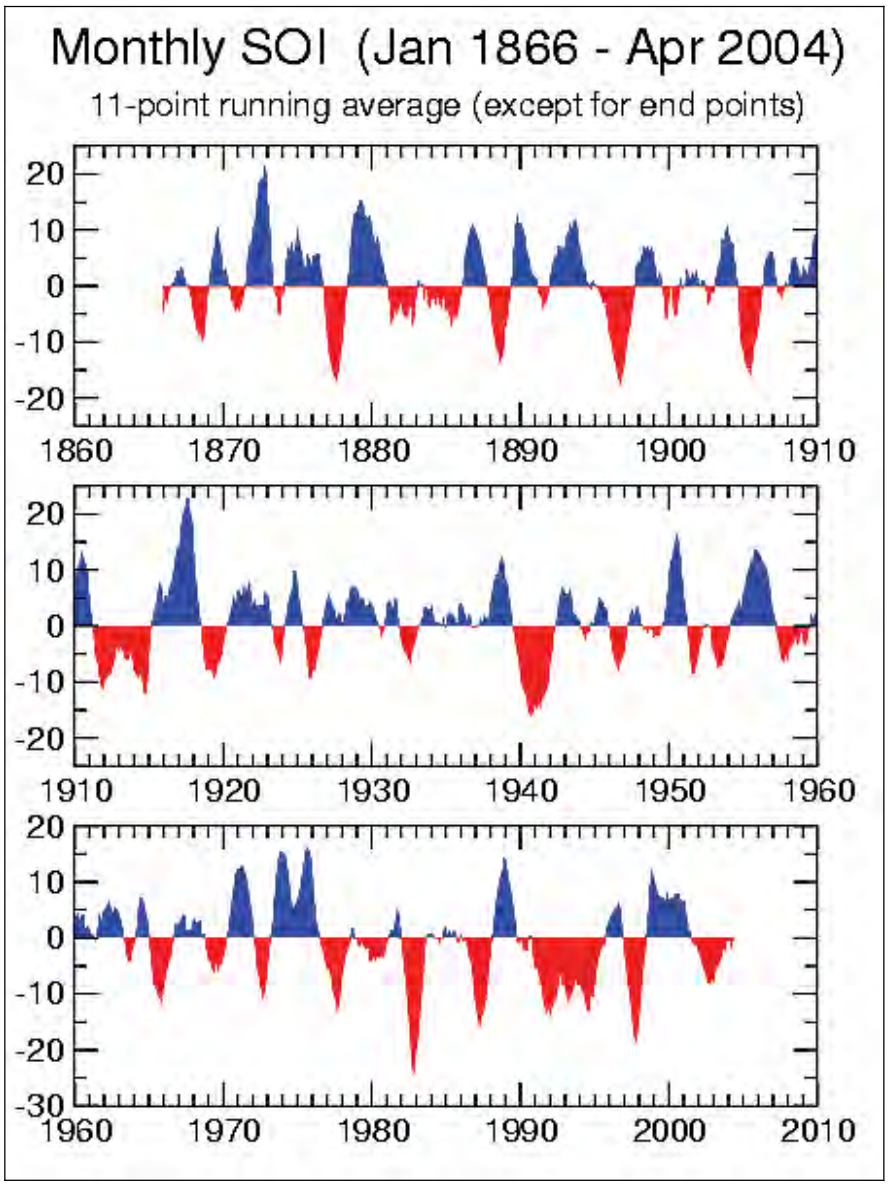

Figure 1.7. Monthly Southern Oscillation Index (SOI), 1866-2004. Based on the mean and standard deviation of the 1933-1992 period. Negative departures (red) correspond to El Niño conditions, while positive excursions of the SOI (blue) are indicative of La Niña episodes. Note that vertical scale indicates dimensionless SOI units. **Source:** Australian Bureau of Meteorology (http://www.dar.csiro.au/information/soi.html)

A number of studies have examined the reliability of the data and the properties of the SOI (Allan *et al.*, 1996; Trenberth and Caron, 2000). For example, a strong annual MSLP cycle at Darwin and Tahiti makes inter-annual and lower frequency variability a small fraction of explained variance (Trenberth and Caron, 2000). As the SOI is based on just two stations, high frequency phenomena such as the Madden-Julian Oscillation may obscure oscillations attributed to the Southern Oscillation (Trenberth, 1997).

Troup (1965) noted that the centres of action involved in the SO vary in position and activity. Prior to 1935, Tahiti has a number of missing values and periods when the correlation between Tahiti–Darwin atmospheric pressure was low despite evidence that the SO was present from other stations (Trenberth and Hoar, 1996). This highlights the need for high-quality, homogeneous climate series (Allen *et al.*, 1991) and the potential for misinterpreting past climate variability based on a sole index of this complex phenomenon. Nevertheless, the SOI is essentially a good representative of the Southern Oscillation, with the advantage of a relatively long record length when compared with SST records (Brassington, 1997).

1.2.4 Late twentieth century ENSO & anthropogenic climatic change

The response of ENSO to anthropogenic warming remains an important and controversial topic (Latif *et al.*, 1997; Trenberth and Hoar, 1997; Allan and D'Arrigo, 1999; Timmermann *et al.*, 1999; Fedorov and Philander, 2000; Jones *et al.*, 2001; Cane, 2004). Attributing any observed recent changes to greenhouse gas forcing ultimately requires a broader baseline of ENSO observation than currently exists temporally, spatially, and with respect to multiple processes. The question of whether ENSO is influenced by greenhouse gas levels may also be partly addressed by examining its sensitivity to past periods of altered boundary conditions (Clement *et al.*, 2000; Tudhope *et al.*, 2001; Cobb *et al.*, 2003; Cane, 2004; Mann *et al.*, 2005).

Several studies support potential links between ENSO and increasing greenhouse gas concentrations (Trenberth and Hoar, 1996; Trenberth and Hoar, 1997; Timmermann *et al.*, 1999). The shift towards generally more ENSO-like conditions in 1976 is consistent with atmospheric Global Circulation Models (GCMs) predictions of an intensified hydrologic cycle under doubled CO_2 scenarios (Graham, 1995; Collin, 2005). It has also been suggested that the recent tendency for more El Niño and the prolonged warm episodes that persisted through the early 1990s are unprecedented in the instrumental climate record and may reflect the influence of anthropogenic global warming (Trenberth and Hoar, 1996; Trenberth and Hoar, 1997; Dunbar and Cole, 1999; Jones *et al.*, 2001).

Simple statistical models have indicated that given the characteristics of the instrumental record, anomalous ENSO episodes experienced during the 1990s would have a very low probability of occurrence in a stationary system (Trenberth and Hoar,

1996; Timmermann, 1999; Cane, 2004; Collins, 2005). This result raises the question of whether recent ENSO anomalies occurred as a result of increasing greenhouse gases (Rajagopalan *et al.*, 1997; Trenberth and Hoar, 1997). However, some studies utilising palaeoclimatic records suggest that similar anomalies of the duration of the 1990-95 event have occurred over the past three centuries, thereby implying no relation to recent greenhouse gas increases (Latif *et al.*, 1997; Allan and D'Arrigo, 1999).

Using model simulations, Timmermann *et al.* (1999) suggested that the mean climate by the middle of the 21st century in the tropical Pacific region will change towards a state corresponding to present-day El Niño conditions. Events typical of El Niño are predicted to also become more frequent, and stronger inter-annual variability will be superimposed on the changes in the mean state. This suggests that year-to-year variations may become more extreme under enhanced greenhouse conditions (Timmermann *et al.*, 1999). Furthermore, Timmermann *et al.* (1999) asserted that projected inter-annual variability would be more strongly skewed, with strong La Niña events (relative to an El Niño mean state) becoming more frequent. Although the model was successful in simulating and predicting ENSO, the response of the phenomenon to greenhouse warming may depend on processes such as role of cloud feedback systems that are currently not well understood (Timmermann *et al.*, 1999).

1.2.5 ENSO teleconnections

Mid-latitude anomalies associated with decadal (IPO/PDO) variability differ from those associated with inter-annual ENSO variations (Zhang *et al.*, 1998). A number of palaeoclimate studies have revealed that long term drifts in ENSO teleconnections have varied as the mean state of ENSO fluctuates (Stahle *et al.*, 1998; Mann *et al.*, 2000; Cobb *et al.*, 2003; Hendy *et al.*, 2003). As already implicated, the predictability of ENSO translates to predictability of anomalies in many tropical and extra tropical regions (Dunbar and Cole, 1999). Variations in regional teleconnections may result from changes in 'centres of action' locations, seasonal timing, intensity of anomalies of ENSO, complex interactions of ENSO with mid-latitude anomalies or other inter-decadal varying aspects of climate (Kumar and Hoerling, 1997). Accordingly, ARTS have identified the further characterisation of the temporal and spatial stability of ENSO teleconnections as being a significant research priority (Dunbar and Cole, 1999).

Understanding the nature and causes of teleconnection instability is crucial for ongoing regional climate prediction efforts related to ENSO.

1.2.6 Issues with instrumental records of ENSO

Most instrumental observations of tropical climate span only the past few decades and only a handful of instrumental records from the tropics predate the early 1900s (Dunbar and Cole, 1999). Thus, state-of-the-art predictive models are based only on the information available from the past several decades. As instrumental records have lengthened through high-quality palaeoclimate reconstructions, climate dynamicists and modelers have recognised the significance of decadal and longer variability in these tropical systems (Dunbar and Cole, 1999).

Recently, issues associated with observational records of ENSO have been revisited (Trenberth and Stepaniak, 2001; Hanley *et al.*, 2003; Gergis and Fowler, 2005). For example during the mid-1970s, it was observed that ENSO events tended to develop first along the coast of South America and then spread westward, as was found in the composites of Rasmusson and Carpenter (1982) based on six warm ENSO events from 1951 to 1972 (Wang, 1995; Fedorov and Philander, 2000). Beginning from the 1982-83 El Niño, however, it was shown that on average El Niños originate in the far western equatorial Pacific and slowly propagate eastward to the central equatorial Pacific (Clarke and Van Gorder, 2001). Such non-stationarities suggests that an inappropriate index of average SST taken from one region, such as the traditionally defined El Niño region of South America, may not adequately characterise the Pacific basin-wide occurrence of an event.

In addition, atmospheric and oceanic components of ENSO can be out of phase with one another (Trenberth, 1997; Kane, 1999). The 2004-05 El Niño was an instructive example of a decoupled ENSO event. SST anomalies exceeded 0.5°C in the western-central Pacific (Niño 4, Niño 3.4 and Niño 3 regions), while warming exceeding 1°C did not expanded eastward of 140°W, resulting in near zero anomalies along the 'classical' El Niño region off the west coast of South America (Niño 1+2 SST region) (Lyon and Barnston, 2005). The atmosphere failed to couple with SST conditions until late in the austral summer when in February 2005, the SOI reached its lowest level since the 1982-83 event (Lyon and Barnston, 2005). Interestingly, this weak El Niño was detected by the Niño 3.4 SST index for at least six months, while the Niño 3 SST index

(commonly used to calibrate ENSO proxy records) only indicated anomalous conditions for 1-2 months (Lyon and Barnston, 2005). Clearly, ENSO experiences significant variation from its currently defined state.

1.2.7 Defining ENSO for palaeoclimate applications

Clarification of the definition of ENSO has long been recognised as an issue of practical relevance by CLIVAR (Trenberth, 1997). Nevertheless, limited consensus exists within the scientific community working on ENSO as to which index best defines ENSO years, and the strength, timing and duration of events (Trenberth, 1997; Hanley *et al.*, 2003; Elsey, 2004; Gergis and Fowler, 2005; Lyon and Barnston, 2005). ENSO is still inadequately understood due to its complex nature, which further complicates efforts to define the morphology of ENSO events (Hanley *et al.*, 2003; Mc Phaden, 2004).

The common approach for climate reconstruction from proxies is to use statistical regression to establish a connection between instrumental records and the variability of the proxy over the period of overlap (Jones *et al.*, 2001; Mann, 2002; Jones and Mann, 2004). This calibration process provides a transfer function that enables the proxy to be used as a surrogate of past climate.

Unfortunately, palaeo-ENSO researchers rarely incorporate indices from both components of ENSO into the calibration process, which has resulted in a persistently fragmented description of the coupled ocean-atmosphere system. To date, reconstructive efforts have tended to focus on only one aspect of the ENSO phenomenon, commonly the Southern Oscillation Index (SOI) (Stahle *et al.*, 1998) or oceanic Niño 3 SST region (Mann *et al.*, 1998; 2000; Evans *et al.*, 2002), thereby only partially characterising ENSO perturbations.

In the absence of a firm consensus, palaeoclimatologists often verify any 'ENSO signal' in a proxy record by comparing it to the suite of historical chronologies of El Niño events first compiled by Quinn *et al.* (1987), and most recently revised by Ortlieb (2000). These lists of past El Niño events recorded in South America have been widely viewed as the major reference for any long-term analysis of ENSO (Diaz and Markgraf, 2000). This is despite the fact that the record is only representative of past ENSO conditions experienced in the eastern Pacific teleconnection region, excludes La Niña episodes, and is not a direct record of instrumental registration of ENSO conditions.

Although, various lists of instrumental ENSO events are available (e.g. Allan *et al.*, 2003, Kiladis and Diaz, 1989, Trenberth, 1997), there is no established chronology of unambiguous events that combines both oceanic and atmospheric aspects of the coupled phenomenon. This is somewhat surprising considering that the accurate characterisation of past episodes is vital for the ongoing climate prediction efforts related to ENSO (Trenberth, 1997; Folland *et al.*, 2001; Allan *et al.*, 2003). As such, a practical need exists for a composite index of the synchronous atmosphere-ocean ENSO anomalies to provide a more comprehensive chronology of past ENSO episodes.

Chapter 2 addresses the issues associated with the complexity of ENSO characterisation through comparing the event capture ability of currently used indices of ENSO. Consequently, the Coupled ENSO Index (CEI) is proposed as a combined classification index for the instrumental period. A list of simultaneous oceanic and atmospheric ENSO anomalies was compiled to assist the palaeoenvironmental community in identifying distinct, unambiguous 'ENSO signals' contained within proxy records, encouraging the development of proxy records for use in detecting imprints of past ENSO behaviour. The development of the CEI was intended to facilitate the characterisation of the seasonal timing and teleconnection signatures of individual events using existing palaeoarchives (Gergis and Fowler, 2005).

1.3 High-Resolution Palaeoclimate Data

1.3.1 Data availability and limitations

High-resolution records derived from corals, tree rings, varved sediments and ice cores have the advantage of precisely registering discrete seasonal to annual environmental signals that may be attributed to single ENSO events (Markgraf and Diaz, 2000). Characteristic ENSO signals include drought, fires, floods, temperature and precipitation fluctuations, SST anomalies and changes in ocean salinity (Markgraf and Diaz, 2000). These records expand upon limited instrumental and documentary data sets allowing the long-term behaviour of oscillations like ENSO to be examined.

There are, however, a number of limitations associated with high temporal resolution palaeoclimatic reconstructions. Unfortunately, high-resolution records are difficult to obtain and often have restricted geographic availability, evident from Figure 1.8.

(Markgraf and Diaz, 2000). Environmental constraints may include a lack of tree species with annual growth rings in low-mid latitude areas of the Southern Hemisphere and the restriction of coral records to tropical warm-water regions of the equatorial Pacific. Such spatial limitations on the location of study sites dictate the type of climatic and oceanic influences that can be resolved (Harrison and Dodson, 1993; Allan and Lindsay, 1998). As a result, regions in which data is sparse or absent present major problems in achieving a spatially balanced understanding of important components of the global climatic system such as ENSO (Allan and Lindsay, 1998).

1.4 Multiproxy Approaches to ENSO Reconstruction

1.4.1 Rationale

A major challenge facing palaeoclimatic studies is to integrate findings from numerous palaeoenvironmental sources analysed at varying spatial and temporal resolutions (Cronin, 1999). Markgraf and Diaz (2000) emphasised the importance of comparing a variety of proxy indicators that represent regional responses to different aspects of the ENSO phenomenon. By doing so, multiproxy investigations taken from spatially distributed locations dramatically reduce the possibility that non-ENSO environmental factors are responsible, allowing the effective study of past ENSO behaviour (Markgraf and Diaz, 2000).

The limitations and potential biases that are specific to each type of palaeoclimate proxy are well understood (Jones and Mann, 2004). For example, differences in temporal resolution (seasonal versus annual), or inherent limitations in temporal coverage varies from a few centuries using corals and historical documentary sources, to thousands of years in the case of tree-ring and ice core sequences (Jones and Mann, 2004). Thus, each proxy represents unique signals from different regions of the globe (tropics versus extra tropics, terrestrial versus marine environments) allowing complementary information on the widespread nature of ENSO event signatures to be investigated (Jones and Mann, 2004).

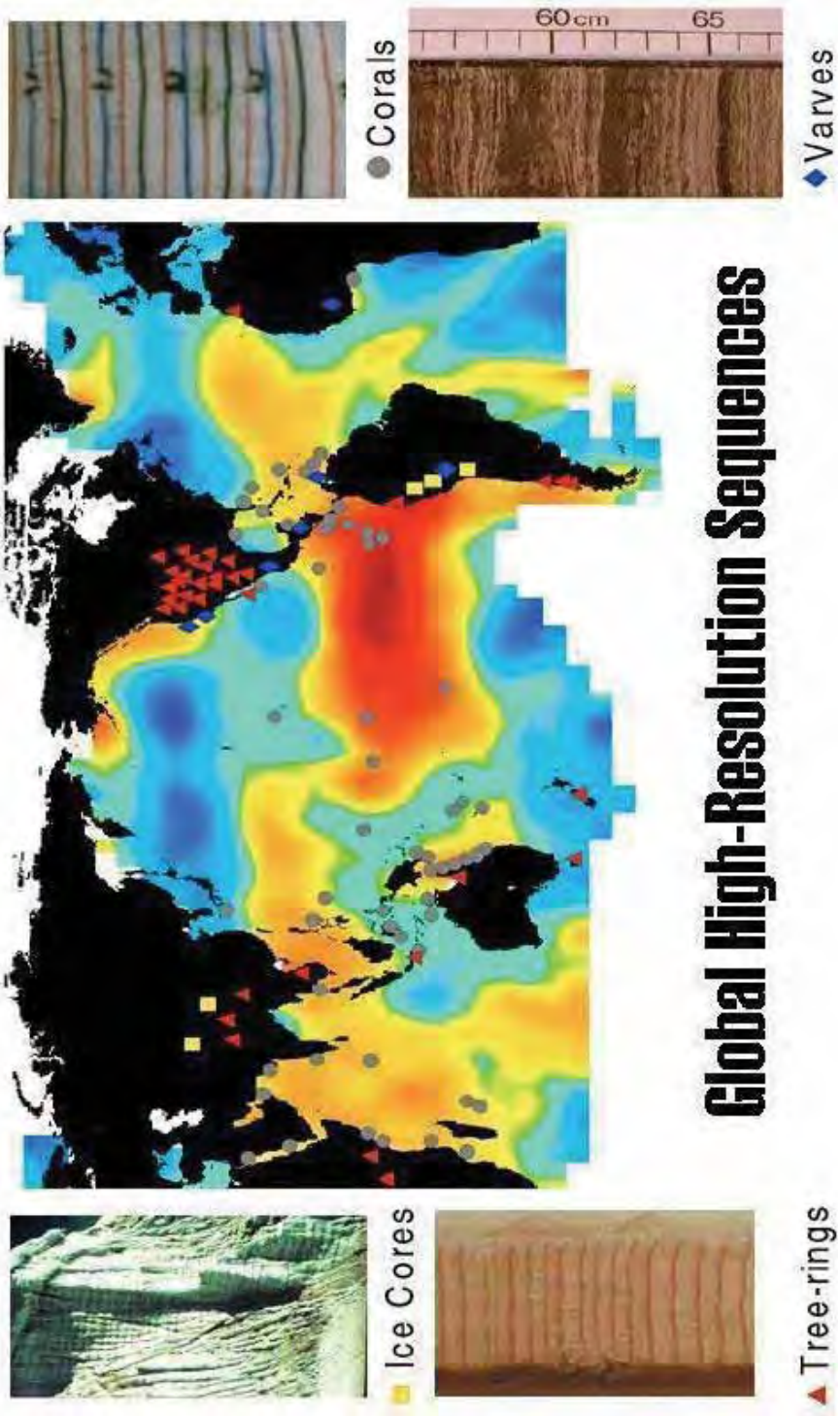

Figure 1.8. Generalised distribution of high-resolution proxy records overlain on average Sea Surface Temperature (SST) anomaly map for December 1877 derived from the Kaplan SST data set (http://ingrid.ldeo.columbia.edu/SOURCES/.KAPLAN). Coral (grey circles), tree-rings (red triangles), ice cores (yellow squares) and sediments (blue diamonds) palaeoclimate records that provide a means for assessing seasonal-annual climate variability in pre-instrumental times. Note the general lack of long Southern Hemisphere and western Pacific proxy records. **Source:** Modified from Annual Records of Tropical Systems (ARTS) http://pangea.stanford.edu/research/Oceans/ARTS/arts_report/arts_report_home.html

As alluded to in Section 1.2.4, the dynamic nature of ENSO makes any reconstruction using proxy archives problematic. ENSO episodes are known to differ in terms of their relative strengths, season of onset, maturity and the location of maximum SST anomalies in the tropical Pacific (Rasmusson and Carpenter, 1982; Allan *et al.*, 1996; Lyon and Barnston, 2005). Consequently, 'multiproxy' approaches have been employed to take advantage of the complementary strengths of a selected number of ENSO-sensitive data sources, allowing event signatures in core and key teleconnection areas to be investigated (Stahle *et al.*, 1998; Mann *et al.*, 2000; D'Arrigo *et al.*, 2005).

1.4.2 Previous approaches to multiproxy ENSO reconstruction

Mann *et al.* (2000) proposed an alternative approach to single proxy ENSO reconstruction which employed a network of diverse, globally distributed, high-resolution proxy records. Through exploiting the complementary information shared by a wide network of different proxy climate indicators, the multiproxy approach to climatic reconstruction diminishes the impact of weaknesses in any individual type or location of indicator, and makes use of the mutual strength of diverse data.

Two common approaches to ENSO reconstruction can be grouped into two broad categories of (i) discrete event analysis and (ii) extension of instrumental ENSO time series. Chapters 5 and 6 detail previous research undertaken in both these areas and provide a critique of both reconstruction techniques. Chapter 5 presents a new discrete ENSO event chronology using widespread tree-ring, coral, ice and documentary data for the period A.D. 1525-2002. In Chapter 6, instrumental indices of ENSO are extended back to A.D. 1525 using Principal Component Analysis (PCA) regression techniques.

Ortlieb (2000) noted that practically all the decadal-centennial variability studies during the 1990s that used dendroclimatology, coral records, tropical ice cores or other proxy sequences were verified using Quinn's El Niño event chronologies (see for example, Mann *et al.* (2000), Stahle *et al.* (1998), Rodbell *et al.* (1999), Diaz and Markgraf (2000)). Importantly, discrete ENSO event chronologies provide an independent means of verifying PCA based reconstructions of ENSO indices, illustrated in Figure 1.9.

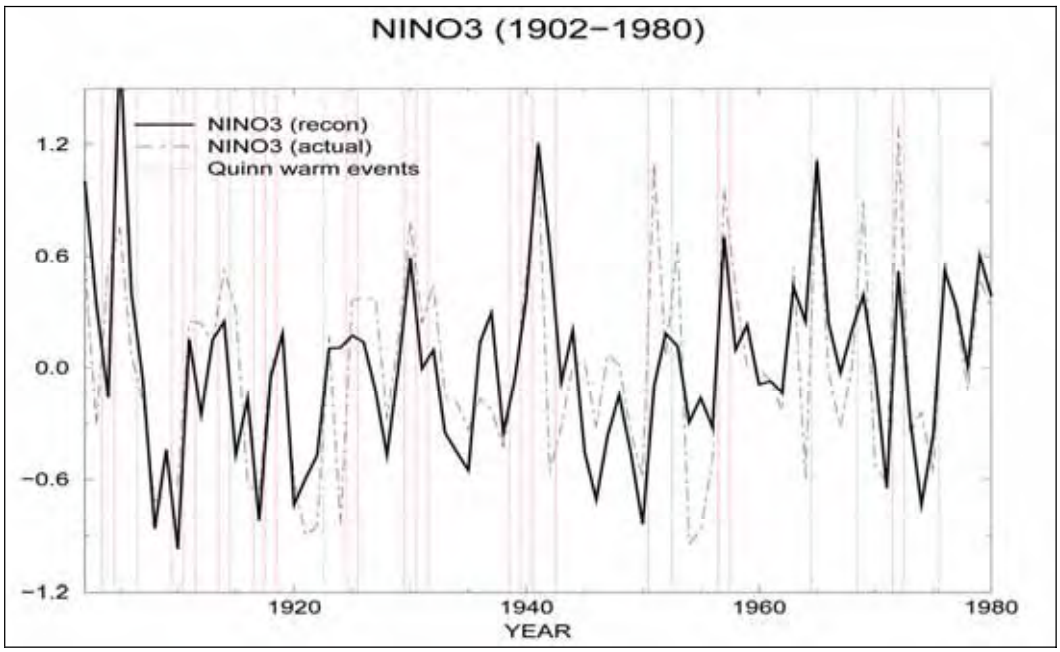

Figure 1.9. Comparison of instrumental and reconstructed Niño 3 SSTs for the 1902-1980 calibration period (Mann *et al.*, 2000). Discrete El Niño events listed in the Quinn and Neal (1992) are annotated to provide independent verification of reconstructed El Niño conditions. Note the considerable mismatch between instrumental and reconstructed Niño 3 SST event amplitude and discrepancies in the timing of Quinn and Neal (1992) El Niño episodes. **Source:** Mann *et al.*, (2000).

1.5 Thesis Outline

The intention of Chapter 1 was to establish the motivation and background to the primary objectives targeted in this study. A technical overview of key research areas provided a synopsis of problematic issues associated with each objective. In conclusion, the following provides an overview of the structure and content of the material presented in the individual chapters contained in this thesis.

- **Chapter 1** is intended to preface the conceptual framework underpinning the objectives targeted in this research. Background to recent climate variability and the role of El Niño-Southern Oscillation (ENSO) in global inter-annual climate variability, the sources, availability and limitations of proxy data and the significance of the development of new proxies from the 'data sparse' mid-latitudes of the Southern Hemisphere is outlined. Finally, a review of the methodologies used in previous reconstructions and a rationale for multiproxy approaches to ENSO reconstruction applied in this study are presented.

- **Chapter 2** addresses the complexities associated with the definition of ENSO. Assessments of the event capture characteristics of instrumental atmospheric, oceanic and coupled ENSO indices are discussed with regard to the implications for subsequent palaeoclimate reconstructions. The Coupled ENSO Index (CEI) is introduced as a new composite calibration index to simultaneously reconstruct both oceanic and atmospheric components of the ENSO system using high-resolution proxy records. Late 20th century ENSO variability is assessed from the perspective of the instrumental period (A.D. 1871-2002).

- **Chapter 3** details the individual proxy tree-ring, coral, ice and documentary records used in the multiproxy analysis. A review and methodological comparison of (i) discrete event and (ii) principal component regression approaches used in previous reconstructions, and the rationale for both multiproxy approaches to ENSO reconstruction is presented.

- **Chapter 4** is concerned with contributing to a new, high-resolution tree-ring ENSO proxy from the 'data sparse' Southern Hemisphere location of New Zealand. A brief overview of the New Zealand Kauri tree-ring database and suitability for ENSO reconstruction is provided. The methodology of primary collection of Kauri tree-ring data and results of the development of two dendroclimatic chronologies are discussed. The benefits of updating dendroclimatic records for subsequent climate applications are presented.

- **Chapter 5** presents novel methodology for the development of a discrete ENSO event chronology using tree-ring, coral, ice and documentary data for the period A.D. 1525-2002. Issues associated with proxy calibration, ENSO event magnitude classification, reconstruction skill quantification and reconstruction verification are detailed. Late 20th century ENSO extremes are assessed from this multiproxy perspective spanning the past five centuries.

- **Chapter 6** describes principal component regression and spectral analysis approaches used to further assess changes in the frequency and amplitude of ENSO variability since A.D. 1525. Multiproxy reconstructions of seasonal atmospheric, oceanic and coupled indices of ENSO are provided and compared against existing global and regional multiproxy ENSO reconstructions. Finally,

an assessment of the stability of regional ENSO teleconnections and nature of late 20th century ENSO is presented.

- **Chapter 7** provides an overall discussion of the results and issues raised in this thesis. Concluding remarks and recommendations for future research are provided.

1.6 References

Allan, R., Reason, C., Lindesay, J. and Ansell, T. (2003). Protracted ENSO episodes and their impacts in the Indian Ocean region. *Deep Sea Research Part II* **50** (12-13): 2331–2347.

Allan, R. (2000). ENSO and climatic variability in the past 150 years. *El Niño and the Southern Oscillation: Multiscale Variability and Global and Regional Impacts.* H. Diaz and V. Markgraf. Cambridge, Cambridge University Press: 3-35.

Allan, R. and D'Arrigo, R. (1999). 'Persistent' ENSO sequences: how unusual was the 1990-1995 El Niño ? *The Holocene* **9** (1): 101-118.

Allan, R. and Lindsay, J. (1998). Past Climates of Australasia. *Climates of the Southern Continents: Present, Past and Future.* J. Hobbs, J. Lindsay and H. Bridgman. London, John Wiley and Sons Ltd.

Allan, R., Lindsay, J. and Parker, D. (1996). *El Niño Southern Oscillation and climate variability.* Melbourne, Australia, CSIRO.

Allan, R., Nicholls, N., Jones, P., and Butterworth, I. (1991). A further extension of the Tahiti-Darwin SOI, early SOI results and Darwin pressure. *Journal of Climate* **4**: 743-749.

Baumgartner, T., Michaelsen, J., Thompson, L., Shen, G., Soutar, A. and Casey, R. (1989). The recording of interannual climatic change by high-resolution natural systems: tree rings, coral bands, glacial ice layers and marine varves. *Aspects of Climate Variability in the Pacific and Western Americas. Geophysical Monograph*. D. Peterson. Washington, American Geophysical Union. **55:** 1-14.

Bjerknes, J. (1966). A possible response of the atmospheric Hadley circulation to equatorial anomalies of ocean temperature. *Tellus* **XVIII** (4): 820-829.

Bjerknes, J. (1969). Atmospheric teleconnections from the equatorial Pacific. *Monthly Weather Review* **97**: 163-172.

Bouma, M., Kovats, R., Goubet, S., Cox, J. and Haines, A. (1997). Global assessment of El Niño's disaster burden. *The Lancet* **350**: 1435-1438.

Bradley, R. (1996). Are there optimum sites for global paleotemperature reconstruction? *Climate Variations and Forcing Mechanisms of the Last 2000 years.* P. Jones, R. Bradley and J. Jouzel. Berlin, Springer-Verlag: 603-624.

Brassington, G. (1997). The Modal Evolution of the Southern Oscillation. *Journal of Climate* **10**: 1021-1034.

Briffa, K., Osborn, T., Schweingruber, F., Harris, I., Jones, P., Shiyatov, S. and Vaganov, E. (2001). Low frequency temperature variations from a northern tree ring density network. *Journal of Geophysical Research* **106** (D3): 2929-2941.

Cane, M. (1983). Oceanographic Events During El Niño. *Science* **95**: 1189-1195.

Cane, M. (2004). The evolution of El Niño, past and future. *Earth and Planetary Science Letters* **164**: 1-14.

Caviedes, C. (2001). *El Niño In History: Storming Throughout the Ages.* Gainesville, USA, University Press of Florida.

Chen, C., Mc Carl, B. and Adams, R. (2001). Economic Implications of Potential ENSO Frequency and Strength Shifts. *Climatic Change* **49**: 147–159,.

Chen, D., Cane, M., Kaplan, A., Zebiak, S. and Huang, D. (2004). Predictability of El Niño over the past 148 years. *Nature* **428**: 733-735.

Chen, W. (1982). Assessment of Southern Oscillation sea-level pressure indices. *Monthly Weather Review* **110**: 800-807.

Clark, C., Cole, J. and Webster, P. (2000). Indian Ocean SST and Indian Summer Rainfall: Predictive Relationships and Their Decadal Variability. *Journal of Climate* **13**: 2503-2519.

Clarke, A. and Van Gorder, S. (2001). ENSO prediction using an ENSO trigger and a proxy for western equatorial Pacific warm pool movement. *Geophysical Research Letters* **28** (4): 579-582.

Clement, A., Seager, R. and Cane, M. (2000). Suppression of El Niño during the mid-Holocene by changes in the Earth's orbit. *Palaeoceanography* **15** (6): 731-737.

CLIVAR Scientific Steering Group (1995). *CLIVAR: A Study of Climate Variability and Predictability, Science Plan.* Geneva, Switzerland, World Meteorological Organisation.

Cobb, K., Charles, C., Cheng, H. and Edwards, L. (2003). El Niño/Southern Oscillation and tropical Pacific climate during the last millennium. *Nature* **424**: 271-276.

Collins, M. (2005). El Niño or La Niña-like climate change? *Climate Dynamics* **24**: 89-104.

Cook, E., D'Arrigo, R. and Mann, M. (2002). A Well-Verified, Multiproxy Reconstruction of the Winter North Atlantic Oscillation Index since A.D. 1400. *Journal of Climate* **15**: 1754-1764.

Cronin, T. (1999). *Principles of Palaeoclimatology.* New York, Columbia University Press.

Crowley, T. (2000). Causes of Climate Change over the Past 1,000 years. *Science* **289**: 270-277.

D'Arrigo, R., Cook, E., Wilson, R., Allan, R. and Mann, M. (2005). On the variability of ENSO over the past six centuries. *Geophysical Research Letters* **32** (L03711): 1-4.

D'Arrigo, R., Jacoby, G. and Krusic, P. (1994). Progress in Dendroclimatic Studies in Indonesia. *Terrestrial, Atmospheric and Oceanographic Sciences* **5**: 349-363.

Diaz, H. and Markgraf, V. (2000). *El Niño and the Southern Oscillation; Multiscale Variability and Global and Regional Impacts.* Cambridge, Cambridge University Press.

Diaz, H. and Pulwarty, R. (1994). An analysis of the time scales of variability in centuries-long ENSO-sensitive records in the last 1000 years. *Climatic Change* **26**: 317–342.

Dunbar, R. and Cole, J. (1999). *Annual Records of Tropical Systems (ARTS); Recommendations for Research.* Geneva, Switzerland, IGBP Science Series.

Easterling, D., Meehl, G., Parmesan, C., Changnon, S., Karl, T. and Mearns, L. (2000). Climate extremes: observations, modeling, and impacts. *Science* **289**: 2068-2074.

Elsey, L. (2004). ENSO Defined. *Weatherwise* **January/February 2004**: 11-12.

Esper, J., Cook, E. and Schweingruber, F. (2002). Low-frequency signals in long tree-ring chronologies for reconstructing past temperature variability. *Science* **295**: 2250-2253.

Evans, M., Kaplan, A. and Cane, M. (2002). Pacific sea surface temperature field reconstruction from coral $\delta^{18}O$ data using reduced space objective analysis. *Palaeoceanography* **17** (1): 7/1-7/13.

Fairbanks, R., Evans, M., Rubenstone, J., Mortlock, R., Broad, K., Moore, M. and Charles, C. (1997). Evaluation of climate indices and their geochemical proxies measured in corals. *Coral Reefs* **16** (Supplement): S93-S100.

Fedorov, A. and Philander, G. (2000). Is El Niño changing? *Science* **288**: 1997-2002.

Folland, C., Karl, T., Christy, J., Clarke, R., Gruza, G., Jouzel, J., Mann, M., Oerlemans, J., Salinger, M. and Wang, S. (2001). Observed Climate Variability and Change. *Climate Change 2001: The Scientific Basis. Contribution of Working Group 1 to the Third Assessment Report of the Intergovernmental Panel on Climate Change.* J. Houghton, Y. Ding, D. Griggs *et al.* United Kingdom and New York, Cambridge University Press.

Gedalof, Z. and Mantua, N. (2002). A multi-century perspective of variability in the Pacific Decadal Oscillation: new insights from tree rings and coral. *Geophysical Research Letters* **29** (24): 57/1-57/3.

Gergis, J. and Fowler, A. (2005). Classification of synchronous oceanic and atmospheric El Niño-Southern Oscillation (ENSO) events for palaeoclimate reconstruction. *International Journal of Climatology* **25**: 1541–1565.

Graham, N. (1995). Simulation of recent global temperature trends. *Science* **267**: 686-671.

Grove, R. and Chappell, J. (2000). El Niño chronology and the history of global crises during the Little Ice Age. *El Niño- History and Crisis.* R. Grove and J. Chappell. Cambridge, The White Horse Press: 5-34.

Hanley, D., Bourassa, M., O'Brian, J., Smith, S. and Spade, E. (2003). A Quantitative Evaluation of ENSO Indices. *Journal of Climate* **16**: 1249-1258.

Harrison, S. and Dodson, J. (1993). Climates of Australia and New Guinea since 18000 yr BP. *Global Climates Since the Last Glacial Maximum.* H. Wright Jr, J. Kutzbach and T. Webb. Minneapolis, USA., University of Minnesota Press: 265-293.

Hendy, E., Gagan, M. and Lough, J. (2003). Chronological control of coral records using luminescent lines and evidence for non-stationarity ENSO teleconnections in north-eastern Australia. *The Holocene* **13** (2): 187-199.

Hoerling, M., Kumar, A. and Zhong, M. (1997). El Niño, La Niña, and the Nonlinearity of Their Teleconnections. *Journal of Climate* **10**: 1769-1786.

Horii, T. and Hanawa, K. (2004). A relationship between the timing of El Niño onset and subsequent evolution. *Geophysical Research Letters* **31** (L06304): 1-4.

Huang, S. (2004). Merging Information from Different Resources for New Insights into Climate Change in the Past and Future. *Geophysical Research Letters* **31**: L13205/L13208.

Jones, P., Briffa, K., Barnett, T. and Tett, S. (1998). High-resolution Palaeoclimatic Records for the last Millennium: Interpretation, Integration and Comparison with General Circulation Model Control-run Temperatures. *The Holocene* **8**: 455-471.

Jones, P. and Mann, M. (2004). Climate over past millennia. *Review of Geophysics* **42**: 1-42.

Jones, P. and Moberg, A. (2003). Hemispheric and large-scale surface air temperature variations: An extensive revision and an update to 2001. *Journal of Climate* **16**: 206-223.

Jones, P., Osborn, T. and Briffa, K. (2001). The Evolution of Climate Over the Last Millennium. *Science* **292** (5517): 662-669.

Kane, R. (1999). El Niño timings and rainfall extremes in India, South-east Asia and China. *International Journal of Climatology* **19**: 653-672.

Karl, T., and Easterling (1999). Climate extremes: selected review and future research directions. *Climatic Change* **42**: 309-325.

Keskin, S. and Olmez, I. (2004). Tracking the El Niño events from Antarctic ice core records. *Journal of Radioanalytical and Nuclear Chemistry* **259** (1): 199-202.

Kumar, A. and Hoerling, M. (1997). Interpretation and Implications of the Observed Inter-El Niño Variability. *Journal of Climate* **10**: 83-91.

Latif, M., Kleeman, R. and Eckert, C. (1997). Greenhouse Warming, Decadal Variability, or El Niño? An Attempt to Understand the Anomalous 1990s. *Journal of Climate* **10**: 2221-2239.

Latif, M., Sperber, L., Arblaster, J., Braconnot, P., Chen, D., Colman, A., Cubasch, U., Cooper, C., Delecluse, P., De Witt, D., Fairhead, L., Flato, G., Hogan, T., Ji, M., Kimoto, M., Kitoh, A., Knutson, T., Le Treut, H., Li, T., Manabe, S., Marti, O., Mechoso, C., Meehl, G., Power, S., Roeckner, E., Sirven, J., Terray, L., Vintzileos, A., Voss, R., Wang, B., Washington, W., Yoshikawa, I., Yu, J. and Zebiak, S. (2001). ENSIP: the El Niño simulation intercomparison project. *Climate Dynamics* **18**: 255-276.

Lyon, B. and Barnston, A. (2005). The evolution of the weak El Niño of 2004-2005. *US CLIVAR Variations* **3** (2): 1-4.

Mann, M. (2002). The value of multiple proxies. *Science* **297**: 1481-1482.

Mann, M. (2003a). Global surface temperatures over the past two millennia. *Geophysical Research Letters* **30** (15): 5/1-5/4.

Mann, M. (2003b). On Past Temperatures and Anomalous Late-20th Century Warmth. *Eos* **84** (27): 1-3.

Mann, M., Bradley, R. and Hughes, M. (1998). Global-scale temperature patterns and climate forcing over the past six centuries. *Nature* **392**: 779-787.

Mann, M., Bradley, R. and Hughes, M. (1999). Northern Hemisphere Temperatures During the Past Millennium: Inferences, Uncertainties, and Limitations. *Geophysical Research Letters* **26** (6): 759-762.

Mann, M., Bradley, R. and Hughes, M. (2000). Long-term variability in the El Niño/Southern Oscillation and associated teleconnections. *El Niño and the Southern Oscillation; Multiscale Variability and Global and Regional Impacts.* H. Diaz, and Markgraf, V. Cambridge, Cambridge University Press: 327-372.

Mann, M., Cane, M., Zebiak, S. and Clement, A. (2005). Volcanic and Solar Forcing of the Tropical Pacific over the Past 1000 Years. *Journal of Climate* **18**: 447-456.

Mantua, N. and Hare, S. (2002). The Pacific Decadal Oscillation. *Journal of Oceanography* **58** (1): 35-44.

Mantua, N., Hare, S., Zhang, Y., Wallace, J. and Francis, R. (1997). A Pacific interdecadal climate oscillation with impacts on Salmon Production. *Bulletin of the American Meteorological Society* **78** (6): 1069-1079.

Markgraf, V. and Diaz, H. (2000). The past-ENSO record; A Review. *El Niño and the Southern Oscillation; Multiscale Variability and Global and Regional Impacts*. V. Markgraf, Diaz, H. New York, Cambridge University Press: 465-488.

Mc Phaden, M. (2004). Evolution of the 2002/03 El Niño. *Bulletin of the American Meteorological Society* **85** (5): 677-695.

Moberg, A., Sonechkin, D., Holmgren, K., Datsenko, N. and Karlen, W. (2005). Highly variable Northern Hemisphere temperature reconstructed from low and high resolution proxy data. *Nature* **433**: 613-617.

Oerlemans, J. (2005). Extracting a Climate Signal from 169 Glacier Records. *Science* **308**: 375-677.

Ortlieb, L. (2000). The documentary historical record of El Niño events in Peru: An update of the Quinn record (sixteenth through nineteenth centuries). *El Niño and the Southern Oscillation: Variability, Global and Regional Impacts.* H. Diaz and V. Markgraf. Cambridge, Cambridge University Press: 207-295.

Power, S., Casey, T., Folland, C., Colman, A. and Mehta, V. (1999). Inter-decadal modulation of the impact of ENSO on Australia. *Climate Dynamics* **15**: 319-324.

Quinn, W., Neal, V. and Antunez de Mayola, S. (1987). El Niño occurrences over the past four and a half centuries. *Journal of Geophysical Research* **92** (C13): 14449–14461.

Quinn, W., Zopf, D., Short, K. and Yang, R. (1978). Historical trends and statistics of the southern oscillation, El Niño and Indonesian droughts. *Fishery Bulletin* **76** (3): 663-678.

Rajagopalan, B., Lall, U. and Cane, M. (1997). Anomalous ENSO occurrences: an alternate view. *Journal of Climate* **10**: 2351-2357.

Rasmusson, E. and Carpenter, T. (1982). Variations in tropical sea surface temperature and surface wind fields associated with the Southern Oscillation/El Niño. *Monthly Weather Review* **110**: 354-384.

Rasmusson, E. and Carpenter, T. (1983). The relationship between eastern equatorial Pacific sea surface temperatures and rainfall over India and Sri Lanka. *Monthly Weather Review* **111**: 517-528.

Rasmusson, E. and Wallace, J. (1983). Meteorological Aspects of the El Niño/Southern Oscillation. *Science* **222**: 1195-1202.

Rodbell, D., Seltzer, G., Anderson, D., Abbott, M., Enfield, D. and Newman, J. (1999). An ~15 000-year record of El Niño driven alluviation in south-western Ecuador. *Science* **283**: 516-520.

Ropelewski, C. and Halpert, M. (1987). Global and regional scale precipitation patterns associated with the El Niño/Southern Oscillation. *Monthly Weather Review* **115**: 1606-1625.

Ropelewski, C. and Halpert, M. (1989). Precipitation patterns associated with the high index phase of the Southern Oscillation. *Journal of Climate* **2**: 268-284.

Salinger, M., Renwick, J. and Mullan, A. (2001). Interdecadal Pacific Oscillation and South Pacific Climate. *International Journal of Climatology* **21**: 1705-1721.

Soon, W. and Baliunas, S. (2003). Proxy climatic and environmental changes of the past 1000 years. *Climate Research* **23**: 89–110.

Stahle, D., D'Arrigo, R., Krusic, P., Cleaveland, M., Cook, E., Allan, R., Cole, J., Dunbar, R., Therrell, M., Gay, D., Moore, M., Stokes, M., Burns, B., Villanueva-Diaz, J. and Thompson, L. (1998). Experimental dendroclimatic reconstruction of the Southern Oscillation. *Bulletin of the American Meteorological Society* **79** (10): 2137-2152.

Timmermann, A. (1999). Detecting the nonstationary response of ENSO to greenhouse warming. *Journal of Atmospheric Sciences* **56**: 2313-2325.

Timmermann, A. (2001). Changes of ENSO Stability Due To Greenhouse Warming. *Geophysical Research Letters* **28** (10): 2062-2064.

Timmermann, A., Oberhuber, J., Bacher, A., Esch, M., Latif, M. and Roeckner, E. (1999). Increased El Niño frequency in a climate model forced by future greenhouse warming. *Nature* **398**: 694-697.

Trenberth, K. (1997). The Definition of El Niño. *Bulletin of the American Meteorological Society* **78** (12): 2771-2777.

Trenberth, K. and Caron, J. (2000). The Southern Oscillation revisited: sea level pressures, surface temperatures, and precipitation. *Journal of Climate* **13**: 4358-4365.

Trenberth, K. and Hoar, T. (1996). The 1990-1995 El Niño Southern Oscillation event: Longest on Record. *Geophysical Research Letters* **23** (1): 57-60.

Trenberth, K. and Hoar, T. (1997). El Niño and climate change. *Geophysical Research Letters* **24** (23): 3057-3060.

Trenberth, K. and Stepaniak, D. (2001). Indices of El Niño evolution. *Journal of Climate* **14**: 1697-1701.

Troup, A. (1965). The Southern Oscillation. *Quarterly Journal of the Royal Meteorology Society.* **91**: 490-506.

Tsonis, A., Hunt, A. and Elsner, J. (2003). On the relation between ENSO and global climate change. *Meteorology and Atmospheric Physics* **84**: 229-242.

Tudhope, A., C., C., Mc Culloch, M., Cook, E., Chappell, J., R., E., Lea, D., Lough, J. and Shimmield, G. (2001). Variability in the El Niño Southern Oscillation through a glacial-interglacial cycle. *Science* **291**: 1511-1517.

Turner, J. (2004). The El Niño-southern oscillation and Antarctica. *International Journal of Climatology* **24** (1): 1-31.

Wang, B. (1995). Interdecadal changes in El Niño onset in the last four decades. *Journal of Climate* **8** (2): 267-285.

Walker, G., and Bliss, E. (1932). World Weather V. *Mem. Royal Meteorological Society,* **4**(36): 53–84.

Wang, H., Zhang, R., Cole, J. and Chavez, F. (1999). El Niño and the related phenomenon Southern Oscillation (ENSO): The largest signal in interannual climate variation. *Proceedings of the National Academy of Sciences* **96**: 11071-11072.

Zhang, R., Rothstein, L. and Busalacchi, A. (1998). Origin of upper-ocean warming and El Niño change on decadal scales in the tropical Pacific Ocean. *Nature* **391** (879-883).

CHAPTER 2.
INSTRUMENTAL RECORDS OF ENSO

2.1 Introduction

Despite the global influence exerted by ENSO on society, limited consensus exists within the scientific community as to which index best defines the timing, duration and strength of ENSO events (Trenberth, 1997; Hanley *et al.*, 2003; Elsey, 2004). ENSO is still inadequately understood due to its complex nature, which further complicates efforts to define the morphology of ENSO events (Hanley *et al.*, 2003; Mc Phaden, 2004).

Palaeo-ENSO researchers rarely incorporate indices from both oceanic and atmospheric components of ENSO into the calibration process. To date, reconstructive efforts have tended to focus on only one aspect of the ENSO phenomenon, commonly the Southern Oscillation Index (SOI) (Stahle *et al.*, 1998) or oceanic Niño 3 Sea Surface Temperature (SST) region (Mann *et al.*, 1998; 2000; Evans *et al.*, 2002; D'Arrigo *et al.*, 2005). This only partially characterises the entirety of ENSO perturbations, which may result in a fragmented description of the coupled ocean-atmosphere system.

In the absence of a firm consensus on how to define ENSO, palaeoclimatologists often verify any 'ENSO signal' in a proxy record by comparing it to the suite of historical chronologies of El Niño events first compiled by Quinn *et al.* (1987), and most recently revised by Ortlieb (2000). As a result these lists of past El Niño events recorded in South America have been widely viewed as the major reference for any long-term analysis of ENSO. This is despite the fact that they only represent past ENSO conditions experienced in the eastern Pacific region, excludes La Niña episodes and are not a direct instrumental record of ENSO conditions.

As introduced in Chapter 1, SST anomalies in the traditional 'El Niño' region defined by the Niño 1+2 SST zone have long been recognised to fluctuate considerably, compared to the waters further west in the central Pacific or the SOI (see for example,

Trenberth and Hoar (1996), and Deser and Wallace (1987)). In fact, using five SST indices and the SOI, Hanley *et al.* (2003) found the east Pacific Niño 1+2 region to: (i) have less sensitivity to El Niño conditions than the SOI, (ii) be the least responsive to La Niña conditions; and (iii) include the highest instances of missed events and false positive cases of all the SST indices analysed for El Niño events. This questions the uncritical, pervasive use of SSTs from this classically defined 'El Niño' region in any contemporary appraisal of past ENSO behaviour. In fact, recently it was proposed that El Niño forecasts should be labelled as 'basin-wide El Niño', 'coastal El Niño', or a 'dateline El Niño' to account for the spatial differences of each episode (Glantz, 2005).

Although various lists of instrumental ENSO events are available (e.g. Allan *et al.*, 2003, Kiladis and Diaz, 1989, Trenberth, 1997), there is no established chronology of unambiguous events that combines both oceanic and atmospheric aspects of the coupled phenomenon. This is somewhat surprising considering that the accurate characterisation of past episodes is vital for the ongoing climate prediction efforts related to ENSO (Trenberth, 1997; Folland *et al.*, 2001; Allan *et al.*, 2003). As such, there is a practical need for an index of the synchronous atmosphere-ocean ENSO anomalies that provides a more comprehensive chronology of past ENSO episodes.

This chapter addresses the issues associated with the complexity of ENSO characterisation through comparing the 'event capture' capability of two currently used indices of ENSO. Here, event capture refers to how accurately each index registers the occurrence and duration of individual ENSO episodes. To more effectively describe the nature and evolution of ENSO conditions a Coupled ENSO Index (CEI) was devised to identify synchronous oceanic (Niño 3.4 SST) and atmospheric (Southern Oscillation Index) anomalies associated with ENSO for the instrumental period (1871-2003). The CEI is a composite, instrumental index of ENSO designed to simultaneously reconstruct both components of the ENSO system (Gergis and Fowler, 2005). Anomalies expressed in only one of the indices (indicative of decoupled and lead/lag ENSO characteristics) are maintained in the CEI, while coupled ocean-atmospheric anomalies results in the amplification of ENSO magnitude indicated by the CEI.

Using the CEI, a list of simultaneous oceanic and atmospheric ENSO anomalies was compiled to assist the palaeoenvironmental community in identifying distinct, unambiguous 'ENSO signals' contained within proxy records. It is hoped that the CEI will facilitate the seasonal timing and teleconnection signatures of individual events to

be suitably characterised using existing palaeoenvironmental archives and encourage the development of proxy records for use in detecting imprints of past ENSO behaviour.

2.2 Instrumental Definitions of ENSO

2.2.1 Oceanic definition of ENSO; El Niño

For the oceanic characterisation of ENSO, monthly Sea Surface Temperatures (SSTs) from the Niño 3.4 zone (5°N-5°S, 120°-170°W) obtained from the National Oceanic and Atmospheric Administration's (NOAA) Climate Prediction Centre (http://www.cpc.ncep.noaa.gov/data/indices/index.html) were used for the 1950-2003 period. Higher mean temperatures than the often-quoted Niño 3 zone, and its proximity to the west Pacific warm pool and main centres of ocean convection, account for the physical importance of the Niño 3.4 region (Trenberth, 1997). Most recently, the significance of this SST region was acknowledged by its selection as the geographical basis for NOAA's operational Oceanic Niño Index (ONI), representing 40% of the distance between the Niño 3 and Niño 4 SST regions (Elsey, 2004; Mc Phaden, 2004). Data from this area represent *in situ* measurements of sea surface temperature variability, thus are considered to be the best available *direct* record of ENSO conditions. Hanley *et al.* (2003) provide a detailed analysis of the sensitivity of currently used ENSO SST indices.

Following the method of Trenberth (1997), SSTs were standardised to the 1950-79 base period and smoothed with a five-month running mean to minimise intra-seasonal noise. This 30-year base period avoids the post-1979 bias of El Niño events identified in the literature (Trenberth and Hoar, 1996; Trenberth, 1997). An ENSO event is defined here as a five month running mean of SST anomalies for a minimum of six months, with no more than two consecutive neutral months impeding ENSO conditions (Trenberth, 1997; Allan and D'Arrigo, 1999; Hanley *et al.*, 2003). The ±0.5°C threshold is consistent with the ONI. To allow event capture discrepancies to be investigated a threshold sensitivity analysis using 0.1 standard deviation increments ranging from ±0.1 to ±0.5 was carried out for the ±0.4°C ENSO definition given by Trenberth (1997) and Trenberth and Stepaniak (2001).

Pre-1950, the interpolated Niño 3.4 SSTs data set of Trenberth and Stepaniak (2001) based on sparse data from 'ships of opportunity', (hereafter referred to as the 'reconstructed Niño 3.4 SSTs'), were used. For the 1871-1981 period, the HadISST (Hadley Centre Sea Ice and Sea Surface Temperature) dataset was used. To make use of high quality satellite data, the National Center for Environmental Protection (NCEP) data was used from October 1981 onwards. Both data sets were based on 1° x 1° latitude/longitude grids with all area averages and interpolation computations calculated at full resolution (Trenberth and Stepaniak, 2001). The period of overlap between observational and 'reconstructed' SSTs was analysed to assess the ability of the latter to serve as a reliable 'pre-instrumental' extension of the Niño 3.4 SST data set, details of which are found in Section 2.3.

2.2.2 Atmospheric definition of ENSO: Southern Oscillation

For the atmospheric definition of ENSO the Southern Oscillation Index (SOI) sourced from the Australian Bureau of Meteorology (http://www.bom.gov.au/climate/current/soihtm1.shtml) was used. Based on the Troup (1965) method, this SOI time series (1871-2003) is the standardised anomaly of the mean sea level pressure difference between Tahiti and Darwin relative to the 1933-1992 base period (Allan *et al.*, 1996). The SOI is presented in standard deviation units around a mean of zero, with significant positive/negative departures representing La Niña/El Niño conditions. Following Trenberth and Hoar (1996) and Allan *et al.* (2003), the SOI was smoothed with a 11-month running mean to remove high frequency fluctuations caused by phenomenon such as the Madden-Julian Oscillation.

Unlike Niño 3.4 region SSTs, there is no published consensus on the SOI threshold values used to define ENSO events. The suitability of using a SOI value of ±0.5 for La Niña/El Niño events for a period of at least six months was tested, consistent with the SST methodology. This definition was applied to the post-1949 SOI time series to examine the occurrence of ENSO episodes recorded by the atmosphere, discussed further in Section 2.3.2.

2.3 Instrumental Event Capture Comparisons

2.3.1 Oceanic event capture

Instrumental and reconstructed Niño 3.4 SST data were compared to assess the utility of the reconstruction as a pre-1950 substitute. The post-1949 observational record indicated 15(13) El Niño (La Niña) events compared to 15(9) for the reconstruction (Figure 2.1). Both SST records capture the same 15 El Niño events, however, the overall onset and duration of events varied slightly. For example, the reconstruction exaggerates the persistence of El Niño conditions by up to seven months (e.g. 1977/78). Mean El Niño duration from the reconstruction was 13.7 months compared to 13.1 months for observed SSTs. The onset of three El Niños were delayed using the reconstruction by one month (1991), four months (1968) and six months (1979/80). A tendency for the reconstruction to amplify the magnitude of positive anomalies (El Niño events) was most conspicuous in the case of the strong El Niños (e.g. 1972, 1982, and 1997), seen in Figure 2.1.

The four La Niñas 'missed' by the SST reconstruction event related to instances where neutral conditions (not exceeding the defined event threshold) in the observational record punctuated the duration criteria for the classification of an ENSO episode. This resulted in the 1954-55, 1955-56, 1970-71, 1971-72, 1973-74, 1975-76, 1998-99 and 1999-00 La Niñas being distinguished as discrete events in the observational SST record, whereas the reconstruction combines them into four longer events spanning 1954-56, 1970-72, 1973-76 and 1998-2000.

An increase in neutral months elevated the mean duration of La Niñas from the reconstruction to 18.6 months, compared to the more frequent, shorter La Niñas averaging 8.4 months from observed SSTs. Furthermore, the reconstruction shows some La Niñas starting one (1970, 1973, 1984, 1998) or two months (1954, 1964, 1988) earlier, which results in the extension of the length of these five events by two (1996) to 10 months (1956).

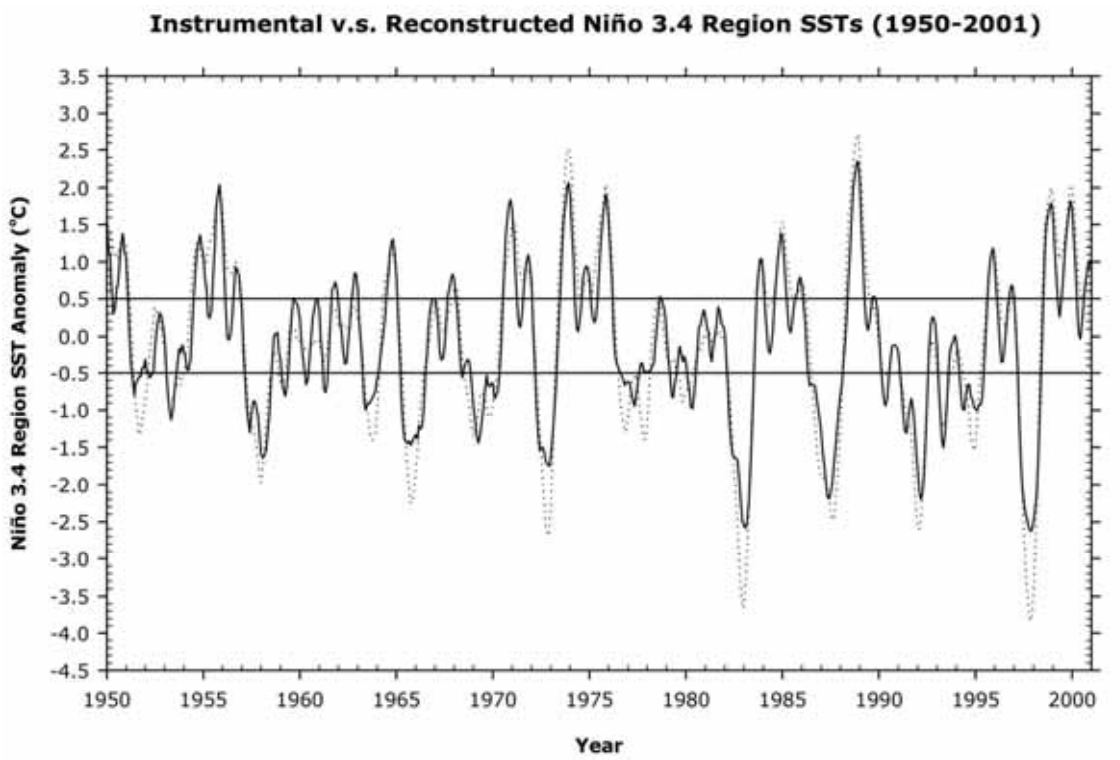

Figure 2.1. Five-month running mean of instrumental (solid) and reconstructed (dashed) Niño 3.4 Region SSTs for the 1950-2001 period of overlap. Horizontal lines represent La Niña and El Niño ±0.5 threshold conditions.

The discrepancies between instrumental and reconstructed Niño 3.4 SSTs identified the potential issues of underestimating the number of La Niñas and overestimating the magnitude of El Niño events prior to 1950. Nevertheless, the striking similarity of the reconstruction shown in Figure 2.1 indicates that the latter is an acceptable, albeit imperfect, extension of the Niño 3.4 SSTs data set.

To examine the sensitivity of ENSO event capture relative to a given threshold, a sensitivity analysis was carried out (Table 2.1). Adjusting the threshold mainly impacted the ratio of neutral and La Niña conditions, as implied by the greater variability in La Niña event capture seen in Table 2.1. The maximum number of El Niño events was captured using the ±0.3 threshold, while the maximum number of La Niñas was obtained using ±0.1.

Table 2.1. 1950-2003 ENSO event capture threshold sensitivity test for Niño 3.4 region SSTs using ±0.1 standard deviation increments (relative to a 1950-1979 base period). Positive/negative SST anomalies denote El Niño/ La Niña conditions.

ENSO Phase	+/- 0.1	+/-0.2	+/- 0.3	+/- 0.4	+/- 0.5
El Niño					
	17	18	19	16	16
La Niña					
	19	15	18	17	13

Increasing the SST event capture threshold raises the number of neutral conditions, which sometimes leads to a 'splitting' of discrete events, impacting event counts. For example, when using the ±0.3 threshold, the 1979-80 El Niño is recorded as two discrete episodes in 1979 and 1980. Similarly, the 1984-86 La Niña given by the ±0.1 threshold is recorded as two separate events (1984-85, 1985-86) by all the other thresholds. This accounts for the somewhat counter-intuitive increase in event capture sometimes associated with raising threshold values.

The ±0.4 definition used by Trenberth (1997) agrees well with the ENSO episodes identified by the ±0.5 definition. The main disparity was that the ±0.4 threshold identified five additional La Niña events during 2000-01, 1985-86, 1983-84, 1974-75 and 1967-68. In all these instances, the ±0.5 threshold was breached for five rather than the six months required for ENSO event capture.

2.3.2 Atmospheric ENSO event capture

Applying the ±0.5 threshold defined in Section 2.2.2 to the post-1949 SOI time series identified twelve El Niño and nine La Niña episodes. In line with the SST analysis, a sensitivity test was used to examine the threshold-dependent changes in ENSO event capture (Table 2.2). A maximum of 14 El Niño episodes were recorded from the SOI using ±0.1 and ±0.2 thresholds, while ±0.1 yielded a maximum of 13 La Niña events. Threshold manipulation altered the frequency of La Niña episodes more so than El Niño event registration due to the weaker magnitude of La Niña events recorded by the SOI.

Table 2.2. 1950-2003 threshold sensitivity for ENSO event capture of the Southern Oscillation Index using ±0.1 standard deviation increments (relative to a 1933-1992 base period). Negative/positive phase in the SOI refers to El Niño /La Niña conditions.

ENSO Phase	+/- 0.1	+/- 0.2	+/- 0.3	+/- 0.4	+/- 0.5
El Niño					
	14	14	13	12	12
La Niña					
	13	12	10	10	9

The threshold-dependent variability in ENSO event capture for the SOI for the upper and lower thresholds used in the sensitivity analysis are shown in Figure 2.2. The minimum (maximum) occurrence of both ENSO phases was registered for the ±0.5 (±0.1) definitions. These differences relate to the registration of an additional four La Niña events (1984-85, 1981, 1966-68, 1959-61) and two weak El Niños (1979-80, 1963-64) using ±0.1.

Instead of splitting events, raising the SOI event capture threshold increases the number of neutral conditions which reduces event duration. For example, using the ±0.1 definition, the 26 month 1957-59 El Niño progressively shortens to 17, 11, 8 and 7 months as the threshold is elevated. This process accounts for changes in the mean duration of El Niño (La Niña) episodes of 20.4 (20.8) months using ±0.1 compared to 14.4 (16.9) months El Niños (La Niñas) produced by using a SOI threshold of ±0.5. It is possible this may reflect the filtering applied to each of the data sets, as discussed further in Section 2.3.3.

The only instance of event splitting noted using a +0.1 threshold is the La Niña of 1966-68, which breaks into 2 events (1966-67, 1967-68) using the +0.2 threshold. The validity of this is questionable as there is only a four-month period of neutral conditions in 1967 that impedes the registration of a continuous event. The fact that these events are not recorded at all by the higher thresholds of Table 2.2 implies a mild atmospheric effect for this moderate La Niña. Similarly, the ±0.1 defined 1959-61 event is only recorded up to the -0.4 threshold, suggesting that relatively weak La Niña events may not be adequately accounted for using a SOI threshold value of ±0.5. In addition, high SOI thresholds appear insensitive to weaker El Niño events. For example, the 1963-64 episode is captured using ±0.1 or ±0.2 thresholds, however, is not when thresholds higher than ±0.3 are used.

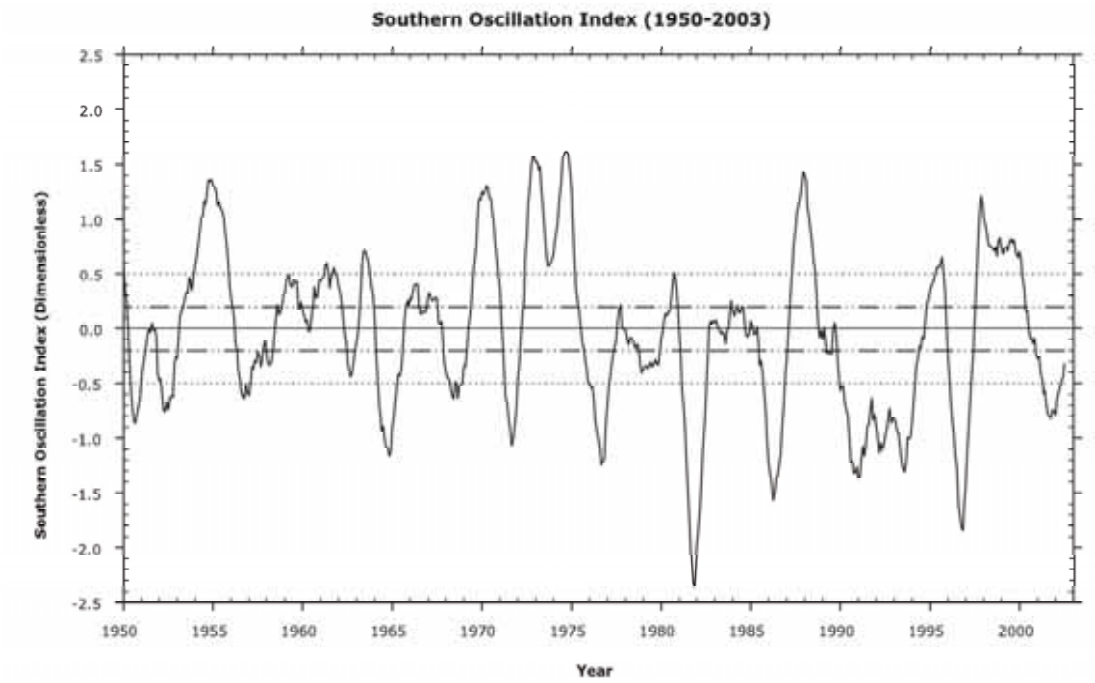

Figure 2.2. Monthly Southern Oscillation Index (SOI) from 1950-2003 smoothed with an 11-month running mean. ENSO event capture comparison using ±0.5 (dotted) and ±0.2 (dashed) thresholds to highlight the impact of threshold selection on event capture.

Nevertheless, 70% of both La Niña and El Niño events identified by ±0.1 are captured by the ±0.5 definition. Very slight differences result from altering the threshold to ±0.3 and ±0.4 (Table 2.2); both record 77% of ±0.1 El Niños, while one extra La Niña event increases event capture from 86% to 93%. There is very little difference between ±0.2 and ±0.1 thresholds; the ±0.2 threshold captures 100% of El Niños and one fewer La Niña resulting in a 92% agreement with ±0.1 events.

2.3.3 Comparison of SST and SOI event analysis

It is evident from comparisons of Tables 2.1 and 2.2 that event capture varies considerably with each index of ENSO and the threshold imposed. Interestingly, no SOI threshold was able to yield enough events to completely agree with the minimum number of events captured by the SST record. The SST analysis identified a minimum of 16(13) El Niños (La Niñas) in the post-1949 period, compared to a maximum of 12(9) El Niño (La Niña) episodes using the ±0.5 SOI definition (see Section 2.3.2).

Compared to the SST event capture, four fewer El Niño and four La Niña events were recorded by the ±0.5 SOI threshold. Two of the El Niños seen from SSTs were not

present at all in the SOI (1980, 1963-64). The other two differences in El Niño capture relate to the 1990-95 SOI El Niño being recorded as three discrete SST events (1991-92, 1993 and 1994-95). Similarly, the 1998-2001 La Niña seen from the SOI is recorded as two separate SST events (1998-99, 1999-00). This was also noted for the La Niñas of 1973-76, 1970-72, and 1955-56. The higher number of ENSO episodes noted from SSTs highlights the event splitting tendency of the oceanic index, raised in Section 2.3.1.

There are also considerable differences in the mean duration of ENSO events seen from the SST and SOI records. Notably, the mean duration of La Niña events from SSTs is 8.4 months compared with a maximum of 16.9 months using ±0.5 for the SOI. Differences are not as marked for El Niños, where the average SST event is 13 months compared to 14.4 months observed from the SOI. This may reflect true differences in the duration of ENSO conditions in the atmospheric and oceanic components, or may be an artefact of the data smoothing and subsequent threshold selection.

The SST event splitting tendency (detailed in Section 2.3.1) impacts the examination of relatively lower magnitude, protracted events defined as 24 months or more of ENSO conditions from the SOI (Trenberth and Hoar, 1996; Allan and D'Arrigo, 1999; Allan *et al.*, 2003). Significantly, strictly applying the 24-month definition to the post-1949 SST record identifies no persistent events from the oceanic record. The maximum duration of any ENSO event recorded from instrumental SSTs is a 22-month El Niño event spanning 1986-88, which falls two months short of the duration criteria (Trenberth and Hoar, 1996; Allan and D'Arrigo, 1999; Allan *et al.*, 2003).

The lack of protracted SST events differs from the three protracted El Niños (1990-95, 1976-78, 1957-59) and three extended La Niñas (1998-2001, 1973-1976, 1954-57) identified using a ±0.1 SOI threshold. For example, the longest SOI El Niño event on record (1990-95) identified by Trenberth and Hoar (1996), is a 50-month event using the most conservative -0.5 SOI threshold, compared to a total of 39 anomalous months combined from the three corresponding discrete SST events (1991-92, 1993, 1994-95). In addition, there are four weak SOI La Niñas (1959-61, 1961-63, 1966-68, and 1981) that occur independently of a corresponding SST response. There are no El Niños that occur independently of a SOI response.

To further complicate matters, the timing of atmospheric and oceanic components of ENSO can be out of phase with one another (Deser and Wallace, 1987; Trenberth, 1997; Kane, 1999), as seen in Figure 2.3. For example, seven El Niños (e.g. 1982, 1990, 1997) and seven La Niñas (e.g. 1988, 1979, 1970) from the SOI start earlier than their oceanic counterparts. Atmospheric El Niños were noted between five (1954, 1964) and eight months (1979) in advance of anomalous SST conditions. By contrast, the ocean was found to precede three El Niños (1957, 1963, and 1986) one month earlier than the SOI, and two La Niñas (1984 and 1995) two months earlier than atmospheric anomalies.

Likewise, ENSO events recorded in the atmosphere appear to have greater persistence compared to the SST record. The atmosphere was found to lag oceanic ENSO signatures for seven La Niñas (e.g. 1976, 1989, 2001) and seven El Niños (e.g. 1951, 1982, 2003). SOI persistence varied up to 12 months (1977-78) for El Niños and 14 months (2000-01) for La Niña episodes. By contrast, there are only four instances where the ocean lags the atmosphere (1964, 1970, 1973, 1988 El Niños), and no indication of oceanic lag from the post-1949 La Niñas. As previously noted, there is a possibility that such trends do not represent true features of ENSO dynamics, but rather a construct of the smoothing applied to the time series.

The differences in event capture characteristics noted above may account for the observed variation in event lists based on SSTs and the SOI. As noted, a sole ENSO index only has the ability to resolve one physical aspect of the phenomenon, and is likely to contain unique information about the dynamics of ENSO evolution. This has considerable implications for the use of a single ENSO index for palaeoclimatic calibration applications.

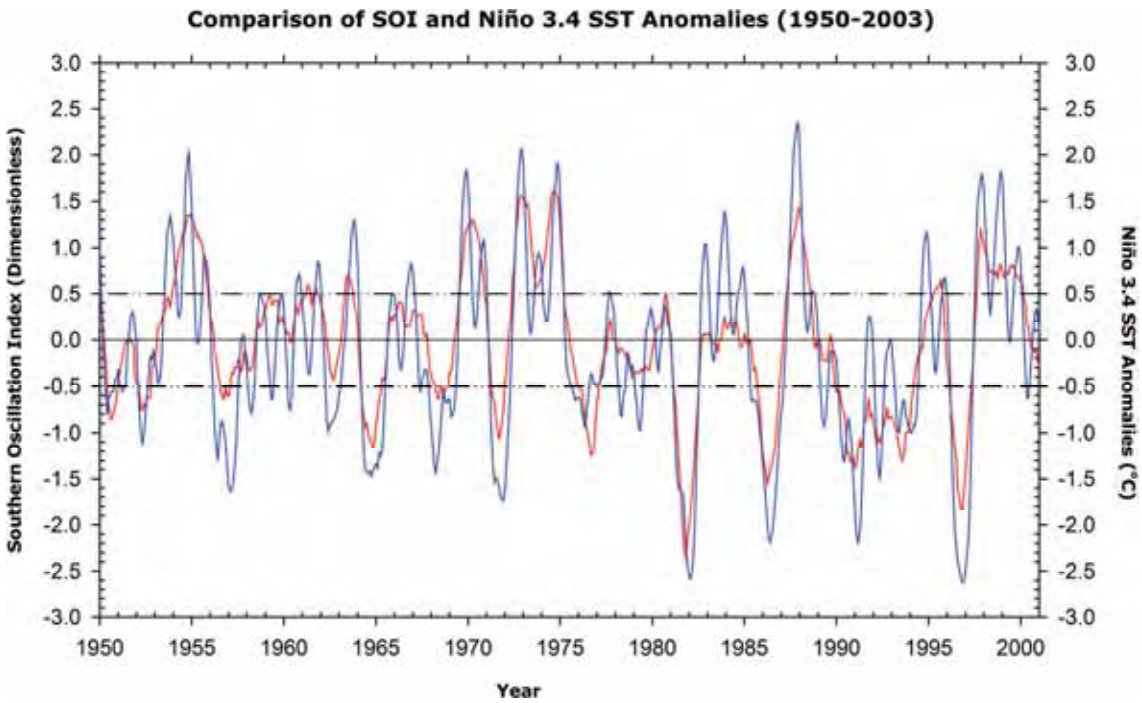

Figure 2.3. Monthly SOI smoothed with an 11-month running mean (red) superimposed on 5-month running mean of instrumental Niño 3.4 Region SSTs (blue) for the 1950-2003 period. SSTs have been inverted to show El Niño SSTs as negative departures to facilitate comparison with the SOI.

2.4 Coupled ENSO Index (CEI)

2.4.1 Rationale

Obviously, the widely used indices of ENSO detailed in Section 2.3 have limitations to their usefulness for describing past ENSO behaviour. Furthermore, a number of studies have examined issues associated with the quality of the station data and the properties of the SOI (Allan *et al.*, 1996; Trenberth and Caron, 2000). For example, Troup (1965) noted that the centres of action involved in the Southern Oscillation vary in position and activity. Similarly, there are very few continuously recorded measurements of tropical oceans in existence prior to 1950 (Fairbanks *et al.*, 1997; Folland *et al.*, 2001). Time series of ocean temperature may be corrupted by changes in the measurement process, such as the gradual switch from bucket to engine intake water starting around 1940 (Fairbanks *et al.*, 1997; Folland *et al.*, 2001). Post-1949 SSTs therefore represent the best available, *in situ* measurements of sea surface temperature variability.

To date, ENSO reconstruction efforts have tended to focus on only one aspect of the ENSO phenomenon, commonly the Southern Oscillation Index (SOI), which only

partially characterises the entirety of ENSO perturbations. Considerable research has also focused on the oceanic Niño 3 region SSTs (Mann *et al.*, 1998; Timmermann, 1999; Latif *et al.*, 2001; Evans *et al.*, 2002; D'Arrigo *et al.*, 2005), despite the fact that in recent years it has become apparent that the key region for coupled atmospheric-oceanic interactions involved in ENSO is located further west than traditionally defined by eastern Pacific ENSO zones (Wang, 1995; Trenberth and Hoar, 1996; Trenberth, 1997; Trenberth and Hoar, 1997).

In the context of such issues, the use of a sole ENSO index is considered undesirable as it can only represent a single aspect of the coupled ocean-atmosphere system. Unless elements of both physical components are included in the calibration process, the description of ENSO will remain incomplete. This in turn may hinder efforts to redefine the phenomenon's life cycle through proxy archives. Clearly, there is a need for a combined ocean-atmosphere index if an integrated reconstruction of ENSO is desired.

A notable attempt to integrate a number of ENSO variables is the Multivariate ENSO Index (MEI) developed by Wolter and Timlin (1993). The MEI is based on six observed variables over the tropical Pacific including sea level pressure, zonal and meridional components of the surface wind, SST, surface air temperature, and total cloudiness fraction of the sky from 1950 to the present (Wolter and Timlin, 1993). Values of the MEI are available online from NOAA's Climate Diagnostics Centre (http://www.cdc.noaa.gov/ENSO/enso.mei_index.html).

Recently, Hanley *et al.* (2003) observed that the MEI had a higher correlation to the Niño 3 index than the SOI or other SST indices. Their analysis also revealed that the Niño 3 SST index is less sensitive for capturing both El Niño and La Niña events than Niño 3.4 SSTs (Hanley *et al.*, 2003), a result also reported by Trenberth (1997). Furthermore, Hanley *et al.* (2003) noted issues associated with the MEI index to include the relatively short length of the time series, a tendency to over-predict the frequency of ENSO events and a weaker relationship with SOI than the other SST indices. Due to "data limitations with the MEI" (Hanley *et al.*, 2003), they were also unable to completely assess the MEI's response and sensitivity to ENSO. Thus, the MEI time series length was considered to be too short to be useful for palaeoclimatic calibration applications, thus is excluded from the analysis presented here.

2.4.2 CEI classification scheme

A classification scheme incorporating both ocean and atmosphere components of ENSO was devised to accurately distinguish unambiguous ENSO events as summarised in Figure 2.4. The basic inputs were monthly values of Niño 3.4 SSTs and the SOI, smoothed using running means of five and eleven months, respectively, as detailed in Section 2.2.

Based on the arguments presented in Sections 2.2.1 and 2.3.1, post-1949 Niño 3.4 SSTs were adopted as the most appropriate direct instrumental record of ENSO conditions. The ±0.5 threshold recently proposed by NOAA to distinguish El Niño, La Niña and neutral months was adopted (Elsey, 2004; Mc Phaden, 2004; Lyon and Barnston, 2005).

Having established the SST-based monthly ENSO classification, a SOI-based sensitivity analysis was undertaken to identify the SOI threshold giving the best agreement with the SST analysis. This was done to ensure near-equal weighting for the oceanic and atmospheric components of ENSO when the two sources were subsequently combined. The results of this sensitivity analysis are presented in Section 2.4.3.

The SOI-based threshold sensitivity analysis (detailed in Section 2.3.2) provided threshold values which were used to classify El Niño, La Niña and neutral months. This was combined with the equivalent analysis undertaken on Niño 3.4 SSTs to produce a composite CEI time series. Where the two series were in agreement, an unambiguous classification for those months resulted. In other cases, any ambiguity was flagged and information about the nature of the ambiguity was retained (see Section 2.4.5 for details).

Following Trenberth (1997) and Hanley *et al.* (2003), a minimum duration of six consecutive months was adopted as the requirement for confident identification of an ENSO event. However, in line with Allan and D'Arrigo (1999), a sequence of ENSO event months to be punctuated by a maximum of two neutral or ambiguous months was allowed. Section 2.4.4 details the application of the method used to derive unambiguous ENSO episodes.

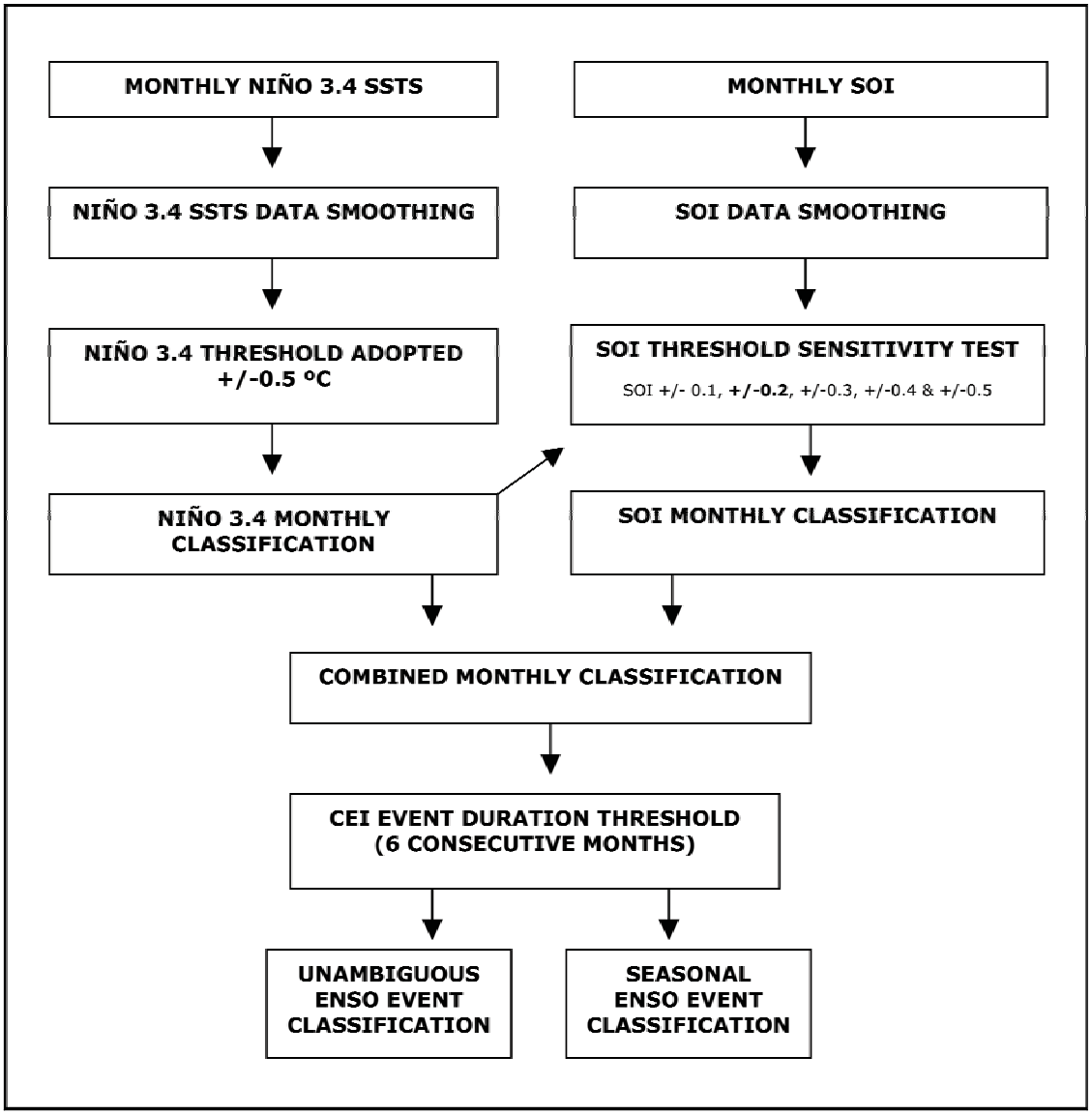

Figure 2.4. Coupled ENSO Index (CEI) classification flowchart showing in monthly and seasonal ENSO classification processes.

The final step in the method was to derive a seasonal version of the CEI to facilitate investigation of proxy-ENSO relationships over various parts of the year. Because of the smoothing inherent to both the SST and SOI data sets, middle month values for the commonly defined austral seasons of summer (DJF), autumn (MAM),winter (JJA), and spring (SON) (i.e. January, April, July and October) were extracted. Results are presented in Section 2.4.5. A monthly listing of the CEI and each component index classification can be found in Appendix 1.

2.4.3 SOI threshold sensitivity analysis

To produce a combined ocean-atmosphere ENSO index it was necessary to identify the SOI threshold needed to achieve the best agreement with Niño 3.4 SST event capture. The sensitivity analysis, using 0.1 standard deviation increments ranging from ±0.1 to ±0.5 (see Section 2.2.1), was next compared to the ENSO events captured using the ±0.5 SST definition from the post-1949 event period. These results are presented in Table 2.3 as percentage of SOI agreement with SST-determined ENSO months.

The high ±0.5 threshold proposed in Section 2.2.2 appears to miss the occurrence of lower magnitude episodes such as the 1908-11 (30 month) and 1949-54 (17 month) La Niñas. As noted in Section 2.3.3, the nature of this omission may have considerable implications for the detection of notable protracted events such as those experienced during the late 20th century (Trenberth and Hoar, 1996; Allan and D'Arrigo, 1999; Allan *et al.*, 2003). In light of a potential loss of important information about the development of ENSO episodes, use of a high SOI threshold (±0.5/0.4) was deemed inappropriate.

Table 2.3. Post-1949 sensitivity test for SOI event capture related to threshold adjustment using ±0.1 standard deviation increments. Values are percentage of agreement with SST-determined ENSO phase months (from Niño 3.4 SSTs for a threshold of ±0.5 for at least six consecutive months) using different SOI thresholds. A SOI threshold of ±0.2 (shaded) yields the most satisfactory agreement with oceanic ENSO events and maintenance of neutral conditions.

ENSO Phase	SOI +/-0.1	SOI +/-0.2	SOI +/-0.3	SOI +/-0.4	SOI +/-0.5
El Niño					
	91%	86%	80%	69%	62%
La Niña					
	90%	83%	77%	70%	64%
Neutral					
	19%	33%	48%	57%	67%

The similarity of agreement between the SOI ±0.1, ±0.2 and ±0.3 thresholds and the SST record is obvious. Although ±0.1 yielded the highest percentage agreement for both ENSO phases, it identified one additional La Niña (1981) compared to ±0.2. This episode is not concurrently observed in the SST record, therefore was considered to be a false positive case (in light of the use of SST anomalies as a basis for defining the presence of ENSO episodes). Similarly, using a ±0.3 SOI threshold does not capture

the 1963-64 El Niño recorded in the SST record. Despite the SST record indicating anomalies reaching 1.0°C during this 10-month event, this episode is not captured using the upper three thresholds of Table 2.3. As a result, the ±0.3 (±0.1) thresholds were rejected on the grounds of potentially being insensitive (oversensitive) to capturing moderate ENSO events.

Finally, the choice of the most appropriate SOI threshold was based on the highest event capture and an adequate agreement of monthly neutral conditions registered by the ocean index. A SOI threshold of ±0.2 was considered to yield the most optimal event capture with respect to the Niño 3.4 SST record while maintaining a satisfactory 1/3 agreement of neutral conditions.

2.4.4 Unambiguous ENSO event classification

Achieving unambiguous ENSO event classification involved addressing the uncertainties presented in Table 2.4. The number of identified events was affected when ENSO conditions were disrupted by more than two neutral or ambiguous months from one index. This results in event splitting for example the La Niñas of 1970-71 and 1971-72. In recognition that characteristics recorded by each sole index may contain meaningful information about the nature of ENSO events, individual classifications were maintained (see Table 2.4 and Section 2.4.5). Using the CEI scheme, 28 distinct El Niño and 26 La Niña episodes were identified from the post-1870 period (Table 2.5), representing synchronous anomalies common to both components of the ENSO system.

Table 2.4. Monthly ENSO classification processes for Niño 3.4 SSTs, SOI and CEI where a maximum of two neutral or ambiguous months are allowed to punctuate ENSO conditions (dark shading). (i) Classification of the 17 month 1949-51 La Niña. (ii) 1970-71 (6 months) and 1971-2 (8 months) La Niña event 'splitting' resulting from 4 consecutive months of neutral conditions in SST record. (iii) Potentially useful lead/lag relationships (light shading) classifications are maintained for seasonal ENSO classification presented in Section 2.4.5.

(i)	M	Niño 3.4 SST	SOI	CEI
1951	2	NIÑA	NIÑA	NIÑA
1951	1	NIÑA	NIÑA	NIÑA
1950	12	NIÑA	NIÑA	NIÑA
1950	11	NIÑA	NIÑA	NIÑA
1950	10	NIÑA	NIÑA	NIÑA
1950	9	NIÑA	NIÑA	NIÑA
1950	8	NIÑA	NIÑA	NIÑA
1950	7	NIÑA	NIÑA	NIÑA
1950	6	NEUTRAL	NIÑA	SOI NIÑA
1950	5	NEUTRAL	NIÑA	SOI NIÑA
1950	4	NIÑA	NIÑA	NIÑA
1950	3	NIÑA	NIÑA	NIÑA
1950	2	NIÑA	NIÑA	NIÑA
1950	1	NIÑA	NIÑA	NIÑA
1949	12	NIÑA	NIÑA	NIÑA
1949	11	NIÑA	NIÑA	NIÑA
1949	10	NIÑA	NIÑA	NIÑA
1949	9	NIÑA	NEUTRAL	N3.4 NIÑA

(ii)	M	Niño 3.4 SST	SOI	CEI
1972	1	NIÑA	NIÑA	NIÑA
1971	12	NIÑA	NIÑA	NIÑA
1971	11	NIÑA	NIÑA	NIÑA
1971	10	NIÑA	NIÑA	NIÑA
1971	9	NIÑA	NIÑA	NIÑA
1971	8	NIÑA	NIÑA	NIÑA
1971	7	NEUTRAL	NIÑA	SOI NIÑA
1971	6	NEUTRAL	NIÑA	SOI NIÑA
1971	5	NEUTRAL	NIÑA	SOI NIÑA
1971	4	NEUTRAL	NIÑA	SOI NIÑA
1971	3	NIÑA	NIÑA	NIÑA
1971	2	NIÑA	NIÑA	NIÑA
1971	1	NIÑA	NIÑA	NIÑA
1970	12	NIÑA	NIÑA	NIÑA
1970	11	NIÑA	NIÑA	NIÑA
1970	10	NIÑA	NIÑA	NIÑA
1970	9	NIÑA	NIÑA	NIÑA
1970	8	NIÑA	NIÑA	NIÑA

(iii)	M	Niño 3.4 SST	SOI	CEI
1998	6	NEUTRAL	NIÑO	SOI NIÑO
1998	5	NIÑO	NIÑO	NIÑO
1998	4	NIÑO	NIÑO	NIÑO
1998	3	NIÑO	NIÑO	NIÑO
1998	2	NIÑO	NIÑO	NIÑO
1998	1	NIÑO	NIÑO	NIÑO
1997	12	NIÑO	NIÑO	NIÑO
1997	11	NIÑO	NIÑO	NIÑO
1997	10	NIÑO	NIÑO	NIÑO
1997	9	NIÑO	NIÑO	NIÑO
1997	8	NIÑO	NIÑO	NIÑO
1997	7	NIÑO	NIÑO	NIÑO
1997	6	NIÑO	NIÑO	NIÑO
1997	5	NIÑO	NIÑO	NIÑO
1997	4	NIÑO	NIÑO	NIÑO
1997	3	NEUTRAL	NIÑO	SOI NIÑO
1997	2	NEUTRAL	NIÑO	SOI NIÑO
1997	1	NEUTRAL	NIÑO	SOI NIÑO

Table 2.5. Unambiguous ENSO events from 1871-2003 derived from Coupled ENSO Index (CEI) classification scheme incorporating the atmospheric SOI and oceanic SSTs from the Niño 3.4 region. Unambiguous status indicates ENSO conditions were simultaneously registered in both instrumental indices. When applicable, event duration includes a maximum of two neutral or ambiguous months as defined in Section 2.4.2. Mean and maximum event magnitude CEI values (detailed in Section 2.4.7) are shown alongside event duration. Extreme events (CEI values exceeding ±3) referred to in Section 2.4.7 are bolded. An asterisk (*) indicates that although ±3 threshold was achieved, this event is not considered extreme as a minimum 50% duration was not observed independently from the SOI in order to reduce the uncertainty associated with the Niño 3.4 SST reconstruction.

El Niño Start	El Niño End	Duration (Months)	Mean CEI Magnitude	Maximum CEI Value	La Niña Start	La Niña End	Duration (Months)	Mean CEI Magnitude	Maximum CEI Value
Mar-2002	Jun-2003	16	-1.74	-2.18	Jul-1999	Mar-2000	9	2.06	2.65
Apr-1997	**May-1998**	14	-3.32	**-4.47**	Aug-1998	Mar-1999	8	2.35	2.96
Apr-1994	May-1995	14	-1.77	-2.17	**Jun-1988**	**Mar-1989**	10	2.87	**3.79**
Feb-1993	Aug-1993	7	-2.07	-2.61	**Jul-1975**	**Mar-1976**	9	2.75	**3.47**
Mar-1991	**Jul-1992**	17	-2.44	**-3.45**	**Jul-1973**	**Mar-1974**	9	2.89	**3.62**
July-1986	**Jan-1988**	19	-2.31	**-3.65**	Aug-1971	Jan-1972	6	1.59	1.85
Mar-1982	**Jul-1983**	17	-3.23	**-4.60**	**Aug-1970**	**Mar-1971**	8	2.48	**3.02**
Feb-1980	Jul-1980	6	-1.10	-1.32	Jul-1964	Dec-1964	6	1.57	1.78
Oct-1976	Jul-1977	10	-1.33	-1.79	**Jul-1955**	**Feb-1956**	8	2.74	**3.39**
Apr-1972	Feb-1973	11	-2.23	-2.71	Aug-1954	Mar-1955	8	1.55	1.71
Dec-1968	Mar-1970	16	-1.38	-1.99	Oct-1949	Feb-1951	17	2.01	2.54
Apr-1965	Jul-1966	16	-2.04	-2.58	Feb-1945	Nov-1945	10	1.04	1.20
Jul-1963	Dec-1963	6	-1.18	-1.31	Jul-1942	Apr-1943	10	1.81	2.36
June-1957	Jul-1958	14	-1.66	-2.19	Jun-1938	Mar-1939	10	1.75	2.01
Mar-1953	Aug-1953	6	-1.57	-1.89	Jul-1933	Feb-1934	8	1.44	1.59
May-1951	Oct-1951	6	-1.28	-1.45	Jun-1924	Mar-1925	10	1.51	1.96
Nov-1939	**Mar-1942**	29	-2.60	**-3.67**	**May 1916**	**Mar-1917**	11	2.54	**3.41**
Aug-1925	Jul-1926	12	-2.30	-2.97	Sep-1908	Feb-1911	30	1.71	2.62
Aug-1923	Jan-1924	6	-1.59	-1.97	Sep-1903	Mar-1904	7	1.71	1.98
Aug-1918	Feb-1920	19	-1.82	-2.77	Dec-1897	Jun-1898	7	1.13	1.24
Oct-1913	Feb-1915	17	-1.82	-2.25	Mar-1892	Jun-1894	28	2.03	2.81
Oct-1911	May1912	8	-2.16	-2.67	Aug-1889	Nov-1890	16	2.33	3.30*
Oct-1904	**Apr 1906**	19	-2.43	**-3.33**	May-1886	Jul-1887	15	2.01	2.64
Sep-1889	Sep-1900	13	-1.89	-2.59	May-1879	May-1880	13	2.03	2.47
Jun-1896	**Apr-1897**	11	-2.89	**-3.75**	Apr-1874	Jun-1876	27	1.66	2.19
Jan-1888	**Apr-1889**	16	-2.43	**-3.79**	**Dec-1871**	**May-1873**	18	2.24	**3.22**
May-1884	Dec-1885	20	-1.10	-1.72					
Dec-1876	**Apr-1878**	17	-3.29	**-4.77**					

To investigate the nature of ENSO characteristics observed from the CEI for the instrumental period, event frequency and duration characteristics for the pre-1950 and post-1949 periods were evaluated against the sole indices of ENSO for these two sub-intervals (Table 2.6). Using the CEI there is an apparent switch from a predominance of La Niña conditions in the pre-1950 period, to heightened El Niño activity post-1949. This is reflected in a an decrease in the total number of La Niña events from 15 to 11, and a corresponding increase in the frequency of El Niños from 12 to 16 in the post-1949 period. This is accompanied by a decline in the mean duration of El Niños (La Niñas) from 15.6 (14.6) to 11.8 (9.2) months. This represents an increase in the frequency of El Niño events from one in every 6.6 years prior to 1950, to one in every 3.4 years in the post 1950 period. However, the overall frequency of La Niña events indicates very little change from one in every 5.3 years prior to 1950, to one in every 4.9 years in the post 1950 period.

Table 2.6. 1871-2003 comparison of pre- and post-1949 ENSO event characteristics using various indices: the CEI (this study); SST (±0.5 from the Niño 3.4 region) and SOI (threshold of ±0.2). Note the differences in the length of the time periods presented and that the CEI produces a higher number of post-1949 CEI El Niños than the SOI due to the event splitting tendency noted for the SST record (see Section 2.3.1). The discrepancy relates to the 1991-92, 1993, and 1994-95 SST El Niños being recorded as one continuous event spanning 1990-1995 in the SOI. This leads to an additional two events in the CEI (highlighting our SST bias), rather than the lowest value of 14 expected from the SOI.

ENSO Phase & Index	Post-1949 Frequency (Total)	Post-1949 Mean Duration (Months)	Pre-1950 Frequency (Total)	Pre-1950 Mean Duration (Months)	Post-1949 Maximum Duration (Months)	Post-1949 Minimum Duration (Months)	Pre-1950 Maximum Duration (Months)	Pre-1950 Minimum Duration (Months)
El Niño								
CEI	16	11.8	12	15.6	19	6	29	6
SST	16	13.1	14	18.8	22	6	29	7
SOI	14	18.4	15	19.3	55	6	46	6
La Niña								
CEI	11	9.2	15	14.6	17	6	28	7
SST	13	8.4	15	16.3	14	6	35	7
SOI	12	18.7	21	19.3	37	8	36	6

Once again, these results highlight the need for caution when investigating ENSO based on a sole index. For example, using the SST record alone, the trend towards more frequent El Niños is not as marked. This contrasts greatly to the SOI results which show a notable decline in the frequency of La Niñas from a pre-1950 peak of 21 events, to 12 observed post-1949. Furthermore, atmospheric ENSO events appear to last

longer than SST anomalies as seen from the maximum duration of El Niño/ La Niñas (55/37 months) in the post-1949 period (noted in Section 2.3.3).

Using the CEI, however, it is possible to avoid the ambiguity associated with using a sole record of the SOI or SSTs. This is not to suggest, however, that trends observed in either of the records are not meaningful. The purpose of this study, however, is concerned with focusing on the simultaneous climate signature common to both components of the ENSO system.

2.4.5 Seasonal ENSO classification

Palaeoclimatologists often deal with proxy records of varying resolution such as the monthly scale of many coral sequences or the annual dating of tree-ring chronologies. To facilitate further insight into ENSO evolution from subsequent proxy reconstructions, seasonal ENSO classifications were categorised by addressing the discrepancies in SOI and SST ENSO classifications outlined in Table 2.4. The seasonal classification preserves information about the individual SOI and SST conditions of the CEI that may provide important evolutive detail on the nature of ENSO events, such as atmosphere/ocean lead/lag signatures. Thus, event lists based on seasonal conditions were generated for the commonly defined seasons (DJF, MAM, JJA, SON) to help identify characteristics such as the onset or peak ENSO conditions from a given proxy record.

Slight discrepancies between the monthly unambiguous event results presented in Table 2.5 and the seasonal compilation of Table 2.7 were observed. These were often related to a modification of the duration, rather than the occurrence, of an event. For example, the 1968-70 El Niño of Table 2.5 is only seen for 1969-70 using the seasonal data in Table 2.7. This is likely an artefact of transferring from monthly to seasonal detail and a reflection of the weak nature of this event (see Table 2.5). The complex issues of seasonal lead/lag relationships were not pursued beyond preserving the ENSO classification generated for the SOI and SST indices. These elements are highlighted in Table 2.7, and not addressed further in this study to avoid detracting from the primary scope of this chapter which seeks to establish a list of unambiguous ENSO events for the instrumental era. Nevertheless, this information is intended to encourage the investigation of the subtleties of discrete ENSO evolution from subsequent proxy reconstruction.

Table 2.7. CEI seasonal classification, 1872-2002. 'NIÑO' (light shading) and 'NIÑA' (dark shading) represent synchronous ENSO conditions, a '?' indicates disagreement, and 'Neutral' no ENSO. 'N 3.4' or 'SOI' preceding 'NIÑO' or 'NIÑA' indicates an event independently flagged in the Niño 3.4 SST or SOI record.

YEAR	DJF	MAM	JJA	SON
2002	SOI NIÑO	NIÑO	NIÑO	NIÑO
2001	NIÑA	SOI NIÑA	Neutral	Neutral
2000	NIÑA	SOI NIÑA	SOI NIÑA	NIÑA
1999	NIÑA	SOI NIÑA	NIÑA	NIÑA
1998	NIÑO	NIÑO	Neutral	NIÑA
1997	SOI NIÑO	NIÑO	NIÑO	NIÑO
1996	NIÑA	SOI NIÑA	SOI NIÑA	NIÑA
1995	NIÑO	NIÑO	Neutral	N3.4 NIÑA
1994	SOI NIÑO	NIÑO	NIÑO	NIÑO
1993	SOI NIÑO	NIÑO	NIÑO	SOI NIÑO
1992	NIÑO	NIÑO	NIÑO	SOI NIÑO
1991	SOI NIÑO	NIÑO	NIÑO	NIÑO
1990	Neutral	NIÑO	NIÑO	Neutral
1989	NIÑA	SOI NIÑA	SOI NIÑA	N3.4 NIÑA
1988	NIÑO	SOI NIÑA	NIÑA	NIÑA
1987	NIÑO	NIÑO	NIÑO	NIÑO
1986	N3.4 NIÑA	Neutral	NIÑO	NIÑO
1985	N3.4 NIÑA	SOI NIÑA	SOI NIÑA	N3.4 NIÑA
1984	N3.4 NIÑA	Neutral	Neutral	N3.4 NIÑA
1983	NIÑO	NIÑO	NIÑO	N3.4 NIÑA
1982	Neutral	NIÑO	NIÑO	NIÑO
1981	Neutral	Neutral	Neutral	SOI NIÑA
1980	SOI NIÑO	NIÑO	NIÑO	SOI NIÑO
1979	Neutral	N3.4 NIÑO	N3.4 NIÑO	Neutral
1978	SOI NIÑO	SOI NIÑO	Neutral	SOI NIÑA
1977	NIÑO	NIÑO	NIÑO	SOI NIÑO
1976	NIÑA	SOI NIÑA	Neutral	NIÑO
1975	NIÑA	SOI NIÑA	NIÑA	NIÑA
1974	NIÑA	SOI NIÑA	SOI NIÑA	NIÑA
1973	NIÑO	N3.4 NIÑO	NIÑA	NIÑA
1972	NIÑA	NIÑO	NIÑO	NIÑO
1971	NIÑA	SOI NIÑA	SOI NIÑA	NIÑA
1970	NIÑO	N3.4 NIÑO	SOI NIÑA	NIÑA
1969	NIÑO	NIÑO	NIÑO	NIÑO
1968	NIÑA	SOI NIÑA	SOI NIÑA	Neutral
1967	SOI NIÑA	SOI NIÑA	SOI NIÑA	N3.4 NIÑA
1966	NIÑO	NIÑO	NIÑO	Neutral
1965	N3.4 NIÑA	NIÑO	NIÑO	NIÑO
1964	N3.4 NIÑO	SOI NIÑA	NIÑA	NIÑA
1963	NIÑA	Neutral	NIÑO	NIÑO
1962	SOI NIÑA	SOI NIÑA	SOI NIÑA	NIÑA
1961	Neutral	N3.4 NIÑO	Neutral	NIÑA
1960	SOI NIÑA	SOI NIÑA	SOI NIÑA	Neutral
1959	SOI NIÑO	NIÑO	Neutral	Neutral
1958	NIÑO	NIÑO	NIÑO	SOI NIÑO
1957	SOI NIÑA	N3.4 NIÑO	NIÑO	NIÑO
1956	NIÑA	SOI NIÑA	SOI NIÑA	NIÑA
1955	NIÑA	SOI NIÑA	NIÑA	NIÑA
1954	SOI NIÑO	Neutral	SOI NIÑA	NIÑA
1953	SOI NIÑO	NIÑO	NIÑO	SOI NIÑO
1952	SOI NIÑO	N3.4 NIÑO	Neutral	Neutral

YEAR	DJF	MAM	JJA	SON
1951	NIÑA	Neutral	NIÑO	NIÑO
1950	NIÑA	NIÑA	NIÑA	NIÑA
1949	SOI NIÑO	Neutral	Neutral	NIÑA
1948	SOI NIÑA	N3.4 NIÑO	Neutral	Neutral
1947	SOI NIÑO	Neutral	SOI NIÑA	N3.4 NIÑA
1946	Neutral	SOI NIÑO	SOI NIÑO	SOI NIÑO
1945	Neutral	NIÑA	NIÑA	NIÑA
1944	Neutral	Neutral	Neutral	Neutral
1943	NIÑA	NIÑA	SOI NIÑA	Neutral
1942	NIÑO	Neutral	NIÑA	NIÑA
1941	NIÑO	NIÑO	NIÑO	NIÑO
1940	NIÑO	NIÑO	NIÑO	NIÑO
1939	NIÑA	SOI NIÑA	Neutral	SOI NIÑO
1938	SOI NIÑA	SOI NIÑA	NIÑA	NIÑA
1937	Neutral	Neutral	Neutral	Neutral
1936	?	SOI NIÑA	Neutral	Neutral
1935	Neutral	SOI NIÑA	Neutral	Neutral
1934	NIÑA	N3.4 NIÑA	Neutral	Neutral
1933	SOI NIÑO		NIÑA	NIÑA
1932	SOI NIÑO	NIÑO	SOI NIÑO	SOI NIÑO
1931	?	?	?	SOI NIÑA
1930	?	N3.4 NIÑO	N3.4 NIÑO	N3.4 NIÑO
1929	SOI NIÑA	SOI NIÑA	SOI NIÑA	?
1928	Neutral	SOI NIÑA	SOI NIÑA	SOI NIÑA
1927	SOI NIÑA	SOI NIÑA	SOI NIÑA	Neutral
1926	NIÑO	NIÑO	NIÑO	Neutral
1925	NIÑA	SOI NIÑA	N3.4 NIÑO	NIÑO
1924	NIÑO	Neutral	NIÑA	NIÑA
1923	NIÑA	Neutral	SOI NIÑO	NIÑO
1922	SOI NIÑA	SOI NIÑA	SOI NIÑA	SOI NIÑA
1921	SOI NIÑA	NIÑA	SOI NIÑA	SOI NIÑA
1920	NIÑO	N3.4 NIÑO	SOI NIÑA	SOI NIÑA
1919	NIÑO	NIÑO	NIÑO	NIÑO
1918	NIÑA	SOI NIÑA	N3.4 NIÑO	NIÑO
1917	NIÑA	SOI NIÑA	SOI NIÑA	SOI NIÑA
1916	SOI NIÑA	SOI NIÑA	NIÑA	NIÑA
1915	NIÑO	N3.4 NIÑO	?	SOI NIÑA
1914	NIÑO	NIÑO	NIÑO	NIÑO
1913	SOI NIÑO	SOI NIÑO	SOI NIÑO	NIÑO
1912	NIÑO	NIÑO	SOI NIÑO	SOI NIÑO
1911	NIÑA	N3.4 NIÑA	SOI NIÑO	NIÑO
1910	NIÑA	NIÑA	NIÑA	NIÑA
1909	NIÑA	NIÑA	NIÑA	NIÑA
1908	Neutral	SOI NIÑA	SOI NIÑA	NIÑA
1907	SOI NIÑA	Neutral	Neutral	Neutral
1906	NIÑO	NIÑO	SOI NIÑA	NIÑA
1905	NIÑO	NIÑO	NIÑO	NIÑO
1904	NIÑA	SOI NIÑA	?	NIÑO
1903	N3.4 NIÑO	?	SOI NIÑA	NIÑA
1902	Neutral	N3.4 NIÑO	N3.4 NIÑO	NIÑO
1901	N3.4 NIÑO	SOI NIÑA	Neutral	SOI NIÑA

YEAR	DJF	MAM	JJA	SON
1900	NIÑO	NIÑO	NIÑO	N3.4 NIÑO
1899	NIÑA	Neutral	N3.4 NIÑO	NIÑO
1898	NIÑA	NIÑA	SOI NIÑA	NIÑA
1897	NIÑO	NIÑO	SOI NIÑO	Neutral
1896	NIÑO	SOI NIÑO	NIÑO	NIÑO
1895	N3.4 NIÑA	Neutral	SOI NIÑO	NIÑO
1894	NIÑA	NIÑA	N3.4 NIÑA	N3.4 NIÑA
1893	NIÑA	NIÑA	NIÑA	NIÑA
1892	Neutral	NIÑA	NIÑA	NIÑA
1891	N3.4 NIÑA	Neutral	SOI NIÑO	SOI NIÑO
1890	NIÑA	NIÑA	NIÑA	NIÑA
1889	NIÑO	NIÑO	SOI NIÑA	NIÑA
1888	NIÑO	NIÑO	NIÑO	NIÑO
1887	NIÑA	NIÑA	NIÑA	Neutral
1886	N3.4 NIÑO	SOI NIÑA	NIÑA	NIÑA
1885	NIÑO	NIÑO	NIÑO	NIÑO
1884	SOI NIÑO	SOI NIÑO	NIÑO	NIÑO
1883	N3.4 NIÑA	Neutral	Neutral	Neutral
1882	?	SOI NIÑO	SOI NIÑO	?
1881	N3.4 NIÑO	NIÑO	SOI NIÑO	SOI NIÑO
1880	NIÑA	NIÑA	SOI NIÑA	SOI NIÑA
1879	NIÑA	SOI NIÑA	NIÑA	NIÑA
1878	NIÑO	NIÑO	?	NIÑA
1877	NIÑO	NIÑO	NIÑO	NIÑO
1876	NIÑA	NIÑA	SOI NIÑA	Neutral
1875	NIÑA	NIÑA	NIÑA	NIÑA
1874	N3.4 NIÑA	NIÑA	NIÑA	NIÑA
1873	NIÑA	NIÑA	Neutral	?
1872	NIÑA	NIÑA	NIÑA	NIÑA

2.4.6 Verification of the CEI classification scheme

To test the veracity of the CEI events, the results in Table 2.5 were compared to eight published lists of past ENSO events available in the literature (Rasmusson and Carpenter, 1983; Kiladis and Diaz, 1989; Quinn and Neal, 1992; Whetton and Rutherfurd, 1994; Mullan, 1995; Trenberth, 1997; Ortlieb, 2000; Allan *et al.*, 2003). Of the five published event lists that extend prior to 1950, three of these are instrumentally based (Rasmusson and Carpenter, 1983; Kiladis and Diaz, 1989; Allan *et al.*, 2003), while the remaining three are historical lists provided by Ortlieb (2000) (pre-1901), Quinn and Neal (1992) (post-1900) and Whetton and Rutherfurd (1994). The latter three are proxy assemblages rather than direct instrumental records, so should be interpreted with a degree of caution.

Differences in temporal coverage make a quantitative comparison between various ENSO event lists problematic. Furthermore, converting a monthly classification into a yearly event list resulted in the need to introduce a 'BOTH' status to the CEI list to accommodate 'phase-flipping', which denotes a switch from El Niño to La Niña conditions (or vice versa) within the same year. Nevertheless, the results presented in Tables 2.8 and 2.9 indicate a good agreement between the CEI and previous work. During the post-1949 period (Table 2.8), every ENSO episode identified by the CEI was verified by at least one other independent list, with the exception of the most recent 2002/03 warm event, which is yet to be incorporated into the event literature, but has been documented by dynamical studies such as Mc Phaden (2004) and Vecchi and Harrison (2003).

For the pre-1950 period (Table 2.9), the CEI was found to have the closest agreement to the list developed initially by Reason *et al.* (2000) and later updated to 2001 by Allan *et al.* (2003). This agreement perhaps relates to the composite approach employed here. Reason *et al.* (2000:1287) referred to using the "magnitude of the Southern Oscillation Index and SST in the Niño 3 and Niño 4 regions to identify ENSO events", however precise details of this methodology are not detailed. Discrepancies observed with the other lists shown in Tables 2.5 and 2.6 are often associated with phase-flipping ('BOTH') cases such as 1911, 1925, and 1951 where other event lists have tended to exclude the occurrence of La Niña conditions.

Table 2.8. Post –1949 comparison of Coupled ENSO index and 7 published event lists. An Asterisk (*) denotes no temporal coverage, while a dash (-) indicates the absence of ENSO conditions. 'BOTH' denotes phase-flipping.

Year	Coupled ENSO Index	Allan et al. (2003)	Trenberth (1997)	Kiladis & Diaz (1989)	Quinn& Neal (1992)	Whetton & Rutherford (1994)	Rasmusson & Carpenter (1983)	Mullan (1995)
2003	NIÑO	*	*	*	*	*	*	*
2002	NIÑO	*	*	*	*	*	*	*
2001	-	NIÑA	*	*	*	*	*	*
2000	NIÑA	NIÑA	-	-	-	-	-	-
1999	NIÑA	NIÑA	*	*	*	*	*	*
1998	BOTH	NIÑA	*	*	*	*	*	*
1997	NIÑO	-	*	*	*	*	*	*
1996	-	-	NIÑA	*	*	*	*	*
1995	NIÑO	-	BOTH	*	*	*	*	*
1994	NIÑO	-	NIÑO	*	*	*	*	*
1993	NIÑO	NIÑO	NIÑO	*	*	*	*	*
1992	NIÑO	NIÑO	NIÑO	*	*	*	*	*
1991	NIÑO	NIÑO	NIÑO	-	-	-	-	-
1990	-	NIÑO	-	*	*	*	*	*
1989	NIÑA	NIÑA	NIÑA	*	*	*	*	NIÑA
1988	NIÑA	NIÑA	BOTH	NIÑA	*	*	*	NIÑA
1987	NIÑO	NIÑO	NIÑO	-	*	*	*	-
1986	NIÑO	NIÑO	NIÑO	NIÑO	*	*	*	-
1985	-	-	NIÑA	-	*	*	*	-
1984	-	-	NIÑA	-	*	*	*	-
1983	NIÑO	NIÑO	NIÑO	-	*	*	NIÑO	NIÑO
1982	NIÑO	NIÑO	NIÑO	NIÑO	*	*	-	NIÑO
1981	-	-	-	-	*	*	-	NIÑO
1980	NIÑO	-	NIÑO	-	*	*	-	NIÑO
1979	-	-	NIÑO	-	*	*	-	-
1978	-	-	NIÑO	-	*	*	-	NIÑO
1977	NIÑO	-	NIÑO	-	-	-	-	NIÑO
1976	BOTH	-	BOTH	NIÑO	NIÑO	-	NIÑO	NIÑO
1975	NIÑA	NIÑA	NIÑA	NIÑA	*	*	*	NIÑA
1974	NIÑA	NIÑA	NIÑA	-	-	-	-	NIÑA
1973	BOTH	BOTH	BOTH	NIÑA	NIÑO	-	-	BOTH
1972	BOTH	NIÑO	BOTH	NIÑO	NIÑO	NIÑO	NIÑO	NIÑO
1971	NIÑA	NIÑA	NIÑA	-	-	-	-	NIÑA
1970	BOTH	NIÑA	BOTH	NIÑA	NIÑO	-	-	NIÑA
1969	NIÑO	-	NIÑO	NIÑO	-	-	NIÑO	NIÑO
1968	NIÑO	-	NIÑO		-	-	-	NIÑA
1967	-	-	-	-	-	-	-	NIÑA
1966	NIÑO	NIÑO	NIÑO	*	NIÑO	NIÑO		NIÑO
1965	NIÑO	NIÑO	BOTH	NIÑO	-	NIÑO	NIÑO	NIÑO
1964	BOTH	NIÑO	BOTH	NIÑA	-	-	-	BOTH
1963	NIÑO	NIÑO	NIÑO	NIÑO	-	-	NIÑO	NIÑA
1962	-	-	-	-	-	-	-	NIÑA
1961	-	-	-	-	-	-	-	-
1960	-	-	-	-	-	-	-	-
1959	-	-	-	-	-	-	-	NIÑO
1958	NIÑO	NIÑO	NIÑO		NIÑO		-	NIÑO
1957	NIÑO	NIÑO	NIÑO	NIÑO	NIÑO	NIÑO	NIÑO	NIÑO
1956	NIÑA	NIÑA	NIÑA	-	-	-	-	NIÑA
1955	NIÑA	NIÑA	NIÑA	-	-	-	-	NIÑA
1954	NIÑA	NIÑA	NIÑA	NIÑA	-	-	-	-
1953	NIÑO	-	NIÑO	NIÑO	NIÑO	-	NIÑO	NIÑO
1952	*	*	NIÑO	*	*	NIÑO		NIÑO
1951	BOTH	-	BOTH	NIÑO	NIÑO	NIÑO	NIÑO	BOTH
1950	NIÑA	NIÑA	NIÑA	-	-	-	-	NIÑA

Table 2.9. 1871-1949 ENSO event comparison of Coupled ENSO index and five published event lists. An Asterisk (*) denotes end of temporal coverage, and a dash (-), the absence of ENSO conditions. The lists of Ortlieb (2000), Quinn and Neal (1992) and Whetton and Rutherfurd (1994) lists are proxy based. The other three are derived from instrumental records. 'BOTH' denotes phase-flipping.

YEAR	Coupled ENSO Index	Allan et al. (2003)	Kiladis & Diaz (1989)	Quinn& Neal (1992) Ortlieb (2000)	Whetton & Rutherford (1996)	Rasmusson& Carpenter (1983)
1949	NIÑA	NIÑA	NIÑA	-	-	-
1948	-	-	-	-	-	-
1947	-	-	-	-	-	-
1946	-	-	-	-	-	-
1945	NIÑA	-	-	-	-	-
1944	-	-	-	-	-	-
1943	NIÑA	NIÑA		NIÑO	-	-
1942	BOTH	BOTH	NIÑA	-	-	-
1941	NIÑO	NIÑO	-	NIÑO	NIÑO	NIÑO
1940	NIÑO	NIÑO	-	NIÑO	-	-
1939	NIÑO	NIÑA	NIÑO	NIÑO	NIÑO	NIÑO
1938	-	NIÑA	NIÑA	-	-	-
1937	-	-	-	-	-	-
1936	-	-	-	-	-	-
1935	-	-	-	-	-	-
1934	NIÑA	NIÑA	-	-	-	-
1933	NIÑA	NIÑA	-	-	-	-
1932	-	-	NIÑO	NIÑO	-	NIÑO
1931	-	NIÑO	NIÑA		-	
1930	-	NIÑO	-	NIÑO	-	NIÑO
1929	-	-	-	-	-	-
1928	-	-	NIÑA	-	-	-
1927	-	-	-		-	-
1926	NIÑO	NIÑO	-	NIÑO	-	-
1925	BOTH	BOTH	NIÑO	NIÑO	NIÑO	NIÑO
1924	BOTH	NIÑA	NIÑA	-	-	-
1923	NIÑO		NIÑO	NIÑO		NIÑO
1922	-	-	-	-	-	-
1921	-	-	-	-	-	-
1920	NIÑO	-	NIÑA	-	-	-
1919	NIÑO	NIÑO	-	NIÑO		
1918	NIÑO	BOTH	NIÑO	NIÑO	NIÑO	NIÑO
1917	NIÑA	NIÑA	-	NIÑO	-	-
1916	NIÑA	NIÑA	NIÑA	-	-	-
1915	NIÑO	NIÑO	-	NIÑO	NIÑO	NIÑO
1914	NIÑO	NIÑO	-	NIÑO	-	-
1913	NIÑO	NIÑO	NIÑO	-	NIÑO	-
1912	NIÑO	NIÑO		NIÑO	-	-
1911	BOTH	NIÑO	NIÑO	NIÑO	-	NIÑO
1910	NIÑA	NIÑA	-	NIÑO		-
1909	NIÑA	NIÑA	-	-	-	-
1908	-	-	NIÑA	-	-	-
1907	-	-	-	NIÑO	NIÑO	-
1906	NIÑO	NIÑO	NIÑA		NIÑA	-
1905	NIÑO	NIÑO	-	NIÑO	NIÑO	NIÑO
1904	BOTH	-	NIÑO	NIÑO	NIÑO	-
1903	BOTH	NIÑO	NIÑA	-	-	-
1902	NIÑO	NIÑO	NIÑO	NIÑO	NIÑO	NIÑO
1901	-	-	-	-	-	-
1900	NIÑO	NIÑO	-	NIÑO	-	-
1899	NIÑO	NIÑO	NIÑO	NIÑO	NIÑO	NIÑO
1898	NIÑA	-	NIÑA	-	-	-
1897	BOTH	NIÑO		NIÑO		-
1896	NIÑO	NIÑO	NIÑO	-	-	NIÑO
1895	-	-	-	-	-	-
1894	NIÑA	-	-	-	NIÑA	-
1893	NIÑA	NIÑA	-	-	-	-
1892	NIÑA	NIÑA	NIÑA	-	-	-
1891	-	-	NIÑO	NIÑO	NIÑO	NIÑO
1890	NIÑA	NIÑA	-	-	-	-
1889	BOTH	BOTH	NIÑA	NIÑO	-	-
1888	NIÑO	NIÑO	NIÑO	NIÑO	NIÑO	-
1887	NIÑA	NIÑA	-	NIÑO	-	NIÑO
1886	NIÑA	NIÑA	NIÑA	-	-	-
1885	NIÑO	-			-	-
1884	NIÑO	-	NIÑO	NIÑO	-	NIÑO
1883	-	-	-	-	-	-
1882	-	-	-	-	-	-
1881	-	-	-	-	-	-
1880	NIÑA	NIÑA	NIÑO	NIÑO	-	NIÑO
1879	NIÑA	NIÑA		-	NIÑA	-
1878	NIÑO	NIÑO	-	NIÑO	-	-
1877	NIÑO	NIÑO	NIÑO	NIÑO	NIÑO	NIÑO
1876	BOTH	*	*	-	-	*
1875	NIÑA	*	*	-	-	*
1874	NIÑA	*	*	NIÑO	NIÑA	*
1873	NIÑA	*	*	-	-	*
1872	NIÑA	*	*	-	-	*
1871	NIÑA	*	*	-	-	*

Notably, the historical El Niño event list of Quinn and Neal (1992) and Ortlieb (2000) appears to 'mislabel' the years 1874, 1910, 1917 and 1943 as El Niños, while the available instrumental records have indicated La Niñas. Only 34 of the 45 CEI El Niño years for their period of overlap (1976-1871) are found in these South American historical chronologies, representing a 70% agreement to the instrumentally based CEI. Furthermore, there are an additional four El Niños (1932, 1930, 1907, and 1891) identified by Quinn and Neal (1992) and Ortlieb (2000) that are not found using the CEI. This highlights the issue of referring to ENSO events as simply 'El Niños', and the important implications for palaeo-ENSO reconstructions of the uncritical use of historical records such as the frequently cited 'Quinn' records for proxy calibration or verification purposes.

Defining an ENSO event based just on SSTs or the SOI also has the potential to introduce similar classification ambiguities. For example, Trenberth's (1997) Niño 3.4 index indicates oceanic La Niña conditions during 1984-85 and 1997, and El Niño conditions during 1952 and 1978-79. These 'events' are absent in the CEI, representing the absence of a simultaneous atmospheric response in the SOI, again emphasising the value of a coupled ENSO classification system for palaeoclimate reconstruction.

2.4.7 CEI extreme event analysis

Having verified the accuracy of the CEI, it was then possible to examine changes in the frequency and strength of extreme ENSO events for the instrumental era. So far this study has focused on ENSO phase classification and duration, which does not quantify the magnitude of an event. The need to identify event magnitude from the instrumental record is considered important so that information on event amplitude is preserved in the analysis and interpretation of subsequent proxy reconstructions. Accurately accounting for the strength of past ENSO episodes from proxy archives is imperative to providing a long-term context for extreme ENSO events noted for the late 20th century.

To quantify the magnitude of ENSO events indicated by the CEI, monthly Niño 3.4 SST anomalies were multiplied by −1 to allow warm SST values to directionally correspond to low SOI values (indicative of El Niño conditions). These monthly SSTs were then added to the corresponding monthly SOI value to produce a numeric value for the CEI. This ranged from a minimum of -4.77 in November 1878 to a maximum

of 3.79 recorded in December 1988. Magnitude characteristics for all CEI-identified ENSO events are detailed in Table 2.5.

To examine the suitability of combining the SOI and SST records, the respective variances of the records were analysed. Negative CEI values produced a standard deviation of 0.51 from the SOI compared to 0.66 from SSTs, while positive CEI values corresponded to a standard deviation value of 0.48 for the SOI and 0.65 for SSTs. This is further reflected in the slightly higher correlation between the CEI and the SST (r = 0.955) than with the SOI (r = 0.922). This indicates that there is likely to be a greater weighting of SSTs than the SOI in the combined index.

To investigate extreme events, the upper 1/3 of the 28 El Niños and 26 La Niñas identified from the CEI were examined (Table 2.5). This definition corresponded to a CEI value of ±3. Examination of Table 2.5 and Figure 2.5 indicates that El Niño events tend to attain greater magnitudes than La Niña episodes. This is exemplified by the 1876-78, 1982-83, and 1997-1998 El Niños which exceeded a CEI value of -4 representing the upper 1% of all ENSO cases. To address the uncertainty introduced by the use of the reconstructed Niño 3.4 dataset pre-1950 period, the SOI response was independently examined in terms of standard deviation departures relative to the 1933-1992 base period (see Sections 2.2.1 and Figure 2.2). To qualify as an extreme event during the 1871-1949 interval, the SOI was independently required to display a minimum of ±1.5 standard deviation anomalies consecutively for a minimum of 50% of the overall duration of each event defined in Table 2.5.

Examining Table 2.5, extreme El Niño events all exceeded a minimum duration of 11 months (1896-97), lasting up to 29 months (1939-42). In contrast, the most extreme La Niñas, experienced in 1988-89, followed by 1973-74, and 1975-76, were on average nine months long, and did not exceed a CEI value of 3.79 (1988-89). The maximum duration of an extreme La Niña event was 18 months during 1871-73, achieving a maximum CEI value of 3.22.

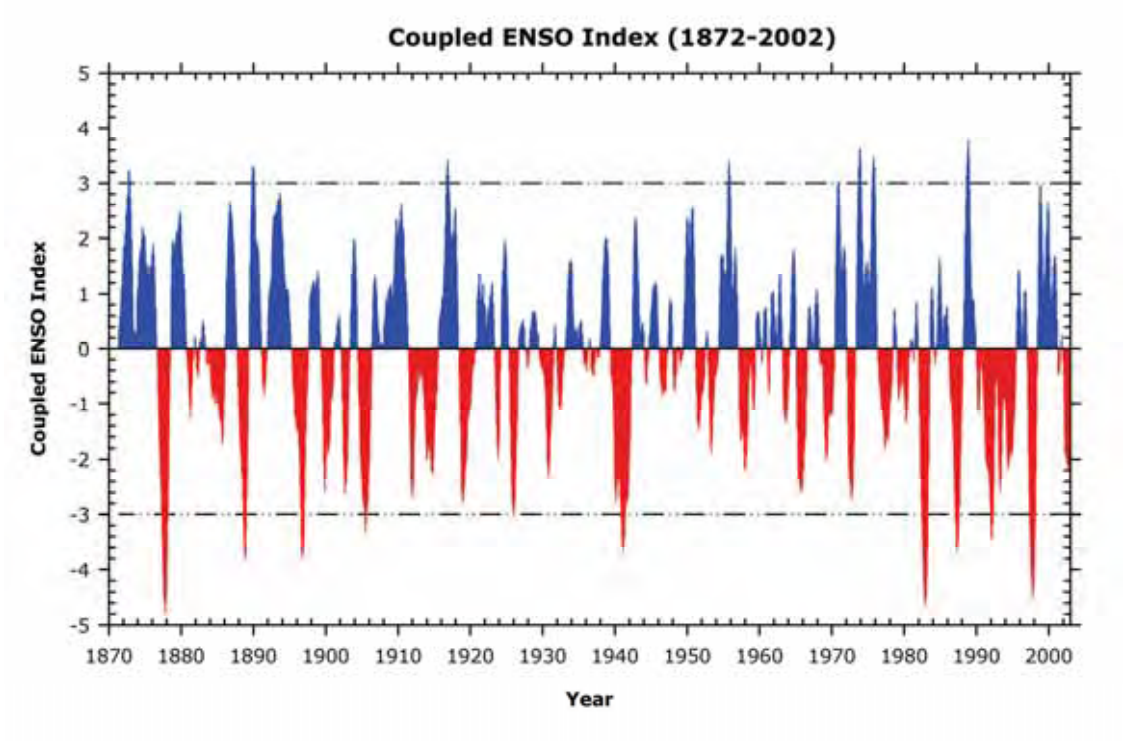

Figure 2.5. CEI event magnitude for 1872-2003 (start and end years omitted due to incomplete seasonal coverage). Extreme ENSO events are defined as a CEI index of ±3, indicated by dashed lines.

Of the 16 extreme ENSO episodes indicated in Table 2.5, nine occur post-1949. In fact, eight of these extreme events (four El Niños and four La Niñas) are observed since 1970. Remembering that the CEI is comprised of observed, rather than reconstructed Niño 3.4 SST anomalies and the SOI for this post-1949 period, there is a lack of the amplitude enhancing effects of the reconstructed SST data noted in Section 2.3.1. The most comparable period of heightened ENSO activity is seen between 1871 and 1917 when four extreme El Niños (1876-1878, 1888-1889, 1896-97, 1904-06) and two La Niñas (1871-73 and 1916-17) are observed.

The most extreme El Niño of the entire time series is a 17-month event spanning 1876-78, including seven months when the SOI exceeded two standard deviations (not shown). An event of a similar magnitude does not reoccur in the record until the two extreme El Niños of 1982-83 and 1997-98 (exceeding two standard deviations in the SOI for nine and six months, respectively). During the 1982-83 El Niño, the SOI independently exceeded three standard deviations for three months from October to December 1982, representing the highest observed SOI anomaly for the instrumental period (3.35 standard deviations in November 1982). Overall, there is a shift in the

frequency of (both phase) extreme ENSO events from 1 in 11.3 years prior to 1950, to 1 in 6.0 years in the post-1949 period.

The examination of protracted events (≥ 24months) from the CEI revealed three La Niñas (1908-1911, 1892-94, 1874-76) and one El Niño (1939-42) episode. With the exception of the 1939-42 El Niño, these events are not extreme in terms of magnitude, they are however, considered extreme in terms of their duration (Table 2.5). For example, the longest La Niña (El Niño) event is a 30(29)-month episode spanning 1908-11(1939-42) with an average magnitude of 1.71(-2.6), and a peak CEI value of 2.62 (-3.67). This suggests that persistent El Niño events identified from the CEI attain higher magnitudes than their La Niña counterparts.

2.5 Discussion

In an attempt to better describe the nature and evolution of ENSO events a classification scheme that captured the synchronous dynamics of the coupled ocean-atmosphere system was devised. The dangers of using a sole index were highlighted through the analyses presented in Sections 2.3 and 2.4. For example, the SOI has a tendency of extending event duration (relative to SSTs) and the Niño 3.4 SST reconstruction has a propensity to over-estimate the magnitude of El Niño events.

This study addressed the complexities associated with generating a combined ENSO index for the instrumental era. To do so it was necessary to investigate the threshold-dependent event capture characteristics of the atmosphere (SOI) and oceanic (Niño 3.4 SSTs) components for both ENSO phases. Comparing features such as event capture and duration allowed the identification of a SOI threshold of ±0.2 which gave the most suitable agreement with NOAA's recently proposed ONI definition of ±0.5 from the Niño 3.4 SST region.

Lack of direct pre-1950 instrumental SST measurements required reliance on a SST reconstruction from the Niño 3.4 SST zone. Section 2.3.1 raised the issues of missing some low magnitude La Niñas and overestimating the magnitude of El Niño events. This may influence, for example, the slightly longer event duration of pre-1950 SSTs (noted in Table 2.6) compared to the instrumental SST record. This bias may also be reflected in the slightly unequal weighting of the SST data when generating the

combined ENSO index (see Section 2.4.7). Nevertheless, with the above-mentioned provisos in mind, the striking similarity of instrumental and reconstructed SSTs suggests that the latter is a reliable record of oceanic ENSO conditions.

Imposing the fairly strict criteria of SOI and SST synchronous agreement for ENSO classification resulted in the exclusion of potentially important lead/lag relationships that are likely to provide additional information on ENSO event evolution. Recognition of this issue resulted in the generation of the seasonal classification scheme which preserved ENSO classifications for the individual SOI and SST components of the CEI (presented in Section 2.4.5). This provided the CEI with the flexibility to reintroduce this level of sophistication, as warranted, without detracting from the primary objective of identifying distinct ENSO event classification.

The CEI also maintains information relating to various seasonal windows in an attempt to encourage the palaeo-ENSO community to reinvestigate proxies for important evolutive detail. To date, ENSO reconstructions such as the tree-ring SOI reconstruction of Stahle *et al.* (1998) have focused on only one seasonal window, typically the boreal winter/austral summer months of DJF. This is when ENSO conditions are generally at their peak maturity (Rasmusson and Carpenter, 1982), and is therefore likely to be the season most clearly recorded in the proxy response.

Recent work by Horii and Hanawa (2004), however, reported that the evolution of ENSO events from the Niño 3.4 region differs considerably depending on the timing of onset. For example, they found that El Niños that begin in April-June tend to develop into high magnitude events that peak during the boreal winter/austral summer, while events developing from July-October are relatively weaker in magnitude and have more irregular decay dynamics. Reporting seasonal ENSO conditions from the CEI (see Section 2.4.5) may assist the recovery of important evolutive information from proxy reconstructions based on calibrating to one season. As Allan *et al.* (2003) recently emphasised, resolving more of the ENSO life cycle is critical if greater modeling precision is be achieved.

From the perspective of a palaeoclimatologist, the CEI has the flexibility to allow the investigation of ENSO on monthly, seasonal and yearly timescales. This is of practical relevance as the community is often dealing with proxy records of varying resolution such as the monthly scale of many coral sequences or the annual dating of tree-ring

chronologies. However, it is recognised that transferring from monthly to seasonal resolution involves issues associated with the arbitrary construct of selecting the middle month of the commonly defined seasonal windows. To avoid further smoothing of the data, ENSO classification for the middle month was presented as a partial representation of the entire seasonal conditions, as necessitated by the methodology adopted here.

This study importantly raised the issues associated with calibrating proxies to the coarser resolution, non-instrumentally based historical chronologies such as the widespread use of Quinn and Neal (1992). The potential danger of uncritical use of these major references for the long-term analysis of ENSO (examined in Section 2.4.6), was highlighted from the somewhat low 70% agreement of the South American El Niño record with the list of CEI events. Failing to incorporate advances in the description of the ENSO system into the analytical treatment of records may detrimentally impact efforts to accurately decipher the wealth of information contained within proxy archives.

As evident through even a basic extreme event analysis for the instrumental period, the magnitude of ENSO events has varied considerably through time. An apparent switch from a predominance of La Niña conditions in the pre-1950 period, to heightened El Niño activity post-1949 was noted in Section 2.4.4. Notably, the discernable increase in the frequency and magnitude of ENSO events since the mid-1970s identified in the literature (Wang, 1995;Fedorov and Philander, 2000; Folland *et al.*, 2001; Wang and Soon-II, 2001; Philander and Fedorov, 2003) was also confirmed from the CEI (Section 2.4.7). The frequency and intensity of post-1970 ENSO events appear anomalous in the context of at least the past century, with 50% of all extreme events noted from the CEI occurring in this period. This finding underscores the need to further investigate the long-term context and nature of recently anomalous ENSO sequences from appropriately calibrated proxy archives.

This study highlighted the significant implications of appropriate threshold selection on ENSO event sensitivity for subsequent palaeoclimate applications. There is a vital need to ensure that ENSO reconstructions attempt to maintain event magnitude resolution through the appropriate use of instrumental records if an assessment of late 20th century ENSO variability from a multi-centennial context is to be accurately achieved. This reinforces the need for 'amplitude preservation' in proxy calibration to refine the details

essential for subsequent applications such as the validation of palaeoclimate model variability (Hegerl *et al.*, 2004).

The need for palaeoclimatic disciplines to work collaboratively to establish standard protocols, such as the consistent statistical treatment of proxy records suggested by Lough (2004) to facilitate ready intercomparison of proxy records, is advocated by this study. The CEI classification scheme presented could serve as an instrumental benchmark to facilitate the calibration of proxy records for analysing ENSO in the pre-observational era (Gergis *et al.*, 2004).

Currently, some climate models have great difficulty in realistically simulating ENSO as they often fail to adequately integrate both oceanic and atmospheric aspects of the phenomenon (Latif *et al.*, 2001; Cane, 2004). Often the primary variables analysed for ENSO are SSTs, which are often biased towards the eastern Pacific, despite the obvious predictive success recently attained by Chen *et al.* (2004) using SSTs from the Niño 3.4 region. Indeed, the development of a coupled ENSO index based on this region appears well justified, and indeed timely, for incorporation into the palaeo-ENSO community.

2.6 Summary

In an attempt to describe more of the nature and evolution of ENSO events, the Coupled ENSO Index (CEI) was devised to identify synchronous oceanic (Niño 3.4 SST) and atmospheric (Southern Oscillation Index) anomalies associated with ENSO for the instrumental period (1871-2003). The CEI is of practical relevance to the ENSO community as it provides an amplitude preserving instrumental baseline for the calibration of proxy records to simultaneously reconstruct both components of the ENSO system.

Analysis of the nature of instrumental ENSO events from the CEI suggests that the frequency and intensity of post-1970 ENSO events (when 50% of all extreme events identified occur) appears the most anomalous in the context of at least the past century. It is hoped that the CEI will facilitate palaeo-ENSO research to systematically resolve the long-term context of past ENSO behaviour. In doing so it may be possible to reliably assess whether the apparently anomalous nature of late 20th century variability is unprecedented within existing palaeoarchives.

2.7 References

Allan, R., Chambers, D., Drosdowsky, W., Hendon, H., Latif, M., Nicholls, N., Smith, I., Stone, R. and Tourre, Y. (2001). Is there an Indian Ocean dipole, and is it independent of the El Niño - Southern Oscillation? *CLIVAR Exchanges* **21**: 1-4.

Allan, R. and D'Arrigo, R. (1999). 'Persistent' ENSO sequences: how unusual was the 1990-1995 El Niño ? *The Holocene* **9** (1): 101-118.

Allan, R., Lindsay, J. and Parker, D. (1996). *El Niño Southern Oscillation and climate variability.* Melbourne, Australia, CSIRO.

Allan, R., Reason, C., Lindesay, J. and Ansell, T. (2003). Protracted ENSO episodes and their impacts in the Indian Ocean region. *Deep Sea Research Part II* **50** (12-13): 2331–2347.

Cane, M. (2004). The evolution of El Niño, past and future. *Earth and Planetary Science Letters* **164**: 1-14.

Chen, D., Cane, M., Kaplan, A., Zebiak, S. and Huang, D. (2004). Predictability of El Niño over the past 148 years. *Nature* **428**: 733-735.

D'Arrigo, R., Cook, E., Wilson, R., Allan, R. and Mann, M. (2005). On the variability of ENSO over the past six centuries. *Geophysical Research Letters* **32** (L03711): 1-4.

Deser, C. and Wallace, J. (1987). El Niño Events and Their Relation to the Southern Oscillation: 1925-1986. *Journal of Geophysical Research* **92** (C13): 14,189-14,196.

Elsey, L. (2004). ENSO Defined. *Weatherwise* **January/February 2004**: 11-12.

Evans, M., Kaplan, A. and Cane, M. (2002). Pacific sea surface temperature field reconstruction from coral $\delta^{18}O$ data using reduced space objective analysis. *Palaeoceanography* **17** (1): 7/1-7/13.

Fairbanks, R., Evans, M., Rubenstone, J., Mortlock, R., Broad, K., Moore, M. and Charles, C. (1997). Evaluation of climate indices and their geochemical proxies measured in corals. *Coral Reefs* **16** (Supplement): S93-S100.

Fedorov, A. and Philander, G. (2000). Is El Niño changing? *Science* **288**: 1997-2002.

Folland, C., Karl, T., Christy, J., Clarke, R., Gruza, G., Jouzel, J., Mann, M., Oerlemans, J., Salinger, M. and Wang, S. (2001). Observed Climate Variability and Change. *Climate Change 2001: The Scientific Basis. Contribution of Working Group 1 to the Third Assessment Report of the Intergovernmental Panel on Climate Change.* J. Houghton, Y. Ding, D. Griggs *et al.* United Kingdom and New York, Cambridge University Press.

Gergis, J. and Fowler, A. (2005). Classification of synchronous oceanic and atmospheric El Niño-Southern Oscillation (ENSO) events for palaeoclimate reconstruction. *International Journal of Climatology* **25**: 1541–1565.

Gergis, J., Fowler, A. and Mooney, S. (2004). A Multiproxy Analysis of El Niño Southern Oscillation (ENSO) Variability. *1st International CLIVAR Science Conference: Understanding and Predicting Our Climate System*, June 21-25, 2004, Baltimore, Maryland, USA.

Glantz, M. (2005). Usable Science 9: El Niño Early Warning for Sustainable Development in the Pacific Rim and Islands. Report of workshop held 13–16 September 2004 in the Galapagos Islands, Ecuador. Bolder, Colarado.

Hanley, D., Bourassa, M., O'Brian, J., Smith, S. and Spade, E. (2003). A Quantitative Evaluation of ENSO Indices. *Journal of Climate* **16**: 1249-1258.

Hegerl, G., Karl, T., Allan, M., Bindoff, N., Karoly, D., Gillet, N. and Zwiers, F. (2004). Climate change detection and attribution: Beyond mean temperature signals. *1st International CLIVAR Science Conference: Understanding and Predicting Our Climate System*, June 21-25, 2004, Baltimore, Maryland, USA.

Horii, T. and Hanawa, K. (2004). A relationship between the timing of El Niño onset and subsequent evolution. *Geophysical Research Letters* **31** (L06304): 1-4.

Jones, P. and Mann, M. (2004). Climate over past millennia. *Review of Geophysics* **42**: 1-42.

Kane, R. (1999). El Niño timings and rainfall extremes in India, South-east Asia and China. *International Journal of Climatology* **19**: 653-672.

Kiladis, G. and Diaz, H. (1989). Global climatic anomalies associated with extremes in the Southern Oscillation. *Journal of Climate* **2**: 1069-1090.

Latif, M., Sperber, L., Arblaster, J., Braconnot, P., Chen, D., Colman, A., Cubasch, U., Cooper, C., Delecluse, P., De Witt, D., Fairhead, L., Flato, G., Hogan, T., Ji, M., Kimoto, M., Kitoh, A., Knutson, T., Le Treut, H., Li, T., Manabe, S., Marti, O., Mechoso, C., Meehl, G., Power, S., Roeckner, E., Sirven, J., Terray, L., Vintzileos, A., Voss, R., Wang, B., Washington, W., Yoshikawa, I., Yu, J. and Zebiak, S. (2001). ENSIP: the El Niño simulation intercomparison project. *Climate Dynamics* **18**: 255-276.

Lough, J. (2004). A strategy to improve the contribution of coral data to high-resolution palaeoclimatology. *Palaeogeography, Palaeoclimatology, Palaeoecology* **204**: 115-143.

Lyon, B. and Barnston, A. (2005). The evolution of the weak El Niño of 2004-2005. *US CLIVAR Variations* **3** (2): 1-4.

Mann, M., Bradley, R. and Hughes, M. (1998). Global-scale temperature patterns and climate forcing over the past six centuries. *Nature* **392**: 779-787.

Mann, M., Bradley, R. and Hughes, M. (2000). Long-term variability in the El Niño/Southern Oscillation and associated teleconnections. *El Niño and the Southern Oscillation; Multiscale Variability and Global and Regional Impacts.* H. Diaz, and Markgraf, V. Cambridge, Cambridge University Press**:** 327-372.

Mc Phaden, M. (2004). Evolution of the 2002/03 El Niño. *Bulletin of the American Meteorological Society* **85** (5): 677-695.

Mullan, A. (1995). On the linearity and stability of Southern Oscillation-climate relationships for New Zealand. *International Journal of Climatology* **15**: 1365-1386.

Ortlieb, L. (2000). The documentary historical record of El Niño events in Peru: An update of the Quinn record (sixteenth through nineteenth centuries). *El Niño and the Southern Oscillation: Variability, Global and Regional Impacts.* H. Diaz and V. Markgraf. Cambridge, Cambridge University Press**:** 207-295.

Philander, G. and Fedorov, A. (2003). Is El Niño Sporadic or Cyclic ? *Annual Reviews of Earth and Planetary Sciences* **31**: 579-594.

Quinn, W. and Neal, V. (1992). The historical record of El Niño events. *Climate Since A.D. 1500*. R. Bradley and P. Jones. London, Routledge.**:** 623–648.

Quinn, W., Neal, V. and Antunez de Mayola, S. (1987). El Niño occurrences over the past four and a half centuries. *Journal of Geophysical Research* **92** (C13): 14449–14461.

Rasmusson, E. and Carpenter, T. (1982). Variations in tropical sea surface temperature and surface wind fields associated with the Southern Oscillation/El Niño. *Monthly Weather Review* **110**: 354-384.

Rasmusson, E. and Carpenter, T. (1983). The relationship between eastern equatorial Pacific sea surface temperatures and rainfall over India and Sri Lanka. *Monthly Weather Review* **111**: 517-528.

Reason, C., Allan, R., Lindsay, J. and Ansell, T. (2000). ENSO and Climatic Signals Across the Indian Ocean Basin in the Global Context: Part I, Interannual Composite Patterns. *International Journal of Climatology* **20**: 1285–1327.

Stahle, D., D'Arrigo, R., Krusic, P., Cleaveland, M., Cook, E., Allan, R., Cole, J., Dunbar, R., Therrell, M., Gay, D., Moore, M., Stokes, M., Burns, B., Villanueva-Diaz, J. and

Thompson, L. (1998). Experimental dendroclimatic reconstruction of the Southern Oscillation. *Bulletin of the American Meteorological Society* **79** (10): 2137-2152.

Timmermann, A. (1999). Detecting the nonstationary response of ENSO to greenhouse warming. *Journal of Atmospheric Sciences* **56**: 2313-2325.

Trenberth, K. (1997). The Definition of El Niño. *Bulletin of the American Meteorological Society* **78** (12): 2771-2777.

Trenberth, K. and Caron, J. (2000). The Southern Oscillation revisited: sea level pressures, surface temperatures, and precipitation. *Journal of Climate* **13**: 4358-4365.

Trenberth, K. and Hoar, T. (1996). The 1990-1995 El Niño Southern Oscillation event: Longest on Record. *Geophysical Research Letters* **23** (1): 57-60.

Trenberth, K. and Hoar, T. (1997). El Niño and climate change. *Geophysical Research Letters* **24** (23): 3057-3060.

Trenberth, K. and Stepaniak, D. (2001). Indices of El Niño evolution. *Journal of Climate* **14**: 1697-1701.

Troup, A. (1965). The Southern Oscillation. *Quarterly Journal of the Royal Meteorology Society.* **91**: 490-506.

Vecchi, G. and Harrison, D. (2003). On the termination of the 2002-03 El Niño event. *Geophysical Research Letters* **30** (18): 7/1-7/4.

Wang, B. (1995). Interdecadal changes in El Niño onset in the last four decades. *Journal of Climate* **8** (2): 267-285.

Wang, B. and Soon-II, A. (2001). Why the Properties of El Niño Changed During the Late 1970s. *Geophysical Research Letters* **28** (19): 3709-3712.

Whetton, P. and Rutherfurd, I. (1994). Historical ENSO teleconnections in the Eastern Hemisphere. *Climatic Change* **28**: 221-253.

Wolter, K. and Timlin, M. (1993). Monitoring ENSO in COADS with a seasonally adjusted principal component index. *Proceedings of the 17th Climate Diagnostics Workshop, Norman Oklahoma, 52-57*, NOAA/NMC/CAC.

CHAPTER 3.
HIGH-RESOLUTION PROXY DATA

3.1 Introduction

3.1.1 Background

Studies of high-resolution palaeoarchives provide considerable potential for documenting various aspects of the ENSO phenomena. When considered together, ENSO sensitive proxy records can reveal how individual events vary spatially across the equatorial Pacific and over areas of ENSO teleconnection influence (Baumgartner *et al.*, 1989; Allan and D'Arrigo, 1999; Mann *et al.*, 2000).

Further, to determine whether the characteristics of ENSO during the late 20th century were unusual, it is essential to place them in the context of longer-term climate variability. Due to the sparseness of instrumental data prior to the mid 19th century, estimates of global climate variability during past centuries rely on indirect proxy indicators derived from sensitive natural archives and the sparse network of historical documentary records. These proxies of past climate must be calibrated against instrumental data for meaningful climate interpretation (Jones and Mann, 2004).

Estimates of seasonal, annual or decadal climate variations must be derived from sources that are capable of resolving annual or seasonal climatic variations. Continuously recording, high-resolution systems all generate distinct layering as a response to climatic variation from one season to the next (Baumgartner *et al.*, 1989). High-resolution records generally result from the growth of living organisms that produce structures such as tree-rings and coral banding, or from complex depositional processes producing for example, dust layers within glacial ice, or the lamina couplets in varved sediments (Fisher, 2002). Proxy variables include width and density measurements from tree-rings, layer thickness from laminated sediments, and accumulation and/or oxygen isotope geochemistry indicators from annually resolved ice and coral records.

These kinds of proxy climate data provide records of climate variations several centuries into the past, with the potential to resolve large-scale patterns of climate change prior to the instrumental period, albeit with important limitations and uncertainties (Jones and Mann, 2004). In recent years, the latest studies based on 'multiproxy' data have proved particularly useful for describing global or hemispheric patterns of climate variability in past centuries (Mann *et al.*, 1998; 2000; Esper *et al.*, 2002; Fisher, 2002; Gedalof and Mantua, 2002; Bradley *et al.*, 2003; Linsley *et al.*, 2004; Moberg *et al.*, 2005; Oerlemans, 2005). Such estimates allow the observed trends of the 20th century to be put into a longer-term perspective, allowing improved comparisons with possible forcing functions.

In this thesis, two approaches to multiproxy ENSO reconstruction are found in Chapters 5 and 6. The intention of this chapter is to provide an overview of high-resolution proxies including the identification of the limitations associated with each data source and details of each of the individual tree-ring, coral, ice and documentary records used in this study. Finally, the issue of data filtering is reviewed in the context of preparing records for high-frequency ENSO analysis.

3.1.2 Proxy data quality issues

There are a number of issues that arise from the use of multiple proxy sources (Mann *et al.*, 1998; Fisher, 2002). Potential limitations specific to each type of proxy data series must be carefully taken into account while structuring a multiproxy network for climatic assessment (Mann *et al.*, 1998). Dating errors in a given record, such as incorrectly assigned annual layers or rings, are particularly detrimental if common information is sought to describe climate patterns on a year-by-year basis, as is the case for ENSO which is characterised by discrete events operating on inter-annual timescales (Mann *et al.*, 1998; Markgraf and Diaz, 2000).

Standardisation of certain biological proxy records relative to estimated growth trends, and the limits of constituent chronology segment lengths can restrict the maximum timescale of climate variability that is recorded (Esper *et al.*, 2002). For example, millennia-long tree-ring chronologies are constructed by averages of many tree-ring sequences from living and sub-fossil trees. The segment lengths of these series are typically several centuries long with the overlapping individual series exactly aligned by calendar year and connected in time using cross-dating (see Section 4.2.2). When the

segment lengths are substantially shorter than the length of the overall chronology being developed, it is difficult to preserve multi-centennial variation in tree-ring series (Cook *et al.*, 1995; Esper *et al.*, 2002). This results from the need to remove age-related biological growth trends that represent noise for the purpose of climate reconstruction (Esper *et al.*, 2002).

Dendrochronologists usually eliminate growth trends by detrending each tree-ring width series with a fitted mathematical growth function (Cook and Peters, 1981; Holmes *et al.*, 1986; Esper *et al.*, 2002). As a result, the maximum wavelength of recoverable climatic information is fundamentally limited by the segment lengths of the individual detrended series (Cook *et al.*, 1995; Esper *et al.*, 2002). Thus, a 100-year-long tree ring sequence will not contain any climatic variance at periods longer then 100 years if it is explicitly detrended by a fitted growth curve (Esper *et al.*, 2002). Consequently, it is possible to miss long-term trends in millennia-length tree-ring chronologies due to using detrended series that are short relative to the multi-centennial fluctuations due to climate (Cook *et al.*, 1995; Esper *et al.*, 2002).

Fisher (2002) identified further problems associated with heterogeneous data compilations. It is often necessary to include records with imperfect transfer functions, the statistical relationship between proxy climate records and direct meteorological variables, which may limit the accuracy of any climatic information gained. Differing seasonal sensitivities, resolutions/spectral sensitivities, high local noise levels and inconsistent resolution of some records are also accredited as posing potential obstacles to palaeo-climatic reconstructions (Fisher, 2002). The reconstruction of tropical ENSO variability and the associated extra tropical climate impact is further complicated by the fact that climate proxies are not consistently accurate in recording their local climate or oceanographic environment in both time and space (Stahle *et al.*, 1998). Furthermore, the sometimes narrow seasonal response of even the most climate sensitive proxies may not perfectly coincide with the seasonality of the local ENSO teleconnection (Stahle *et al.*, 1998).

Despite such considerations, Mann *et al.* (1998) noted that with appropriate data treatment, the common signal recorded by a diverse and widely distributed set of independent climate indicators more accurately captures any consistent climate signal present than single proxy analysis. Importantly, this reduces the compromising effects of the biases and weaknesses inherent to individual proxy records (Mann *et al.*, 1998).

3.2 Dendroclimatology

Dendroclimatology is a powerful technique for the reconstruction of climate in temperate and highly seasonal locations (Fritts, 1976; Schweingruber, 1988; Cook and Kairiukstis, 1990; Fritts, 1991). Some tree species form annual growth ring couplets of early and late wood (Figure 3.1) in response to seasonal stimuli (Fritts, 1976; Schweingruber, 1988; Cook and Kairiukstis, 1990). At sites where climatic parameters are limiting to tree growth, the width, density, and other aspects of these annual bands have been correlated to climate variability with considerable success.

A well-developed set of chronological and statistical procedures is employed subsequently to confirm the presence of a climate signal in a dendroclimatic study (Fritts, 1976; Schweingruber, 1988; Cook and Kairiukstis, 1990; Fritts, 1991). Firstly, sequences from many trees are compared (Figure 3.2), using standard cross-dating techniques, to identify and eliminate age errors associated with extra or missing rings. This process ensures absolute annual dating of the final chronology, composed of many individual sequences, and enhances the climatic signal over potential biological noise. Subsequently, conservative standardisation procedures are applied to remove biological influences such as growth trends with age and persistence (Cook and Peters, 1981; Cook and Kairiukstis, 1990).

3.2.1 ENSO sensitive tree-ring records

The length of tree-ring records are excellent sources for evaluating the long-term stability of ENSO teleconnected climate patterns. Existing dendroclimatic reconstructions, overwhelmingly derived from temperate climates, are beginning to be compiled and incorporated into reconstructions that enable evaluation of broad patterns of change in regional temperature and moisture availability (Stahle *et al.*, 1998; Overpeck and Trenberth, 2003; Cook *et al.*, 2004; Woodhouse *et al.*, 2005). These large-scale palaeoclimate reconstructions can then be used to evaluate the changing influence of tropical systems like ENSO on extra tropical regions by developing gridded fields of reconstructed climate data for validating model output (Cook *et al.*, 2004).

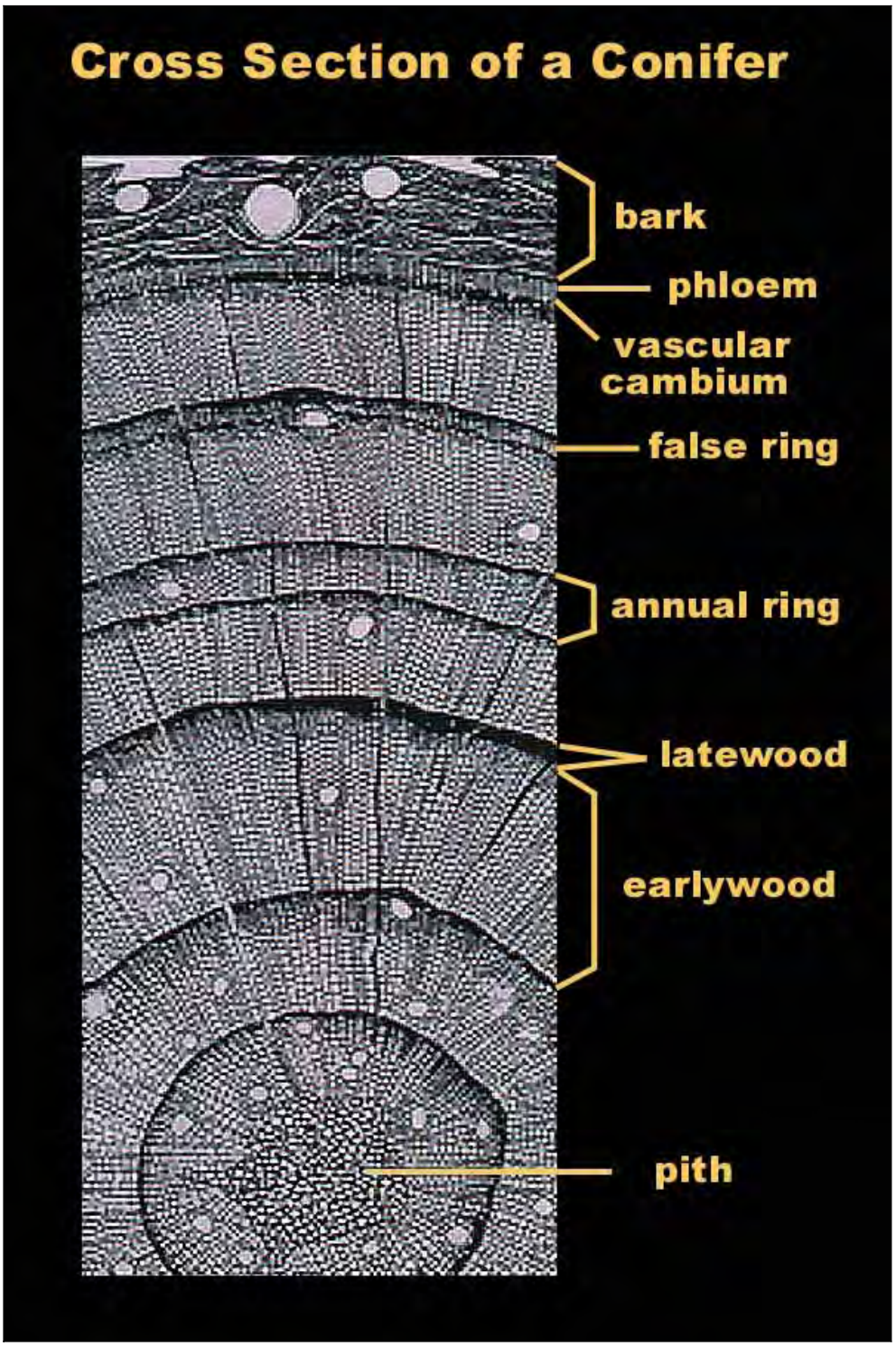

Figure 3.1. Cross section of a conifer indicating the structural anatomy associated with annual tree-ring growth (Adapted from Fritts, 1976). **Source:** Fritts (1976) modified by Connie Woodhouse and Bruce Bauer, National Oceanic and Atmospheric Administration (NOAA) Palaeoclimatology Program (http://www.ncdc.noaa.gov/palaeo/slides).

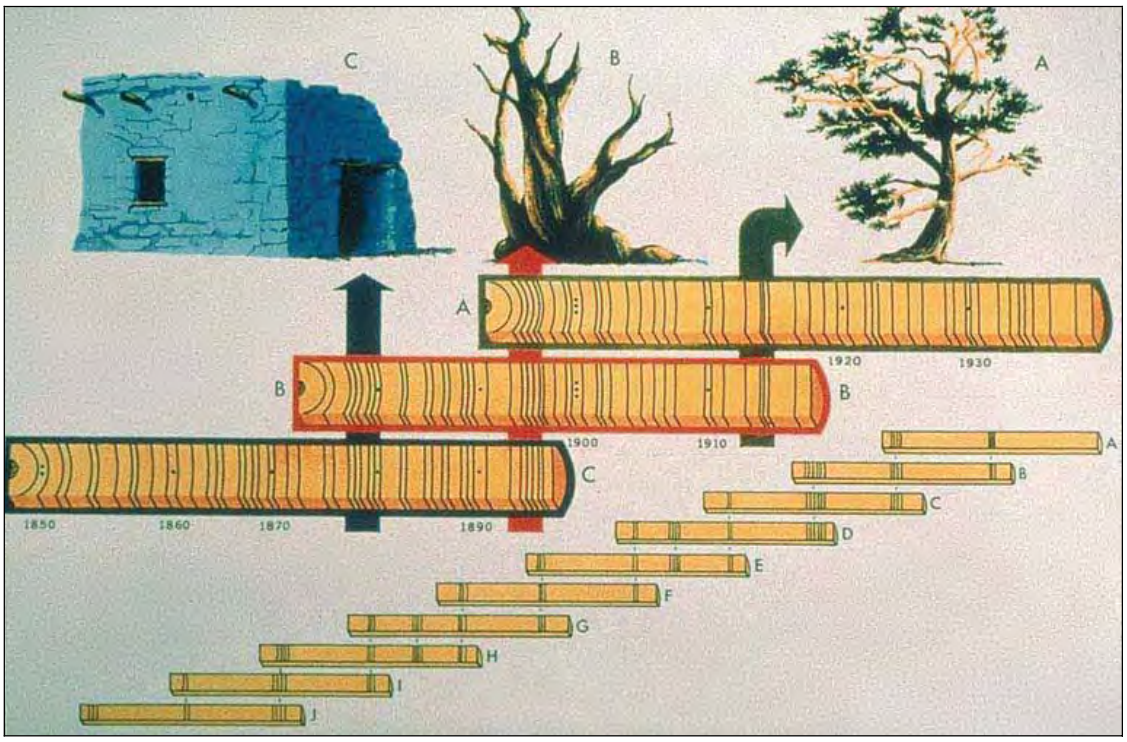

Figure 3.2. The process of cross-dating based on (a) living trees, (b) relict materials derived from standing dead, stump and (c) building timbers. **Source:** Connie Woodhouse and Bruce Bauer, National Oceanic and Atmospheric Administration (NOAA) Palaeoclimatology Program (http://www.ncdc.noaa.gov/palaeo/slides).

The extreme scarcity of long, exactly dated tree-ring chronologies from tropical forests is the fundamental problem preventing the development of long ENSO records from the equatorial core zone (Dunbar and Cole, 1999; Cook *et al.*, 2000a; Evans and Schrag, 2004; Poussart *et al.*, 2004). The vast majority of tropical forest species do not produce anatomically distinct annual growth rings, and therefore cannot be used for palaeoclimate reconstruction given present understanding and technology. However, a small subset of tree species native to the tropics has been conclusively shown to form reliable annual growth rings, and a few species within this subset are also long-lived and sensitive to tropical climate variability (D'Arrigo *et al.*, 1994; Dunbar and Cole, 1999; Evans and Schrag, 2004; Poussart *et al.*, 2004).

A number of dendroclimatic reconstructions of the SOI have been attempted based on tree-ring records from ENSO-sensitive teleconnection regions such as south-western North America (Cleaveland *et al.*, 1992; Meko, 1992; Michaelsen and Thompson, 1992; Cleaveland *et al.*, 2003), combined Mexican/south-western U.S. latewood density (Stahle and Cleaveland, 1993) and combinations of tropical Pacific and North

American chronologies (Stahle *et al.*, 1998;Cook *et al.*, 2000a). Using an updated version of the tree-ring dataset used by Stahle *et al.*, (1998), D'Arrigo *et al.*, (2005) recently developed a reconstruction for the Niño 3 SST region, discussed further in Chapter 6.

Mann *et al.* (2000) caution, however, that reliance on purely extra-tropical dendroclimatic records may assume a stationarity (stability) in the extra-tropical response to tropical ENSO events that may not be warranted. Hence, an obvious priority of tree-ring research is to target chronology development within ENSO sensitive locations in both tropical and extra tropical regions where strong and consistent climate teleconnections to ENSO have been demonstrated through rigorous calibration with modern instrumental data (Dunbar and Cole, 1999; Fowler *et al.*, 2004; Fowler, 2005).

3.2.2 West Pacific ENSO proxy New Zealand Kauri (*Agathis australis*)

The potential of tree-rings for resolving annual climatic phenomenon such as ENSO has been repeatedly demonstrated (Lough and Fritts, 1985; D'Arrigo and Jacoby, 1991; Cleaveland *et al.*, 1992; Stahle *et al.*, 1998). However, most tree-ring data with potential for ENSO reconstruction come from eastern Pacific teleconnection regions, rather than from the areas influenced by the western Pacific warm pool region. Long tree-ring records from the western Pacific and Southern Hemisphere in general, have long been sought after by the palaeoclimate community to allow recent ENSO variability to be placed into a Pacific Basin-wide context (Stahle *et al.*, 1998; Dunbar and Cole, 1999; Briffa, 2000; Jones and Mann, 2004).

This study directly contributes to the development of a high-resolution tree-ring record from the 'data sparse' Southern Hemisphere location of New Zealand (Chapter 3). New Zealand is one of only four temperate zone landmasses in the Southern Hemisphere that extends poleward of 30° south. Its location across the Subtropical Front, an important oceanic boundary defined by Nowlin and Klinck (1986), places New Zealand at a crucial location for detecting changes in broad-scale circulations associated with changes to the South Pacific Convergence Zone (SPCZ) on timescales from decades to centuries (Fowler *et al.*, 2000; Salinger *et al.*, 2001). Research over several decades has defined many of ENSO's essential characteristics and identified strong relationships with the climate of some extra-tropical regions (teleconnections), including New

Zealand (see Figure 1.2) (Kiladis and Diaz, 1989; Mullan, 1995; Salinger and Mullan, 1999; Diaz *et al.*, 2001).

Over twenty years of dendroclimatological research on New Zealand's Kauri (*Agathis australis*), has determined that the species carries a significant ENSO signal in its growth rings (Fowler *et al.*, 2000; 2004; 2005b; Fowler, 2005). Although individual specimens are capable of attaining ages greater than 1,000 years (Figure 3.3), extending the temporal scale of the Kauri data base has also been possible through the recovery of house timbers, museum relicts of the logging era (Figure 3.4), and the excavation of preserved logs buried in swamps for thousands of years in Northland (Ogden *et al.*, 1992; Buckley *et al.*, 2000; Boswijk *et al.*, 2002; 2006) (Figure 3.5).

Given the strength of the ENSO signal in Kauri and century scale evidence of a strong/persistent New Zealand region teleconnection with ENSO (Fowler *et al.*, 2004; Fowler, 2005), it is recognised that these dendrochronological sequences have great potential to investigate the high-resolution character of ENSO variability at decadal to millennial timescales. The hitherto absence of ENSO sensitive tree-ring data from New Zealand in recent multiproxy ENSO reconstructions highlights the considerable significance of bringing a new teleconnection region into play (Stahle *et al.*, 1998; Mann *et al.*, 2000; D'Arrigo *et al.*, 2005). This is of particular importance as it contributes to the data sparse extra-tropical regions of the Southern Hemisphere teleconnection variability identified by Annual Records of Tropical Systems (ARTS) as being a significant research priority (Dunbar and Cole, 1999; Buckley *et al.*, 2000; Fowler *et al.*, 2000; 2004).

Until recently, the longest tree-ring records from the Southern Hemisphere include a 3,622 year *Fitzroya cupressoides* record from south-central Chile (Lara and Villalba, 1993), and a subalpine *Lagarostrobos franklinii* (Huon Pine) chronology from Tasmania, which (discontinuously) extends back to 2146 BC (Cook *et al.*, 2000b). However, recent revisions of the modern Kauri database (Chapter 4) and the development of new sub-fossil chronologies has resulted in a record that continuously covers 3,722 years from 1724 B.C. to A.D. 2002 (Boswijk *et al.*, 2006) (Figure 3.6), making it the longest tree-ring record available from the western Pacific. In addition, ancient Kauri radiocarbon dated to 20,000-40,000 years BP has been recovered from swamps, providing a unique opportunity to decipher South Pacific climate variability on annual-millennial timescales from Holocene and pre-last glacial maximum periods (Fowler *et al.*, 2004).

Figure 3.3. One of largest living Kauri trees in New Zealand, the Yakkas tree, Waipoua Forest, Northland, New Zealand. With a diameter girth of 4.6 metres, this tree is reputed to be more than 1,000 years old. **Source:** Joëlle Gergis, 2003.

Figure 3.4. Peter Crossley and Gretel Boswijk examining a stump found in Herekino forest, Northland. **Source:** Andrew Lorrey, 2004.

Figure 3.5. Swamp Kauri found buried in bog lands of Northland, New Zealand has cross-dated to material from living trees, extending the continuous length of the Kauri record 3,722 years back in time to the calendar year 1724 B.C. **Source:** Andrew Lorrey, 2002.

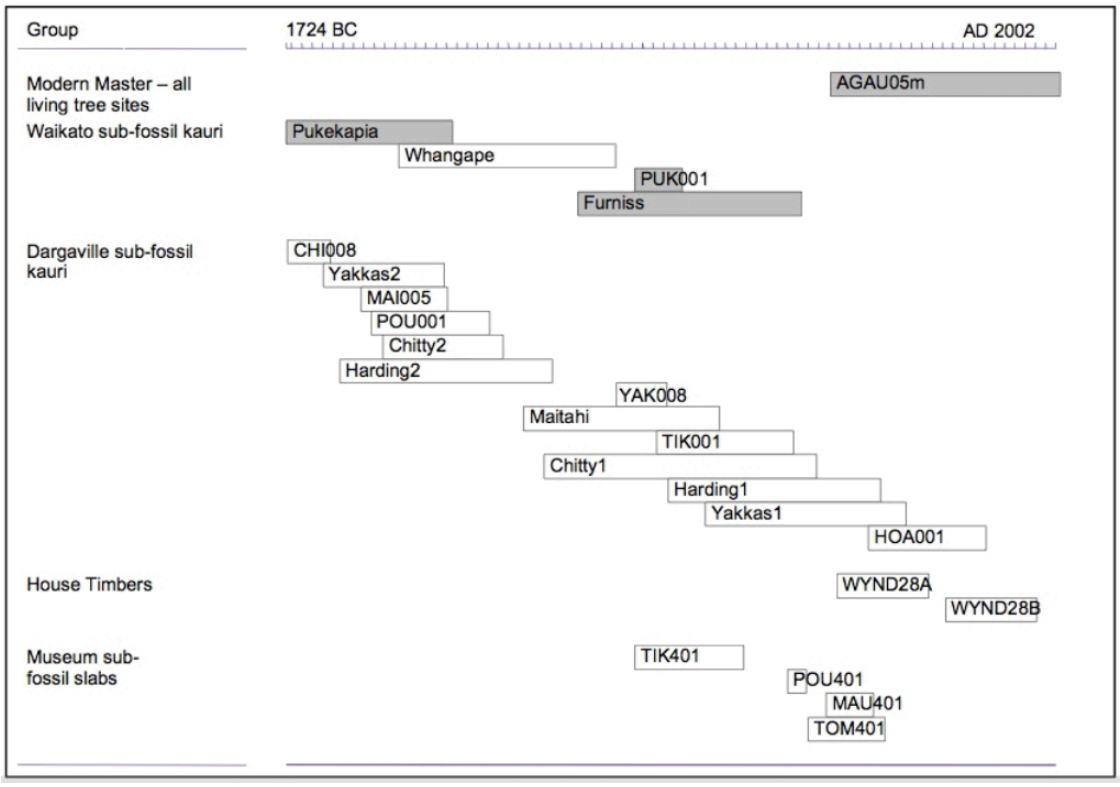

Figure 3.6. Temporal distribution of Kauri site chronologies (e.g. Pukekapia) and tree-sequences (e.g. PUK001) between 1724 BC and A.D. 2002. Shaded bars indicate chronologies built during the 1990s. All other sub-fossil and house-timber chronologies were developed between 2002-2004. The modern Kauri 'master' chronology (AGAU05) 149 trees (344 series) derived from 17 individual sites from the upper North Island. **Source:** Gretel Boswijk, 2005.

Significantly, the Kauri chronology is the longest continuous tree-ring proxy record of past ENSO variability available in the world. Revisions of the Kauri modern master database (detailed in Chapter 4) have considerably improved the quality of instrumental-proxy calibration, facilitating the assessment of ENSO extremes experienced during the late 20th century from a multi-century context (Gergis and Fowler, 2005a; 2005b; Gergis *et al.*, 2005a; 2005b; 2005c; 2005d).

3.3 Coral Records

Corals are particularly useful in the Southern Hemisphere and at lower latitudes where they can provide proxy climate records from shallow-water tropical marine regions in areas poorly represented by tree rings and ice cores (Fisher, 2002). Corals have the ability to track climate changes within the annual cycle, allowing sea-surface conditions

to be reconstructed with reference to specific seasons (Dunbar and Cole, 1999; Gagan *et al.*, 2000; Fisher, 2002). Seasonally resolved coral records are essential for reconstructing dynamic climate systems including ENSO, the monsoon, and wind-driven oceanic upwelling (Dunbar and Cole, 1999; Gagan *et al.*, 2000).

The ability of $\delta^{18}O$ and Sr/Ca ratios in the coral genera *Porites* and *Pavona* to monitor interannual climate fluctuations in the tropical Pacific region, such as the ENSO, has been demonstrated with live coral specimens (Cole *et al.*, 1993; Dunbar *et al.*, 1994; Evans *et al.*, 1998; Guilderson and Schrag, 1999; Urban *et al.*, 2000; Pelejero *et al.*, 2005) and fossil corals for time slices since the last interglacial (Correge *et al.*, 2000; Tudhope *et al.*, 2001; Gagan *et al.*, 2004; Mc Gregor and Gagan, 2004).

Many tropical corals reflect Sea Surface Temperature (SST) or salinity records, and are strongly affected by ENSO conditions (Quinn *et al.*, 1998; Dunbar and Cole, 1999; Cole *et al.*, 2000; Cobb *et al.*, 2001; Hendy *et al.*, 2002). When seawater $\delta^{18}O$ or Sr/Ca varies in response to changes in the balance between precipitation, evaporation, and water advection, the coral $\delta^{18}O$ or Sr/Ca ratios changes accordingly (Druffel, 1997; Fairbanks *et al.*, 1997; Dunbar and Cole, 1999; Gagan *et al.*, 2000; Fisher, 2002). The aragonite skeletons of reef-building corals also carry isotopic and chemical indicators that track site-specific features such as runoff, upwelling intensity and changes in oceanic pH (Gagan *et al.*, 2000; Hendy *et al.*, 2003; Pelejero *et al.*, 2005). Coral response to SST varies depending on location, proximity to upwelling zones, contractions and expansion of west Pacific warm pool (Gagan *et al.*, 2000).

During an El Niño event when eastern equatorial Pacific SSTs are generally anomalous warm, the region of the south-west Pacific is typically associated with cooler SSTs and below average monsoon rainfall, recorded as an enhancement of $\delta^{18}O$ values (Gagan *et al.*, 2000; Watanabe *et al.*, 2003). Changes in SSTs in the south-western Pacific are less marked during La Niña events (when the eastern equatorial Pacific is cooler than average), but rainfall is enhanced because of a more vigorous summer monsoon, registered as a lowering of $\delta^{18}O$ values (Gagan *et al.*, 2000; Watanabe *et al.*, 2003).

The ENSO signal in coral $\delta^{18}O$ records from the central western Pacific is considered strong and unambiguous (Cole *et al.*, 1993; Guilderson and Schrag, 1999; Urban *et al.*, 2000). In this region, El Niño events bring small SST increases of less than 1.5°C and enhanced rainfall associated with the migration of intense convection from the

Indonesian region, as the warm, fresh pool of the western Pacific expands eastward (Urban *et al.*, 2000). These changes combine to generate negative $\delta^{18}O$ anomalies recorded in the coral skeleton (Cole *et al.*, 1993). La Niña events experience relatively cool and dry conditions that produce positive $\delta^{18}O$ anomalies (Urban *et al.*, 2000).

To date, most of the studies of past climate have used the coral genus *Porites* because it is abundant throughout the Indo-Pacific region and can be sampled at high temporal resolution because it grows quickly (8-24mm/yr) (Watanabe *et al.*, 2003; Bagnato *et al.*, 2004). However, at present continuous geochemical records from *Porites* do not extend past approximately 300-400 years (Watanabe *et al.*, 2003). Similar age barriers have been noted by studies using *Pavona* from the equatorial Pacific and the Caribbean (Watanabe *et al.*, 2003). Recently, studies based on the massive, annually banded coral *Diploastrea heliopera* that is known to live for up to 1,000 years throughout the tropical Indian and Pacific Oceans have been presented (Watanabe *et al.*, 2003; Bagnato *et al.*, 2004).

Diploastrea is well preserved in Late Quaternary raised coral reefs within the Pacific warm pool regions of Indonesia, Papua New Guinea and Vanuatu representing significant opportunities for the development of long tropical palaeoclimate records (Watanabe *et al.*, 2003). Individual colonies are known to grow 3-4m high and could potentially double the typical time span of existing coral palaeoclimatic records (Watanabe *et al.*, 2003). In addition, *Diploastrea* records ENSO inter-annual variability in SST and salinity across the south-western Pacific indicating that it should yield dependable palaeo-ENSO records, providing an important new coral archive of a key component of the global climate system (Watanabe *et al.*, 2003; Bagnato *et al.*, 2004).

Currently the science of building coral chronologies is not as well developed as for tree-rings and ice cores, however corals are unique in their ability to resolve key uncertainties in our knowledge of tropical climates which are critical in our understanding of ENSO (Dunbar and Cole, 1999; Gagan *et al.*, 2000; Fisher, 2002). Like trees, fossil coral stratigraphies can be cross-correlated and made into longer chronologies (Correge *et al.*, 2000; Tudhope *et al.*, 2001; Hendy *et al.*, 2003), although this work is not nearly as developed as with tree-ring chronologies (e.g. Roig *et al.*, 2001; Cook *et al.*, 2002; Boswijk *et al.*, 2006).

3.3.1 Coral dating issues

The dating accuracy of any palaeoclimate record is an important factor in determining the value of a given proxy-climate record (Mann *et al.*, 1998; Fisher, 2002). Typical errors associated with coral age estimates are generally only 1-2 years per century, although greater errors have been reported (Dunbar *et al.*, 1994). Thus, strict dating control is recognised as being critical to maintaining the reliability of coral records and the climate reconstructions to which they contribute (e.g. Mann *et al.*, 1998; 2000; Dunbar and Cole, 1999; Lough, 2004).

Dating typically involves successively counting the density bands back from the date of collection at the top of the coral or are dated from the annual cycle of the measured isotope (Hendy *et al.*, 2003). Difficulties can arise due to changing growth orientation down the coral core and the three-dimensional structure of the coral skeleton which can produce artifacts in the X-radiograph such as multiple peaks and ambiguous banding patterns (Hendy *et al.*, 2003). Stable isotopic analysis is also commonly used to cross verify age estimates (Dunbar *et al.*, 1994; Quinn *et al.*, 1998).

Ideally, a more rigorous approach to coral dating accuracy, comparable to cross-dating techniques routinely used in dendroclimatology, would be desirable. Realistically, however, conservation issues associated with the sampling of multiple coral colonies from tropical areas are likely to be problematic. Nonetheless, regional composites made up of individual coral cores are beginning to be compiled, revealing vital information on large-scale patterns of past oceanic variability (Hendy *et al.*, 2003; Linsley *et al.*, 2004).

Recently, Hendy *et al.* (2003) applied cross-dating techniques adapted from dendrochronology to produce an eight coral core, multi-century regional chronology for the Great Barrier Reef. Characteristic patterns of distinct luminescent lines within the coral skeletons were matched between coral cores (Figure 3.7) from inshore and mid-shelf reefs in the central Great Barrier Reef to produce a master chronology of river flood events back to A.D. 1615 (Hendy *et al.*, 2003).

This study demonstrated for the first time that cross-dating techniques adopted from dendrochronology may be successfully applied to coral records (Hendy *et al.*, 2003). The authors emphasised the need to combine records from more than one coral from a particular location both to ensure dating accuracy (through improved replication) and to demonstrate that a common climatic signal is being recorded. In doing so, the degree of

random noise that may be registered by a single coral record will be minimised (Hendy *et al.*, 2003).

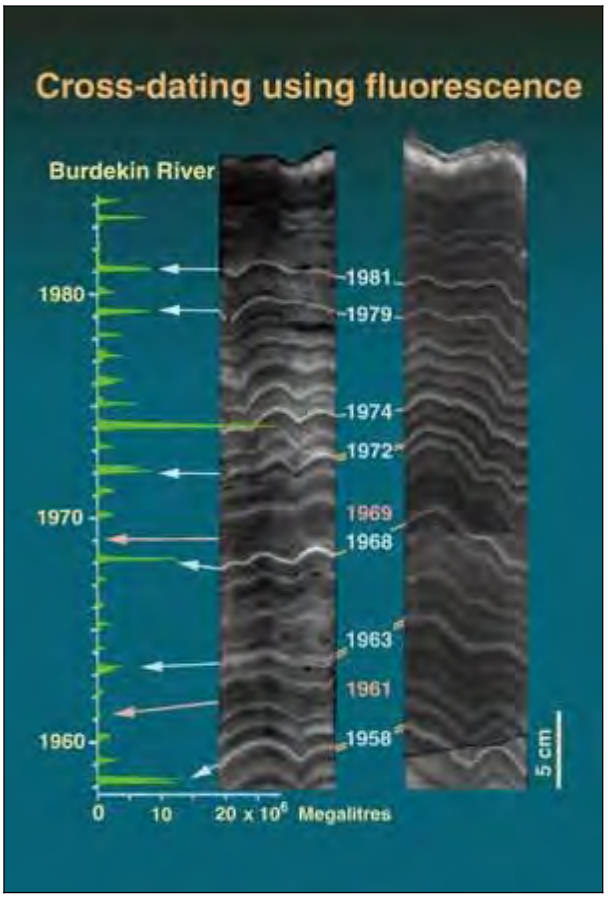

Figure 3.7. Example of cross-dating luminescent lines in two coral cores from the Great Barrier Reef, Australia calibrated to instrumental Burdekin River outflow data. **Source:** Erica Hendy (www.onlineopinion.com.au/images/Coral_Record1.gif).

3.4 Ice-Core Data

Some ice caps and ice sheets continuously record the chemical and physical nature of the Earth's atmosphere on seasonal, annual, decadal and centennial time scales (Oerlemans, 2005). Ice cores have been recovered from both polar and lower latitudes, the longest of which covers eight glacial cycles spanning the past 740 000 years (EPICA, 2004). Data from the upper sections of these cores have been integrated with other proxy indicators to yield a high-resolution global perspective of the Earth's climate over the past 1,000 years (Mann *et al.*, 1998; Moberg *et al.*, 2005; Oerlemans, 2005).

Ice cores provide climate information over multiple millennia from the polar regions of the Northern and Southern Hemispheres, as well as tropical and subtropical alpine environments (Thompson *et al.*, 1985; Thompson *et al.*, 2000a; Bradley *et al.*, 2003; Jones and Mann, 2004). In particular, records recovered from low-latitude ice caps are of particular interest as they are located in areas where climatic changes may directly and significantly affect human activities (Thompson, 2000; Thompson *et al.*, 2000b; Thompson *et al.*, 2002). Currently, over 75% of the world's population lives in areas directly impacted by variations in tropical climate, which underscores the importance of deciphering long-term climate records from these regions (Thompson, 2000; Yang *et al.*, 2000).

Ice core information is thus spatially complementary to that provided by either tree-rings or corals, but it is available only over a very small fraction of the global surface (Fisher, 2002). Ice cores can provide several climate related indicators, including the fraction of melting ice, the rate of accumulation of precipitation, and concentrations of various chemical constituents (including trace gases) that provide information about the atmospheric environment at the time the bubbles in the ice were trapped (Thompson *et al.*, 1979). Ice cores also contain cosmogenic isotopes of beryllium and volcanic dust, both providing sources of vital information regarding the past radiative forcing of climate (Zielinski *et al.*, 1994; Fiedel *et al.*, 1995; Zielinski, 2000; Shindell *et al.*, 2001; Shindell *et al.*, 2003).

Annual dating in ice sequences is sometimes possible, but in practice it is often quite difficult (Jones and Mann, 2004). Use of stratigraphic markers, such as known volcanic dust events are also used in conjunction with isotopic indicators to help anchor any age model (Zielinski, 2000). Stacking of multiple annual ice core records can reduce the age model uncertainty in chronologies and reduce site specific variability (Fisher, 2002). In regions with low snowfall, one year's accumulation may represent a number of discrete precipitation events. In such cases, annual dating may not be possible and there is furthermore the potential for a substantial temporal (and seasonal) sampling bias. In regions where accumulation is high (e.g., Law Dome, Antarctica) or where a number of cores can be cross-dated like trees (e.g., Greenland), seasonal resolution is possible (Thompson *et al.*, 1984; Goodwin *et al.*, 2004).

Like all proxy records, ice sequences can also suffer from the issue of dating inaccuracies. Annual layer thickness from the Quelccaya ice-core ranges from 1.2m at

the surface to 0.01m at the base, estimated to A.D. 744 (see Figure 3.8) (Thompson *et al.*, 1985). The timescale is, however, subject to errors due to factors such layers being thinned and stretched as new snow accumulated each year (Thompson *et al.*, 1985). Nonetheless, back to A.D. 1500, the estimated dating uncertainty is ±2 years, while dating on the lower sections is estimated at ±20 years (Thompson *et al.*, 1986). Consequently, only the post A.D. 1525 net accumulation data of the summit core is analysed in this study (see Section 4.10).

Figure 3.8. Ice cliff on Quelccaya ice cap, Peru, with visible annual accumulation layers. The distinct seasonality of precipitation at Quelccaya (November-April) results in the deposition of the dry season dust bands seen in the ice cliff. According to a recent report by Nash (2002), this ice cliff no longer exists due to accelerated global warming experienced in recent decades. **Source:** Lonnie Thompson, Byrd Polar Research Centre, The Ohio State University, (http://www.ncdc.noaa.gov/palaeo/slides).

3.5 Documentary Records

Documentary sources provide information about past weather events which can, under certain circumstances, provide information about past climate variability. These include records of frost dates, droughts, floods famines, the freezing of water bodies, duration of snow and sea ice cover, and phenological evidence such as the dates of flowering of plants and the ranges of various species of plants (Lamb, 1982; Jones and Mann, 2004). All can provide insight into past climate conditions, however, they are generally limited to regions with long written traditions, such as Europe, eastern Asia and North America (Jones and Mann, 2004).

However, logs from Spanish galleons crossing the Pacific Ocean during the 16th–19th centuries (Garcia Herrera *et al.*, 2003) provide possible insights into variations in the strength of the prevailing winds, and documentary information from South America has allowed a chronology of El Niño to be developed over the past few centuries (Quinn and Neal, 1992; Ortlieb, 2000). Human accounts through the form of artistic depictions of mountain glacier retreats and advances during past centuries have also provided evidence of climate change on more low-frequency timescales (Fisher, 2002).

Despite the wealth of data available in some regions, documentary sources alone are not useful for detailing truly global-scale climate variations. This caution is necessary as they are not equivalent in their reliability to actual instrumental measurements of meteorological variables (Folland *et al.*, 2001; Jones and Mann, 2004). Historical documentary information also often emphasise extreme conditions such as heat waves and cold snaps, which may provide a highly misleading sense of the true seasonal or annual mean climate anomalies that are of interest in discussing climate change (Folland *et al.*, 2001; Jones and Mann, 2004).

3.6 Proxy Data Sources

3.6.1 Proxy selection

Data was primarily collected from the World Data Centre for Palaeoclimatology (http://www.ngdc.noaa.gov/palaeo/data) and through direct collaboration with researchers engaged in high-resolution palaeoclimatic studies. Coral, tree-ring, documentary and ice records were selected for representation of *in situ* oceanic processes

and associated atmospheric (terrestrial) conditions from ENSO affected regions (Figure 3.9).

Proxies used in this study are predominately published records from core ENSO or key teleconnection areas previously identified as containing an 'ENSO signal' from both eastern and western Pacific locations back to A.D. 1525 (Table 3.1). Detailed statistical relationships between each proxy and seasonal CEI data for each proxy with one year lead and lag times can be examined in Appendix 2. Coral sequences were limited to those with sufficient, continuous record length and to those which were given a positive assessment by Lough (2004). This resulted in a number of shorter and/or discontinuous coral records being excluded from this analysis (Cole *et al.*, 2000; Urban *et al.*, 2000; Cobb *et al.*, 2003).

Although a number of the records listed in Table 1 extend well beyond A.D. 1525 (e.g. the Quelccaya ice core data and all tree-ring records except for the Indonesian Teak), the lack of long-term coral data from tropical regions makes it difficult to establish evidence of global teleconnections associated with ENSO events (Whetton and Rutherfurd, 1994; Grove and Chappell, 2000). Furthermore, as exact dating associated with older sections of individual records become more uncertain due to a loss of overall internal replication or dating issues, the few records that are available become less reliable back in time (Thompson *et al.*, 1986; D'Arrigo *et al.*, 1994). Accordingly, here the analysis was limited to the A.D. 1525-2002 period.

With the exception of the Kauri, Pink Pine and Teak raw tree-ring data was obtained from NOAA's World Data Centre-A for Palaeoclimatology. Kauri, Pink Pine, Teak, the North Chinese rainfall index and Nile flood data were sourced via personal communication (Whetton and Rutherfurd, 1994; Fenwick, 2003; Fowler *et al.*, 2004).

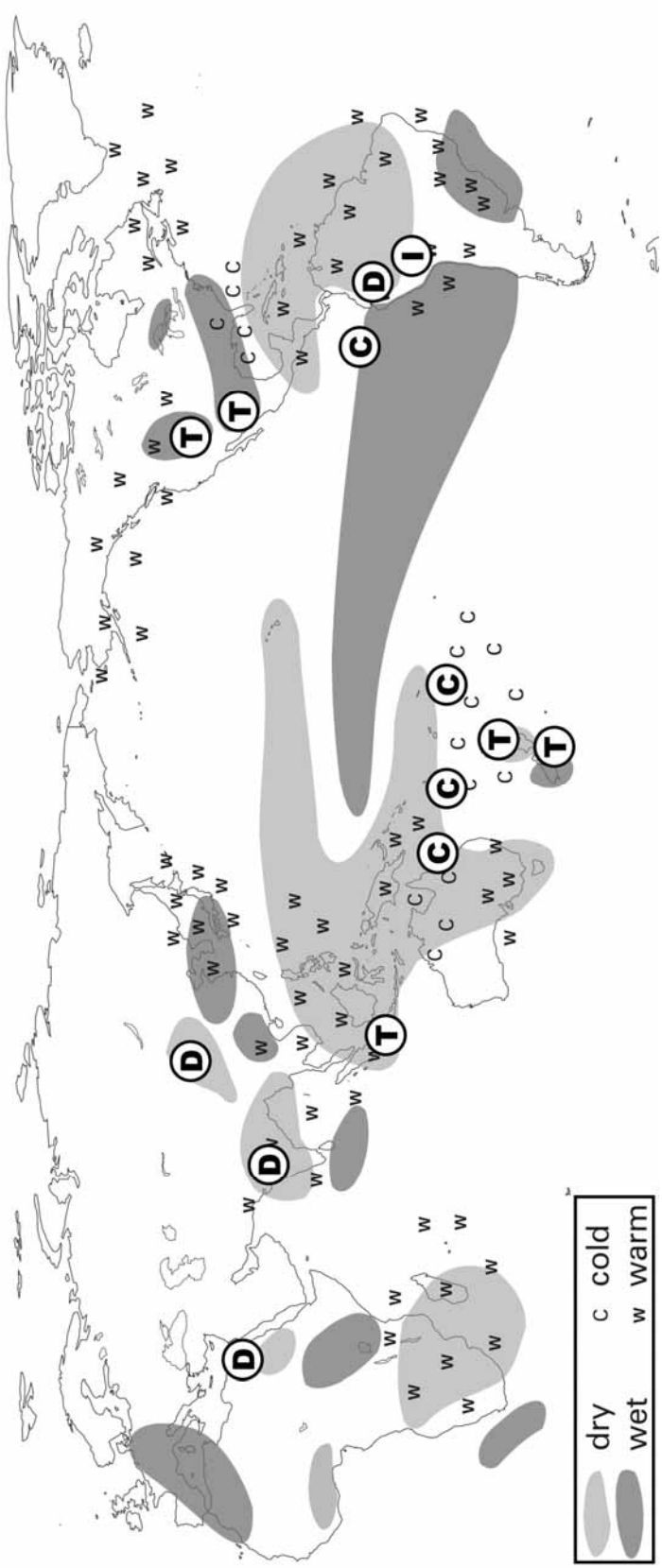

Figure 3.9. Location of proxy records used in this study shown with regard to El Niño teleconnection characteristics. Rainfall anomalies are represented by light grey shading (dry) and dark shading (wet). Temperature anomalies indicated by 'c' (cool) and 'w' (warm) annotation. 'T' denotes tree-ring records, 'C' coral sequences, 'D' documentary source and 'I' ice core data. Details of each record are listed in Table 3.1. **Source:** Modified from Fowler *et al.* (2005a).

Table 3.1. Details of proxy climate records used in this study. Proxy locations are shown in Figure 3.9. Note that each proxy is calibrated to the specific season of strongest agreement with the instrumental ENSO conditions as indicated by the CEI (see Chapter 2).

Proxy Record	Dates (A.D.)	Data filter	ENSO Zone	Season	Climate Variable
Tree-rings					
Berlage Indonesian Teak [a*]	1525-1929	10-year Gaussian	West Pacific	SON	Total Ring Widths
D'Arrigo Indonesian Teak [b*]	1841-1995	20-year Spline	West Pacific	SON	Total Ring Widths
New Zealand Kauri [c]	1525-2002	20-year Spline	West Pacific	SON	Total Ring Widths
New Zealand Pink Pine [d]	1525-1998	20-year Spline	West Pacific	JJA	Total Ring Widths
Mexican Douglas Fir [e]	1525-1998	20-year Spline	East Pacific	DJF	Total Ring Widths
SW USA Pinyon Pine [f]	1525-2000	20-year Spline	East Pacific	DJF	Total Ring Widths
Coral					
Great Barrier Reef [g]	1612-1985	3-year Gaussian	South-west Pacific	DJF	Luminescence SSS
New Caledonia [h]	1658-1992	3-year Gaussian	South-west Pacific	SON	δO^{18} SST
Galapagos Islands [i]	1607-1982	3-year Gaussian	East Pacific	DJF	δO^{18} SST
Rarotonga [j]	1726-1997	3-year Gaussian	Central Pacific	DJF	Sr/Ca SST
Ice					
Quelccaya Ice Core [k]	1525-1984	3-year Gaussian	East Pacific	DJF	Net accumulation
Historical Records					
Quinn/Ortlieb [l]	1525-1987	N/A	East Pacific	JJA	Rainfall
Nile [m]	1587-1984	10-year Gaussian	North Africa Teleconnection	MAM	Rainfall
India Drought [n]	1525-1984	N/A	South Asia Teleconnection	SON	Rainfall
China [o]	1525-1979	10-year Gaussian	North Asia Teleconnection	DJF	Rainfall

[a] Berlage (1931), Murphy and Whetton (1989), Whetton and Rutherfurd (1994), Whetton *et al.* (1996).

[b] D'Arrigo *et al.* (1994), IGBP Pages/WDC-A for Palaeoclimatology Contribution Series 1999-063

[c] Fowler *et al.* (2000; 2004), Gergis *et al.* (2004b; 2004a)

[d] Fenwick (2003)

[e] Cleaveland *et al.*(2003)

Stahle and Cleaveland, (2002), IGBP Pages/WDC-A for Palaeoclimatology Contribution Series 2002-004.

Greybill (1994) IGBP Pages/WDC-A for Palaeoclimatology Contribution Series 1994-003

Grissino-Mayer and Swetnam (1992) IGBP Pages/WDC-A for Palaeoclimatology Contribution Series 1992-012

Dean (1993) IGBP Pages/WDC-A for Palaeoclimatology Contribution Series 1993-021

Grow (2000) IGBP Pages/WDC-A for Palaeoclimatology Contribution Series 2003-094

[f] Stahle *et al.*, (1998), IGBP Pages/WDC-A for Palaeoclimatology Contribution Series 2002-004.

[g] Hendy *et al.* (1998), IGBP Pages/WDC-A for Palaeoclimatology Contribution Series 2002-009

[h] Quinn *et al.* (1998), IGBP Pages/WDC-A for Palaeoclimatology Contribution Series 1999-003.

[i] Dunbar *et al.* (1994), IGBP Pages/WDC-A for Palaeoclimatology Contribution Series 1994-013

[j] Linsley *et al.* (2000), IGBP Pages/WDC-A for Palaeoclimatology Contribution Series 2000-065.

[k] Thompson *et al.* (1992) IGBP Pages/WDC-A for Palaeoclimatology Contribution Series 1992-008

[l] Quinn and Neal (1992), Ortlieb (2000)

[m] Hassan (1981), Whetton and Rutherfurd (1994), Whetton *et al.* (1996)

[n] Whetton and Rutherfurd (1994), Whetton *et al.* (1996)

[o] Wang and Zhao (1981), Whetton and Rutherfurd (1994), Whetton *et al.* (1996)

* Berlage Indonesian Teak sequence used from 1525-1929, D'Arrigo Teak used from 1930-1995. Raw tree-ring widths could not be obtained for the Berlage record, obstructing the development of a single Teak chronology for Java.

3.7 Tree-Ring Data

3.7.1 Kauri (*Agathis australis*) - North Island, New Zealand

Kauri (*Agathis australis* D. Don Lindley) belongs to the genus *Agathis*, found in rainforests of the western Pacific, including Papua New Guinea, Australia, New Caledonia and New Zealand (Salmon, 1980). To date, 426 crossdated series from 191 trees from the seventeen individual sites listed in Table 3.2 were used to construct a master total ring width chronology for the period A.D. 1525-2002.

Kauri tree-rings are negatively correlated with both temperature and precipitation during the spring growing season (SON) (Fowler *et al.*, 2005b). However, Fowler *et al.* (2000) identified stronger correlations between Kauri tree rings and the SOI than with local precipitation and surface air temperature, with correlations peaking in spring, then declining through the rest of the growing season (Fowler *et al.*, 2000; Fowler *et al.*, 2005b).

In the case of El Niño episodes, increases in the frequency and/or strength of south-westerly winds bringing relatively cool–dry conditions to Northern New Zealand, are associated with a wide ring in Kauri. During warm–wet conditions characteristic of La Niña, narrow growth rings in Kauri are generally observed (Fowler *et al.*, 2000; Fowler, 2005).

Table 3.2. Listing of all Kauri (*Agathis australis*) chronologies used to develop a regional master chronology for the upper North Island, New Zealand, A.D. 1525-2002.

Site	Site Code	Dates (A.D.)	Contributor
Upper North Island			
Cascades Kauri Park	CASC	1559-1982	Fowler, A. Boswijk, G.
Huapai Scientific Reserve	HUPI	1483-1997	Fowler, A. Boswijk, G.
Katikati	KATI	1698-1996	Ahmed, M. Ogden, J. Buckley, B.
Hidden Valley, Great Barrier	HIDV	1697-2002	Boswijk, G. Xiong, L.
Huia, Waitakere Ranges	HUIA	1720-1981	Boswijk, G.
Kawhia	KAWH	1710-1996	Boswijk, G.
Konini Forks	KOND	1770-1976	La Marche, V.
Onekura Bluff, Puketi Forest	PUBL	1623-1982	Ahmed, M. Ogden, J.
Puketi Forest South	PUKF	1504-2002	Gergis, J. Ahmed, M.
Thumb Track, Little Barrier	LTBR	1790-1981	Ahmed, M. Ogden, J.
Manaia Sanctuary	MASC	1269-1998	Boswijk, G. Ogden, J. Fowler, A.
Mt Moehau	MOEH	1360-1980	Boswijk, G. Palmer, J.
Mt William	MWIL	1580-1981	Boswijk, G.
Trounson Kauri Park	TROU	1529-2002	Gergis, J. Ahmed, M.
Waipoua Forest	WAID	1628-1903	Palmer, J. Xiong, L.
Waitakere Dam	WTDM	1727-2002	Lorrey, A.
Warawara Forest	WARA	1640-1979	Ahmed, M. Ogden, J.

3.7.2 Pink Pine (*Halocarpus biformis*) - South Island, New Zealand

Pink Pine (*Halocarpus biformis* (Hook.) Quinn) is an indigenous evergreen conifer in New Zealand (Fenwick, 2003). Here, total ring-width chronologies were used to develop a master chronology from Westland, New Zealand, using 296 series from 173 trees from 13 sites listed in Table 3.3. Fenwick (2003) reported that tree growth is positively correlated with temperature over the entire growing season, approximately from September to May, and the strongest and most consistent relationships occurred in January-March (Fenwick, 2003). Chronologies were negatively correlated with January precipitation, but in general, the influence of rainfall on tree growth was negligible (Fenwick, 2003).

The relationship with SOI was direct during the growing season (in agreement with the temperature response), and inverse when calculated for a lag of two years. Generally, El Niño (La Niña) events registered as narrow (wide) growth rings in the Pink Pine master chronology used in this analysis (see Chapter 5).

Table 3.3. Listing of all Pink Pine (*Halocarpus biformis)* chronologies used to develop a regional master chronology for the Westland South Island, New Zealand, A.D. 1525-1999. **Source:** Adapted from Fenwick (2003).

Site	Site Code	Dates (A.D.)	Contributor
Westland, South Island			
Mt. Bonar	BON	1463-1999	Fenwick, P.
Camp Creek	CCP	1410-1998	Fenwick, P.
Croesus Track	CRS	1783-1999	Fenwick, P.
Eldrik Peak	ELD	1776-1980	Fenwick, P.
Mt. Glasgow	GLS	1461- 1999	Fenwick, P.
Matiri Range	MAT	1508-1999	Fenwick, P.
Mt. Elliot	MEL	1440-1999	Fenwick, P.
Mt. Greenland	MGR	1720-1980	Fenwick, P.
Mt. French	MTF	1675-1969	Fenwick, P.
Omoeroa Saddle	OMO	1771-1912	Fenwick, P.
Slopedown Hill	SPD	1761-1997	Fenwick, P.
Mt. Te Kinga	TKG	1754-1970	Fenwick, P.
Totara Saddle	TOS	1784-1910	Fenwick, P.

3.7.3 Pinyon Pine (*Pinus edulis*) - South-Western USA

Ten Pinyon Pine (*Pinus edulis*) total ring width chronologies from Utah, Arizona and New Mexico listed in Table 3.4 were used here to develop a regional master chronology for south-western USA for the A.D. 1525-2000 period. Chronologies are significantly

correlated with the DJF SOI even though the growing season of the sample trees does not begin until spring or early boreal summer (JJA) (Stahle *et al.*, 1998).

Boreal cool season (December and May) precipitation over south-western USA is significantly correlated with indices of ENSO (Ropelewski and Halpert, 1989). This ENSO teleconnection to tree growth exists because El Niño (La Niña) events during the boreal cool season tend to enhance (reduce) boreal winter and early spring precipitation over subtropical North America (Stahle *et al.*, 1998).

These chronologies are strongly correlated with precipitation (October–March), which is the season of strongest ENSO influence on climate in this region (Stahle *et al.*, 1998). The tree-growth response in subtropical North America during El Niño years is characterised by a wide ring in the Pinyon Pine master record, while and dry La Niña conditions corresponds to the deposition of a narrow growth ring.

Table 3.4. Listing of all Pinyon Pine (*Pinus edulis*) chronologies used to develop a regional master chronology for south-western USA, A.D. 1525-2000.

SW USA Pinyon Pine (PIED) Site Name	Site Code	Date (A.D.)	Contributors	NOAA World Data Centre A-Paleoclimatology Contribution ID
Utah				
Coal Bench	CBN	1555-2000	Grow, D.	2003-094
Deer Springs Mesa	DSM	1477-1998	Grow, D.	2003-094
Lower Henderson Canyon	HCL	1507-1999	Grow, D.	2003-094
Round Valley Draw	RVD	1561-1999	Grow, D.	2003-094
Skutumpah Road #1	SK1	1590-2000	Grow, D.	2003-094
Skutumpah Road #2	SK2	1406-2000	Grow, D.	2003-094
Navajo Mountain	NAV	1469-1971	Dean, J. Bowden, D.	1993-021
Arizona				
Eagle Creek	EPN	1640-1987	Graybill, D.	1994-003
New Mexico				
Paliza		1658-1972	Dean, J.	1993-021
Oscura Peak White Sands Missile Range	OSC	1644-1981	Grissino-Mayer, H. Swetnam, T.	1992-012

3.7.4 Douglas Fir (*Pseudotsuga menziesii*) - Mexico

Eight individual Douglas Fir (*Pseudotsuga menziesii*) sites chronologies listed in Table 3.5 were used to develop a regional master chronology for Mexico for the period A.D. 1525-1998. Although earlywood and latewood chronologies have been developed

(Cleaveland, 1986, 1988; Stahle *et al.*, 1998), limited late 20th century replication of earlywood chronologies and a desire for consistency with the other tree-ring chronologies, resulted in the analysis of total ring width chronologies.

Tropical Pacific SSTs strongly influence precipitation in Mexico between December and May particularly during ENSO episodes (Cleaveland *et al.*, 2003). This ENSO teleconnection to the climate of northern Mexico is clearly reflected in the growth of Douglas Fir trees from the Sierra Madre Occidental of Chihuahua and Durango in November to March precipitation (Stahle *et al.*, 1998; Cleaveland *et al.*, 2003).

Table 3.5. Listing of all Douglas Fir (*Pseudotsuga menziesii*) chronologies used to develop a regional master chronology for the southwest USA, A.D. 1525-1998.

Mexican Douglas Fir (PSME) Site Name	Site Code	Date (A.D.)	Contributors	NOAA World. Data Centre A-Paleoclimatology Contribution ID
Mexico				
Cerro Potosi	POT	1845-1995	D.Stahle, M.Therrell, M.Cleaveland, G.Paull	2002-004
Creel International Airport	CIA	1644-1993	D.Stahle, M.Cleaveland, B.Burns	2002-004
El Salto recollection (inc 3 Tucson LTRR sites)	SAL	1481-1993	D.Stahle, B.Burns, M.Cleaveland	2002-004
El Tabacote & Tomochi	TAB	1583-1993	D.Stahle B.Burns, M.Cleaveland	2002-004
Villareal	VIL	1710-1998	D.Stahle M.Therrell M.Cleaveland, J.Villanueva-Diaz	2002-004
Mesa de Campanero	CAM	1806-1993	D.Stahle, M.Cleaveland B.Burns	2002-004
Las Tinajas	TIN	1621-1993	D.Stahle, B.Burns M.Cleaveland	2002-004
Cerro Baraja & Los Angeles Sawmill	BLA	1376-1993	D.Stahle, M.Cleaveland B.Burns	2002-004

The Tropical Rainfall Index (TRI) (Wright,1982), representing an estimate of ENSO-related rainfall anomalies from the central Pacific, correlates significantly with instrumental and tree-ring reconstructed winter precipitation (r=0.49 and 0.55, respectively), reflecting the strong ENSO modulation of cool season climate over northern Mexico (Cleaveland *et al.*, 2003). From the ring width chronology analysed here, El Niño (La Niña) episodes associated with enhanced (reduced) rainfall over northern Mexico; correspond to wide (narrow) tree-rings in the Douglas Fir chronology.

3.7.5 Teak (*Tectona grandis*) - Java, Indonesia

The Teak chronology, first published by Berlage (1931), remains one of the few high-resolution palaeoclimate records available from the western equatorial Pacific. Berlage (1931) was the first to develop a Javanese Teak chronology for the period A.D. 1514-1929, and his ring-width chronology has been partially confirmed with new specimens from Java (D'Arrigo *et al.* 1994). A major component of the long chronology was based on disks taken from two trees (back to A.D. 1514 and 1527). Between A.D. 1514-1825 the chronology is based on between 10-22 individual series and after the year A.D. 1929 it is based on a maximum of 89 series (Murphy and Whetton, 1989).

A reanalysis of the Berlage (1931) chronology undertaken by Murphy and Whetton (1989) is the used for the period A.D. 1525-1840 (Whetton and Rutherfurd, *pers comm.*). An exponential function with a high-order polynomial was used to fit a biological growth curve and subsequently used to develop a modified tree-ring index chronology (Murphy and Whetton, 1989; Whetton and Rutherfurd, 1994). To remove the prominent low frequency fluctuations detected by spectral analysis (Murphy and Whetton, 1989), the chronology was smoothed with a 11-year Gaussian filter to facilitate high-frequency analysis associated with ENSO (Murphy and Whetton, 1989; Whetton and Rutherfurd, 1994). Murphy and Whetton (1989) found a significant relationship with the SOI in the dry season between May-October (peaking in July) when Indonesian rainfall is most responsive to ENSO (Murphy and Whetton, 1989).

Between A.D. 1841-1995, the more recent chronology of D'Arrigo *et al.* (1994), smoothed here using a 20-year cubic spline, is used. The chronology includes many trees more than 200 years old, and the derived chronology is well replicated from A.D. 1700-1995. The chronology is significantly correlated with the winter SOI for the period A.D. 1879-1977, both concurrently (r=0.19; $P < 0.10$) and following the SOI by two seasons ($r = -0.35$; $P < 0.001$) (D'Arrigo *et al.*, 1994).

Rainfall in the Indonesian archipelago is directly linked to convection associated with the Indonesian low-pressure cell, a key element of the ENSO system. During an El Niño phase there is a tendency for droughts when the Indonesian low migrates eastward into the central Pacific (D'Arrigo *et al.*, 1994). Conversely, during La Niña events, above normal rainfall and flooding tends to occur in Indonesia (D'Arrigo *et al.*, 1994).

The link between rainfall in Java and ENSO appears to be strongest during the dry monsoon season from June to November (D'Arrigo *et al.*, 1994). This is when Teak growth appears to be most sensitive to variations in rainfall and ENSO (D'Arrigo *et al.*, 1994). Generally, enhanced rainfall experienced during a La Niña corresponds to the deposition of a wide growth ring, while dry El Niño conditions are associated with narrow tree-rings.

3.8 Coral Data

3.8.1 Galapagos Islands, Ecuador – eastern Pacific

Situated within the eastern Pacific SST 'centre of action', the Galapagos Island record provides the longest coral record of ENSO-related variability from this region (Dunbar *et al.*, 1994). An uplifted colony of *Pavona clavus* was sampled for $\delta^{18}O$ in annual increments determined from high-density couplets and stable isotope profiles (Dunbar *et al.*, 1994). Climatic interpretation was based on near monthly $\delta^{18}O$ analyses of *Porites gigantea* coral, 1961-1983, which was significantly correlated with local monthly SSTs (r=-0.90, including annual cycle) (Dunbar *et al.*, 1994).

Significant correlations were reported between annual average $\delta^{18}O$ and regional SSTs (r=0.88), Wright's SST index (r=0.74), Wright's rainfall index (r=0.64) but no significant correlation with Wright's SOI (r=0.47) for the 1965-1982 period (Wright, 1982; Dunbar *et al.*, 1994). On the basis of the younger, short coral records, authors suggest that annual $\delta^{18}O$ can be used to reconstruct eastern Pacific SSTs and identify past ENSO events. A significant correlation (r=0.66) was reported between annual $\delta^{18}O$ values in the longer core and Puerto Chicama SSTs for the A.D. 1936-1953 period (Dunbar *et al.*, 1994).

During El Niño events, the trade winds weaken allowing warm water from the western Pacific to move eastward, causing the Indonesian low to shift much further east towards the dateline and southward toward the equator (Dunbar *et al.*, 1994). This shift results in a diminished SST gradient across the region, leading to weak trade winds and a suppression of upwelling (Dunbar *et al.*, 1994). Consequently, sea level and SSTs rise and precipitation increase throughout most of the tropical Pacific. The opposite

tendency occurs during La Niña episodes. For the purposes herein, El Niño (La Niña) conditions are registered as a less (more) negative $\delta^{18}O$ index.

Importantly, the Galapagos coral record is recognised as containing several dating issues (Dunbar and Cole, 1999). Before A.D. 1936, a cumulative age error estimate of ±3 years to band couplets continues until A.D. 1906 (Dunbar *et al.*, 1994). Before A.D. 1906, an additional age error estimate of ±2 years is given, resulting in a net maximum cumulative error of ±5 years. These errors result from possible inaccuracies in band counting and short hiatuses in coral growth (Dunbar *et al.*, 1994). Accordingly, caution should be exercised when interpreting any apparent ENSO signal recorded independently of verification with other proxy records.

3.8.2 Rarotonga – central-western Pacific

In a study from Rarotonga in the central western Pacific, *Porites lutea* were sampled for Sr/Ca and $\delta^{18}O$ at 1-2 mm resolution (Linsley *et al.*, 2000a). A chronology was established for the period A.D. 1726-1995 by assuming annual minima in Sr/Ca occurred in February (month of average warmest SSTs) and annual maxima in Sr/Ca in August-September (the months of coldest average SSTs) (Linsley *et al.*, 2000a). Herein, Sr/Ca values were used starting from A.D. 1727, as data is only available for one season (SON) of the year A.D. 1726.

Rarotonga is located in the Cook Islands in the region of the eastern South Pacific Convergence Zone (SPCZ) where maximum SSTs occur between February and March (Linsley *et al.*, 2000a). The region had been identified as a 'centre of action' in the Southern Oscillation (Glantz *et al.*, 1991; Allan *et al.*, 1996). A greater proportion of common variance is reported between Sr/Ca and SSTs (r=0.86) than between the coral $\delta^{18}O$ record (r=0.73) (Linsley *et al.*, 2000b).

During El Niño events, the SPCZ moves to the north-east joining the Intertropical Convergence Zone (ITCZ) in the central-western tropical Pacific (Linsley *et al.*, 2000a). This leads to cooler and drier than average conditions in the region, registering as enhanced Sr/Ca ($\delta^{18}O$) in the coral record (Linsley *et al.*, 2000a). During La Niña events, the situation reverses, resulting in a warming of SSTs and enhanced rainfall associated with the intensification of the ITCZ, corresponding to a low Sr/Ca ($\delta^{18}O$) values (Linsley *et al.*, 2000a).

3.8.3 New Caledonia - south-western Pacific

In a study of *Porites lutea* from New Caledonia, coral was sampled at a resolution of twelve measurements per year between A.D. 1992-1952, and at frequency of four samples per year over the remainder of the coral (Quinn *et al.*, 1998). Using annual density band couplets and stable isotope analysis, dating of the chronology was established back to the year A.D. 1657, making the sequence a very valuable proxy of long-term climate variability from the tropics (Quinn *et al.*, 1998; Dunbar and Cole, 1999; Gagan *et al.*, 2000). Indeed, along with records from the Great Barrier Reef (Australia) and the Galapagos Islands (Ecuador), the record is one of three Pacific coral records to continuously extend beyond A.D. 1700 (Gagan *et al.*, 2000).

The climate of the southwest Pacific in the vicinity of New Caledonia is influenced by annual variations in the relative positions of the belt of sub-tropical lows to the south and the South Pacific Convergence Zone (SPCZ) to the north (Quinn *et al.*, 1998). Rainfall and air temperatures reach a maximum between December and April due to the southward displacement of the SPCZ (Quinn *et al.*, 1998). During the remainder of the year, rainfall and air temperatures decrease in response to the northward migration of the SPCZ (Quinn *et al.*, 1998). Correlation between monthly $\delta^{18}O$ and monthly SSTs, A.D. 1967-1991, was r=0.88 (including the annual cycle which may enhance strength of correlations), with an annual average correlation of 0.57 over the same period (Quinn *et al.*, 1998). On an annual basis for the A.D. 1903-1991 period, a significant correlation of 0.56 was observed between coral $\delta^{18}O$ and SSTs (Quinn *et al.*, 1998).

Seasonal $\delta^{18}O$ variations are mainly controlled by SSTs but variations in salinity may be more important on inter-annual time scales, perhaps accounting for the reduced strength of the relationship on annual time scales (Quinn *et al.*, 1998). However, due to New Caledonia's location near the 'hinge line' separating regions of opposite response in the Southern Oscillation, fluctuations in the region may not correlate as strongly with records derived from areas closer to eastern or western centres of action (Allan, 1988; Glantz *et al.*, 1991; Quinn *et al.*, 1998). Nonetheless, El Niño events which generally correspond to a SST cooling and a decrease in rainfall in the region are registered as less negative $\delta^{18}O$ value in the coral record (Quinn *et al.*, 1998). Conversely, La Niña conditions, associated with SST warming and enhanced rainfall, correspond to a more negative $\delta^{18}O$ signal in the coral geochemistry (Quinn *et al.*, 1998).

3.8.4 Great Barrier Reef, Australia - western Pacific

Eight multi-century, *Porites* coral cores were used by Hendy *et al.* (2003) to develop a 373-year chronology from the Great Barrier Reef, Australia. Using cross-dating techniques adapted from dendrochronology, characteristic patterns of distinct luminescent lines within the coral skeletons were matched between coral cores from inshore and mid-shelf reefs (see Section 4.3.1). Skeleton-plots of luminescent banding were produced for each core and combined into a master chronology back to A.D. 1615. In addition to improving dating control, the luminescence master chronology provides a proxy for Burdekin River runoff associated with Queensland DJF rainfall (Hendy *et al.*, 2003).

The luminescence master chronology is significantly correlated (r=0.82, 1894–1985) with the extended instrumental record of Burdekin River flow and an index of Queensland summer rainfall (r=0.65,1891–1985) (Hendy *et al.*, 2003). The Great Barrier Reef usually experiences reduced summer monsoon rainfall during El Niño years, along with warmer SST anomalies in late summer, and higher surface radiation as a result of reduced cloud cover. The opposite situation occurs in La Niña years when the summer monsoon circulation tends to be more vigorous, leading to above-average rainfall and river flow, lower salinity and higher turbidity of reef waters. Thus, reduced (enhanced) rainfall events associated with El Niños (La Niñas) are generally registered as narrow (wide) bands in the luminescence coral record.

3.9 Ice-Core Data

3.9.1 Quelccaya, Peru

The first long-term tropical ice core records ever recovered came from the Quelccaya ice cap in the southern Andes of Peru (Thompson *et al.*, 1979; Thompson *et al.*, 1984; Thompson *et al.*, 1985; Thompson *et al.*, 1986). Two cores from the summit (5670 m above sea level) provided a 1,500 year history of climate and general environmental conditions including droughts, volcanic activity, moisture sources, temperature, and glacier net balance (Thompson *et al.*, 1985). Annual variations in visible dust layers, dust concentrations, $\delta^{18}O$, conductivity, plus calibration by the identification of an ash layer

from the documented eruption of Huaynaputina (A.D. 1600), permitted accurate dating and time-scale verification (Thompson *et al.*, 1986).

The annual mass balance of this ice cap represents the balance between annual precipitation and radiation (Thompson *et al.*, 1984).The precipitation on Quelccaya originates over the Amazon Basin to the east which is physically linked to sea surface temperature anomalies in the eastern equatorial Pacific (Thompson *et al.*, 1984). The oxygen isotopic composition exhibits an annual cycle with least negative values associated with winter snowfall (Thompson *et al.*, 1986). Major El Niño occurrences on Quelccaya ice cap correspond to periods of substantially reduced snow accumulation (Thompson *et al.*, 1984).

On an annual basis for eight years between 1976-1983, positive SST anomalies in the Puerto Chicama (Niño 1+2) region are significantly correlated (r=0.66) with a decrease in the snow accumulation on Quelccaya (Thompson *et al.*, 1984). Periods of lower mass balance are better correlated with positive SSTs anomalies (r=0.45) than with negative SOI pressure anomalies (r=0.35) (Thompson *et al.*, 1984).The thickness of the annual dust layers may also reflect annual snow accumulation influenced by changes in ENSO behaviour (Thompson *et al.*, 1979; Thompson *et al.*, 1984; Thompson *et al.*, 1986). In general, visible dust layers characteristic of the dry season (July) are associated with high micro particle concentrations, less negative $\delta^{18}O$ ratios and high conductivities (Thompson *et al.*, 1986) Thus, El Niño events are associated with high dust concentrations and more positive $\delta^{18}O$ concentrations while La Niña episodes are characterised by very negative $\delta^{18}O$ levels and thin dust horizons (Thompson *et al.*, 1984; Thompson *et al.*, 1986).

3.10 Documentary Data

3.10.1 Quinn El Niño chronologies

The seminal paper for the historical chronology of El Niño events was that of Quinn *et al.* (1987). Quinn's list of past El Niño events back to A.D. 1525 has been viewed as the major reference for any long-term analysis of ENSO (Ortlieb, 2000). This pioneer paper proposed an intensity scale of events that has been generally adopted by the scientific community working on ENSO and climate variability (Ortlieb, 2000). The

chronology was developed by compiling documentary data dealing with reports of anomalous rainfalls and storm events on the coast of Peru, travel time of ships in the eastern Pacific, or anomalous SST and air-temperature episodes in western South America (Ortlieb and Vargas, 2002). However, it is important to note that the record only documents the El Niño phase of the ENSO phenomenon and excludes La Niña episodes.

The most complete pre-instrumental record of El Niño events from South America is the historical series compiled by Quinn and Neal (1992), hereafter referred to as 'QN92'. This chronology records low SOI events which are associated with unusual climatic events such as failure of the anchovy fisheries or coastal flooding in Peru. El Niño events are classified in seven classes based on very strong, strong, moderate, and weak categories. The QN92 El Niño series updates the Quinn *et al.* (1987) chronology, and includes many more medium to weak events in the earlier part of the record, and it also revised the strength classification for several events.

Subsequently, researchers such as Ortlieb and Machare (1993) questioned the occurrence, magnitude and reliability of some of the events recorded in the South American regional El Niño indices given by QN92. Some authors questioned the occurrence of some of the reconstructed events (A.D. 1525-1900), or the inferred intensity of some other events (Ortlieb, 2000). More recently, Ortlieb (2000) updated the regional South American chronology, by completing the revision of all available documentary sources dealing with climatic anomalies between the 16th to 19th centuries in Peru and southern Ecuador (Ortlieb, 2000).

Through this process, two chronological records of climatic anomalies were established (Ortlieb, 2000). One was considered to be of 'global' relevance, based on all the available data from East Africa and Indian and Pacific Oceans has been (ambiguously) referred to as the 'ENSO Chronology' (Quinn, 1992). Another was called the 'regional El Niño chronology' which was established from eastern Pacific and western South American data (Quinn and Neal, 1992; Ortlieb, 2000).

Only a regional teleconnection signal from the core Eastern Pacific ENSO zone is required for the purposes of this study. To circumvent the biases noted by Whetton *et al.* (1996), a chronology derived purely from South American sources was incorporated. The El Niño record assembled by Ortlieb (2000) was used from A.D. 1525 until 1900

(inclusive). From 1901 onward, the classification reverted to the Quinn and Neal (1992) chronology, continuing on from where the update by Ortlieb (2000) terminates.

As detailed in Chapter 2, SST El Niños are not always synchronous with variations observed from the SOI. From A.D. 1877-1984, Whetton and Rutherfurd (1994) note four (20%) of the 20 strong El Niños and nine (45%) of the 20 weak and moderate El Niños they identified are associated with high or zero SOI where they should be associated with negative SOI. Similarly, during three major periods of negative SOI there were no El Niños. Nevertheless, the QN92 chronology remains the longest, and most extensively studied documentary record of ENSO available, justifying its inclusion in this study.

3.10.2 Nile River flood record, Egypt

Sahelian rainfall is characterised by long period fluctuations, such as the general decline in rainfall since 1960 (Janowiak, 1988). In addition it appears that the rainfall of the region also shows an ENSO signal (Hassan, 1981; Eltahir and Wang, 1999). This signal, which is one of reduced rainfall during El Niño events, appears to be strongest in the east including the region of the Ethiopian highlands (Janowiak, 1988). The Blue Nile rises in these highlands and contributes most of the interannual variability in the Nile discharge (Janowiak, 1988). Whetton and Rutherfurd (1994) report that for the period 1870 to 1986 there is a significant correlation between Nile discharge and the SOI index (r=0.38), and a stronger correlation (r=0.51) if long period fluctuations are removed from the Nile record.

This ENSO signal in Nile flow is of particular interest here because a 1300-year record of Nile flood height is available (Whetton and Rutherfurd, 1994). This record consists of annual maximum and minimum river heights measured on the Nilometer at Roda Island, Cairo, from A.D. 622. Quinn (1992) suggested that the height of the Nile flood forms a 1368 year record of the Southern Oscillation.

The version of the data set used here was supplied by F. Hassan of Washington State University to Whetton and Rutherfurd (*pers comm.*). Hassan (1981) removed the trend in the data due to silting of the Nile's bed, and converted the series from cubits to metres above sea-level. The data is complete from A.D. 622-1470, but from then onwards there are some lengthy gaps, particularly between A.D. 1523 and 1700, and the record terminates at A.D. 1921 (Whetton and Rutherfurd, 1994).

To update the record to A.D. 1986 Whetton and Rutherfurd (1994) used a version of annual discharge for the Nile which employs the discharge measured at Aswan until the building of the Aswan High Dam in A.D. 1964, after which it uses discharge from Dongola upstream of the dam. The Roda flood height data and the discharge data are significantly correlated (r=0.88) for the years of overlap (A.D. 1871-1921) (Whetton and Rutherfurd, 1994). Linear regression estimates of flood height using discharge values were used to update the flood height record to 1986 (Whetton and Rutherfurd, 1994).

Whetton and Rutherfurd (1994) removed the long-period (greater than 10 years) oscillations in the Nile series that obscured the annual and biennial oscillations. This was done by expressing annual variations as anomalies away from an 11-year Gaussian filtered version of the series with the ends of the series padded (Whetton and Rutherfurd, 1994). Estimation of the anomalies was complicated by the periods of missing data in the series before 1824, thus, the smoothed series could only be defined for the periods 1587-1625, 1720-1800, and 1824-1921 (Whetton and Rutherfurd, 1994). The occasional missing value in these periods were filled by the local mean value to produce the smoothed series, and any such filled values were removed from the final differenced series (Whetton and Rutherfurd, 1994).

In general, high Nile levels were found to correspond more strongly to La Niña conditions, while discharge periods were found to periodically coincide with El Niño episodes (see Chapter 5).

3.10.3 Northern China rainfall index

During the 20th century, rainfall fluctuations in northern China have been associated with ENSO (Wang and Zhao, 1981; Wang *et al.*, 2000). As an example, Whetton and Rutherfurd (1994) described an index of northern Chinese rainfall as significantly correlated (r = 0.38) with June-August (wet-season) SOI over the period A.D. 1870-1979. The index used by Whetton and Rutherfurd (1994) was constructed from data in the Chinese Atlas of Floods and Droughts which contains data from A.D 1470 to 1979 (Whetton and Rutherfurd, 1994). The reliability of the atlas is discussed in detail in Wang and Zhao (1981), but in simple terms, the rainfall index classifies annual rainfall at up to 120 stations into classes, based mainly on historical information, supplemented by records of actual rainfall where they exist. The classes range from one (extreme

wetness) to five (extreme dryness). In the atlas index values for each year are both mapped, and given in tabulated form.

In this study, a northern Chinese rainfall index spanning A.D. 1525-1979 was used. The index was calculated from the atlas by averaging data for 49 stations north of the Changjiang (Yangtse) River (which flows west to east across China around 30°N) (Whetton and Rutherfurd, 1994). Of these stations only those having more than 75% of the full record were used (35 in number). The five-point rainfall index was inverted, so that low rainfall was associated with a low value (Whetton and Rutherfurd, 1994). Similar to the Nile flood record, the series was high-pass filtered by Whetton and Rutherfurd (1994) by differencing from a function smoothed using an 11-year Gaussian filter for the purpose of ENSO analysis (Whetton and Rutherfurd, 1994). In general, high rainfall was found to weakly correspond to El Niño episodes, while low discharge periods corresponded more closely with La Niña events.

3.10.4 Indian drought chronology

Sir Gilbert Walker is traditionally associated with significant early attempts at monsoon forecasting in India. The link with Indian rainfall was specific in Walker's original definition of the Southern Oscillation (Walker and Bliss, 1932). Over the past few decades, the search for useful predictive relationships between Indian summer monsoon rainfall and the SOI has continued (Rasmusson and Carpenter, 1983; Nicholls, 1995; Kane, 1998; Torrence and Webster, 1999; Yu *et al.*, 2002; Allan *et al.*, 2003). In El Niño years associated with low SOI values, Indian monsoon rainfall tends to be low, producing droughts. While no continuous time series of Indian rainfall is available prior to the late 18th century (Allan *et al.*, 2002), extensive historical records of drought and famine associated with rainfall are available (Whetton and Rutherfurd, 1994). Using a wide number of sources, Whetton and Rutherfurd (1994) developed a chronology of Indian drought/famine extending back to A.D. 1500 using historical sources for comparison with the Quinn series.

Whetton and Rutherfurd (1994) highlighted that the chronology for the A.D. 1500-1769 is much less reliable than the chronology from A.D. 1770 onwards and is primarily a chronology of famine rather than drought. It is cautioned that some of the famine years before A.D. 1770 may not have been caused by drought, however the problem was described as "unlikely to be serious" (Whetton and Rutherfurd, 1994:232),

as the great majority of famines during the 19th and 20th centuries are known to have been triggered by droughts. As such, the drought chronology presented by Whetton and Rutherfurd (1994) for the A.D. 1525-1982 period is considered useful for El Niño reconstruction in the context of a multiproxy analysis.

3.11 Proxy Data Filtering

3.11.1 Data detrending

The estimated spectrum of a time series shows how the variance of a particular time series is distributed as a function of frequency (Ghil and Yiou, 1996). Depending on the purpose of analysis, some frequencies may be of greater interest than others, and it may be helpful to reduce the amplitude of waves of undesired frequencies by statistically filtering them out before analysing a time series. Thus, before being ready for climate analysis it may be necessary to appropriately filter proxy data for its intended application (Fowler and Boswijk, 2003).

A trend in a time series refers to a slow, gradual change in some property of the series (such as growth-age relationships) over the entire period under investigation. The term trend is sometimes loosely defined as a long term change in the mean (Chatfield, 1975), but can also refer to change in other statistical properties. For example, tree-ring series of measured ring width frequently have a trend in variance as well as mean. The gradual change need not persist indefinitely to be regarded as trend, and indeed is often a part of oscillations with periods long timescales compared to the record (Chatfield, 1975; Zwiers and Von Storch, 2004).

Detrending is a form of filtering that removes this gradual change in some property from a time series. A familiar use of detrending to dendrochronologists is the removal of 'age trend' from measured ring-width series in the production of tree-ring indices (Fritts, 1976; Schweingruber, 1988; Cook and Kairiukstis, 1990; Fritts, 1991). In this sense, detrending is intended to remove a feature thought to distort or obscure the relationships of interest (Fritts, 1976; Cook and Kairiukstis, 1990).

Whether to detrend depends on the data and the purpose of analysis. Sometimes the trend itself is of interest. For example, the trend in long-term temperature records might be used as evidence of global warming. Detrending the temperature records

before analysis of a global temperature trend would thus defeat the purpose. The removal of a trend is appropriate when trend is considered unrelated to the signal of interest. Statistical methods are often used to identify a trend in a given time series. The most straightforward is the fitting of a least squares straight line as a function of time. General approaches to detrending include fitting a negative exponential such as a straight line, or piecewise polynomials such as a cubic smoothing spline (Fritts, 1976; Cook and Peters, 1981; Holmes *et al.*, 1986).

The advantage of a linear approach to detrending is its simplicity, however, a straight line may be unrealistic in restricting the functional form if the trend in mean is assumed to be linear. A much more sophisticated method is found by fitting a cubic smoothing spline of known frequency response. The cubic smoothing spline is widely used in dendrochronology for detrending (Cook and Peters, 1981; Cleaveland *et al.*, 2003; Fowler and Boswijk, 2003; D'Arrigo *et al.*, 2005). Splines are adaptable and easily applied to a wide range of types of 'age trend' or 'growth trend' found in tree-ring data. The application of the spline to dendrochronology was first proposed by Cook and Peters (1981), who derived a useful relationship for the spline parameter p as a function of the 50% frequency response, that is, the frequency at which the amplitude of the frequency response of the spline is 0.50 (see Figure 3.10).

The frequency response of the detrending function describes the effect that detrending has on the original series. The frequency response of a spline is high for those frequencies tracked closely by the spline (Fowler and Boswijk, 2003). In the subsequent removal of the trend line, these frequencies are mostly removed. Frequencies at which the frequency response of the spline is high are therefore those at which the spectrum of the detrended series is low. In general, at the lowest frequencies, the spectrum of the detrended series will be diminished relative to the spectrum of the original data (Cook and Peters, 1981). The more flexible the spline, the higher the frequency-range affected by the detrending (Fowler and Boswijk, 2003).

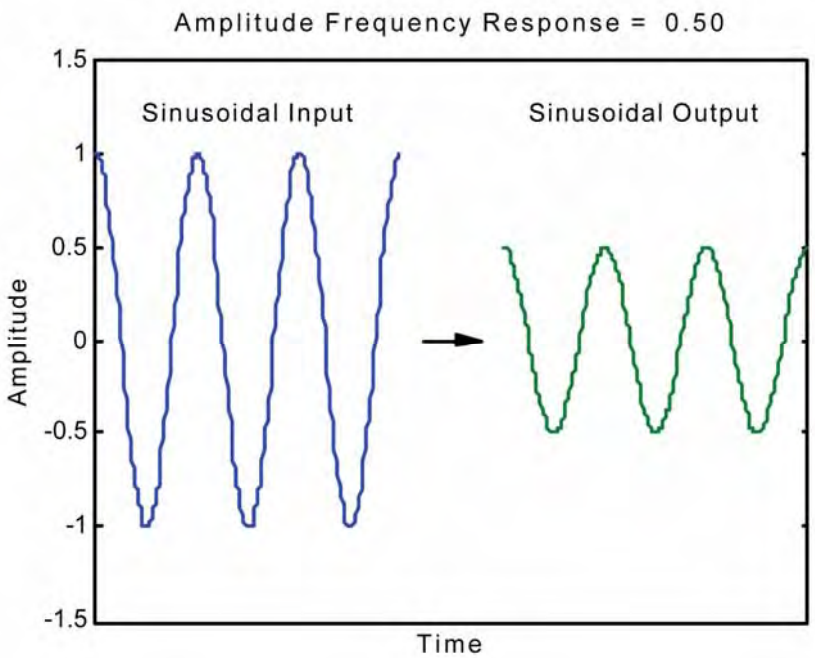

Figure 3.10. Effect on a sine wave of filtering by a filter with 0.50 amplitude of frequency response at the wavelength of the sinusoid. **Source:** Meko, 2002 (http://www.ltrr.arizona.edu/~dmeko/).

3.11.2 Tree-ring standardisation

For tree-ring analyses the standardisation process involves fitting a curve to the ring-width series (detrending) and then dividing or subtracting each ring-width value by the corresponding detrended curve values (Holmes *et al.*, 1986; Cook and Kairiukstis, 1990). The chronology then represents the departure of growth for a given year in relation to the 'expected' mean value for a given year, and is expressed as a four digit integer with 1000 representing the long-term mean (Holmes *et al.*, 1986; Cook and Kairiukstis, 1990). Thus, higher or lower values for a given year represent proportionally higher or lower tree growth years for that year, which is then used to interpret a proxy environmental signal in the data (Holmes *et al.*, 1986; Cook and Kairiukstis, 1990).

Once a trend line has been fitted to the data, that line may be regarded as representing the trend. For the purpose of standardization, there are two options available for the removal of a given trend. The first is to subtract the value of the trend line from the original data, giving a time series of residuals from the trend (Holmes *et al.*, 1986). This 'difference' option is attractive for its simplicity and gives a convenient breakdown of the variance. The residual series is in the same units as the original series, and the total sum

of squares of the original data can be expressed as the trend sum-of-squares and residual sum-of-squares (Holmes *et al.*, 1986).

The 'ratio' option is often more appropriate for some kinds of data because the ratio is dimensionless, and the ratio operation tends to remove any trend in the variance that might accompany trend in mean (Holmes *et al.*, 1986). Tree-ring width is one such data type. The variance of ring width tends to be high when mean ring width is high, and low when mean ring width is low (Holmes *et al.*, 1986). To allow high frequency variability associated with ENSO events to be inferred, 20-year splines (using the 'ratio' method for indexing) were applied to tree-ring records using the dendrochronology program ARSTAN (Cook and Peters, 1981; Holmes *et al.*, 1986).

All tree-ring sequences listed in Table 3.1 (except the Berlage Teak record) were standardised using the program ARSTAN (Holmes *et al.*, 1986) to remove the effects of biological growth for climate analysis. Tree-ring data was filtered using a smoothing spline with 50% variance cut off at 20 years, suitable for high-frequency ENSO analysis, precluding the analysis of low frequency trends (Fowler and Boswijk, 2003). To overcome any site specific bias in individual locations, all standardised series available for a given species were next combined into tree means and then averaged to produce a regional 'master chronology' using the tree-ring chronology development software of Fowler and Boswijk (2003).

The Berlage Teak record used in this study is a version of the Berlage (1931) chronology modified by Murphy and Whetton (1989). Biological trends in the tree-ring series were removed using a linear-logarithmic approximation to produce a tree-ring index series with approximately zero mean (Murphy and Whetton, 1989). The tree-ring index was then filtered to remove long-period fluctuations using a 11-year Gaussian filter, as was done for the Nile and North Chinese Rainfall records (also supplied by Whetton and Rutherfurd (*pers comm.*)).

3.11.3 Coral and ice data filtering

Unlike tree-ring data, coral records do not appear to show any significant trends in geochemical tracers due to upward growth in the water column, changes in growth rates or colony age (Hendy, *pers comm.*). As such, there is no need to extract the signal of interest from any other influences related to factors such as biological growth in trees by the processes of detrending detailed in Section 4.7. Similarly, for the only ice core

record used (Quelccaya, Peru), analysis was confined to net accumulation rates for the upper profile (post A.D. 1500) where dating errors due to factors such as compression are estimated to be a very low (±2 years) (Thompson *et al.*, 1986). The core stratigraphy was further constrained by annual variations in micro-particles, oxygen isotopes and the presence of a prominent volcanic ash layer, increasing confidence in the accuracy of the dating (Thompson *et al.*, 1986).

Differences in the length of coral records resulted in a short base period of thirty years between 1931-1960, which was inconsistent with the base periods of the instrumental data used (see Chapter 2). As a result, absolute values of the various coral isotopic indices (rather than data normalised relative to a given period's mean and standard deviation characteristics) were used to allow the assessment of long-term trends contained within the coral records (Tudhope *et al.*, 2001; Lough, 2004). Consequently, it was only necessary to high-pass filter the absolute data to reduce low frequencies that may obscure high-frequency variability.

Since ENSO events generally last for one or two years, proxy records were high-pass filtered to remove longer period fluctuations in the data that would obscure annual fluctuations, necessarily excluding the analysis of low frequency (decadal-centennial) ENSO trends. In an effort to be consistent with approaches designed for high frequency ENSO analysis noted elsewhere in the relevant proxy literature (Whetton and Rutherfurd, 1994; Diaz and Markgraf, 2000; Linsley *et al.*, 2004; Lough, 2004; D'Arrigo *et al.*, 2005), all coral records were smoothed using a three-year high-pass Gaussian filter. This results in the exclusion of frequencies greater than three years from the data, facilitating the investigation of discrete ENSO events. The only ice core record used in this analysis (Quelccaya, Peru) was similarly filtered in line with the treatment of the coral data and previous studies (Diaz and Markgraf, 2000; Goodwin *et al.*, 2004)

A Gaussian filter has a response curve that approximates an ideal Gaussian distribution (Chatfield, 1975). The Gaussian filter is derived by setting the weights equal to the ordinates of the Gaussian (normal) probability density function (Chatfield, 1975). Similar to splines, the Gaussian filter is particularly convenient because the standard deviation of the appropriate normal distribution can be specified in terms of the 50% frequency response of the filter (Chatfield, 1975).

3.12 Summary

This Chapter provides an overview of the type of proxy records (tree-ring, coral, ice and documentary records) used in this thesis. Details of specific ENSO signals and potential weaknesses in each of the proxies used were discussed, highlighting the need for a multiproxy approach to ENSO reconstruction. Finally, implications of proxy data filtering was reviewed as a prelude to the climate analyses presented in Chapters 4-6.

3.13 References

Allan, R. (1988). El Niño Southern Oscillation influences in the Australasian Region. *Processes in Physical Geography* **12**: 4-40.

Allan, R. and D'Arrigo, R. (1999). 'Persistent' ENSO sequences: how unusual was the 1990-1995 El Niño ? *The Holocene* **9** (1): 101-118.

Allan, R., Lindsay, J. and Parker, D. (1996). *El Niño Southern Oscillation and climate variability.* Melbourne, Australia, CSIRO.

Allan, R., Reason, C., Carroll, P. and Jones, P. (2002). A reconstruction of Madras (Chennai) mean sea level pressure using instrumental records from the late 18th and early 19th centuries. *International Journal of Climatology* **22:**1119-1142.

Allan, R., Reason, C., Lindesay, J. and Ansell, T. (2003). Protracted ENSO episodes and their impacts in the Indian Ocean region. *Deep Sea Research Part II* **50** (12-13): 2331–2347.

Bagnato, S., Linsley, B., Howe, S., Wellington, G. and Salinger, J. (2004). Evaluating the use of the massive coral *Diploastrea heliopera* for palaeoclimate reconstruction. *Palaeoceanography* **19** (PA1032): 1-12.

Baumgartner, T., Michaelsen, J., Thompson, L., Shen, G., Soutar, A. and Casey, R. (1989). The recording of interannual climatic change by high-resolution natural systems: tree rings, coral bands, glacial ice layers and marine varves. *Aspects of Climate Variability in the Pacific and Western Americas. Geophysical Monograph*. D. Peterson. Washington, American Geophysical Union. **55:** 1-14.

Berlage, H. (1931). On the relationship between thickness of tree rings of Djati and rainfall on Java. *Tectona* **24**: 939-953.

Boswijk, G., Fowler, A. and Ogden, J. (2002). Tree Ring Chronologies of New Zealand, 1: Kauri (Agathis australis), Living and recently dead trees. School of Geography and Environmental Science, University of Auckland Occasional Paper 44. Auckland: 1-113.

Boswijk, G., Fowler, A., Lorrey, A., Palmer, J., and Ogden, J. (2006). Extension of the New Zealand Kauri (Agathis australis) chronology to 1724 BC. *The Holocene* **16** (2): 188-199.

Bradley, R., Vuille, M., Hardy, D. and Thompson, L. (2003). Low latitude ice cores record Pacific sea surface temperatures. *Geophysical Research Letters* **30** (4): 23/1-23/4.

Briffa, K. (2000). Annual climate variability in the Holocene: interpreting the message of ancient trees. *Quaternary Science Reviews* **19**: 87-105.

Buckley, B., Ogden, J., Palmer, J., Salinger, J. and Fowler, A. (2000). Dendroclimatic interpretation of tree-rings in Agathis australis (Kauri) 1; Climatic correlation functions and master chronology. *Journal of the Royal Society of New Zealand* **30** (3): 263-275.

Chatfield, C. (1975). *The analysis of time series: theory and practice*. London, Chapman and Hall.

Cleaveland, M., Cook, E. and Stahle, D. (1992). Secular variability of the Southern Oscillation detected in tree-ring data from Mexico and the southern United States. *El Niño: Historical and Palaeoclimatic Aspects of the Southern Oscillation.* H. Diaz and V. Markgraf. Cambridge, Cambridge University Press: 271–291.

Cleaveland, M., Stahle, D., Therrell, M., Villanueva-Diaz, J. and Burns, B. (2003). Tree-ring Reconstructed Winter Precipitation and Tropical Teleconnections in Durango, Mexico. *Climatic Change* **59**: 369–388.

Cobb, K., Charles, C., Cheng, H. and Edwards, L. (2003). El Niño/Southern Oscillation and tropical Pacific climate during the last millennium. *Nature* **424**: 271-276.

Cobb, K., Charles, C. and Hunter, D. (2001). A central tropical Pacific coral demonstrates Pacific, Indian, and Atlantic decadal climate connections. *Geophysical Research Letters* **28** (11): 2209-2212.

Cole, J., Dunbar, R., Mc Clanahan, T. and Muthiga, N. (2000). Tropical Pacific forcing of decadal SST variability in the Western Indian Ocean over the past two centuries. *Science* **287** (5453): 617-619.

Cole, J., Fairbanks, R. and Shen, G. (1993). Recent variability in the Southern Oscillation; isotopic results from a Tarawa atoll coral. *Science* **260**: 1790-1793.

Cook, E., Briffa, K., Meko, D., Graybill, A. and Funkhouser, G. (1995). The 'segment length curse' in long tree-ring chronology development for palaeoclimatic studies. *The Holocene* **5** (2): 229-237.

Cook, E., D'Arrigo, R., Cole, J., Stahle, D. and Villalba, R. (2000a). Tree-ring records of past ENSO variability and forcing. *El Niño and the Southern Oscillation; Multiscale Variability*

and Global and Regional Impact. H. Diaz, and Markgraf, V. New York, Cambridge University Press: 297-323.

Cook, E., Buckley, B., D'Arrigo, R., and Peterson, M. (2000b). Warm-season temperatures since 1600 BC reconstructed from Tasmanian tree rings and their relationship to large-scale sea surface temperature anomalies. *Climate Dynamics* **16**: 79-91.

Cook, E. and Kairiukstis, L. (1990). *Methods of Dendrochronology.* Dordrecht, The Netherlands, Kluwer Academic Publishers.

Cook, E., Palmer, J., Cook, B., Hogg, A. and D'Arrigo, R. (2002). A multi-millennial palaeoclimatic resource from *Lagarostrobos colensoi* tree-rings at Oroko Swamp, New Zealand. *Global and Planetary Change* **33**: 209-220.

Cook, E. and Peters, K. (1981). The smoothing spline: a new approach to standardizing forest interior tree-ring width series for dendroclimatic studies. *Tree Ring Bulletin* **41**: 45-53.

Cook, E., Woodhouse, C., Eakin, M., Meko, D. and Stahle, D. (2004). Long-Term Aridity Changes in the Western United States. *Science* **306**: 1015-1018.

Correge, T., Delcroix, T., Recy, J., Beck, W., Cabioch, G. and Le Cornec, F. (2000). Evidence for stronger El Niño-Southern Oscillation (ENSO) events in a mid-Holocene massive coral. *Palaeoceanography* **15** (4).

D'Arrigo, R., Cook, E., Wilson, R., Allan, R. and Mann, M. (2005). On the variability of ENSO over the past six centuries. *Geophysical Research Letters* **32** (L03711): 1-4.

D'Arrigo, R. and Jacoby, G. (1991). A thousand year record of north-western New Mexico winter precipitation reconstructed from tree rings and its relation to El Niño and the Southern Oscillation. *The Holocene* **1/2**: 95–101.

D'Arrigo, R., Jacoby, G. and Krusic, P. (1994). Progress in Dendroclimatic Studies in Indonesia. *Terrestrial, Atmospheric and Oceanographic Sciences* **5**: 349-363.

Diaz, H., Hoerling, M. and Eischieid, J. (2001). ENSO Variability, Teleconnections and Climate Change. *International Journal of Climatology* **21**: 1845-1862.

Diaz, H. and Markgraf, V. (2000). *El Niño and the Southern Oscillation; Multiscale Variability and Global and Regional Impacts.* Cambridge, Cambridge University Press.

Druffel, E. (1997). Geochemistry of corals: Proxies of past ocean chemistry, ocean circulation, and climate. *Proceedings of the National Academy of Sciences* **94**: 8354-8361.

Dunbar, R. and Cole, J. (1999). *Annual Records of Tropical Systems (ARTS); Recommendations for Research.* Geneva, Switzerland, IGBP Science Series.

Dunbar, R., Wellington, G., Colgan, M. and Glynn, P. (1994). Eastern Pacific sea surface temperature since 1600 A.D: the $\delta^{18}O$ record of climate variability in Galapagos corals. *Palaeoceanography* **9**: 291–316.

Eltahir, E. and Wang, G. (1999). Nilometers, El Niño and Climate Variability. *Geophysical Research Letters* **26** (4): 489-492.

EPICA, C. M. (2004). Eight glacial cycles from an Antarctic ice core. *Nature* **429**: 623-628.

Esper, J., Cook, E. and Schweingruber, F. (2002). Low-frequency signals in long tree-ring chronologies for reconstructing past temperature variability. *Science* **295**: 2250-2253.

Evans, M., Fairbanks, R. and Rubenstone, J. (1998). A proxy index of ENSO teleconnections. *Nature* **394**: 732-733.

Evans, M. and Schrag, D. (2004). A stable isotope-based approach to tropical dendroclimatology. *Geochimica et Cosmochimica Acta,* **68** (16): 3295-3305.

Fairbanks, R., Evans, M., Rubenstone, J., Mortlock, R., Broad, K., Moore, M. and Charles, C. (1997). Evaluation of climate indices and their geochemical proxies measured in corals. *Coral Reefs* **16** (Supplement): S93-S100.

Fenwick, P. (2003). Reconstruction of past climates using Pink Pine (*Halocarpus biformis*) tree-ring chronologies. Christchurch, New Zealand, Soil Plant and Ecological Sciences, Linclon University.

Fiedel, S., Southon, J. and Brown, T. (1995). The GISP ice core record of volcanism since 7000 B.C. *Science* **267** (5195): 256-258.

Fisher, D. (2002). High-resolution multiproxy climatic records from ice cores, tree-rings, corals and documentary sources using eigenvector techniques and maps: assessment of recovered signal and errors. *The Holocene* **12** (4): 401-419.

Folland, C., Karl, T., Christy, J., Clarke, R., Gruza, G., Jouzel, J., Mann, M., Oerlemans, J., Salinger, M. and Wang, S. (2001). Observed Climate Variability and Change. *Climate Change 2001: The Scientific Basis. Contribution of Working Group 1 to the Third Assessment Report of the Intergovernmental Panel on Climate Change.* J. Houghton, Y. Ding, D. Griggs *et al.* United Kingdom and New York, Cambridge University Press.

Fowler, A. (2005). Mean sea-level pressure composite mapping dendroclimatology: advocacy and an Agathis australis (Kauri) case study. *Climate Research*: 73-84.

Fowler, A. and Boswijk, G. (2003). Chronology stripping as a tool for enhancing the statistical quality of tree-ring chronologies. *Tree Ring Research* **59** (2): 53-62.

Fowler, A., Boswijk, G., Gergis, J. and Lorrey, A. (2005a). Insights into 422 years of ENSO history from *Agathis australis* (Kauri) tree-rings. *International Journal of Climatology*: *in prep*.

Fowler, A., Boswijk, G. and Ogden, J. (2004). Tree-ring studies on Agathis australis (Kauri): a synthesis of development work on Late Holocene chronologies. *Tree Ring Research* **60** (1): 15-29.

Fowler, A., Lorrey, A. and Crossley, P. (2005b). Seasonal growth characteristics of Kauri. *Tree Ring Research* **61** (1): 3–19.

Fowler, A., Palmer, J., Salinger, J. and Ogden, J. (2000). Dendroclimatic interpretation of tree-rings in Agathis australis (Kauri) 2; Evidence of a significant relationship with ENSO. *Journal of Royal Society of New Zealand* **30** (3): 277-292.

Fritts, H. (1976). *Tree Rings and Climate*. London, Academic Press Inc.

Fritts, H. (1991). *Reconstructing Large-Scale Climatic Patterns from Tree-Ring Data; A Diagnostic Analysis*. Tucson, USA, University of Arizona Press.

Gagan, M., Ayliffe, L., Beck, J., Cole, J., Druffel, E., Dunbar, R. and Schrag, D. (2000). New views of tropical palaeoclimates from corals. *Quaternary Science Reviews* **19**: 45-64.

Gagan, M., Hendy, E., Haberle, S. and Hantoro, W. (2004). Post-glacial evolution of the Indo-Pacific Warm Pool and El Niño-Southern oscillation. *Quaternary International* **2004** (118-119): 127-143.

Garcia Herrera, R., Garcia, R., Rosario Prieto, M., Hernandez, E., Gimeno, L., and Daz, H. (2003). The use of Spanish historical archives to reconstruct climate variability. *Bulletin of the American Meteorological Society* **84**: 1025-1035.

Gedalof, Z. and Mantua, N. (2002). A multi-century perspective of variability in the Pacific Decadal Oscillation: new insights from tree rings and coral. *Geophysical Research Letters* **29** (24): 57/1-57/3.

Gergis, J., Boswijk, G. and Fowler, A. (2004a). An update of modern Northland Kauri (*Agathis australis*) tree-ring chronologies 1: Puketi State Forest. New Zealand tree-ring Site Report No.12, School of Geography and Environmental Science Working Paper 12, University of Auckland, New Zealand.

Gergis, J., Boswijk, G. and Fowler, A. (2004b). An update of modern Northland Kauri (*Agathis australis*) tree-ring chronologies 2: Trounson Kauri Park. New Zealand tree-ring Site Report No.13, School of Geography and Environmental Science Working Paper 13, University of Auckland, New Zealand.

Gergis, J. and Fowler, A. (2005a). Classification of synchronous oceanic and atmospheric El Niño-Southern Oscillation (ENSO) events for palaeoclimate reconstruction. *International Journal of Climatology* **25**: 1541–1565.

Gergis, J. and Fowler, A. (2005b). How unusual was late Twentieth Century El Niño-Southern Oscillation (ENSO)? Assessing evidence from tree-ring, coral, ice and documentary archives, A.D. 1525-2002. *Advances in Geosciences*: *in review*.

Gergis, J., Fowler, A., Braganza, K., Mooney, S. and Risbey, J. (2005b). El Niño-Southern Oscillation (ENSO) since A.D. 1525: integrating evidence from tree-ring, coral, ice core and documentary archives. *PAGES 2nd Open Science Meeting: Palaeoclimate, Environmental Sustainability and Our Future*, August 10-12, Beijing, China.

Gergis, J., Fowler, A., Braganza, K., Risbey, J. and Mooney, S. (2005c). Multiproxy approaches to El Niño-Southern Oscillation (ENSO) reconstruction; integrating evidence from tree-ring, coral, ice and documentary archives, A.D. 1525-2002. *Reconstructing Past Climates for Future Prediction: Integrating High-Resolution Palaeo Data for Meaningful Prediction in the Australasian Region*, June 27-28, Canberra, Australia.

Gergis, J., Fowler, A. and Mooney, S. (2004c). A Multiproxy Analysis of El Niño Southern Oscillation (ENSO) Variability. *1st International CLIVAR Science Conference: Understanding and Predicting Our Climate System*, June 21-25, 2004, Baltimore, Maryland, USA.

Gergis, J., Fowler, A. and Mooney, S. (2005d). A Multiproxy Analysis of El Niño-Southern Oscillation Variability. *1st Alexander Von Humboldt International Conference on the El Niño Phenomenon and its Global Impact*, 16-20 May, 2005, Guayaquil, Ecuador, European Geophysical Union pp 35-36.

Ghil, M. and Yiou, P. (1996). Spectral Methods: what they can and cannot do for climatic time series. *Decadal Climate Variability: Dynamics and Predictability.* D. Anderson and J. Willebrand. Berlin, Elsevier: 1-31.

Glantz, M., Katz, R. and Nicholls, N. (1991). *Teleconnections linking worldwide climate anomalies: scientific basis and societal impact.* Cambridge, Cambridge University Press.

Goodwin, I., van Ommen, T., Curran, M. and Mayeweski, P. (2004). Mid latitude winter climate variability in the South Indian and southwest Pacific regions since 1300 A.D. *Climate Dynamics* **22**: 783-794.

Grove, R. and Chappell, J. (2000). El Niño chronology and the history of global crises during the Little Ice Age. *El Niño- History and Crisis*. R. Grove and J. Chappell. Cambridge, The White Horse Press: 5-34.

Guilderson, T. and Schrag, D. (1999). Reliability of coral isotope records from the western Pacific warm pool: A comparison using age-optimized records. *Palaeoceanography* **14** (4): 457-464.

Hassan, F. (1981). Historical Nile Floods and Their Implications for Climatic Change. *Science* **212**: 1142-1145.

Hendy, E., Gagan, M., Alibert, C., Mc Culloch, M., Lough, J. and Isdale, P. (2002). Abrupt Decrease in Tropical Pacific Sea Surface Salinity at End of Little Ice Age. *Science* **295** (5559): 1511-1514.

Hendy, E., Gagan, M. and Lough, J. (2003). Chronological control of coral records using luminescent lines and evidence for non-stationarity ENSO teleconnections in north-eastern Australia. *The Holocene* **13** (2): 187-199.

Holmes, R., Adams, R. and Fritts, H. (1986). Users manual for program ARSTAN. *Tree-ring chronologies of western North America: California, eastern Oregon and northern Great Basin*. Tucson, University of Arizona: 50-65.

Janowiak, J. (1988). An investigation of inter-annual rainfall variability in Africa. *Journal of Climate* **1**: 240-179.

Jones, P. and Mann, M. (2004). Climate over past millennia. *Review of Geophysics* **42**: 1-42.

Kane, R. (1998). Extremes of the ENSO phenomenon and Indian summer monsoon rainfall. *International Journal of Climatology* **18**: 775-791.

Kiladis, G. and Diaz, H. (1989). Global climatic anomalies associated with extremes in the Southern Oscillation. *Journal of Climate* **2**: 1069-1090.

Lamb, S. (1982). *Climate, History and the Modern World.* London, Routledge.

Lara, A. and Villalba, R. (1993). A 3620 year temperature record from Fitzroya cupressoides tree rings in southern South America. *Science* **260**: 1104-1106.

Linsley, B., Ren, L., Dunbar, R. and Howe, S. (2000a). El Niño Southern Oscillation (ENSO) and decadal-scale climate variability at 10N in the eastern Pacific from 1893 to 1994: A coral-based reconstruction of from Clipperton Atoll. *Palaeoceanography* **15** (3): 322-335.

Linsley, B., Wellington, G. and Schrag, D. (2000b). Decadal Sea Surface Temperature Variability in the Subtropical South Pacific from 1726 to 1997 A.D. *Science* **290**: 1145-1149.

Linsley, B., Wellington, G., Schrag, D., Ren, L., Salinger, J. and Tudhope, A. (2004). Geochemical evidence from corals for changes in the amplitude and spatial pattern of

South Pacific interdecadal climate variability over the last 300 years. *Climate Dynamics* **22**: 1-11.

Lough, J. (2004). A strategy to improve the contribution of coral data to high-resolution palaeoclimatology. *Palaeogeography, Palaeoclimatology, Palaeoecology* **204**: 115-143.

Lough, J. and Fritts, H. (1985). The Southern Oscillation and tree rings: 1600–1961. *Journal of Climate and Applied Meteorology* **24**: 952–966.

Mann, M., Bradley, R. and Hughes, M. (1998). Global-scale temperature patterns and climate forcing over the past six centuries. *Nature* **392**: 779-787.

Mann, M., Bradley, R. and Hughes, M. (2000). Long-term variability in the El Niño/Southern Oscillation and associated teleconnections. *El Niño and the Southern Oscillation; Multiscale Variability and Global and Regional Impacts.* H. Diaz, and Markgraf, V. Cambridge, Cambridge University Press: 327-372.

Markgraf, V. and Diaz, H. (2000). The past-ENSO record; A Review. *El Niño and the Southern Oscillation; Multiscale Variability and Global and Regional Impacts*. V. Markgraf, Diaz, H. New York, Cambridge University Press: 465-488.

Mc Gregor, H. and Gagan, M. (2004). Western Pacific coral $\delta^{18}O$ records of anomalous Holocene variability in the El Niño-Southern Oscillation. *Geophysical Research Letters* **31**: L11204/1-L11204/4.

Meko, D. (1992). Spectral properties of tree-ring data in the United States Southwest as related to El Niño/Southern Oscillation. *El Niño: Historical and Palaeoclimatic Aspects of the Southern Oscillation.* H. Diaz and V. Markgraf. Cambridge, Cambridge University Press: 349–375.

Michaelsen, J. and Thompson, L. (1992). A comparison of proxy records of El Niño/Southern Oscillation. *El Niño: Historical and Palaeoclimatic Aspects of the Southern Oscillation.* H. Diaz and V. Markgraf. Cambridge, Cambridge University Press: 7–28.

Moberg, A., Sonechkin, D., Holmgren, K., Datsenko, N. and Karlen, W. (2005). Highly variable Northern Hemisphere temperature reconstructed from low and high resolution proxy data. *Nature* **433**: 613-617.

Mullan, A. (1995). On the linearity and stability of Southern Oscillation-climate relationships for New Zealand. *International Journal of Climatology* **15**: 1365-1386.

Murphy, J. and Whetton, P. (1989). A re-analysis of a tree-ring chronology from Java. *Proceedings of the Koninklijke Nederlandse Akademie van Wetenschappen (Dendrochronology)* **Proceedings B 92** (3): 241-257.

Nash, M. (2002). *El Niño; Unlocking the Secrets of the Master Weather-Maker*. New York, Warner Books Inc.

Nicholls, N. (1995). All-India summer monsoon rainfall and sea surface temperatures around northern Australia and Indonesia. *Journal of Climate* **8**: 1463-1467.

Nowlin, W. and Klinck, J. (1986). The physics of the Antarctic circumpolar current. *Reviews of Geophysics* **24**: 469-491.

Oerlemans, J. (2005). Extracting a Climate Signal from 169 Glacier Records. *Science* **308**: 375-677.

Ogden, J., Wilson, A., Hendy, C. and Newnham, R. (1992). The Late Quaternary history of Kauri (Agathis australis) in New Zealand and its climatic significance. *Journal of Biogeography* **19**: 611-622.

Ortlieb, L. (2000). The documentary historical record of El Niño events in Peru: An update of the Quinn record (sixteenth through nineteenth centuries). *El Niño and the Southern Oscillation: Variability, Global and Regional Impacts*. H. Diaz and V. Markgraf. Cambridge, Cambridge University Press: 207-295.

Ortlieb, L. and Macharé, J. (1993). Former El Niño events: records from western South America. *Global and Planetary Change* **7**: 181–202.

Overpeck, J. and Trenberth, K. (2003). A multi-millennia perspective on drought and implications for the future. *CLIVAR/PAGES/IPCC Workshop A multi-millennia perspective on drought and implications for the future*, Tucson.

Pelejero, C., Calvo, E., McCulloch, M., Marshall, J., Gagan, M., Lough, J. and Opdyke, B. (2005). Preindustrial to modern interdecadal variability in coral reef pH. *Science* **309**: 2204-2207.

Poussart, P., Evans, M. and Schrag, D. (2004). Resolving seasonality in tropical trees: multi-decade, high-resolution oxygen and carbon isotope records from Indonesia and Thailand. *Earth and Planetary Science Letters* **218**: 301-316.

Quinn, T., Crowley, T., Taylor, F., Henin, C., Joannot, P. and Join, Y. (1998). A multi-century stable isotope record from a New Caledonia coral: Interannual and decadal SST variability in the southwest Pacific since 1657. *Palaeoceanography* **13** (4): 412-426.

Quinn, W. (1992). A study of Southern Oscillation-related climate activity for A.D 622-1900 incorporating Nile River flood data. *El Niño: Historical and Palaeoclimatic Aspects of the Southern Oscillation*. H. Diaz, and Markgraf, V. Cambridge, Cambridge University Press.: 119-149.

Quinn, W. and Neal, V. (1992). The historical record of El Niño events. *Climate Since A.D 1500*. R. Bradley and P. Jones. London, Routledge.: 623–648.

Quinn, W., Neal, V. and Antunez de Mayola, S. (1987). El Niño occurrences over the past four and a half centuries. *Journal of Geophysical Research* **92** (C13): 14449–14461.

Rasmusson, E. and Carpenter, T. (1983). The relationship between eastern equatorial Pacific sea surface temperatures and rainfall over India and Sri Lanka. *Monthly Weather Review* **111**: 517-528.

Roig, F., Le-Quesne, C., Boninsegna, J., Briffa, K., Lara, A., Jones, P. and Villagrans, C. (2001). Climate Variability 50 000 years ago in mid-latitude Chile as reconstructed from tree rings. *Nature* **410**: 567-570.

Ropelewski, C. and Halpert, M. (1989). Precipitation patterns associated with the high index phase of the Southern Oscillation. *Journal of Climate* **2**: 268-284.

Salinger, J. and Mullan, A. (1999). New Zealand climate: temperature and precipitation variations and their links with atmospheric circulation 1930-1994. *International Journal of Climatology* **19**: 1049-1071.

Salinger, M., Renwick, J. and Mullan, A. (2001). Interdecadal Pacific Oscillation and South Pacific Climate. *International Journal of Climatology* **21**: 1705-1721.

Salmon, J. (1980). *The Native Trees of New Zealand.* Wellington, New Zealand, Reed Methuen.

Schweingruber, F. (1988). *Tree Rings. Basics and Applications of Dendrochronology.* Dordrecht, The Netherlands, Kluwer Academic Press.

Shindell, D., Schmidt, G., Mann, M., Rind, D. and Waple, A. (2001). Solar Forcing of Regional Climate Change During the Maunder Minimum. *Science* **294**: 2149-2152.

Shindell, D., Schmidt, G., Miller, R. and Mann, M. (2003). Volcanic and Solar Forcing of Climate Change during the Preindustrial Era,. *Journal of Climate* **16**: 4094-4107.

Stahle, D. and Cleaveland, M. (1993). Southern Oscillation extremes reconstructed from tree rings of the Sierra Madre Occidental and southern Great Plains. *Journal of Climate* **6**: 129–140.

Stahle, D., D'Arrigo, R., Krusic, P., Cleaveland, M., Cook, E., Allan, R., Cole, J., Dunbar, R., Therrell, M., Gay, D., Moore, M., Stokes, M., Burns, B., Villanueva-Diaz, J. and Thompson, L. (1998). Experimental dendroclimatic reconstruction of the Southern Oscillation. *Bulletin of the American Meteorological Society* **79** (10): 2137-2152.

Thompson, L. (2000). Ice core evidence for climate change in the Tropics: Implications for our future. *Quaternary Science Reviews* **19**: 19-35.

Thompson, L., Hastenrath, S. and Morales Arnao, B. (1979). Climatic ice core records from the tropical Quelccaya ice cap. *Science* **203**: 1240-1243.

Thompson, L., Henderson, K., Mosley-Thompson, E. and Lin, P. (2000a). The Tropical Ice Core Record of ENSO. *El Niño and the Southern Oscillation: Multiscale Variability and Global and Regional Impacts.* H. Diaz and V. Markgraf. Cambridge, Cambridge University Press.

Thompson, L., Mosley-Thompson, E., Bolzan, J. and Koci, B. (1985). A 1500 year record of tropical precipitation in ice cores from the Quelccaya ice cap, Peru. *Science* **229**: 971-973.

Thompson, L., Mosley-Thompson, E., Dansgaard, W. and Grootes, P. (1986). The Little Ice Age as recorded in the stratigraphy of the tropical Quelccaya ice cap. *Science* **234**: 361-364.

Thompson, L., Mosley-Thompson, E., Davis, M., Henderson, K., Brecher, H., Zagorodnov, V., Mashiotta, T., Lin, P., Mikhalenko, V., Hardy, D. and Beer, J. (2002). Kilimanjaro ice core records: evidence of Holocene climate change in tropical Africa. *Science* **298**: 589-593.

Thompson, L., Mosley-Thompson, E. and Henderson, K. (2000b). Ice-core palaeoclimate records in tropical South America since the Last Glacial Maximum. Journal of Quaternary Science **15** (4): 377-394.

Thompson, L., Mosley-Thompson, E. and Morales Arnao, B. (1984). El Niño-Southern Oscillation events recorded in stratigraphy of the tropical Quelccaya Ice Cap. *Science* **276**: 50-52.

Torrence, C. and Webster, P. (1999). Interdecadal changes in the ENSO–monsoon system. *Journal of Climate* **12**: 2679-2690.

Tudhope, A., C., C., Mc Culloch, M., Cook, E., Chappell, J., R., E., Lea, D., Lough, J. and Shimmield, G. (2001). Variability in the El Niño Southern Oscillation through a glacial-interglacial cycle. *Science* **291**: 1511-1517.

Urban, F., Cole, J. and Overpeck, J. (2000). Influence of mean climate change on climate variability from a 155-year tropical Pacific coral record. *Nature* **407**: 989-993.

Walker, G., and Bliss, E. (1932). World Weather V. *Mem. Royal Meteorological Society,* **4**(36): 53–84.

Wang, B., Wu, R. and Fu, X. (2000). Pacific–East Asian Teleconnection: How Does ENSO Affect East Asian Climate? *Journal of Climate* **13** (1517-1536).

Wang, S. and Zhao, Z. (1981). Droughts and floods in China,1470–1979. *Climate and History*. T. Wigley, M. Ingrasham and G. Farmer, Cambridge University Press: 171–288.

Watanabe, T., Gagan, M., Correge, T., Scott-Gagan, H., Cowley, J. and Hantoro, W. (2003). Oxygen isotope systematics in Diploastrea heliopera: new coral archive of tropical palaeoclimate. *Geochimica et Cosochimica Acta* **67** (7): 1349-1358.

Whetton, P., Allan, R. and Rutherfurd, I. (1996). Historical ENSO teleconnections in the Eastern Hemisphere: comparisons with latest El Niño series of Quinn. *Climatic Change* **32**: 103-109.

Whetton, P. and Rutherfurd, I. (1994). Historical ENSO teleconnections in the Eastern Hemisphere. *Climatic Change* **28**: 221-253.

Woodhouse, C., Kunkel, K., Easterling, D. and Cook, E. (2005). The twentieth-century pluvial in the western United States. *Geophysical Research Letters* **32**: L07701/1-L07701/4.

Wright P. (1982). Homogenized long-period Southern Oscillation indices. *International Journal of Climatology* **9**:33–54.

Yang, M., Yao, T., He, Y. and Thompson, L. (2000). ENSO events recorded in the Guliya ice core. *Climatic Change* **47**: 401–409.

Yu, J., Mechoso, C., McWilliams, J. and Arakawa, A. (2002). Impacts of the Indian Ocean on the ENSO cycle. *Geophysical Research Letters* **29** (8): 46/1-46/4.

Zielinski, G. (2000). Use of palaeo-records in determining variability within the volcanism-climate system. *Quaternary Science Reviews* **19**: 417-438.

Zielinski, G., Mayewski, P., Meeker, L., Whitlow, S., Twickler, M., Morrison, M., Meese, D., Glow, A. and Alley, R. (1994). Record of volcanism since 7000 B.C. from the GISP2 Greenland ice core and implications for the volcano-climate system. *Science* **5161**: 948-952.

Zwiers, F. and Von Storch, H. (2004). On the role of statistics in climate research. *International Journal of Climatology* **24**: 665-680.

CHAPTER 4.
KAURI DENDROCLIMATOLOGY

4.1 Introduction

Kauri (*Agathis australis* D. Don Lindley) belongs to the genus *Agathis*, found in rainforests of the western Pacific, including Papua New Guinea, Australia, New Caledonia and New Zealand (Salmon, 1980). The species reaches its southern limit at latitude 38°S in the forests of northern New Zealand, where it is often a canopy emergent (Ogden *et al.*, 1992). Kauri are New Zealand's most notable native conifers, reaching heights up to 50m (163ft.), with girth sizes greater than 10m (33ft.) and ages in excess of 2,000 years (Salmon, 1980; Department of Conservation, 2003). The longevity of the species and existence of living trees in essentially undisturbed environments makes Kauri a very valuable proxy for the study of long-term climate change of the data sparse south Pacific (Fowler *et al.*, 2004).

More than 20 years of research on Kauri in New Zealand has resulted in a high quality tree-ring master chronology that is now beginning to be used for high-resolution palaeoclimate applications. The first known tree-ring work on Kauri was undertaken by Bell and Bell (1958), however, substantial work leading to the development of chronologies began with the investigations of Dunwiddie (1979) and La Marche *et al.* (1979). A significant phase of work on living trees in the 1980s followed (Palmer, 1982; Ahmed, 1984; Fowler, 1984; Ahmed and Ogden, 1985; 1987). In the 1990s, a major review of the modern Kauri database resulted in the development of the first Kauri master chronology (Buckley *et al.*, 2000).

Further work on modern Kauri (living and standing dead trees) has been undertaken since Buckley *et al.* (2000), including the addition of new sites, the extension of the chronology of some existing sites and detailed quality control of all existing material (Boswijk *et al.*, 2002; Fowler and Boswijk, 2003; Fowler *et al.*, 2004). Extensive analysis of the quality of the modern Kauri master chronology concluded that there were problems associated with low sample depth prior to A.D. 1600 and the late 20th century

(Fowler and Boswijk, 2003; Fowler *et al.*, 2004). Spatially, there was no pre-A.D. 1600 coverage from Northland (far North Island of New Zealand), and the post-1982 period was only represented by four southern sites; Huapai Scientific Reserve, Katikati, Kawhia, and Manaia Sanctuary, seen in Figure 4.1. Significantly, no data existed for any of the Northland sites (Puketi Forest, Puketi Bluff, Trounson, Warawara, Waipoua) for the past 20 years Figure 4.1).

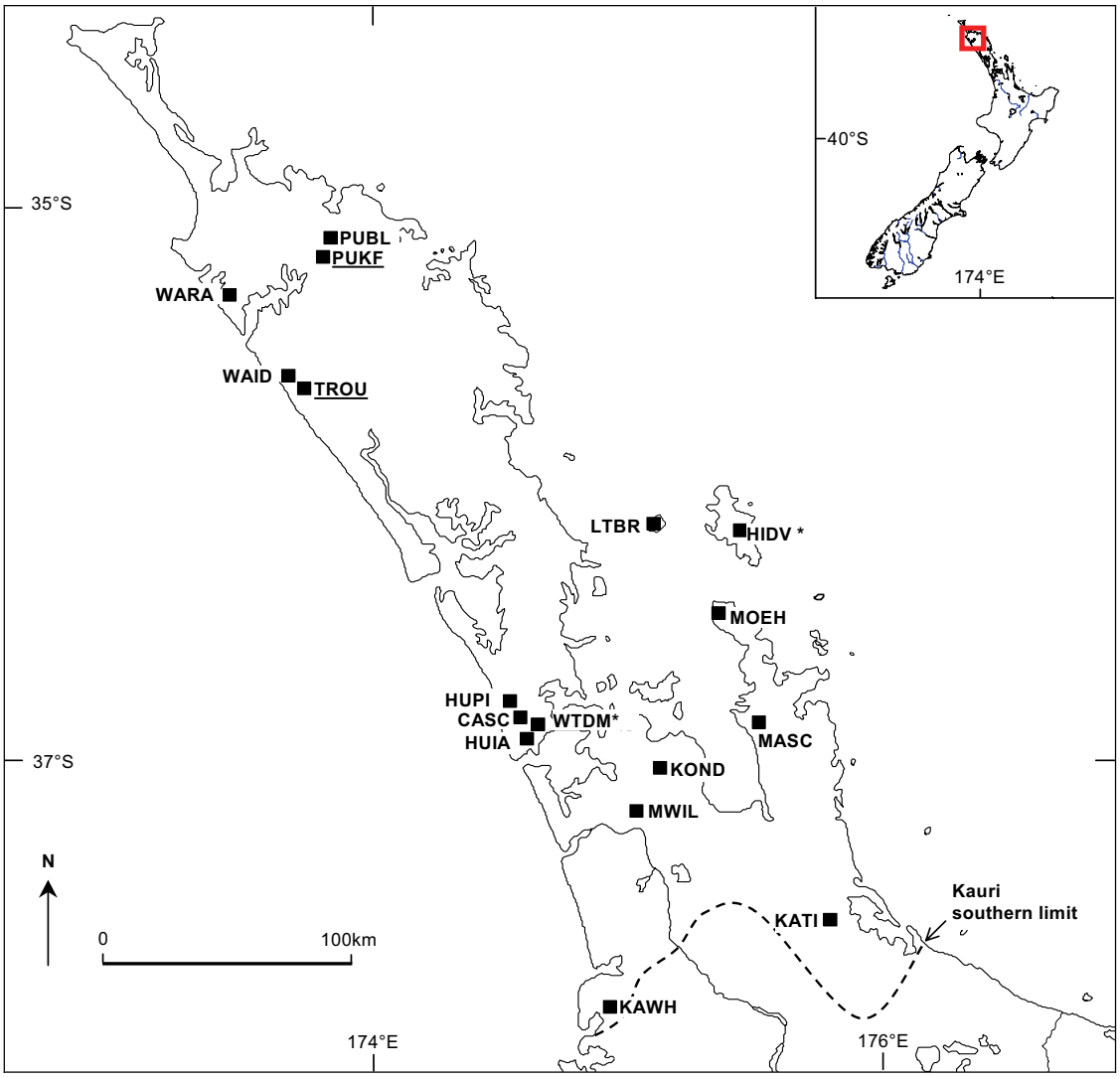

Figure 4.1. Location of the 17 modern Kauri chronologies of the upper North Island of New Zealand. Updated Northland sites are underlined (PUKF, TROU), with new Auckland sites (WTDM, HIDV) asterisked.

Previous dendroclimatological work on Kauri has revealed a significant El Niño-Southern Oscillation (ENSO) signal in its growth ring patterns (Figure 4.2) (Fowler *et al.*, 2000; Fowler *et al.*, 2005b). Although there are hundreds of long, climatically sensitive tree-ring chronologies available worldwide, most are not well suited for ENSO reconstruction because they are located in regions not strongly influenced by ENSO or do not respond to climate during the season of strongest ENSO influence (Stahle *et al.*, 1998). Fortunately, the distribution of Kauri in the upper North Island of New Zealand, coincides with precipitation and temperature variability associated with the influence of ENSO that extends into the South Pacific (Fowler *et al.*, 2000). This places Kauri among a handful of species worldwide that are useful for the study of past ENSO behaviour.

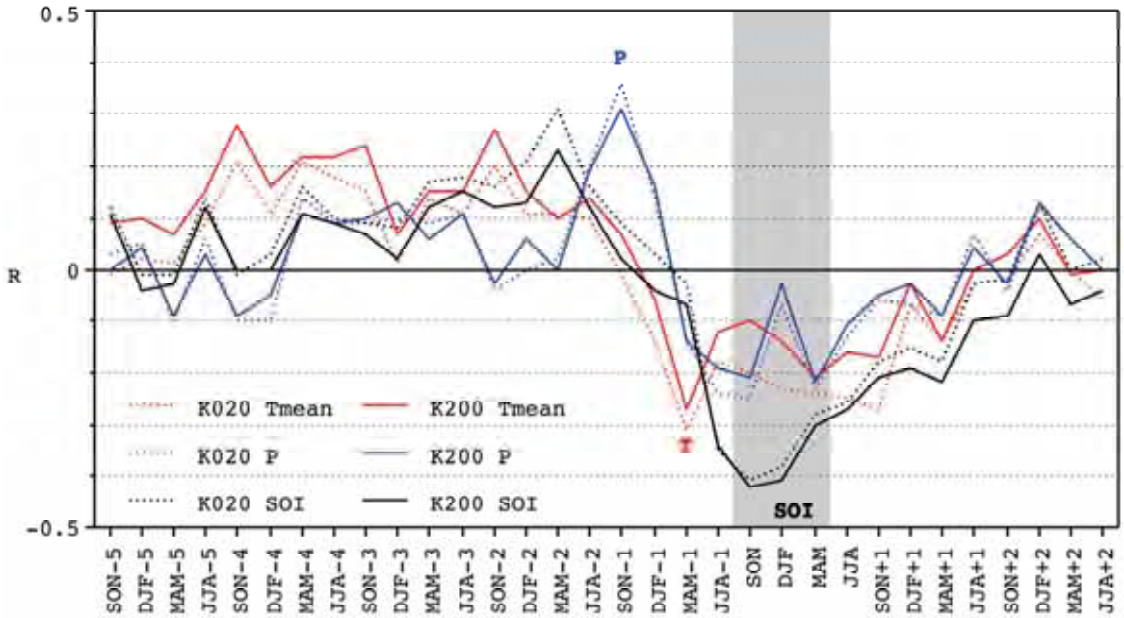

Figure 4.2. Seasonal response function of Kauri growth with temperature (red), precipitation (blue) and the SOI (black). Strongest signal is in the austral spring (shaded). Dashed (solid) lines high (low) pass filtered. i.e. K020 (K200). **Source:** Fowler *et al.* (2000; 2005b).

The value of updating proxies to improve the period of overlap with meteorological data for improved proxy calibration is well recognised (Bradley, 1996). The 1990s are recognised as containing a number of both extreme and prolonged ENSO episodes (Trenberth and Hoar, 1997; Allan and D'Arrigo, 1999). As such, expanded spatial and sample replication of late 20th century variability recorded in Kauri tree-rings was

required to allow a climatically anomalous period to be assessed from a multi-centennial perspective.

This chapter describes the collection of primary tree-ring data and subsequent development of two Northland chronologies, Puketi State Forest and Trounson Kauri Park, from the Upper North Island of New Zealand. The development of updated versions of the modern Kauri master chronologies (AGAUm05a and AGAUm05b) and implications for climate applications are presented.

4.2 Dendrochronological Methods

Living trees were sampled from the targeted area of Northland using a hand-held increment borer (Figure 4.3), producing cores up to 79cm in length and approximately 5mm in diameter. Five mature trees from each site were sampled twice; one short (<30cm) core, and one deep core to a maximum depth of 79cm in an attempt to capture pre-A.D. 1600 growth rings. Three short radii were sampled from 10 trees for the purpose of updating sequences to the end of the 2002-03 growing season. Healthy appearing individuals were selected from Kauri stands where minimal growth competition and general disturbance was believed to have occurred. As the Southern Hemisphere's growing season straddles the change of the calendar year, the year of the annual ring is assigned based on when year ring formation began. Thus, the last complete ring for the trees sampled between October-December 2003 represents the 2002 growth ring. The diameter at breast height (DBH) measurement of each tree was recorded and photographs of the crown and surrounding canopy (Figure 4.4) were taken to facilitate the reidentification of trees and post-sampling monitoring.

Core samples were taken at mean breast height at a slightly upward slope to encourage the sample hole to fill with natural gum and resin (Figure 4.5). In addition, all core holes were treated with the horticultural disinfectant *Vercon* to prevent bacterial infections. Resample cores were labelled with a prefix of 3 to denote sampling in 2003. All core angles, compass direction of each hole and sample height from litter mound were recorded. All core holes were photographed for each tree, in accordance with the New Zealand Department of Conservation's permit requirements.

Figure 4.3. Andrew Lorrey sampling a living Kauri tree using a hand-held increment borer. **Source:** Jenny Lux, 2004.

Figure 4.4. Canopy of a mature Kauri forest, Warawara plateau, Northland. **Source:** Joëlle Gergis, 2004.

Figure 4.5. (left) Jeff Marsden (Panguru Development Trust) showing a post-sample hole filled with natural resin and (right) close up of a sample hole. **Source:** Joëlle Gergis, 2004.

After being air-dried, the cores were glued to wooden mounts with the tracheids vertically aligned. Surfaces were sanded using an industrial sander fitted with a fine-grained belt to clearly reveal the ring sequence (Figure 4.6). Ring widths were then measured to 0.01mm using a binocular microscope and a travelling stage linked to a computer. All data was entered into the 'Dendro for Windows' package (Tyers, 1999).

Figure 4.6. Surfaced wood sample clearly reveals the ring sequence of growth rings. Note bark-edge on far left hand side. **Source:** Jenny Lux.

Computerised crossmatching was undertaken using the tree-ring crossdating program XMATCH developed by Fowler (1998) which provides an on-screen running correlation coefficient (R values) between two samples (Figure 4.7). The position of best fit remains high while the series are correctly crossdated and declines when mismatched due to missing or false rings (Fowler, 1998). Discrepancies displayed in the best-fit anomaly panel (Figure 4.7) suggested areas either side of the current year that required further examination of ring width plots and wood samples.

Figure 4.7 shows a high cross correlation value of r=0.596 for the period of overlap between the individual sample and Puketi Forest site master chronology. A site master is developed by first averaging all radii from each individual tree to form a tree mean sequence. Following this, all tree mean sequences from a given location are averaged to produce a site master chronology. Thus, the discrepancies indicated in the best-fit anomaly panel (bottom) are likely to reflect growth form anomalies inherent to an individual radius from one tree as compared to the entire site chronology.

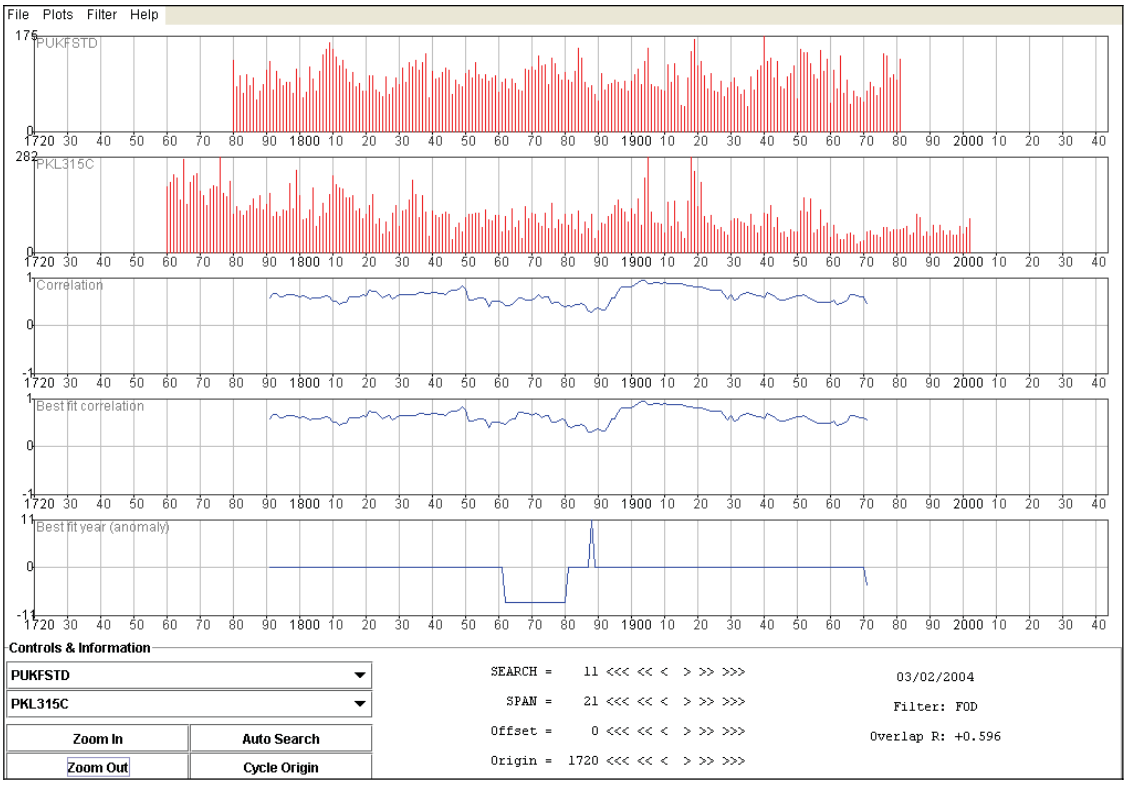

Figure 4.7. XMATCH profile of sample PKL315C crossdated against the master Puketi site chronology.

Dunwiddie (1979) observed that Kauri has some notable growth anomalies that can affect crossdating of samples. Kauri, like many conifers, can occasionally produce 'false' rings where an indistinct boundary is formed during the growing season or a locally absent ring which occurs when an annual ring is not formed around the entire circumference of the tree (see Chapter 3) (Stokes and Smiley, 1968; Dunwiddie, 1979). Where a ring was found to be present on part of one radius or off the measuring track (i.e. locally absent), a measured value for the ring was inserted into the series (Stokes and Smiley, 1968). If a ring was wholly absent from a radius (i.e. a missing ring), a value of one was inserted (Stokes and Smiley, 1968; Baillie, 1982). If the location of problematic rings could not be reliably resolved, the radius sequence was truncated.

The modern Kauri master chronology of Fowler *et al.*, (2004) was used in conjunction with the original site chronologies to facilitate the resolution of the crossmatching issues indicated using XMATCH. All samples were first internally cross checked using XMATCH, then compared to the original site master chronology produced by Ahmed (1984) and the Kauri master chronology (Fowler *et al.*, 2004). The use of the Kauri master chronology enabled temporally unreplicated periods in the new material from long cores to be independently cross verified. An XMATCH profile displaying the correlation of each sample to the original site and Kauri spline 20 master chronologies was produced for each sample for the University of Auckland's Tree-Ring Laboratory's paper archive.

To further verify the crossdating, intra and inter-tree crossmatching and statistical comparison of site chronologies was undertaken using CROS 73 (Baillie and Pilcher, 1973) contained within the Dendro for Windows package (Tyers 1999). This program compares every ring-width series against each other to produce correlation coefficients (r) measured at every position of overlap (Baillie and Pilcher, 1973). Significant matches are expressed statistically using Student's *t*-value, which calculates the degree of similarity between pairs of samples at every position of overlap along a given tree-ring sequence (Baillie and Pilcher, 1973; Baillie, 1982). Following this, sequences were plotted as line graphs and visually compared to assist the resolution of crossmatching difficulties, particularly for the low sample depth periods targeted in this study.

All series were then standardised using the program ARSTAN (Holmes *et al.*, 1986) to remove the effects of biological growth in preparation for climate analysis. Tree-ring indices were first detrended using cubic smoothing splines, detailed in Chapter 3 (Cook

and Peters, 1981). Chronologies developed using splines with a 50% frequency response at 20 and 200 years are suitable for high frequency (ENSO, sunspots) and long-term climate trend analyses (global warming applications) (Fowler and Boswijk, 2003). All standardised series were combined into tree mean sequences which were then averaged to produce spline 20 and 200 versions of the Puketi South and Trounson chronologies.

A further quality control procedure was initiated to test the merit of including each crossdated series in the updated site chronology (Fowler and Boswijk, 2003). This was assessed using the Expressed Population Signal (EPS) statistic (Briffa and Jones, 1990). The 'chronology stripping' procedure discussed by Fowler and Boswijk (2003) involves iteratively removing poor series which lower the chronology EPS. The EPS statistic is calculated from the sample size and the mean within and between tree correlations, and has a possible range from zero to one, where one represents a hypothetical perfect chronology.

4.3 Puketi State Forest, Northland

4.3.1 Background

Tree-ring analysis of Kauri in Puketi State Forest was originally carried out by Ahmed (1984) as part of a wider ecological and dendrochronological study of Kauri from sites across the upper North Island. Ahmed (1984) sampled two stands of Kauri from southern Puketi (Loop track and Te Harua stream) and one stand at Onekura Bluff, in northern Puketi Forest. In 2003, an update of Northland Kauri study sites including Puketi Forest was undertaken by Gergis *et al.* (2005a) to improve pre-A.D. 1600 and post-A.D. 1980 coverage of the modern Kauri record for the purpose of ENSO reconstruction (Fowler *et al.*, 2000). The area was visited and two original sites, the Loop Track in southern Puketi and Onekura Bluff, were resampled. Thirty-nine samples from fifteen trees were obtained from the Loop Track and forty samples from fifteen trees were sampled from Onekura Bluff. Dendrochronological analysis was carried out on the material from the Loop Track to construct a revised chronology for southern Puketi Forest.

4.3.2 Puketi Forest site description

Puketi State Forest is located between the Hokianga and Whangaroa harbours in eastern Northland, New Zealand (Figure 4.1). The forest encloses the Waipapa River catchment which drains into the Hokianga Harbour at Rangiahua. The topography of the region is comprised of rugged, undulating terrain, with steep-moderately steep valleys and numerous relatively flat ridges elevated between 150-460m above sea level (Ahmed, 1984). In the past, the area is known to have suffered disturbances such as logging, gum digging, gum bleeding, burning and grazing (Ahmed, 1984). Although the area has been disturbed, the forest still contains over 10% of the total mature Kauri stands remaining in New Zealand (Department of Conservation, 2003).

Puketi and the adjacent Omahuta Forest form one of the largest continuous tracts of native forest in Northland. A number of large Kauri trees still exist in the area, including Te Tangi o te Tui in Puketi, the fourth largest Kauri in the country with a height of 50.9m (167'), a diameter of 3.94m (12.9'), and a clean bole at more than 30m (98.4') (Adams, 1989; Department of Conservation, 2003). Puketi is an important bird conservation area, providing a breeding habitat for the endangered kokako, North Island brown kiwi and kaka (Adams, 1989; Department of Conservation, 2003).

4.3.3 Loop Track, Puketi South

The original location of the sampling site on the Loop Track was vaguely described by Ahmed (1984) as being "close to the Te Harua Stream", 3km from the Te Harua site. He noted Kauri as the most abundant species found at the site, with 16% of trees falling into 10-30cm DBH size class and a further 10% in the 60-80cm DBH range. Other species associated with Kauri in the closed canopy included *Beilschmiedia tawa*, *Dacrydium kirkii* and *Elaeocarpus dentatus* (Ahmed, 1984). A few large, dead trees were observed in the sampling area, leaving the canopy relatively open in places.

The sub-canopy of the original sample site was described as consisting of *Beilschmiedia tarairi*, *Dacrydium kirkii* and *Elaeocarpus dentatus*, with *Gahnia xanthocarpa*, *Astelia trinervia*, *Blechnum capense* and *Freycinetia banksii* common understorey species (Ahmed, 1984). A number of Kauri of various ages were also recorded and observed around the sample area. In October 2003, 15 trees were sampled by Gergis *et al.* (2005a) from the 'Loop Track' in the Waihoanga Gorge Kauri Walk in southern Puketi Forest (Latitude: 35° 15' 32" S, Longitude: 173° 44' 40" E).

The track is accessed from Puketi Road, traverses through farmland before crossing Waihoanga Creek on a sign-posted trail. Gergis *et al.* (2005a) sampled trees predominately from a northeast facing ridge approximately 320m above sea level close to the Te Tawa Stream near Waihoanga Creek (Figure 4.8). All trees sampled were in the 1.1-2.1m DBH range. The low DBH values noted by Ahmed (1984) for the original sample site suggests that a relatively immature stand was likely to have been sampled compared with the mature stand sampled in 2003. A detailed map of sampled tree locations is found in Figure 4.9.

Figure 4.8. Loop Track sample site, Waihoanga Gorge, southern Puketi Forest. **Source:** Joëlle Gergis.

4.4 Puketi Forest Results

4.4.1 Characteristics of original Loop Track, Puketi South

Ahmed (1984) described the Loop Track and Te Harua Ridge sites as having similar ring width patterns. As a result, data obtained only from those trees on the north-facing slopes from both sites was pooled to increase the sample size of an overall site chronology for Puketi South (PUKF). Mean ring width was 1.56mm and mean sensitivity was 0.2, representing the relative high frequency variance of a series (periods <2 years in length) (Fritts, 1991).

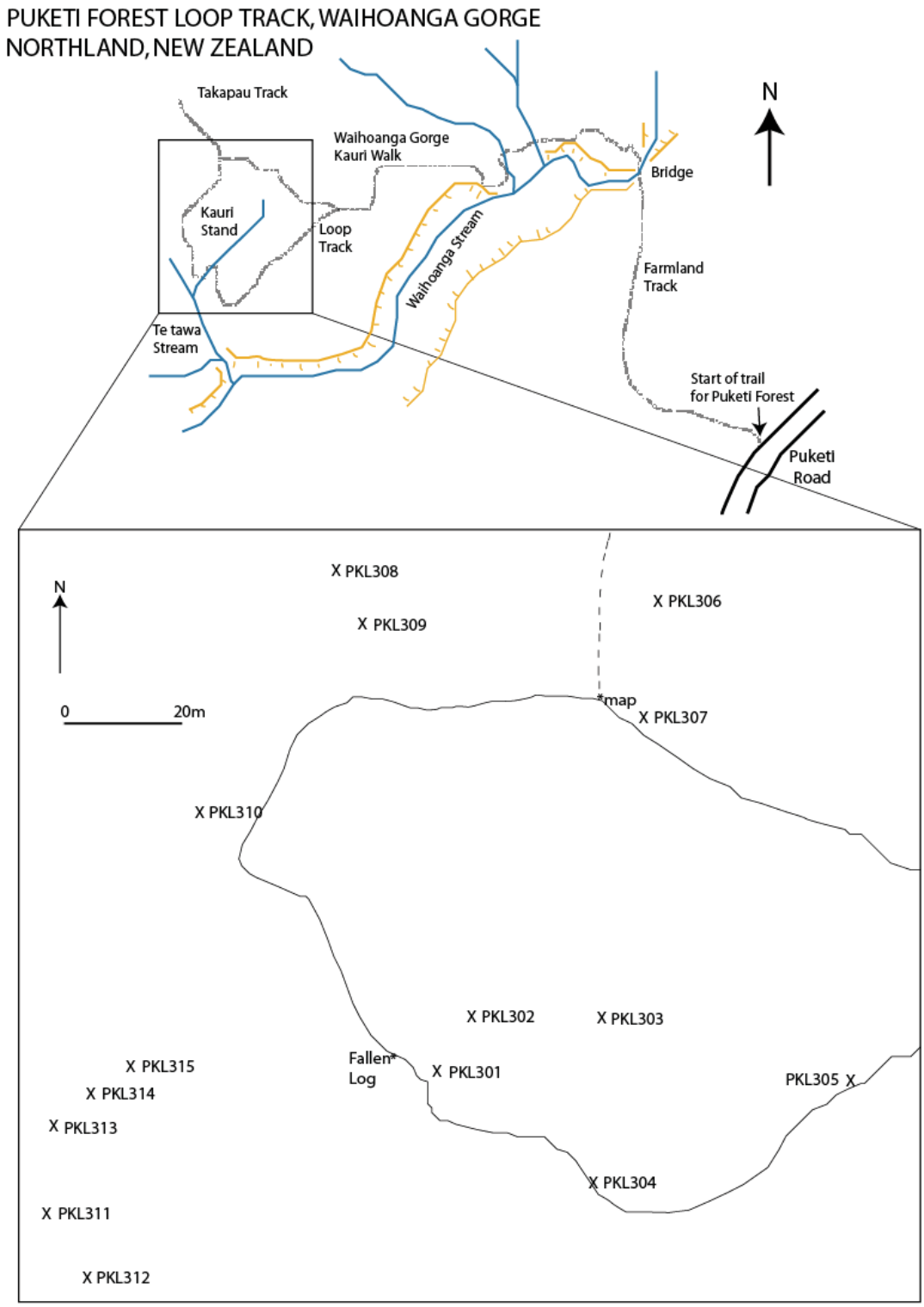

Figure 4.9. Tree location map for Kauri sampled from Waihoanga Gorge Loop Track, Southern Puketi Forest. **Source:** Gergis *et al.* (2005a).

4.4.2 Characteristics of resampled Loop Track, Puketi South

Of the 39 samples collected in 2003, 22 radii from 12 trees were incorporated into an updated site chronology for southern Puketi Forest. Table 4.1 and Table 4.2 indicate the consistently good intra and inter-tree crossmatching of the resample material. Tree PKF315 showed the strongest relationships with all trees included in the chronology, with *t*-values ranging from a low of 3.6 with PKF304 to 14.6 with PKF306 (Table 4.2). Lowest *t*-values were observed for PKF304, however due to the length of this sample (A.D. 1532) it was included in the chronology on the grounds of low sample depth noted for this period.

Trees PKF301, PKF303 and PKF305 either had poor internal or inter-tree correlations and thus were rejected from inclusion in the final site chronology. PKF311 was the only tree truncated due to narrow rings that resulted in unreliable dating. Inter-tree comparisons between Ahmed's (1984) dataset and the 2003 material also revealed consistently good *t*-values, the strongest relationship of t=11.12 noted between PKF312 and PKF012 (Table 4.3).

The revised chronology incorporating both Ahmed's (1984) and resampled data sets included 22 trees spanning A.D. 1504-A.D. 2002 (Figure 4.10). The 499-year combined chronology has an average ring width of 1.69mm, with mean sensitivity of 0.18. A maximum sample depth of 22 trees occurs between A.D. 1900-1964, while 11 trees extending beyond 1981 to 2002 (Appendix 3A). Three trees (PKF302, PKF304, PKF311) extended back beyond A.D. 1600. The longest was PKF302, which dated to A.D. 1504-2002.

A statistical comparison of the original, resampled and revised chronologies for Puketi South were checked against the modern Kauri master chronology (excluding the original Puketi South record) and individual site chronologies to verify crossdating (Table 4.4). This indicates the notable improvement in the statistical robustness (indicated by high *t*-values) of both the resample and revised chronologies when compared to the original chronology of Ahmed (1984).

Table 4.1. Internal Crossmatching for Puketi Loop Resample Trees PKF301-PKF310. t-values over 3.00 shown.\ = overlap < 15 years, - = t-values less than 3.00, * = empty triangle. min t = 0.77 max t = 12.90, mean t = 6.05 s.d. = 2.20

Sample I.D.	Start Dates (A.D.)	End Dates (A.D.)	PKF302b	PKF304a	PKF306a	PKF306b	PKF306c	PKF307c	PKF308b	PKF308c	PKF309a	PKF309b	PKF309c	PKF310a	PKF310b	PKF310c
			A.D.1737 A.D.2002	A.D.1532 A.D.2002	A.D.1834 A.D.2002	A.D.1825 A.D.2002	A.D.1850 A.D.2002	A.D.1745 A.D.2002	A.D.1868 A.D.2002	A.D.1895 A.D.2002	A.D.1880 A.D.2002	A.D.1747 A.D.2002	A.D.1718 A.D.2002	A.D.1744 A.D.2002	A.D.1769 A.D.2002	A.D.1863 A.D.2002
PKF302a	1504	2002	12.66	6.00	9.54	6.40	7.85	5.84	6.26	7.76	4.79	6.13	5.65	7.82	5.62	5.59
PKF302b	1737	2002	*	4.28	7.00	6.06	6.22	5.79	6.31	5.43	3.17	6.83	6.63	6.45	5.75	3.55
PKF304a	1532	2002	*	*	4.77	3.38	4.30	4.51	-	3.60	-	5.98	4.52	4.67	3.87	3.83
PKF306a	1834	2002	*	*	*	12.15	11.34	7.59	7.49	7.01	6.29	9.04	6.62	7.29	7.05	6.89
PKF306b	1825	2002	*	*	*	*	12.46	6.28	7.05	5.28	5.41	8.66	6.74	7.51	7.76	7.18
PKF306c	1850	2002	*	*	*	*	*	5.41	7.12	6.03	5.55	5.86	5.47	7.57	6.79	6.40
PKF307c	1745	2002	*	*	*	*	*	*	3.74	4.57	-	6.38	4.53	5.42	6.38	3.74
PKF308b	1868	2002	*	*	*	*	*	*	*	7.63	7.22	8.22	4.27	4.66	4.75	6.23
PKF308c	1895	2002	*	*	*	*	*	*	*	*	5.62	5.65	3.89	-	4.47	3.29
PKF309a	1880	2002	*	*	*	*	*	*	*	*	*	8.01	4.48	4.89	3.01	6.34
PKF309b	1747	2002	*	*	*	*	*	*	*	*	*	*	9.26	6.77	5.21	5.06
PKF309c	1718	2002	*	*	*	*	*	*	*	*	*	*	*	6.63	5.57	4.27
PKF310a	1744	2002	*	*	*	*	*	*	*	*	*	*	*	*	9.17	10.17
PKF310b	1769	2002	*	*	*	*	*	*	*	*	*	*	*	*	*	7.98
PKF310c	1863	2002	*	*	*	*	*	*	*	*	*	*	*	*	*	*
PKF311a	1587	1964	*	*	*	*	*	*	*	*	*	*	*	*	*	*
PKF312a	1903	2002	*	*	*	*	*	*	*	*	*	*	*	*	*	*
PKF312b	1805	2002	*	*	*	*	*	*	*	*	*	*	*	*	*	*
PKF312c	1830	2002	*	*	*	*	*	*	*	*	*	*	*	*	*	*
PKF313b	1813	2002	*	*	*	*	*	*	*	*	*	*	*	*	*	*
PKF313c	1849	1960	*	*	*	*	*	*	*	*	*	*	*	*	*	*
PKF314a	1771	2002	*	*	*	*	*	*	*	*	*	*	*	*	*	*
PKF314b	1716	2002	*	*	*	*	*	*	*	*	*	*	*	*	*	*
PKF314c	1672	1961	*	*	*	*	*	*	*	*	*	*	*	*	*	*
PKF315a	1729	2002	*	*	*	*	*	*	*	*	*	*	*	*	*	*
PKF315b	1718	2002	*	*	*	*	*	*	*	*	*	*	*	*	*	*
PKF315c	1760	2002	*	*	*	*	*	*	*	*	*	*	*	*	*	*

continued overleaf...

Table 4.1. *continued* Internal Crossmatching for Puketi Loop Resample Trees PKF311-PKF315. *t*-values over 3.00 shown.\ = overlap < 15 years, - = t-values less than 3.00, * = empty triangle. min t = 0.77 max t = 12.90 mean t = 6.05 s.d. = 2.20.

Sample I.D.	Start Dates (A.D.)	End Dates (A.D.)	PKF311a	PKF312a	PKF312b	PKF312c	PKF313b	PKF313c	PKF314a	PKF314b	PKF314c	PKF315a	PKF315b	PKF315c
			A.D.1587 A.D.1964	A.D.1903 A.D.2002	A.D.1805 A.D.2002	A.D.1830 A.D.2002	A.D.1813 A.D.2002	A.D.1849 A.D.1960	A.D.1771 A.D.2002	A.D.1716 A.D.2002	A.D.1672 A.D.1961	A.D.1729 A.D.2002	A.D.1718 A.D.2002	A.D.1760 A.D.2002
PKF302a	1504	2002	9.91	5.44	5.84	6.96	8.08	7.04	5.81	8.46	3.88	7.06	10.18	10.01
PKF302b	1737	2002	8.40	4.89	4.90	5.23	7.76	6.28	5.35	7.47	3.60	8.00	8.33	8.41
PKF304a	1532	2002	5.19	-	3.50	3.92	4.53	5.51	-	-	3.31	-	3.93	5.98
PKF306a	1834	2002	8.25	5.13	8.63	6.64	6.87	6.49	4.31	8.74	3.94	10.38	9.30	9.90
PKF306b	1825	2002	6.74	3.90	7.25	5.59	6.81	5.59	3.94	7.92	4.72	9.63	9.24	8.81
PKF306c	1850	2002	6.13	4.15	6.62	4.75	5.23	5.92	4.10	7.65	3.37	8.12	8.28	9.11
PKF307c	1745	2002	10.40	3.76	5.73	4.40	3.58	4.73	5.17	6.02	4.22	9.12	10.09	7.52
PKF308b	1868	2002	4.29	5.41	5.10	5.43	5.26	3.95	3.92	5.76	3.97	6.55	5.29	7.77
PKF308c	1895	2002	6.49	5.20	4.65	3.41	5.05	4.90	4.10	6.18	-	5.60	7.11	10.38
PKF309a	1880	2002	-	4.35	3.66	3.16	4.49	-	-	3.36	3.61	4.90	3.42	5.12
PKF309b	1747	2002	7.66	-	6.48	5.32	8.58	6.62	3.85	8.32	8.64	10.00	7.77	8.80
PKF309c	1718	2002	7.86	4.26	4.83	3.49	3.79	-	3.52	6.21	5.83	6.75	6.11	7.65
PKF310a	1744	2002	8.14	-	3.38	3.45	7.89	4.81	4.22	10.01	5.22	7.13	8.01	7.64
PKF310b	1769	2002	7.58	-	4.73	4.01	6.17	5.43	5.03	8.91	5.87	8.26	8.03	7.96
PKF310c	1863	2002	4.42	3.01	4.01	-	5.81	3.54	3.68	5.31	4.12	6.07	5.27	7.08
PKF311a	1587	1964	*	4.12	7.03	6.75	8.85	6.98	4.51	8.37	6.31	9.37	12.20	10.09
PKF312a	1903	2002	*	*	5.43	3.59	3.01	-	3.28	3.06	-	3.85	4.32	6.67
PKF312b	1805	2002	*	*	*	8.56	6.99	7.37	4.76	5.37	4.15	7.65	6.60	6.65
PKF312c	1830	2002	*	*	*	*	7.79	5.15	-	4.45	3.92	6.90	6.12	6.96
PKF313b	1813	2002	*	*	*	*	*	9.96	3.61	7.96	4.55	8.47	9.18	8.62
PKF313c	1849	1960	*	*	*	*	*	*	4.28	6.34	4.54	6.56	6.89	5.92
PKF314a	1771	2002	*	*	*	*	*	*	*	8.64	4.71	4.45	5.66	10.67
PKF314b	1716	2002	*	*	*	*	*	*	*	*	5.94	8.34	10.17	10.99
PKF314c	1672	1961	*	*	*	*	*	*	*	*	*	5.84	5.54	6.40
PKF315a	1729	2002	*	*	*	*	*	*	*	*	*	*	12.17	12.90
PKF315b	1718	2002	*	*	*	*	*	*	*	*	*	*	*	10.87
PKF315c	1760	2002	*	*	*	*	*	*	*	*	*	*	*	*

Table 4.2. Puketi Loop 2003 Resample Inter-tree Comparison. t-values over 3.00 shown.\ = overlap < 15 years, - = t-values less than 3.00, * = empty triangle. t = 3.26 max t = 14.67 mean t = 7.84 s.d. = 2.56.

Sample I.D.	Start Dates (A.D.)	End Dates (A.D.)	PKF304a	PKF306	PKF307c	PKF308	PKF309	PKF310	PKF311a	PKF312	PKF313	PKF314	PKF315
			A.D.1532 A.D.2002	A.D.1825 A.D.2002	A.D.1745 A.D.2002	A.D.1868 A.D.2002	A.D.1718 A.D.2002	A.D.1744 A.D.2002	A.D.1587 A.D.1964	A.D.1805 A.D.2002	A.D.1813 A.D.2002	A.D.1672 A.D.2002	A.D.1718 A.D.2002
PKF302	1504	2002	6.18	9.56	6.59	7.66	8.51	8.15	11.20	6.77	9.33	9.08	12.83
PKF304a	1532	2002	*	4.21	4.51	3.41	5.34	5.16	5.19	3.77	4.97	3.26	3.60
PKF306	1825	2002	*	*	7.63	9.42	10.18	10.77	8.10	9.05	8.94	7.27	14.67
PKF307c	1745	2002	*	*	*	4.48	5.87	6.49	10.40	5.98	4.17	7.51	10.54
PKF308	1868	2002	*	*	*	*	7.66	5.56	5.70	7.46	5.74	6.56	10.44
PKF309	1718	2002	*	*	*	*	*	9.24	8.74	7.06	6.92	7.85	11.91
PKF310	1744	2002	*	*	*	*	*	*	8.60	5.80	8.47	8.82	11.39
PKF311a	1587	1964	*	*	*	*	*	*	*	8.13	9.52	8.12	13.29
PKF312	1805	2002	*	*	*	*	*	*	*	*	8.03	6.11	9.86
PKF313	1813	2002	*	*	*	*	*	*	*	*	*	5.96	11.38
PKF314	1672	2002	*	*	*	*	*	*	*	*	*	*	12.62

Table 4.3. Inter-tree comparison of Ahmed's (1984) trees and Puketi Loop 2003 Resample Trees (ID numbers starting with 3). *t*-values over 3.00 shown.\ = overlap < 15 years, - = t-values less than 3.00, * = empty triangle. min t = 2.85 max t = 14.67 mean t = 6.87 s.d. = 2.26.

Sample I.D.	Start Dates (A.D.)	End Dates (A.D.)	PKF009	PKF010	PKF011	PKF012	PKF013	PKF015	PKF016	PKF0172	PKF020	PKF0233
			A.D.1780 A.D.1981	A.D.1824 A.D.1981	A.D.1792 A.D.1981	A.D.1823 A.D.1981	A.D.1835 A.D.1981	A.D.1840 A.D.1981	A.D.1790 A.D.1981	A.D.1900 A.D.1981	A.D.1850 A.D.1981	A.D.1870 A.D.1981
PKF302	1504	2002	5.75	6.76	8.82	11.12	7.92	6.21	9.91	4.58	5.34	4.89
PKF304a	1532	2002	3.60	3.74	5.33	4.12	4.12	3.39	4.28	3.49	-	3.13
PKF306	1825	2002	10.13	9.69	9.98	9.57	9.21	7.81	10.59	5.44	5.83	4.65
PKF307c	1745	2002	7.28	6.83	7.58	6.59	4.65	4.39	5.98	-	3.04	3.53
PKF308	1868	2002	8.77	6.41	6.26	6.19	6.36	4.50	6.71	5.34	5.52	3.16
PKF309	1718	2002	7.17	7.44	8.14	7.26	6.39	4.43	7.54	7.87	3.82	3.09
PKF310	1744	2002	8.60	9.85	6.92	7.86	6.20	6.94	7.01	5.15	5.22	4.11
PKF311a	1587	1964	6.43	7.03	9.17	8.90	6.57	5.13	8.55	3.55	5.20	6.24
PKF312	1805	2002	7.40	6.48	7.94	6.67	6.60	5.02	7.56	4.03	3.50	5.22
PKF313	1813	2002	5.96	6.42	8.31	8.05	8.90	5.74	7.72	3.84	4.43	5.20
PKF314	1672	2002	10.75	6.98	8.10	6.18	6.17	6.82	6.79	3.18	5.32	3.65
PKF315	1718	2002	11.99	8.68	11.01	9.81	8.94	7.84	10.33	6.80	5.78	6.59

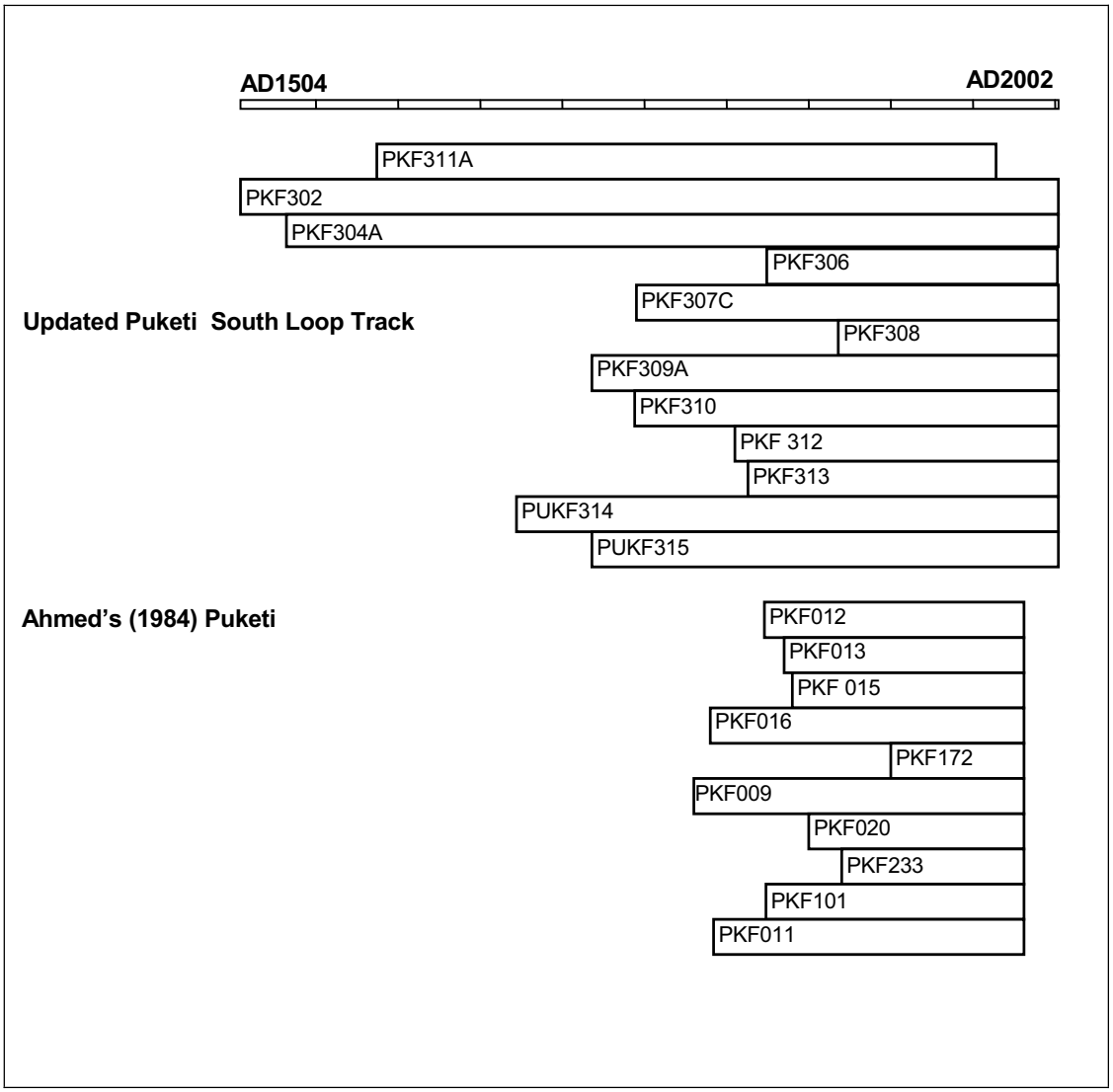

Figure 4.10. Tree sequences used in the revised Puketi South site chronology, A.D. 1504-2002.

T-values increased virtually in all instances with individual site chronologies and associated with the temporally short Waipoua standing dead chronology. The revised chronology had the strongest statistical relationship with Manaia Sanctuary (t=13.41), Puketi Bluff (t=12.72) and Cascades (t= 12.12). There was an overall improvement of the t-value statistic from t=14.95 to a high t=18.63 with the modern master, implying a discernable improvement from the incorporation of resampled material (Table 4.4).

The overall EPS results for both standardised chronologies are presented in Table 4.5. The conservative effect of the spline 200 standardisation was apparent, reducing the length of the high quality period by 76 years and overall EPS statistic by up to 0.04. The trivial drop in EPS further reflects the internal quality of the Puketi chronology.

Table 4.4. Intra-site comparison of original, resampled and revised Puketi with each modern Kauri site chronologies by region. Note that 'Original Puketi Loop' refers to the Ahmed (1984) chronology; 'Resampled Puketi Loop' refers to the material only collected in 2003 and the 'Revised Puketi Loop' incorporates both the original and resampled material (Gergis *et al.*, 2005a).

Master Chronology	Start Dates (A.D.)	End Dates (A.D.)	Original Puketi Loop	Resampled Puketi Loop	Revised Puketi Loop
			A.D. 1780 A.D. 1981	A.D. 1504 A.D. 2002	A.D. 1504 A.D. 2002
Kauri master (ex. Puketi)	1269	1998	14.95	17.82	18.63
Auckland					
Cascades	1559	1982	7.01	12.15	12.12
Hidden Valley	1679	1997	6.19	10.10	9.61
Huapai	1463	1997	6.81	12.04	11.87
Huia	1720	1981	9.67	10.60	10.53
Konini Forks	1770	1976	10.73	9.03	10.55
Little Barrier	1790	1981	10.63	10.53	11.41
Waikato/Bay of Plenty					
Katikati	1698	1996	10.90	10.04	11.10
Manaia	1269	1998	11.05	12.74	13.41
Moehau	1360	1980	6.64	10.47	10.74
Mount William	1580	1981	9.02	10.24	10.95
Northland					
Puketi Bluff	1675	1981	13.76	12.41	12.72
Trounson	1668	1980	6.01	8.13	8.34
Waipoua Dead	1628	1903	4.35	7.56	7.60
Warawara	1660	1979	9.32	9.50	10.32

Table 4.5. Revised chronology stripping Expressed Population Signal (EPS) results for southern Puketi.

Standardisation	EPS Value (All Series)	Highest Quality Period (EPS≥0.80)	Most Significant Series Removal	EPS Improvement
Spline 20	0.959	A.D. 1737-A.D. 2002	PKF310A	+0.959 to +0.959
Spline 200	0.927	A.D. 1813-A.D. 2002	PKF312A	+0.919 to +0.921

Overall the chronology was found to be of a high quality (EPS remained above 0.927 with no series removed) and the effects of stripping (i.e. removal of 'worst' samples) were found to be negligible, particularly in the case of the spline 20 standardisation. As a result, all crossdated series were considered suitable for chronology construction. The inclusion of all series in the final chronology agrees with the conclusion of Fowler and Boswijk (2003) that crossdating alone does indeed provide an effective implicit quality control for Kauri tree-ring chronologies.

4.4.3 Discussion of the revised Puketi chronology

Resampling of Puketi State Forest in 2003 resulted in the development of a robust site chronology being established from 44 radii from 22 trees from southern Puketi. The original chronology for southern Puketi (A.D. 1780-1981) was extended by a total of 297 years through the addition of 27 radii from 12 trees, to span A.D. 1504-2002.

Material from this site did not present problems and was of a high quality. This was reflected in the strong statistical relationships noted between all other modern chronologies from Auckland, Waikato and Northland and high EPS statistics. The strong relationship noted with Manaia Sanctuary (A.D. 1269-1998) and Cascades (A.D. 1559-1982) is likely to reflect the high length of overlap between these two long chronologies. The slight decrease in the statistical relationship between the original and revised PUKF chronologies and nearby Puketi Bluff (A.D. 1623-1983) is perhaps a reflection of the relatively short overlap of the two chronologies.

Overall, the revised site chronology for Puketi was replicated in its entirety by other independent site chronologies and was thus considered to be of a suitably high standard to be included in the Kauri modern master record. Importantly, Puketi is the first of the Northland chronologies to extend past A.D. 1982, and the first of the 17 modern Kauri chronologies to provide all of the 20th century for climate analysis (Gergis *et al.*, 2005a).

4.5 Trounson Kauri Park

4.5.1 Background

Tree-ring analysis of Kauri from Trounson was originally carried out by Ahmed (1984) who sampled a mature stand of Kauri trees between 1979 and 1982, obtaining 43 cores from 20 trees. He constructed a site chronology spanning A.D. 1668-1980 using 20 samples derived from 12 trees, rejecting 21 cores from further analysis. As part of update, the original collection was reassessed for its potential to expand the Trounson chronology for climate analysis. Particular emphasis was placed on reassessing rejected cores and the inner rings of long cores to improve pre- A.D. 1600 replication. In October and December 2003, Gergis *et al.* (2005b) sampled 15 trees from Trounson to improve pre-A.D. 1600 and post-A.D. 1980 replication of the modern Kauri data base for the purpose of ENSO reconstruction (Fowler *et al.*, 2000). Dendrochronological

analysis was carried out using the original and resampled material to extend and improve replication of the Trounson chronology to span A.D. 1529-2002.

4.6 Site Description

Trounson Kauri Park is located east of State Highway 12, between Kaihu and Donnelly's Crossing in the Waima River catchment, on the west coast of Northland (Figure 4.1). The park covers a total area of 573 ha of regenerating broadleaf forest, 231 ha of which is pristine Kauri forest (Ahmed, 1984; Department of Conservation, 2003). Under the jurisdiction of the New Zealand Department of Conservation, Trounson was classified as a 'mainland island' reserve in 1997; one of only six mainland islands in New Zealand, and is the only one in Northland (Department of Conservation, 2003). In fact, Trounson is New Zealand's only fully protected Kauri forest ecosystem, emphasising the area's high conservation status (Department of Conservation, 2003). The park is home to several threatened species such as Kauri snails, banded kokopu, various weta species, kukupa, long-tailed bat, kokako, North Island brown kiwi and a stand of Kauri trees that is recognised as one of the best examples in the country (Department of Conservation, 2003).

Ahmed (1984) described the original study site as "a ridge crest area facing a valley system that extends to Maungonui Bluff on the west coast at an elevation of approximately 146-200m". Trees from a mature Kauri stand on the top and sides of a ridge were sampled. Unfortunately, precise grid references for sampling locations were not accurately recorded by the original collectors making resampling of the original trees problematic.

Although Kauri accounted for 81% of the biomass of the original study site, the canopy also included *Podocarpus ferrugineus* and *Podocarpus hallii* (Ahmed, 1984). *Knightia excelsa*, *Coprosma arborea* and *Myrsine australis* commonly featured in the understorey. Approximately 48% of Kauri fell into the 10-30cm diameter at breast height (DBH) size class, with only 9% of individuals occupying the 50-80cm size bracket (Ahmed, 1984). Young regenerating (<10cm DBH) stands of Kauri were observed in some localities alongside large, mature trees competing with *Beilschmiedia tarairi* (Ahmed, 1984). A number of stumps of old Kauri were observed in the sample plot and in various places in the park (Ahmed, 1984).

In 2003, 15 Kauri trees were sampled from a gently sloping ridge (<10 °) in the north-east portion of the Trounson Kauri Park (Latitude 35° 43' 36"S, Longitude 173° 38' 38"E) along Department of Conservation 'trapping lines' AK and AL (see Figure 4.11). The track was accessed from a path bordering farmland which contained a number of weathered stumps. The update trees were sampled between lines AL 300 AL 420 at an elevation of approximately 260m. Three of the five large trees were cored in the vicinity of AK 380-420, while the other two trees were located at AL 240 and AL 380. All trees sampled ranged between 1.0-2.4m. A detailed map of the location of trees sampled can be found in Figure 4.11.

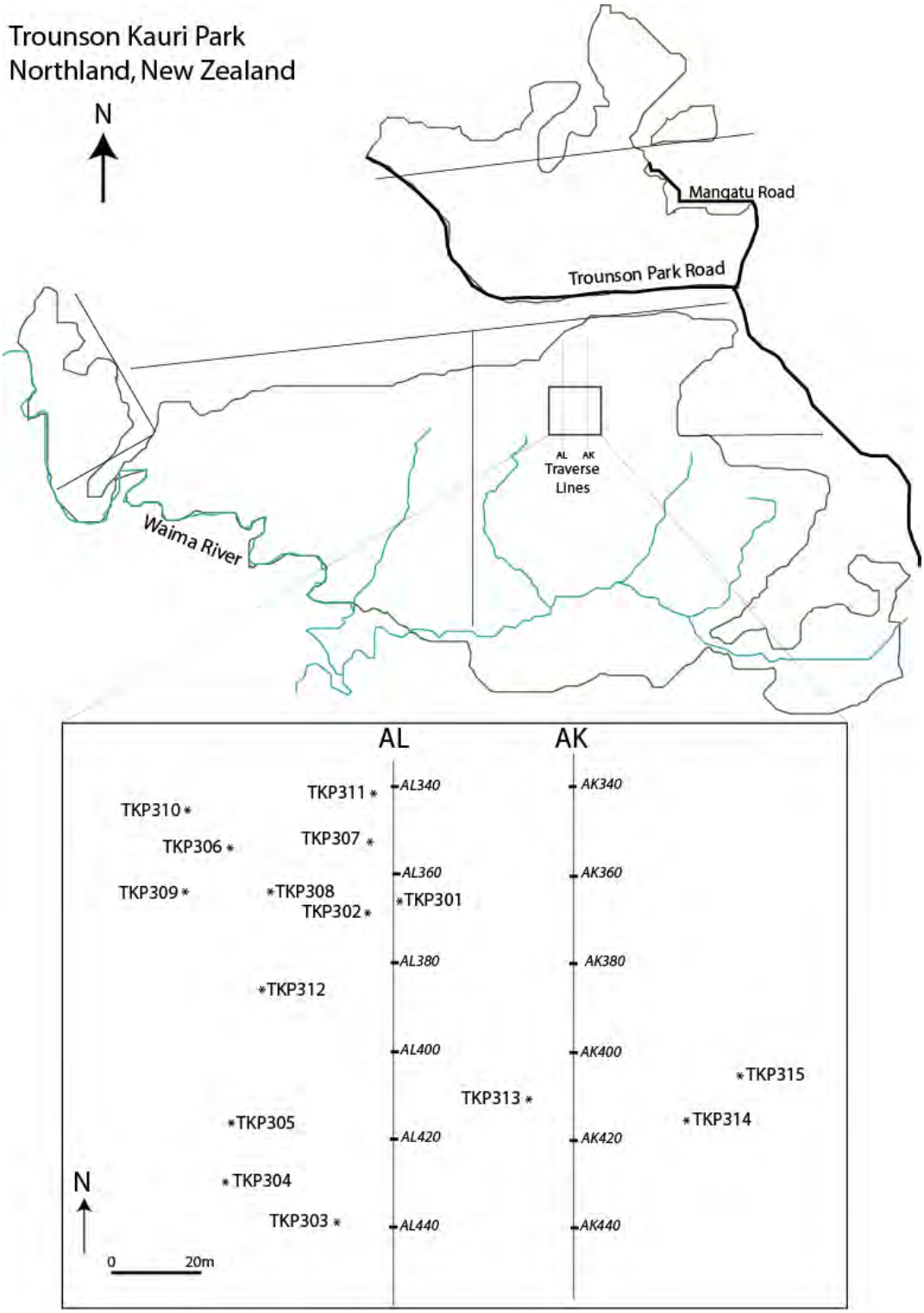

Figure 4.11. Tree location map for Kauri sampled from Trounson Kauri Park, Northland. AL and AK refer to New Zealand Department of Conservation 'trapping lines'. **Source:** Gergis *et al.* (2005b).

4.7 Trounson Results

4.7.1 Characteristics of original Trounson data set

Ahmed (1984) reported that the outer part of several trees displayed significant suppression of growth-rings, mostly between 1920-1981. The resulting dating inaccuracies obscured reliable cross matching which led to the subsequent truncation of numerous sequences. Ahmed (1984:153) alluded to the possibility of an unidentified regional disturbance accounting for similar signatures of growth impediment expressed in sequences obtained from nearby Waipoua Forest, stating "probably Waipoua Coastal and Trounson have suffered the same type of disturbance, but this needs further investigation".

Nevertheless, Ahmed (1984) noted many of the cores that displayed this uncountable, compressed outer portion also contained distinct and sensitive inner rings, which made cross matching with other cores possible. Complacent (insensitive), false and locally absent rings were also noted and easily detected. In general, trees showed good radial uniformity despite being asymmetrical. Ahmed (1984) noted that trees sampled from north-facing slopes produced higher quality data which readily crossmatched with other cores. The original site chronology was established using 20 cores obtained from 10 trees, and spanned A.D. 1668-1980. For ease of reference, Ahmed's (1984) original Trounson chronology has been labelled TROU84.

4.7.2 Remeasurement results

Remeasurement and crossmatching of the existing data set largely confirmed Ahmed's (1984) original observation that material from Trounson were problematic. Table 4.6 presents a Student's *t*-value matrix of the statistical relationship between all cores from the site. Both original and reassessed *t* values are presented in order to allow for comparison between differing analysts and crossmatching techniques. Use of the new XMATCH crossmatching technique developed by Fowler (1998) appeared to assist in the dating of difficult material previously rejected by Ahmed (1984).

Table 4.6. Trounson Remeasure T-Value Matrix. *t*-values over 3.00 shown. \ = overlap < 15 years, - = *t*-values less than 3.00, * = empty triangle. *Italicised* valued denote original Student's 't' statistics and original start/end dates for the original sample. Shading indicates core originally rejected. Date extension flagged by * N = 465 min t = -3.35 max t = 16.31 mean t = 5.18, S.D= 2.72.

Sample ID	Start Year (A.D.)	End Year (A.D.)	TKP 001a	TKP 001b	TKP 002a	TKP 002b	TKP 003a	TKP 003b	TKP 004a	TKP 004b	TKP 005a	TKP 006a	TKP 006b	TKP 007a	TKP 007b	TKP 008a	TKP 008b	TKP 009a	TKP 009b	TKP 011b	TKP 013a	TKP 014a	TKP 014b	TKP 015a	TKP 015b	TKP 018b	TKP 018c	TKP 019a	TKP 019b	TKP 020a	TKP 020d
TKP001a	* 1782	1977	*	13.12	6.00	5.33	4.45	3.46	2.95	3.13	4.48	1.01	2.70	3.04	1.74	3.41	5.47	4.55	5.40	2.93	4.24	6.78	4.60	8.67	5.49	2.03	2.24	3.22	1.56	4.10	3.73
	1800	1978		8.14	3.62	3.87	3.20	-	-	-	-	3.61	3.65	-	-	-	3.44	4.60	6.22	-	-	-	-	4.63	5.03	4.64	-	5.66	-	6.18	-
TKP001b	* 1768	1978	*	*	6.16	8.39	5.36	5.18	2.62	4.93	4.34	4.00	6.94	5.27	4.17	5.33	7.60	8.50	7.26	4.79	7.33	7.69	7.18	13.15	11.38	8.35	5.91	5.62	4.05	6.11	6.85
	1770	1978			5.80	7.47	6.09	-	-	-	-	6.09	7.42	4.56	-	3.78	7.21	8.32	7.37	-	7.39	-	6.82	10.42	7.58	7.04	-	6.01	-	6.84	-
TKP002a	1700	*1940	*	*	*	7.21	3.91	4.31	5.19	6.23	5.20	6.03	6.33	6.53	4.96	4.98	8.30	5.74	6.88	4.81	6.51	6.58	6.23	7.63	7.59	4.26	3.61	7.55	3.71	3.32	5.91
	1700	1920				9.14	3.96	-	-	-	-	7.23	7.53	8.00	-	4.89	9.26	6.80	7.10	-	7.24	-	7.57	8.31	7.97	5.04	-	6.40	-	3.81	-
TKP002b	1701	1920	*	*	*	*	4.18	4.32	3.42	5.24	4.79	6.49	6.20	8.03	6.31	4.06	4.46	6.49	5.60	5.31	5.93	6.75	5.42	7.83	6.44	3.82	3.15	4.48	2.60	3.38	4.32
	1700	1920					4.68	-	-	-	-	7.48	7.38	8.99	-	3.46	5.53	6.90	5.99	-	7.77	-	5.51	7.22	7.56	6.08	-	6.84	-	4.75	-
TKP003a	1700	1976	*	*	*	*	*	6.43	4.85	5.18	4.46	4.42	5.13	4.68	2.82	6.19	5.22	6.56	5.82	2.98	4.64	4.20	4.03	4.47	5.28	4.30	4.34	3.81	1.45	4.74	3.44
	1700	1978						-	-	-	-	4.83	4.89	4.36	-	6.52	5.95	6.19	4.77	-	5.44	-	4.42	4.99	5.75	3.25	-	3.36	-	5.49	-
TKP003b	1670	1900	*	*	*	*	*	*	5.36	3.65	4.50	5.42	4.99	5.58	3.33	4.84	4.28	7.30	7.18	4.35	5.61	5.63	4.87	5.20	4.26	4.49	4.34	5.52	1.15	3.43	2.36
	-	-							-	-	-	-	-	-	-	-	-	-	-	-	-	-	-	-	-	-	-	-	-	-	-
TKP004a	1680	1939	*	*	*	*	*	*	*	10.64	8.69	3.99	4.34	6.13	4.79	5.10	7.14	4.84	5.70	3.59	4.25	4.20	5.54	2.48	2.25	2.78	4.59	4.73	2.39	2.27	4.30
	-	-								-	-	-	-	-	-	-	-	-	-	-	-	-	-	-	-	-	-	-	-	-	-
TKP004b	1720	1900	*	*	*	*	*	*	*	*	7.00	4.86	5.93	6.26	7.13	5.04	7.59	4.36	4.43	6.57	5.27	6.87	6.38	4.90	3.77	3.60	2.38	4.43	3.09	2.32	4.64
	-	-									-	-	-	-	-	-	-	-	-	-	-	-	-	-	-	-	-	-	-	-	-
TKP005a	1705	1899	*	*	*	*	*	*	*	*	*	4.73	4.11	7.48	7.73	5.08	8.01	4.86	6.61	4.02	6.21	4.94	7.12	4.80	5.48	3.75	4.61	4.42	2.10	3.89	6.43
	-	-										-	-	-	-	-	-	-	-	-	-	-	-	-	-	-	-	-	-	-	-
TKP006a	1719	1960	*	*	*	*	*	*	*	*	*	*	11.50	8.18	3.99	7.64	10.63	7.49	8.07	3.56	9.13	6.06	8.16	7.85	9.25	7.89	7.93	7.62	3.44	5.70	4.96
	1720	1900											11.88	9.68	-	6.68	9.94	8.32	11.08	-	9.16	-	8.57	8.99	8.93	8.55	-	8.53	-	7.30	-
TKP006b	*1697	1900	*	*	*	*	*	*	*	*	*	*	*	7.11	7.55	7.74	8.57	7.98	7.77	3.85	8.14	6.83	5.21	7.79	7.46	8.37	5.74	5.94	3.51	3.22	4.43
	1700	1900												6.99	-	7.04	10.67	7.47	8.37	-	9.66	-	6.34	9.20	8.44	8.51	-	6.47	-	6.56	-
TKP007a	1668	1915	*	*	*	*	*	*	*	*	*	*	*	*	8.53	7.26	8.48	7.38	7.87	4.98	6.17	5.84	7.74	7.89	7.29	5.79	5.85	7.08	4.10	4.57	6.82
	1668	1910														5.31	7.59	7.34	7.38	-	6.70	-	8.91	9.32	8.76	5.82	-	7.32	-	6.45	-
TKP007b	1700	1960	*	*	*	*	*	*	*	*	*	*	*	*	*	7.18	6.27	6.24	4.27	3.31	8.43	6.69	6.64	8.74	8.09	4.95	4.17	5.36	1.74	4.49	3.42
	-	-														-	-	-	-	-	-	-	-	-	-	-	-	-	-	-	-
TKP008a	1688	1910	*	*	*	*	*	*	*	*	*	*	*	*	*	*	7.11	11.08	6.08	-	8.09	7.00	5.42	6.92	6.75	5.52	6.45	7.15	2.76	6.23	4.68
	1688	1920															6.41	9.47	5.83	-	7.26	-	5.17	7.92	7.06	-	4.63	6.26	-	7.31	-
TKP008b	*1745	1900	*	*	*	*	*	*	*	*	*	*	*	*	*	*	*	6.64	9.64	3.74	9.01	6.47	9.22	8.06	8.54	6.61	8.10	7.42	4.24	4.46	7.51
	1748	1900																6.65	8.25	-	7.37	-	8.78	7.54	7.91	6.27	-	6.17	-	5.95	-
TKP009a	1708	1960	*	*	*	*	*	*	*	*	*	*	*	*	*	*	*	*	9.02	3.75	7.25	5.78	6.18	8.86	7.62	7.83	6.77	7.68	2.20	5.00	3.81
	1707	1920																	-	-	-	-	-	-	-	-	-	-	-	-	-
TKP009b	1773	1978	*	*	*	*	*	*	*	*	*	*	*	*	*	*	*	*	*	4.75	8.73	4.38	8.01	9.21	10.95	8.81	7.82	8.35	2.91	6.91	6.04
	1773	1978																		-	-	-	-	-	-	-	-	-	-	-	-
TKP011b	1807	1901	*	*	*	*	*	*	*	*	*	*	*	*	*	*	*	*	*	*	3.48	5.96	6.58	7.85	5.52	4.49	3.05	3.96	1.71	2.85	2.49
	-	-																			-	-	-	-	-	-	-	-	-	-	-
TKP013a	1720	1900	*	*	*	*	*	*	*	*	*	*	*	*	*	*	*	*	*	*	*	6.65	6.87	7.88	9.01	6.05	5.15	6.55	3.66	4.95	4.21
	1675	1900																				-	7.87	9.29	9.26	6.34	-	6.43	-	5.84	-
TKP014a	1629	1930	*	*	*	*	*	*	*	*	*	*	*	*	*	*	*	*	*	*	*	*	11.41	9.63	7.36	4.86	3.25	6.69	2.96	5.08	5.77
	-	-																					-	-	-	-	-	-	-	-	-
TKP014b	1724	1900	*	*	*	*	*	*	*	*	*	*	*	*	*	*	*	*	*	*	*	*	*	8.94	8.89	6.43	4.42	8.26	3.47	5.70	5.28
	1720	1900																						8.46	9.27	5.50	-	7.59	-	6.35	-
TKP015a	1690	1910	*	*	*	*	*	*	*	*	*	*	*	*	*	*	*	*	*	*	*	*	*	*	16.31	8.73	6.42	8.67	4.21	5.87	6.90
	1690	1900																							15.52	9.07	-	11.51	-	8.18	-
TKP015b	*1682	1901	*	*	*	*	*	*	*	*	*	*	*	*	*	*	*	*	*	*	*	*	*	*	*	9.83	6.21	8.26	4.49	5.71	7.39
	1730	1910																								8.06	-	10.71	-	10.45	-
TKP018b	* 1760	1900	*	*	*	*	*	*	*	*	*	*	*	*	*	*	*	*	*	*	*	*	*	*	*	*	9.11	6.71	2.74	7.54	5.24
	1790	1980																									-	8.11	-	11.01	-
TKP018c	1775	1907	*	*	*	*	*	*	*	*	*	*	*	*	*	*	*	*	*	*	*	*	*	*	*	*	*	7.03	3.86	6.71	5.10
	-	-																										-	-	-	-
TKP019a	* 1681	1920	*	*	*	*	*	*	*	*	*	*	*	*	*	*	*	*	*	*	*	*	*	*	*	*	*	*	3.92	4.63	4.57
	1780	1920																											-	-	-
TKP019b	1730	1890	*	*	*	*	*	*	*	*	*	*	*	*	*	*	*	*	*	*	*	*	*	*	*	*	*	*	*	1.66	4.01
	-	-																												-	-
TKP020a	* 1747	1960	*	*	*	*	*	*	*	*	*	*	*	*	*	*	*	*	*	*	*	*	*	*	*	*	*	*	*	*	2.65
	1750	1970																													-
TKP020d	1770	1900	*	*	*	*	*	*	*	*	*	*	*	*	*	*	*	*	*												
	-	-																													

Reappraisal of the original collection resulted in 10 additional cores being incorporated into a revised original site chronology. These ten previously rejected cores (shaded in Table 4.6) introduced material from trees TKP04, TKP05 and TKP011, increasing sample size to 29 samples from 16 trees. Date extensions were obtained for the 10 samples denoted by an asterisk in Table 4.6. The most notable extension was due to the incorporation of material from TKP014 which led to an extension of the site master back to A.D. 1629 (Table 4.6). The use of the Kauri master chronology assisted in the dating of previously undated material.

4.7.3 Characteristics of 2003 Trounson resample

Of the 40 samples from 15 trees collected in 2003, only 23 samples from 10 trees were incorporated into an independent site chronology for Trounson referred to here as TROU03. Unfortunately, a number of the sequences were either fast growing (<100 rings) or displayed obscure growth patterns which resulted in trees TKP303, TKP305, TKP306, TKP308, and TKP310 being rejected. This is evident from the low *t*-values obtained for these specimens (Table 4.7).

Additionally, a number of trees from Trounson had uncountable and/or uncrossdatable outer rings. This necessitated the truncation of 10 radii (most commonly between A.D. 1890-1960), which may account for some of the poor internal cross matching statistics observed in Table 4.7. For example, the impact of reducing within tree overlap can be seen clearly for trees TKP315 (t=5.36) and TKP314 (t=5.15).

Nonetheless, high internal cross matching was observed for a number of trees (Table 4.8). The most internally robust trees of the chronology are TKP312 (t=13.88), TKP304 (t=12.17), and TKP311 (t=12.78). The strongest 'between tree' relationship observed from the collection was found between TKP312 and TKP315 which displayed a *t*-value of 10.41. This is most likely a result of the long period (328 years) of overlap common to these two trees. The lowest relationship was observed between TKP302 and TKP312 which overlap for 144 years, between A.D. 1858 and A.D. 2002 (t=3.56).

Table 4.7. Internal Crossmatching for Trounson Kauri Park 2003 resample trees: TKP301-TKP308. t-values over 3.00 shown. \ = overlap < 15 years, - = t-values less than 3.00, * = empty triangle. n = 396 min t = -2.21 max t = 13.89 mean t = 2.98 s.d. = 2.35.

Sample I.D.	Start Year (A.D.)	End Year (A.D.)	TKP301b	TKP301c	TKP302b	TKP302c	TKP303a	TKP303c	TKP304a	TKP304b	TKP304c	TKP305b	TKP305c	TKP306c	TKP307b	TKP307c	TKP308a	TKP308b
			A.D. 1826 A.D. 2002	A.D. 1843 A.D. 2002	A.D. 1890 A.D. 2002	A.D. 1858 A.D. 2002	A.D. 1930 A.D. 2002	A.D. 1895 A.D. 2002	A.D. 1756 A.D. 1880	A.D. 1748 A.D. 1890	A.D. 1743 A.D. 1890	A.D. 1884 A.D. 2002	A.D. 1858 A.D. 2002	A.D. 1915 A.D. 2002	A.D. 1837 A.D. 2002	A.D. 1878 A.D. 2002	A.D. 1913 A.D. 2002	A.D. 1913 A.D. 2002
TKP301a	1852	2002	6.14	6.95	3.20	3.94	-	-	-	-	-	3.28	-	-	-	3.03	-	-
TKP301b	1826	2002	*	10.73	-	3.46	-	-	-	-	3.98	-	3.89	3.14	-	-	-	-
TKP301c	1843	2002	*	*	3.32	3.22	-	-	3.11	3.98	3.71	-	3.39	-	-	3.46	-	-
TKP302b	1890	2002	*	*	*	9.24	-	-	\	\	\	-	-	-	-	4.68	-	-
TKP302c	1858	2002	*	*	*	*	-	-	-	-	-	3.90	-	-	3.66	5.38	3.11	-
TKP303a	1930	2002	*	*	*	*	*	3.03	\	\	\	-	-	-	-	-	-	-
TKP303c	1895	2002	*	*	*	*	*	*	\	\	\	-	-	-	-	-	-	-
TKP304a	1756	1880	*	*	*	*	*	*	*	8.16	9.96	\	-	\	4.34	\	\	\
TKP304b	1748	1890	*	*	*	*	*	*	*	*	12.17	\	3.52	\	3.82	\	\	\
TKP304c	1743	1890	*	*	*	*	*	*	*	*	*	\	-	\	4.04	\	\	\
TKP305b	1884	2002	*	*	*	*	*	*	*	*	*	*	7.49	-	-	-	-	-
TKP305c	1858	2002	*	*	*	*	*	*	*	*	*	*	*	-	-	-	-	-
TKP306c	1915	2002	*	*	*	*	*	*	*	*	*	*	*	*	-	-	3.58	5.37
TKP307b	1837	2002	*	*	*	*	*	*	*	*	*	*	*	*	*	5.31	-	-
TKP307c	1878	2002	*	*	*	*	*	*	*	*	*	*	*	*	*	*	-	-
TKP308a	1913	2002	*	*	*	*	*	*	*	*	*	*	*	*	*	*	*	5.31
TKP308b	1913	2002	*	*	*	*	*	*	*	*	*	*	*	*	*	*	*	*
TKP309a	1900	2002	*	*	*	*	*	*	*	*	*	*	*	*	*	*	*	*
TKP309b	1930	2002	*	*	*	*	*	*	*	*	*	*	*	*	*	*	*	*
TKP309c	1930	2002	*	*	*	*	*	*	*	*	*	*	*	*	*	*	*	*
TKP310a	1910	1982	*	*	*	*	*	*	*	*	*	*	*	*	*	*	*	*
TKP310c	1930	2002	*	*	*	*	*	*	*	*	*	*	*	*	*	*	*	*
TKP311a	1736	2002	*	*	*	*	*	*	*	*	*	*	*	*	*	*	*	*
TKP311b	1552	2002	*	*	*	*	*	*	*	*	*	*	*	*	*	*	*	*
TKP312a	1653	2002	*	*	*	*	*	*	*	*	*	*	*	*	*	*	*	*
TKP312b	1529	1960	*	*	*	*	*	*	*	*	*	*	*	*	*	*	*	*
TKP313a	1745	1920	*	*	*	*	*	*	*	*	*	*	*	*	*	*	*	*
TKP313b	1631	1920	*	*	*	*	*	*	*	*	*	*	*	*	*	*	*	*
TKP314a	1671	1900	*	*	*	*	*	*	*	*	*	*	*	*	*	*	*	*
TKP314b	1632	2002	*	*	*	*	*	*	*	*	*	*	*	*	*	*	*	*
TKP315a	1705	1914	*	*	*	*	*	*	*	*	*	*	*	*	*	*	*	*
TKP315b	1588	1810	*	*	*	*	*	*	*	*	*	*	*	*	*	*	*	*

continued overleaf...

Table 4.7. *continued* Internal Crossmatching for Trounson Kauri Park 2003 resample trees: TKP309-TKP315. Triangular YR-CROS73 matrix: t-values over 3.00 shown. \ = overlap < 15 years, - = t-values less than 3.00, * = empty triangle. n = 396 min t = -2.21 max t = 13.89 mean t = 2.98 s.d. = 2.35.

Sample I.D.	Start Year (A.D.)	End Year (A.D.)	TKP309a	TKP309b	TKP309c	TKP310a	TKP310c	TKP311a	TKP311b	TKP312a	TKP312b	TKP313a	TKP313b	TKP314a	TKP314b	TKP315a	TKP315b
			A.D. 1900 A.D. 2002	A.D. 1930 A.D. 2002	A.D. 1930 A.D. 2002	A.D. 1910 A.D. 1982	A.D. 1930 A.D. 2002	A.D. 1736 A.D. 2002	A.D. 1552 A.D. 2002	A.D. 1653 A.D. 2002	A.D. 1529 A.D. 1960	A.D. 1745 A.D. 1920	A.D. 1631 A.D. 1920	A.D. 1671 A.D. 1900	A.D. 1632 A.D. 2002	A.D. 1705 A.D. 1914	A.D. 1588 A.D. 1810
TKP301a	1852	2002	-	-	-	-	-	-	4.35	3.84	4.27	-	-	-	5.17	-	\
TKP301b	1826	2002	-	-	-	-	-	4.28	5.15	5.74	3.61	3.55	-	-	5.75	3.32	\
TKP301c	1843	2002	-	-	-	-	-	4.12	5.21	5.72	4.64	4.76	4.34	-	4.96	4.02	\
TKP302b	1890	2002	5.07	-	-	-	-	-	3.19	-	-	-	3.11	\	5.13	-	\
TKP302c	1858	2002	3.11	-	-	-	-	4.09	4.77	4.74	-	4.08	5.10	-	5.55	-	\
TKP303a	1930	2002	3.43	4.22	3.49	-	-	-	-	-	-	\	\	\	-	\	\
TKP303c	1895	2002	3.17	-	5.31	-	-	3.28	-	-	-	-	-	\	-	-	\
TKP304a	1756	1880	\	\	\	\	\	5.89	5.64	-	4.41	4.77	-	-	5.00	4.84	3.11
TKP304b	1748	1890	\	\	\	\	\	7.63	8.32	5.82	6.15	6.95	3.85	6.18	5.00	5.92	4.98
TKP304c	1743	1890	\	\	\	\	\	7.95	6.51	4.56	4.61	6.59	4.05	4.67	4.59	4.83	3.91
TKP305b	1884	2002	-	-	-	-	-	-	-	-	-	-	-	-	-	-	\
TKP305c	1858	2002	-	-	-	-	-	3.45	-	-	-	3.33	-	-	-	-	\
TKP306c	1915	2002	-	-	-	-	3.01	-	-	-	-	\	\	\	3.41	\	\
TKP307b	1837	2002	-	-	-	-	-	5.07	4.31	-	-	5.03	6.43	-	3.01	-	\
TKP307c	1878	2002	3.97	3.23	-	-	-	-	4.33	3.29	3.01	-	-	-	4.01	-	\
TKP308a	1913	2002	-	-	-	-	-	-	-	-	-	\	\	\	-	\	\
TKP308b	1913	2002	-	-	-	-	-	-	-	-	-	\	\	\	-	\	\
TKP309a	1900	2002	*	5.25	3.40	-	-	-	4.58	-	-	-	-	\	6.61	-	\
TKP309b	1930	2002	*	*	3.56	-	-	4.20	4.58	-	-	\	\	\	3.22	\	\
TKP309c	1930	2002	*	*	*	-	-	-	-	-	3.98	\	\	\	-	\	\
TKP310a	1910	1982	*	*	*	*	-	-	-	-	-	\	\	\	-	\	\
TKP310c	1930	2002	*	*	*	*	*	-	-	-	-	\	\	\	-	\	\
TKP311a	1736	2002	*	*	*	*	*	*	12.78	4.55	5.51	7.28	6.34	4.03	5.21	4.48	5.20
TKP311b	1552	2002	*	*	*	*	*	*	*	6.21	8.69	6.01	4.79	7.38	7.63	6.09	10.54
TKP312a	1653	2002	*	*	*	*	*	*	*	*	13.88	4.36	-	4.81	4.66	6.11	6.26
TKP312b	1529	1960	*	*	*	*	*	*	*	*	*	4.55	-	5.75	5.01	4.94	7.66
TKP313a	1745	1920	*	*	*	*	*	*	*	*	*	*	9.13	4.64	4.64	5.56	3.20
TKP313b	1631	1920	*	*	*	*	*	*	*	*	*	*	*	3.45	5.91	-	3.77
TKP314a	1671	1900	*	*	*	*	*	*	*	*	*	*	*	*	5.15	4.59	8.58
TKP314b	1632	2002	*	*	*	*	*	*	*	*	*	*	*	*	*	7.86	5.57
TKP315a	1705	1914	*	*	*	*	*	*	*	*	*	*	*	*	*	*	5.35
TKP315b	1588	1810	*	*	*	*	*	*	*	*	*	*	*	*	*	*	*

Table 4.8. Inter-tree comparison for 2003 resample from Trounson Kauri Park. t-values over 3.00 shown. \ = overlap < 15 years, - = t-values less than 3.00, * = empty triangle. n = 44 min t = 0.04 max t = 10.41 mean t = 5.34 s.d. = 2.30.

Tree I.D.	Start Year (A.D.)	End Year (A.D.)	TKP301	TKP302	TKP304	TKP307	TKP309	TKP311	TKP312	TKP313	TKP314	TKP315
			A.D.1826 A.D. 2002	A.D.1858 A.D.2002	A.D.1743 A.D.1890	A.D.1837 A.D.2002	A.D.1900 A.D.2002	A.D.1552 A.D.2002	A.D.1529 A.D.2002	A.D.1631 A.D.1920	A.D.1632 A.D.2002	A.D.1588 A.D.1914
TKP301	1826	2002	*	4.50	4.50	4.15	-	5.82	6.54	4.20	6.61	4.43
TKP302	1858	2002	*	*	-	5.77	4.70	4.82	3.56	5.67	6.52	-
TKP304	1743	1890	*	*	*	3.58	\	9.85	5.86	6.27	6.59	7.55
TKP307	1837	2002	*	*	*	*	5.16	6.12	3.58	4.31	4.28	-
TKP309	1900	2002	*	*	*	*	*	4.35	-	-	6.09	-
TKP311	1552	2002	*	*	*	*	*	*	7.69	7.07	7.90	9.22
TKP312	1529	2002	*	*	*	*	*	*	*	3.66	6.20	10.41
TKP313	1631	1920	*	*	*	*	*	*	*	*	5.93	5.98
TKP314	1632	2002	*	*	*	*	*	*	*	*	*	8.32
TKP315	1588	1914	*	*	*	*	*	*	*	*	*	*

Both original and resampled material was combined into a revised and updated site chronology for Trounson, referred to as TROUNSON. Figure 4.12 displays the structure of the TROUNSON chronology, comprised of original (TKP) and resampled material (TKP with ID numbers starting with 3). Three cores from trees TKP311, TKP312 and TKP315 extended beyond A.D. 1600. The longest sequence of the collection was TKP311B, which spanned 474 years between A.D. 1552-2002 and had consistently high between tree *t*-values as seen in Table 4.7. Seven trees (TKP301, TKP302, TKP307, TKP309, TKP311, TKP312, and TKP314) improved post-1960 replication for the site up until A.D. 2002.

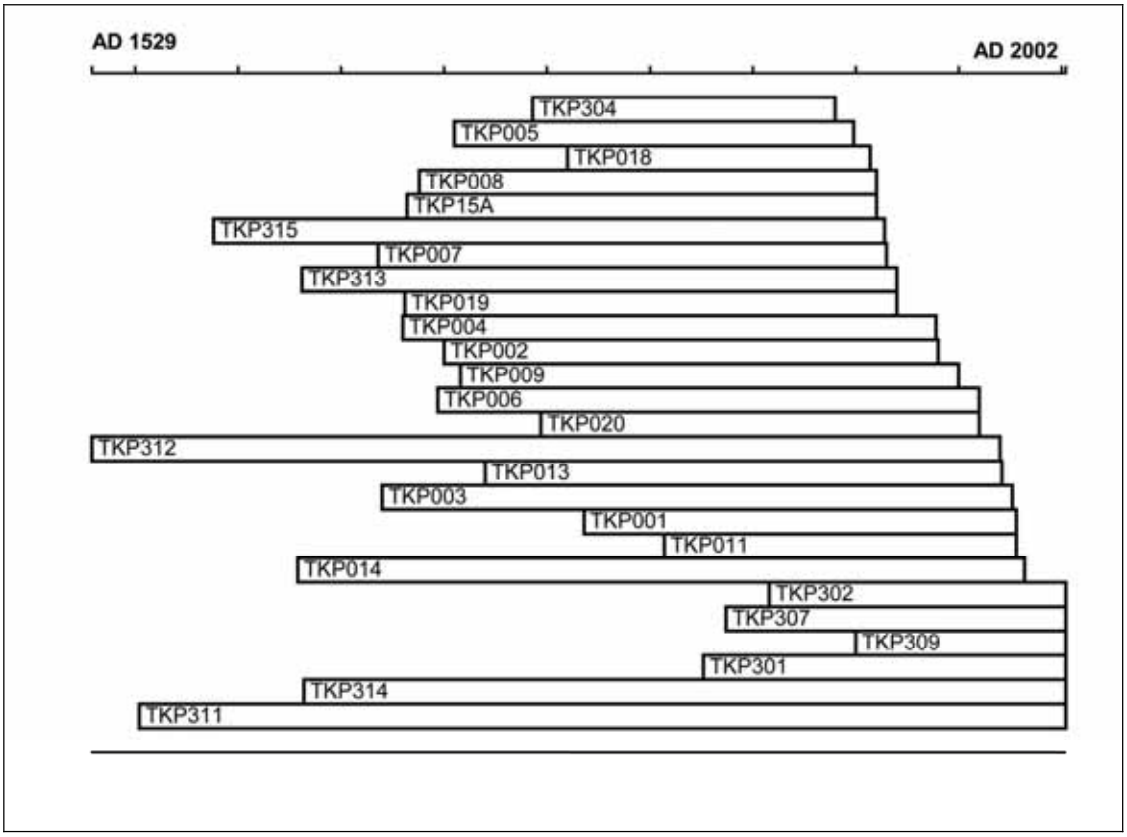

Figure 4.12. Tree sequences used to develop TROUNSON chronology (A.D. 1529-A.D. 2002) including Ahmed's original material and resample 2003 trees which have a TKP prefix and ID numbers beginning with 3 e.g. TKP315.

Inter-tree comparisons for the original and resampled trees included in the TROUNSON chronology are presented in Table 4.9. Statistical relationships between the two subsets were significant but fairly modest, perhaps reflecting the complex structure of the chronology. The strongest relationship was observed between TKP009

and TKP311 (t=9.28). In fact, the long TKP311 sequence had the best agreement with all trees from the original collection. The worst performer of the resample group was TKP309, which only spanned A.D. 1900-2002. This is likely to be due to its short length and its position in the fairly poorly replicated post-1900 period noted from this site. TKP309 did however, show a fairly good relationship with TKP314 (t=6.09), and thus was considered valuable for its role in contributing to the update of the Trounson chronology to A.D. 2002.

To verify crossdating, statistical comparisons between the original, resampled and revised chronologies for Trounson were undertaken against the modern Kauri master chronology (excluding the original Trounson record) and individual site chronologies. The results of this analysis (Table 4.10) indicate an improvement in the statistical robustness of both the resample and revised chronologies compared to the original chronology of Ahmed (1984).

Compared to Ahmed's (1984) chronology, t-values for the revised TROUNSON chronology improved virtually in all instances with individual site chronologies from all regions. The only instance of a weakened relationship was noted between the Huia chronology where the t-value fell from 9.29 to 9.04. The weakest relationship (t=5.28) was noted with the relatively short Konini Forks chronology from the Auckland region. The revised chronology showed greatest affinity for Waipoua standing dead (t=12.99), Cascades (t=11.85) and Huapai (t=11.46). There was an overall improvement of the t-value statistic from t=12.47 to t=14.17 with the modern master, indicating a discernable improvement from the incorporation of resampled material (Table 4.10).

Table 4.9. T-Value matrix for remeasured original (Ahmed, 1984) and 2003 update trees from Trounson Kauri Park. *t*-values over 3.00 shown. \ = overlap < 15 years, - = *t*-values less than 3.00, * = empty triangle. * = empty triangle n = 135 min t = 3.08 max t = 9.28 mean t = 5.28 s.d. = 1.38.

Tree I.D.	Start Year (A.D.)	End Year (A.D.)	TKP301	TKP302	TKP304	TKP307	TKP309	TKP311	TKP312	TKP313	TKP314	TKP315
			A.D.1826 A.D.2002	A.D.1858 A.D.2002	A.D.1743 A.D.1890	A.D.1837 A.D.2002	A.D.1900 A.D.2002	A.D.1552 A.D.2002	A.D.1529 A.D.1970	A.D.1631 A.D.1920	A.D.1632 A.D.2002	A.D.1588 A.D.1914
TKP001	1768	1978	3.26	5.00	6.15	5.46	3.46	3.55	4.55	4.12	6.19	5.15
TKP002	1700	1940	4.08	5.75	5.94	4.94	-	5.49	5.19	6.07	5.37	7.10
TKP003	1670	1976	4.86	5.65	6.46	4.97	4.08	7.72	8.51	5.20	7.89	7.27
TKP004	1680	1939	-	3.68	5.46	3.82	-	6.82	-	6.25	3.58	4.32
TKP005	1705	1899	-	3.92	5.64	3.04	\	5.51	3.59	4.11	5.14	5.51
TKP006	1697	1960	4.33	-	7.93	3.93	-	6.97	5.08	6.40	4.50	5.86
TKP007	1668	1915	-	-	6.11	3.20	-	4.84	3.78	4.89	3.57	4.44
TKP008	1688	1910	-	6.00	6.89	4.46	\	7.81	3.23	7.10	5.45	4.92
TKP009	1708	1950	3.98	4.71	7.71	4.63	-	9.28	6.78	6.53	8.10	7.90
TKP013	1720	1971	-	-	4.81	-	-	3.45	-	4.37	-	4.21
TKP011	1807	1978	-	-	-	-	-	-	-	-	-	-
TKP014	1629	1982	-	-	4.90	-	-	4.24	4.60	5.36	3.47	5.40
TKP015	1682	1910	-	4.05	5.91	4.28	\	4.90	5.64	5.17	5.70	5.21
TKP018	1760	1907	3.51	3.55	5.84	4.10	\	6.12	3.76	7.73	3.99	3.34
TKP019	1681	1920	-	3.08	4.48	-	-	4.17	-	6.89	4.00	4.22
TKP020	1747	1960	3.19	3.32	4.71	4.98	3.10	3.51	4.67	4.42	4.85	3.48

Table 4.10. Intra-site comparison of original (TROU84), resampled (TROU03) and revised Trounson (TROUNSON) chronologies with all modern Kauri site chronologies by region. \ = overlap < 15 years, - = t-values less than 3.00, n = 45 min t = 5.25, max t = 16.33 mean t = 9.37 s.d. = 2.58.

Master Chronology	Start Dates (A.D.)	End Dates (A.D.)	TROU84	TROU03	TROUNSON
			A.D. 1668 A.D. 1980	A.D. 1529 A.D. 2002	A.D. 1529 A.D. 2002
Kauri Master (ex. Trounson)	1269	2002	12.47	16.33	14.17
Auckland					
Cascades	1559	1982	10.76	11.61	11.85
Hidden Valley	1679	2003	7.20	9.53	9.09
Huapai	1483	1997	10.82	11.35	11.46
Huia	1720	1981	9.29	11.50	9.04
Konini Forks	1770	1976	5.25	8.40	5.28
Little Barrier	1790	1981	5.51	8.36	6.22
Waikato/Bay of Plenty					
Katikati	1698	1996	5.25	7.49	5.95
Manaia	1269	1998	7.22	12.11	9.54
Moehau	1360	1980	7.83	10.68	8.75
Mount William	1580	1981	8.30	10.34	9.56
Northland					
Puketi Bluff	1675	1981	5.87	6.44	6.17
Puketi Loop	1504	2002	8.38	13.22	10.57
Waipoua Dead	1628	1903	11.49	9.04	12.99
Warawara	1660	1979	8.33	11.90	8.77

To assess the validity of including all crossdated material in the revised chronology, the EPS results for both standardised chronologies were examined (Table 4.11). Overall, both the chronologies were found to be of a high quality (EPS remained above 0.912 with no series removed) and the effects of stripping were found to be negligible, particularly in the case of the spline 20 standardisation. Removing the statistically 'worst' sample of the chronology (TKP011B from the original collection), resulted in maximum improvement of 0.003 which was considered insignificant. Importantly, the EPS analysis implies that it is not necessary to exclude any of the crossdated series from construction of the revised TROUNSON chronology.

Table 4.11. Revised chronology Stripping Expressed Population Signal (EPS) results for TROUNSON chronology.

Standardisation	EPS Value (All Series)	Highest Quality Period (EPS≥0.80)	Most Significant Series Removal	EPS Improvement
Spline 20	+0.947	A.D. 1680 - A.D.1977	TKP0 11B	+0.946 to +0.947
Spline 200	+0.912	A.D. 1719 - A.D.2002	TKP 011B	+0.904 to +0.907

Overall, the 474-year revised chronology had an average ring width of 1.86 mm and a mean sensitivity of 0.16, representing the relative high frequency variance of a series (periods <2 years in length) (Fritts, 1991). Maximum sample depth of 24 trees occurs between A.D. 1858-1890, with seven update trees extending beyond A.D. 1980-2002 (Appendix 3B). Three trees (TKP311, TKP312, and TKP315) extend the record beyond A.D. 1600 period, the longest (TKP312A) dating to A.D. 1529-2002.

4.7.4 Discussion of the revised Trounson chronology

Revision of Ahmed's original samples and analysis of new material resulted in a robust 26-tree (52 radii) chronology for Trounson Kauri Park. Ten trees of sufficiently high quality were incorporated as a result of the 2003 resample. The TROU03 chronology has the strongest statistical relationship with Puketi Loop (t=13.22) and Warawara (t=11.90), which may be a reflection of the chronology's regional affinity with these other Northland sites. It may be that the strong relationship noted with Puketi Loop also reflects the similar temporal coverage of the revised Puketi chronology (A.D. 1504-2002), reported by Gergis *et al.* (2005a).

It is evident from Table 4.10 that the TROU03 chronology displayed higher t -values than the combined revised TROUNSON chronology. The most obvious example is the TROU03 chronology's relationship to the modern master (t=16.33) which falls to 14.17 for the TROUNSON chronology. This possibly reflects the complex composition of the TROUNSON chronology. Truncation issues noted for the original (TROU84) and resample (TROU03) collections is reflected in the nature of the extension of the revised TROUNSON chronology. For example, there are 15 samples extending beyond A.D. 1960 from the TROU03 chronology compared to eight samples from the TROU84.

The near doubling of sample depth for this period perhaps accounts for the lowered t values observed between the TROU03 and TROUNSON chronologies presented in Table 4.10. This may suggest a greater weighting of the TROU03 chronology for the (relatively unreplicated) post-1960 component of the TROUNSON chronology, which may influence the statistical relationships relative to other regional chronologies. In addition, there are seven samples that contribute to pre-A.D. 1700 sample depth from the TROU03 chronology compared to nine from the TROU84 material. These results may be indicative of real differences in the nature of the original and resampled trees examined from Trounson.

The impact of chronology standardisation is reflected in the length of the high quality period indicated by the EPS results presented in Table 4.11. Discrepancies noted for the late 20th century relate to the EPS value dropping below 0.8 between A.D. 1978 and A.D. 2002 using the spline 20 standardisation. This may be due to a higher signal-to-noise ratio produced by using a high pass filter (i.e. frequencies <20 years enhanced using a 20 year spline), which may highlight the benefits of using a Kauri chronology which has been subjected to more conservative smoothing such as the spline 200. Using the more conservative 200 year smoothing spline, however, served to reduce the length of the high quality period at the older end of the chronology by 39 years. This corresponds to a notable decline in sample depth (see Appendix 3B) where the impact of using material derived from differing populations of trees from the original and resampled collections from Trounson are likely to be more amplified.

Nonetheless, the revised chronology for Trounson was found to match well against all other modern chronologies from Auckland, Waikato and Northland indicating that the site is of a standard sufficient to be included in the modern Kauri master record. This was confirmed by the high EPS statistics noted for both standardised chronologies, thus all series were incorporated into the final chronology.

The Trounson Kauri Park chronology was revised as part of an update of Northland tree-ring chronologies to be used for El Niño-Southern Oscillation research. Existing material from Trounson was remeasured, leading to the incorporation of an additional three trees (10 samples). The original chronology was rebuilt using 10 trees (29 samples) (TROU03). After new trees were sampled in 2003, an additional 23 samples from 10 trees were crossdated to extend Ahmed's (1984) original 13 tree site chronology (A.D. 1668-1980) to a robust 26 tree/52 radii chronology spanning A.D. 1529-2002 (TROUNSON).

A considerable proportion of resampled trees displayed complacent and obscure growth rings, particularly in the post-1900 period. This led to the rejection of five resampled trees from further analysis and the truncation of three trees used in the revised chronology. The resample supports Ahmed's (1984) hypothesis that Trounson and Waipoua may have suffered some sort of regional disturbance. In light of the high degree of biological noise noted from trees from this site, it is recommended that no further dendrochronological sampling be undertaken at Trounson Kauri Park for purposes associated with the reconstruction of climate parameters.

Overall, the reappraisal of material from Trounson resulted in the development of a robust chronology, TROUNSON, representing the fourth longest record of the modern Kauri database. Trounson is the second of the Northland chronologies to extend past A.D. 1982, and the second of the 17 modern Kauri chronologies to span the entirety of the 20th century (Gergis *et al.*, 2005b).

4.8 Revision of the modern Kauri Master Chronology

4.8.1 Introduction

As a prelude to climate reconstruction, Fowler *et al.* (2004) summarised the state of the modern Kauri tree-ring master chronology derived from living and standing dead trees. This clearly demonstrated that Kauri growth variation is primarily a response to regional-scale climate forcing, operating over several degrees of latitude and longitude (Fowler *et al.*, 2004). The presence of pervasive regional forcing led to the development of a multi-site master chronology for palaeoclimate reconstruction.

Recently, the modern Kauri database was revised for the purpose of ENSO reconstruction. Updated material from living Kauri trees were sampled from two Northland sites (Puketi State Forest, Trounson Kauri Park) and two new areas of Hidden Valley and Waitakere Dam (Table 4.12) were incorporated into updated versions of the modern Kauri chronology for climate analysis. In particular, late 20th century and pre A.D. 1600 low sample depth periods were targeted. Prior to the update, 149 trees (344 series) from 15 sites were used to develop the modern Kauri master chronology.

4.8.2 Chronology Construction and Standardisation

All standardised series from 17 modern Kauri sites (CASC, HIDV, HUIA, HUPI, KATI, KOND, KAWH, LTBR, MASC, MWIL, MOEH PUBL, PUKF, TROU, WAID, WARA, WTDM shown in Figure 4.1), plus a display piece of unknown origin were combined into tree mean sequences that were then averaged to produce two versions of the Kauri master chronology; AGAU05a (spline 20) and AGAU05b (spline 200). Note that the KAWH and WAID chronologies not included in the data set used by Fowler *et al.* (2004) are used here, while MOEH remains excluded.

To maximise the common high-frequency climate signal, a master chronology AGAUm05a was developed using a relatively flexible standardisation spline of 50% variance cut-off at 20 years following Fowler *et al.* (2004), who concluded that more conservative standardisation is required for decadal to centennial-scale climate applications. To investigate the implications of standardisation techniques on master chronology development, this analysis focuses on a master record using a conservative smoothing spline with 50% variance cut off at 200 years (AGAUm05b) to allow comparison with results of the spline 20 analysis reported by Fowler *et al.* (2004).

Following standardisation, a quality control procedure was initiated to test the merit of including each crossdated series in the construction of the updated site and master chronologies. This was assessed using the Expressed Population Signal (EPS) statistic (Briffa and Jones, 1990), detailed Section 4.2.

Table 4.12. Chronology details for sites updated since Fowler *et al.* (2004). HIDV and WTDM are new sites and unanalysed material from WARA underlined. 1) Ahmed and Ogden (1985), 2) Gergis *et al.* (2005a), Gergis *et al.* (2005b), 4) Boswijk and Ogden (2005), and 5) Lorrey (2004).

Code	Location	Trees (cores)	Dates (A.D.)	Comments	Refs
PUKF	Puketi Forest South (35º 15'S 173º 44'E) Altitude: 290 m Aspect: N	22 (47)	1504-2002	Original chronology developed by Ahmed (1984) spanned A.D.1780-1982 using 19 radii from 10 trees. Material for this chronology was developed pooling material from the Loop track and Te Harua in southern Puketi. In 2003, 39 samples from 15 trees were sampled from the "Loop Track" (Waihoanga Gorge) in southern Puketi forest. 27 radii from 12 trees were cross matched and incorporated into the original chronology. This resulted in a 297 year extension to the original chronology to now cover A.D. 1504-2002.	1,2
PUBL	Onekura Bluff, Puketi Forest (35º 11'S 173º 45'E) Altitude: 305 m Aspect: N	9 (24)	1623-1982	In 2003, 40 samples from 15 trees were sampled at an average elevation of 320m from Onekura Bluff in northern Puketi. The site was accessed from the quarry site on the Mokau Ridge Road approximately 2km along the Onekura Route trail. Preparation and visual inspection of the material suggests that a sensitive ring patterns is suitable for chronology development to be used for future climate analysis.	1,2
TROU	Trounson Kauri Park (35º 43'S 173º 38'E) Altitude: 175 m Aspect: N	26 (52)	1529-2002	Original chronology developed by Ahmed (1984) spanned A.D. 1668-1980 using 19 radii from 13 trees. The outer part of several trees displayed significant suppression of rings, mostly between 1900-1980. The original collection was also remeasured in an attempt to bolster pre-1600 sample depth. The revaluation of the original material resulted in an addition of 10 radii and three trees previously rejected by Ahmed (1984). In 2004, 40 samples from 15 trees were sampled from a north-eastern portion of Trounson Kauri Park. The resample also identified problematic growth anomalies such as suppression and complacent growth patterns. Nonetheless, 23 samples from 10 trees were cross matched and incorporated into the original chronology. This resulted in a 161 year extension to the original chronology to cover A.D. 1529-2002.	1,3
WARA	Warawara Forest (35º 22'S 173º 17'E) Altitude: 468 m Aspect: N	14 (28)	1640-1979	Original chronology derived from pooling material from a plateau and ridge site, with only one tree covering A.D.1640-1750. In 2004, 31 samples from 12 trees were collected from Warawara Plateau (35º 22', 52" S 173º 17' 11" E) at an elevation of 522m. 27 samples from 10 trees were also sampled from a nearby ridge (35º 24' 25" S 173º 17' 40" E) at 426m. The very mature nature of the trees and visual inspection of the samples appear very promising for extensive chronology development.	1
HIDV	Hidden Valley, Great Barrier (36º 12'S 175º 26'E) Altitude: 220 m Aspect: E	13 (20)	1697-2003	In 1999, 10 Cores were taken from five trees in 'Hidden Valley', growing on an east-facing slope on Great Barrier Island. The core samples were measured by Xiong at the Lincoln University Tree-ring Laboratory but never combined into a site chronology. In 2004, Hidden Valley was revisited by Boswijk and Ogden and five trees originally sampled were identified and a single core obtained from each. Four additional trees and a fallen, rotted log were also sampled. A chronology was subsequently constructed spanning A.D. 1679- 2003, using 20 cores from 13 trees.	4
WTDM	Waitakere Reservoir, Auckland (36º 54'S 174º 32'E) Altitude: 210 m Aspect: NW	7 (22)	1727-2002	In 2004, 32 cores from 8 trees were sampled from the north-east shore of Waitakere Reservoir. Seven kauri cross-matched and were combined into a site chronology, WTDM, which span the period A.D. 1728-A.D. 2002. Trees at this site were once located on a ridge top, but with the construction of the reservoir in the early 1900's the kauri here are now at or near lake-level. It is thought this site could be used as a "swamp" kauri analogue.	5

4.8.3 Revisions of the Puketi State Forest chronology

As detailed in Sections 4.4, 39 samples from 15 Kauri were sampled from Puketi State Forest. The original chronology developed by Ahmed (1984) (A.D. 1780-1981) comprised of 19 radii from 10 trees, was extended by 297 years through the addition of 27 radii from 12 trees (Gergis *et al.*, 2005a). Eleven trees extending beyond 1981 to 2002, and three trees improved replication beyond A.D. 1600, the longest dated from A.D. 1504-2002 (Gergis *et al.*, 2005a). This revision resulted in a 47 radii/22-tree chronology representing the fourth longest chronology in the modern Kauri database (A.D. 1504-2002), the first of the modern Kauri data base to cover the entirety of the 20th century (Gergis *et al.*, 2005a).

The quality of the PUKF chronology is reflected by EPS values which remained above 0.92 with no series removed. A maximum of 0.002 EPS improvement was attained removing the worst performer of the chronology (Gergis *et al.*, 2005a). As a result, none of the crossdated series was omitted from subsequent chronology construction.

4.8.4 Revisions of the Trounson Kauri Park chronology

In 2003, 40 radii from 15 trees were sampled from Trounson. Existing material collected by Ahmed (1984) was also reassessed for its potential to extend the original site chronology to be used for climatic analysis. Remeasurement led to an incorporation of an additional 10 samples and three trees, allowing 29 samples from 16 trees from the original collection to be incorporated into a revised chronology for Trounson (Gergis *et al.*, 2005b).

Following the resample, an additional 23 samples from 10 trees were added, resulting in a considerable revision of the original 13 tree chronology (A.D. 1668-1980). Three trees were responsible for date extension beyond A.D. 1600, the longest sequence spanning 474 years from A.D. 1552-2002. Seven trees from the resample collection improved post-1960 replication to A.D. 2002. The revision resulted in a robust 52 radii/26-tree chronology for Trounson spanning A.D. 1529-2002. This represents the fifth longest chronology of the modern Kauri master database and the second to cover the entirety of the 20th century (Gergis *et al.*, 2005b).

Both the Spline 20 and 200 versions of the TROU chronology were found to be of a high quality, with the EPS remaining above 0.912 with no series removed. The EPS

analysis suggests that it is unnecessary to exclude any of the cross dated series from construction of a revised chronology for Trounson.

4.8.5 Hidden Valley, Great Barrier Island

In 1999, 10 cores were sampled from five trees in 'Hidden Valley', growing on an east-facing slope on Great Barrier Island, however, these samples were not incorporated into any of the Kauri master chronologies (Boswijk *et al.*, 2002). In 2004, Hidden Valley was revisited and five trees originally sampled were identified and a single core obtained from each (Boswijk and Ogden, 2005). Four additional trees and a fallen, log were also sampled. The HIDV chronology was developed using 20 radii from 13 trees, spanning A.D. 1697-2003 (Boswijk and Ogden, 2005). Five trees extend to 2003 while another two date to A.D. 1997. The introduction of HIDV signifies the third site to cover the entirety of the 20th century, importantly introducing material from the east coast into the modern Kauri data base.

The effects of stripping for HIDV were found to be slightly higher than PUKF and TROU. Both the spline 20 (200) chronologies were found to be of a high quality, with an EPS of 0.91(0.84) with no series removed. Removing the statistically 'worst' sample of the chronology (HID 004B), resulting in maximum improvement of 0.009 (0.003) using spline 200 (20) standardisation. The lower quality statistics noted for HIDV are likely to be due to considerably lower sample depth of the new chronology compared to the now very well replicated PUKF and TROU records. Nonetheless, the changes to EPS were once again considered minor, thus it was deemed unnecessary to exclude any of the crossdated series from construction of the HIDV chronology.

4.8.6 Waitakere Dam, West Auckland

The Waitakere Dam site is located 210m above sea level, near Cascades Kauri Park, a regional recreation area in the foothills of the Waitakere Ranges (Lorrey, 2004). In 2004, 32 samples from eight trees were sampled 3m above lake level from the north-eastern shore of Waitakere Reservoir. Lorrey (2004) developed the WTDM chronology using 22 samples from seven trees for the period A.D. 1727-2002. All trees used in the WTDM extended to A.D. 2002, with only one tree (WTD005) covering the pre A.D. 1840 period.

Both the spline 20 and 200 WTDM chronologies were found to be of a good quality; EPS was 0.87 and 0.75, respectively with no series removed. Like HIDV, the lower quality statistics noted for WTDM are likely to be due to considerably lower sample depth of the new chronology compared to PUKF and TROU chronologies. Nonetheless, the changes to EPS were once again considered minor, thus it was deemed unnecessary to exclude any of the crossdated series from construction of the WTDM chronology.

4.8.7 Inter-site comparisons

Inter-site correlations were investigated using a cross-correlation matrix (Table 4.13) for the high quality period A.D. 1840-1920 identified by Fowler *et al.* (2004). A spline 200 version of the Fowler *et al.* (2004) master chronology, AGAU03d, was used to assess statistical robustness of individual site chronologies to all other crossdated material. Inter-site correlations ranged from a low of r=0.08 (WTDM-KAWH) to a maximum r=0.82 (PUKF-PUBL). The mean correlation for each site across all other sites ranges from r=0.24 (KAWH) to r=0.50 (PUKF) (not shown).

Updating PUKF and TROU resulted in some notable revisions in inter-site correlations. Significantly, the chronology from Puketi displayed the highest mean correlation for each site across all other sites (r=0.50). In line with the result of Fowler *et al.* (2004), the highest inter-site relationship of all modern sites was noted between PUKF and PUBL (r=0.82), perhaps an indication of the geographical proximity of the two sites.

PUKF also displayed the second strongest relationship (r=0.77) with the AGAU03d master along with HUPI, following HUIA (r=0.79). Slight declines in correlation were noted between PUKF and three Auckland chronologies of KATI (r=0.57 to r=0.49) and LTBR (r=0.51 to r=0.49), perhaps reflecting a reduction in the interval of overlap shared by these relatively short chronologies.

Table 4.13. Inter-site correlations (r) for 200 spline standardised versions of the modern Kauri chronologies. Following Fowler *et al.* (2004), correlations are based on the A.D. 1840-1920 period, with pre-updated correlations shown in brackets. AGAU03d refers to the spline 200 version of the master chronology reported in Fowler *et al.* (2004).

	CASC	HIDV	HUIA	HUPI	KATI	KAWH	KOND	LTBR	MASC	MOEH	MWIL	PUBL	PUKF	TROU	WAID	WARA	WTDM
CASC	-	0.60	0.56	0.48	0.32	0.35	0.29	0.26	0.61	0.41	0.62	0.47	0.64 (0.47)	0.65 (0.54)	0.25	0.26	0.44
HIDV	0.60	-	0.46	0.47	0.19	0.35	0.37	0.33	0.48	0.42	0.57	0.37	0.53 (N/A)	0.61 (N/A)	0.18	0.25	0.45
HUIA	0.56	0.46	-	0.61	0.41	0.23	0.42	0.50	0.51	0.53	0.66	0.54	0.56 (0.49)	0.51 (0.46)	0.41	0.56	0.44
HUPI	0.48	0.47	0.61	-	0.24	0.32	0.50	0.62	0.33	0.53	0.65	0.34	0.45 (0.37)	0.54 (0.47)	0.37	0.35	0.41
KATI	0.32	0.19	0.41	0.24	-	0.24	0.60	0.39	0.35	0.25	0.26	0.59	0.49 (0.57)	0.30 (0.20)	0.31	0.54	0.29
KAWH	0.35	0.35	0.23	0.32	0.24	-	0.30	0.14	0.32	0.33	0.30	0.09	0.11 N/A	0.45 N/A	0.10	0.24	0.08
KOND	0.29	0.37	0.42	0.50	0.60	0.30	-	0.61	0.32	0.38	0.35	0.44	0.41 (0.38)	0.35 (0.31)	0.32	0.56	0.48
LTBR	0.26	0.33	0.50	0.62	0.39	0.14	0.61	-	0.35	0.33	0.26	0.53	0.49 (0.51)	0.41 (0.32)	0.57	0.54	0.46
MASC	0.61	0.48	0.51	0.33	0.35	0.32	0.32	0.35	-	0.51	0.40	0.54	0.69 (0.56)	0.51 (0.38)	0.28	0.33	0.20
MOEH	0.41	0.42	0.53	0.53	0.25	0.33	0.38	0.33	0.51	-	0.40	0.45	0.42 N/A	0.39 N/A	0.38	0.41	0.26
MWIL	0.62	0.57	0.66	0.65	0.26	0.30	0.35	0.26	0.40	0.40	-	0.42	0.48 (0.34)	0.57 (0.48)	0.16	0.30	0.27
PUBL	0.47	0.37	0.54	0.34	0.59	0.09	0.44	0.53	0.54	0.45	0.42	-	0.82 (0.77)	0.51 (0.36)	0.52	0.57	0.29
PUKF	0.64	0.53	0.56	0.45	0.49	0.11	0.41	0.49	0.69	0.42	0.48	0.82	-	0.65 (0.34)	0.51	0.44	0.34
TROU	0.65	0.61	0.51	0.54	0.30	0.45	0.35	0.41	0.51	0.39	0.57	0.51	0.65 (0.34)	-	0.61	0.41	0.43
WAID	0.25	0.18	0.41	0.37	0.31	0.10	0.32	0.57	0.28	0.38	0.16	0.52	0.51 N/A	0.61 N/A	-	0.42	0.28
WARA	0.26	0.25	0.56	0.35	0.54	0.24	0.56	0.54	0.33	0.41	0.30	0.57	0.44 (0.43)	0.41 (0.41)	0.42	-	0.36
WTDM	0.44	0.45	0.44	0.41	0.29	0.08	0.48	0.46	0.20	0.26	0.27	0.29	0.34 N/A	0.43 N/A	0.28	0.36	-
AGAUm03d	0.70	0.60	0.79	0.77	0.61	0.43	0.68	0.71	0.64	0.59	0.70	0.73	0.77 (0.70)	0.76 (0.67)	0.59	0.68	0.53

Statistical relationships between the longer chronologies included in the master record were strengthened. For example, the correlation between PUKF and MASC improved from r=0.56 to a high r=0.69, which represents the second strongest inter-site relationship (after PUKF-PUBL) of the all modern Kauri sites. This strong relationship between PUKF and MASC was also noted by Fowler *et al.* (2004) using spline 20 standardisation. Marked improvements were observed between PUKF and TROU (r=0.34 to r=0.65) and CASC (r=0.47 to r=0.64). The weakest inter-site correlation of r=0.11 was obtained for the KAWH chronology.

The revised TROU chronology showed an increase in mean correlations for each site across all other sites from r=0.39 to r=0.49. TROU displayed the third highest correlation of r=0.76 with the AGAU03d master chronology, improving from a correlation of r=0.67. Revising TROU resulted in improved correlations with all site chronologies listed in Table 4.13. Marked improvements between TROU were noted for MASC (r=0.38- r=0.51), MWIL (r=0.48- r=0.57) and PUBL (r=0.36 to r=0.51).

The strongest inter-site relationship for TROU (r=0.66) was noted between CASC and PUKF, while the weakest was r=0.30 with KATI. The strong correlations noted against TROU and PUKF may relate to high temporal overlap.

Inter-site correlations for the newly introduced HIDV achieved a mean correlation value of r=0.41 between all other sites, and a r=0.53 relationship with the Fowler *et al.* (2004) master chronology. HIDV showed the greatest affinity with TROU (r=0.59), MWIL (r=0.58), CASC (r=0.52), and HUPI (r=0.47). The weakest correlations were seen against WAID (r=0.15), KATI (r=0.19), and WARA (r=0.28). HIDV does not show evidence for affinity to any particular region.

Inter-site correlations for the newly introduced WTDM achieved a mean correlation value of 0.34 between all other sites, and a relationship of r=0.60 with the Fowler *et al.* (2004) master chronology. WTDM showed the greatest affinity with KOND (r=0.48), LTBR (r=0.46), HIDV (r=0.44), and HUIA (r=0.44). The weakest correlations were seen with KAWH (r=0.08), MASC (r=0.20), MOEH (r=0.26) and MTWIL (r=0.27). Like HIDV, WTDM does not appear to show any evidence for any particular regional affinity.

Improvements in the high quality periods (defined using EPS values ≥ 0.8) of the revised PUKF and TROU chronologies were achieved for both spline 20 and 200 standardisations. The spline 20 version of the updated PUKF is now the third site chronology of the modern master to exceed an EPS values ≥ 0.95 between A.D. 1849-1981. Using spline 200 standardisation, the most marked improvement for PUKF was a 147% increase in the EPS >0.90 between A.D. 1834-1981. Using spline 20 standardisation there was a 54.6% increase in the length of TROU exceeding an EPS≥ 0.90. A notable 116% increase in the proportion of the spline 200 TROU exceeding EPS>0.80 (A.D. 1719-2002).

The marked improvements observed for the spline 200 version of TROU may reflect the relatively lower quality of the original chronology (due to issues such as truncation, see Gergis *et al.* (2004b)) prior to the update. However, the higher quality of the PUKF is suggested by the 132% increase in the length of the spline 20 chronology with an EPS ≥ 0.95. This highlights the obvious benefit increased replication has on the overall quality of Kauri chronologies, irrespective of original quality. Simply speaking, a

relatively poor chronology may be made good and a good chronology made better through increasing sample depth and length at a given site.

The introduction of HIDV resulted in the addition of 291 years (A.D. 1706-1997) of high quality material (EPS>0.80) to the spline 20 chronology. Using spline 200 standardisation, high EPS values were achieved for 277 years (A.D. 1720-1997), signifying the internal quality of the new chronology. Using the WTDM chronology, EPS≥0.80 for both chronologies were identified from the spline 20(200) chronology between A.D. 1869 –2002 (1879-2002). Although the chronology doesn't extend far back in time, it provided useful replication of the late 20th century important for proxy calibration associated with climate analysis.

4.8.8 Updating the modern Kauri master chronology

A total of 344 series from 149 trees were used to develop the spline 200 version of the master chronology (AGAU03d) used by Fowler *et al.* (2004). Following the update, a revised master chronology (AGAU05b), was constructed using 426 series from 191 trees (Figure 4.13). This represents an overall increase of 22% (28%) in the number of trees (series). Details of the percentage increases generated for various sub-intervals between A.D. 1500-2002 are presented in Table 4.14. Using the revised AGAU05b chronology, peak sample depth (A.D. 1900) was improved by 82 series (24%) and 42 trees (28%). Significant improvements in the maximum number of trees were also noted between A.D. 1701-1800 (44%), A.D. 1601-1700 (42%), and A.D. 1501-1600 (40%), representing a considerable bolstering of sample depth within the master chronology.

Table 4.14. Mean and maximum percentage increase of sample depth of updated material relative to spline 200 version of the chronology reported by Fowler *et al.* (2004) (AGAU03d). The periods specifically targeted for the update are in bold.

Dates (A.D.)	Mean % Increase of No. Series	Maximum % Increase of No. Series	Mean % Increase of No. Trees	Maximum % Increase of No. Trees
1501-1600	14.6	23.5	25.0	40.0
1601-1700	16.9	22.9	31.1	42.2
1701-1800	27.3	33.3	37.2	44.4
1801-1900	22.9	24.9	28.7	30.0
1901-1982	25.0	54.1	28.1	57.4
Post-1982	113.1	464.3	100.0	362.5

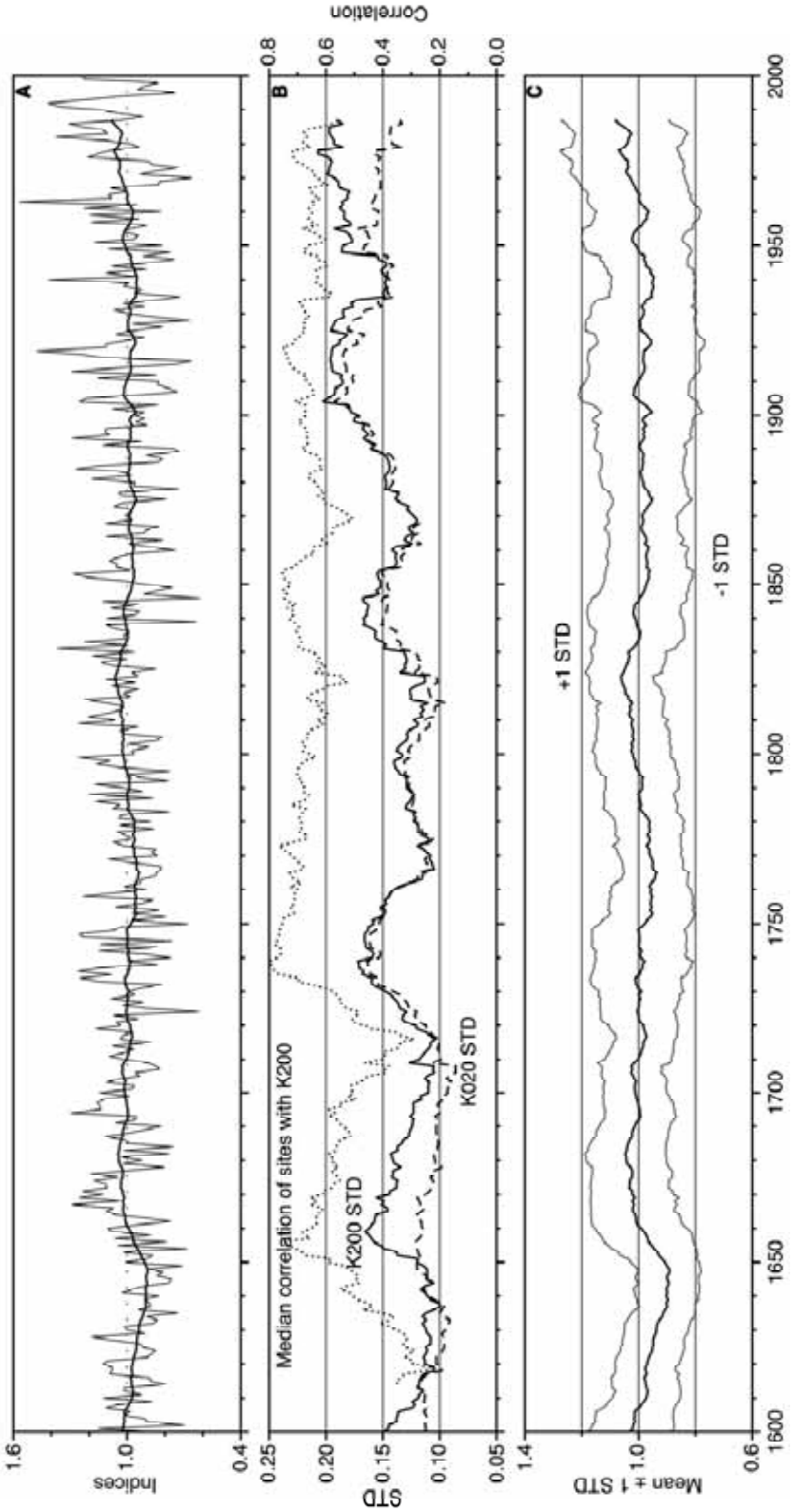

Figure 4.13. Trends in variance of the revised modern Kauri master chronology. Panel A shows low-pass filtered tree-ring indices standardised with a smoothing spline with 50% variance cut off at 200 years. Panel B shows 31-year moving variance of standard deviations for low (K200-solid line) and high (K20-dashed line) pass filtered master chronologies. Dotted line indicates median correlation of sites with K200 master. Panel C shows mean changes in K200 with 1 standard deviation uncertainty estimates. **Source:** Fowler *et al.* (2005a).

The primary objective of the update was to address the sample depth issues noted by Fowler *et al.* (2004) for the post A.D. 1982 period. Prior to the update, peak sample depth for the late 20th century was achieved in A.D. 1983 using 135 series from 61 trees. Following the update, the A.D. 1983 peak rose to 208 series from 96 trees; representing a 57% (54%) increase in trees (series) (Table 4.14). The most notable increases were observed for the post-1982 period when there was, on average of 113% increase in the number of series, with a maximum improvement in replication achieved by 1998 (464%) (Table 4.14).

Table 4.14 indicates the considerable improvement of replication for the late 20th century. Using AGAU03d, there are only 25 series from 15 trees from MASC and HUIA extending to 1997. Following the revision of the master chronology, this increased to 97 series from 48 trees from six sites (HUIA, MASC, PUKF, TROU, HIDV, WTDM), representing a 288% increase in series and 220% rise in the number of trees. Additionally, there was the important introduction of 65 series from 29 trees between A.D. 2000-2002 from four of these sites (HIDV, TROU, PUKF, and WTDM), representing a substantial degree of spatial replication covering the end of the 20th century.

To simply assess sub-sample bias for this period, a sub-master from the previously identified high quality period of A.D. 1840-1920 (Fowler *et al.*, 2004) was built using all the trees presents at A.D. 2002. The sub-chronology comprised of 29 trees from the four sites (HIDV, TROU, PUKF, and WTDM) was then correlated against the Kauri master chronology (all sites). The correlation squared (r^2, the proportion of common variance) of 0.80, indicating that this particular subset of trees shares a very high 80% of common variance with the total master chronology (Fowler *et al.*, 2004).

The pre-A.D. 1600 period was the secondary objective of updating of the Kauri modern master chronology. Prior to the update, there was a maximum of 36 series from 19 trees from four sites (HUPI, MASC, MWIL, DISP) representing the A.D. 1501-100 period. Following the incorporation of the new material, the number of trees rose modestly to a maximum of 42 series from 25 trees from six sites (HUPI, MASC, MWIL, DISP, TROU and PUKF). A sub-master was built from all trees present at A.D. 1550, to produce an r^2 of 0.49 for the A.D. 1840-1920 period. This was a modest improvement on the 46% of variance explained using the sample material discussed in Fowler *et al.* (2004). By A.D. 1650, the r^2 reaches a very high value of 0.80, compared to

A.D. 1600 using the spline 20 version of the master chronology used by Fowler *at al.* (2004).

4.8.9 Trends in the modern Kauri master chronology

To examine long-term changes in mean variance of the Kauri record over time, 31-year sliding variance of high (K20) and low (K200) pass filtered master chronologies were calculated (Figure 4.14). Both records indicate a prominent 50-70 year cycle in variance with a marked increase in variance by ~A.D. 1870. Interestingly, this rise coincides with the timing of the end of the Little Ice Age (~A.D. 1550-1850) and increases in global industrialisation.

There are, however, some slight discrepancies in the variance indicated by the two Kauri master chronologies. Notably, compared to the low pass version of the chronology, the high pass master shows reduced variance between A.D. 1650-1710 and A.D. 1950-1980. From K200 the late 20th century variability appears unprecedented in the context of the past 450 years, while the K20 chronology remains within the range of variability recorded over the past four centuries. Nonetheless, the K200 standardisation is considered to be more conservative due to the removal of high frequency variability that is more influenced by age-growth relationships discussed in Chapter 3, which may suggest a somewhat anomalous late 20th century. However, most significantly, the differences in the trends noted here clearly highlight the uncertainty associated with single proxy analysis.

4.9 Discussion & Conclusions

Expanding the overall number and internal replication of site chronologies resulted in some significant improvements to the modern Kauri master chronology. The quality of the PUKF, TROU HIDV and WTDM chronologies are reflected in the strong relationships noted between all other modern chronologies from Auckland, Waikato and Northland indicating that these sites are of a suitably high standard to be included in the Kauri modern database.

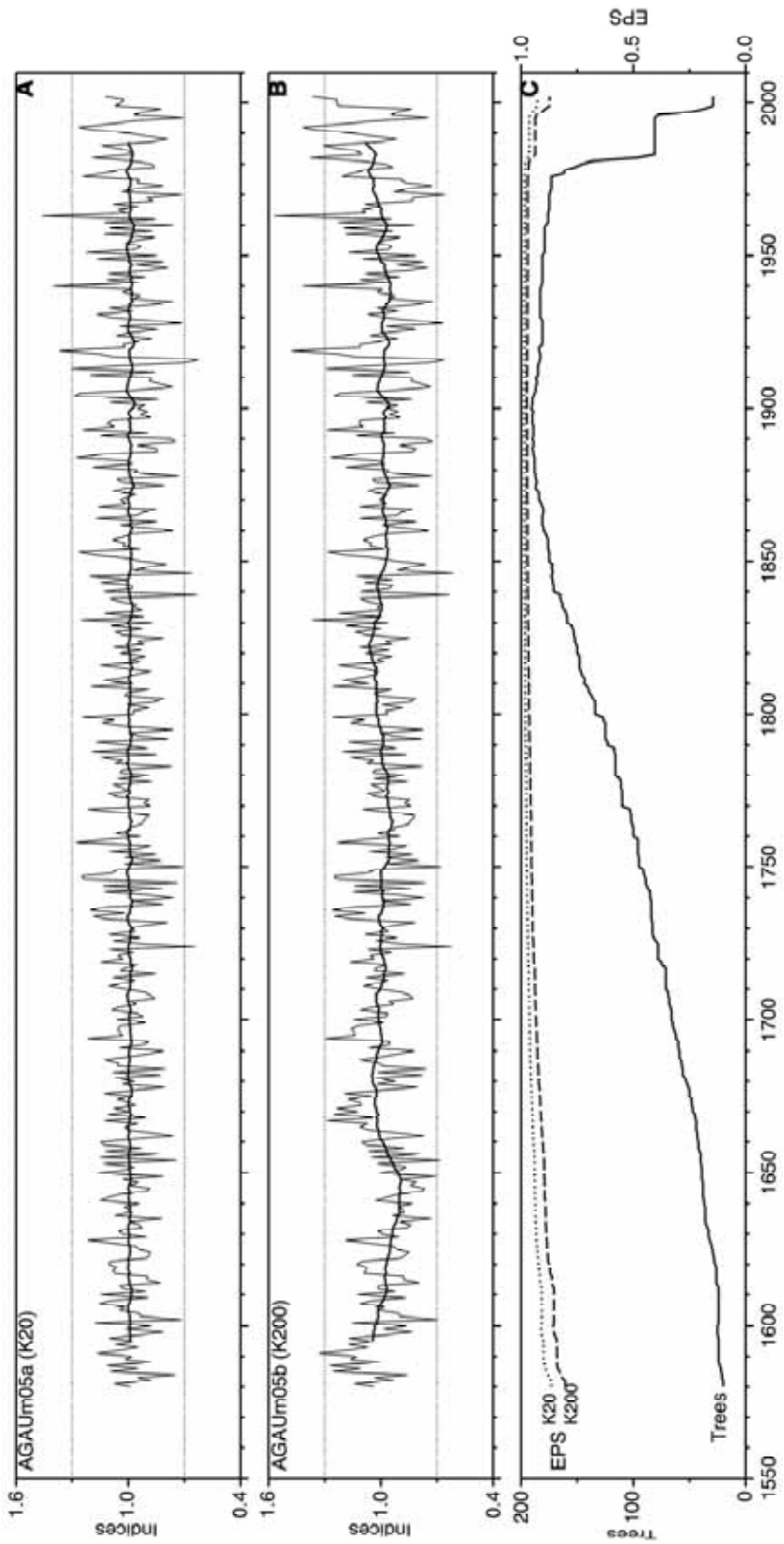

Figure 4.14. Revised modern Kauri master chronology. Panel A shows high-pass filtered tree-ring indices standardised with a smoothing spline with 50% variance cut off at 20 years (K20). Panel B shows low pass filtered tree-ring indices standardised with a smoothing spline with 50% variance cut off at 200 years (K200). Panel C indicates sample depth (number of trees) and overall changes in Expressed Population Statistics (EPS) for both K20 and K200 master chronologies. **Source:** Fowler *et al.* (2005a).

Overall, changes in sample depth related to the addition of new material resulted in changes in the overall EPS quality statistics of the modern master chronology. Using the unrevised AGAU03d, high quality intervals for EPS ≥0.80 recorded for A.D. 1583-1997. Following the update, there was an extension of the high quality interval using the EPS≥0.80 threshold to A.D. 1577-2002 using spline 200 standardisation, and back further to A.D. 1559 using high-pass spline 20 standardisation.

It is acknowledged that using a spline 200 chronology is likely to yield more conservative statistics than those obtained using the spline 20 version of the master presented in Fowler *at al.* (2004). As Fowler and Boswijk (2003) noted, using a more flexible 20 year spline maximises intra-site correlations compared to 200 year spline treatment. As a result, statistical relationships are reduced due to the smoothing of the high frequency (inter-annual) variability that facilitates crossdating between trees and sites. These results highlight the compromises in the length of high quality record necessary for the examination of decadal-century scale variability through time, and the importance of selecting a standardisation technique relevant to the desired climatic application. However, the high quality obtained using the spline 20 chronology may be more suitable for high-frequency discrete event analysis of ENSO (Fowler and Boswijk, 2003).

Material from two other Northland sites, Onekura Bluff and Warawara (see Table 4.12) should be analysed for their potential to considerably revise individual site chronologies. This would improve the relatively weak sample depth periods of the modern master record noted here. The lack of replication noted for the pre-A.D. 1600 period reflects the difficulty of sampling living trees due to Kauri's very large size. As Fowler *et al.* (2004) noted cores from mature trees rarely get close to the pith because of the physical limitations of using non-destructive increment borers.

As such, this analysis supports the proposition of Fowler *et al.* (2004) of targeting this period through archival and relic logging material from fallen trees and stumps rather than further attempts of obtaining material from living trees (see Chapter 3, Figure 3.4.) Nevertheless, in light of the very mature nature of the trees sampled from Warawara, this collection may prove to be a very valuable asset to the modern Kauri database.

Importantly, the incorporation of material from the update sites has not only improved overall replication of the late 20th century, but also improved spatial representation to

include material from the west (TROU, WTDM), north (PUKF) and east (HIDV). Previously, the significance of any climatic interpretation of the post A.D. 1998 period from AGAU03d may have been geographically biased due to lack of spatial replication. Following the significant revision, the Kauri modern master may now be confidently interpreted to represent the large-scale, regional climate forcing suggested by Fowler *et al.* (2004).

The revised Kauri master chronology is now derived from 426 series from 191 trees from 17 sites from Kauri's entire geographic range. As a result, decadal-centennial (inter-annual-decadal) climate reconstruction is now possible between A.D. 1577-2002 (A.D. 1559-2002) using the updated spline 200 (20) versions of the Kauri modern master chronology. Long tree-ring records from the Southern Hemisphere have long been sought after by the palaeoclimate community to allow recent ENSO variability to be placed into long-term context from a key teleconnection area (Lara and Villalba, 1993; Stahle *et al.*, 1998; Briffa, 2000; Jones and Mann, 2004).

4.10 Summary

In 2005, the modern Kauri database was extensively revised for the purpose of ENSO reconstruction. In particular, late 20th century and pre A.D. 1600 low sample depth periods were targeted. Material from living Kauri trees were sampled from Puketi State Forest, Trounson Kauri Park, Hidden Valley and Waitakere Dam were incorporated into the development of updated versions of the modern Kauri master chronologies (AGAUm05a and AGAUm05b) for climate analysis.

Prior to the update, 149 trees (344 series) from 15 sites were used to develop the modern Kauri master chronology. Following revision, replication rose to 191 trees (426 series) from 17 sites. This reflected the considerable expansion of chronologies from Puketi State Forest and Trounson Kauri Park, and the introduction of material from the new sites of Hidden Valley and Waitakere Dam. Significantly there has been a mean increase of 25% in the number of trees replicating the pre-A.D 1600 period and a doubling of post A.D. 1982 replication.

This chapter assessed the implications of the standardisation applied to the development of the modern Kauri master chronology. Following the update, highest quality inter-annual-decadal (decadal-centennial) climate reconstruction is now possible between A.D. 1559-2002 (A.D. 1577-2002) using the updated spline 20 (200) versions of the Kauri modern master chronology.

Significantly, Kauri now joins the handful of tree species in the world which contains an identified ENSO signal in its growth ring patterns, introducing an important long-term counterpart to the eastern Pacific tree-ring chronologies currently available (Stahle *et al.*, 1998; Cook *et al.*, 2000; D'Arrigo *et al.*, 2005). In fact, the Kauri chronology represents the potential to be the longest tree-ring proxy record of past ENSO variability available from the western Pacific.

However, from the initial results presented in this chapter, it is unclear whether the late 20th century variance recorded in Kauri growth rings is unprecedented from a long-term perspective. This highlights the limitations of single proxy analysis, reiterating the merits of multiproxy climate analysis (Gergis *et al.*, 2004; Gergis *et al.*, 2005c; 2005d; 2005e). Accordingly, the Kauri record is further analysed in Chapters 5 and 6 in comparison with a number of other high-resolution proxy records.

4.11 References

Adams, J. G. (1989). *Kauri a King Among Kings.* Auckland, Wilson and Horton Ltd.

Ahmed, M. (1984). Ecological and dendrochronological studies on Agathis australis Salisb. (Kauri). Department of Botany, University of Auckland, New Zealand.

Ahmed, M. and Ogden, J. (1985). Modern New Zealand tree-ring chronologies 3. Agathis australis (Salib.)-Kauri. *Tree Ring Bulletin* **45**: 11-24.

Ahmed, M. and Ogden, J. (1987). Population dynamics of the emergent conifer *Agathis australis* (D. Don) Lindl. (Kauri) in New Zealand. I. Population structures and tree growth rates in mature stands. *New Zealand Journal of Botany* **25**: 217-229.

Allan, R. and D'Arrigo, R. (1999). 'Persistent' ENSO sequences: how unusual was the 1990-1995 El Niño ? *The Holocene* **9** (1): 101-118.

Baillie, M. (1982). *Tree-ring Dating and Archaeology.* London, University of Chicago Press.

Baillie, M. and Pilcher, J. (1973). A simple crossdating program for tree-ring research. *Tree Ring Bulletin* **33**: 7-14.

Bell, V. and Bell, R. (1958). Dendrochronological studies in New Zealand trees. *Tree Ring Bulletin* **22**: 7-11.

Boswijk G., and Ogden J. (2005). Tree-ring analysis of kauri (*Agathis australis*) from Hidden Valley, Great Barrier Island. New Zealand tree-ring Site Report No. 21, Working Paper 31, School of Geography and Environmental Science, Auckland.

Boswijk, G., Fowler, A. and Ogden, J. (2002). Tree Ring Chronologies of New Zealand, 1: Kauri (Agathis australis), Living and recently dead trees. School of Geography and Environmental Science, University of Auckland Occasional Paper 44. Auckland: 1-113.

Bradley, R. (1996). Are there optimum sites for global paleotemperature reconstruction? *Climate Variations and Forcing Mechanisms of the Last 2000 years.* P. Jones, R. Bradley and J. Jouzel. Berlin, Springer-Verlag: 603-624.

Briffa, K. (2000). Annual climate variability in the Holocene: interpreting the message of ancient trees. *Quaternary Science Reviews* **19**: 87-105.

Briffa, K. and Jones, P. (1990). Basic chronology statistics and assessment. *Methods of Dendrochronology: applications in the environmental sciences.* E. Cook and L. Kairiukstis. Dordrecht, Kluwer Academic.

Buckley, B., Ogden, J., Palmer, J., Salinger, J. and Fowler, A. (2000). Dendroclimatic interpretation of tree-rings in Agathis australis (Kauri) 1; Climatic correlation functions and master chronology. *Journal of the Royal Society of New Zealand* **30** (3): 263-275.

Cook, E., D'Arrigo, R., Cole, J., Stahle, D. and Villalba, R. (2000). Tree-ring records of past ENSO variability and forcing. *El Niño and the Southern Oscillation; Multiscale Variability and Global and Regional Impact*. H. Diaz, and Markgraf, V. New York, Cambridge University Press: 297-323.

Cook, E. and Peters, K. (1981). The smoothing spline: a new approach to standardizing forest interior tree-ring width series for dendroclimatic studies. *Tree Ring Bulletin* **41**: 45-53.

D'Arrigo, R., Cook, E., Wilson, R., Allan, R. and Mann, M. (2005). On the variability of ENSO over the past six centuries. *Geophysical Research Letters* **32** (L03711): 1-4.

Department of Conservation (2003). Puketi and Omahuta Forests. Kerikeri, Department of Conservation.

Dunwiddie, P. (1979). Dendrochronological studies of indigenous New Zealand trees. *New Zealand Journal of Botany* **17**: 251-266.

Fowler, A. (1984). A dendroclimatological Study of Kauri (*Agathis australis*). University of Auckland, Auckland, New Zealand.

Fowler, A. (1998). XMATCH98: an interactive tree-ring crossdating program. Occasional Paper 38. Auckland, Department of Geography, University of Auckland.: 1-28.

Fowler, A. and Boswijk, G. (2003). Chronology stripping as a tool for enhancing the statistical quality of tree-ring chronologies. *Tree Ring Research* **59** (2): 53-62.

Fowler, A., Boswijk, G., Gergis, J. and Lorrey, A. (2005a). ENSO history recorded in *Agathis australis* (Kauri) tree-rings, Part A: Kauri's potential as an ENSO proxy. *International Journal of Climatology*: *in review*.

Fowler, A., Boswijk, G. and Ogden, J. (2004). Tree-ring studies on *Agathis australis* (Kauri): a synthesis of development work on Late Holocene chronologies. *Tree Ring Research* **60** (1): 15-29.

Fowler, A., Lorrey, A. and Crossley, P. (2005b). Seasonal growth characteristics of Kauri. *Tree Ring Research* **61** (1): 3–19.

Fowler, A., Palmer, J., Salinger, J. and Ogden, J. (2000). Dendroclimatic interpretation of tree-rings in Agathis australis (Kauri) 2; Evidence of a significant relationship with ENSO. *Journal of Royal Society of New Zealand* **30** (3): 277-292.

Fritts, H. (1991). *Reconstructing Large-Scale Climatic Patterns from Tree-Ring Data; A Diagnostic Analysis*. Tucson, USA, University of Arizona Press.

Gergis, J., Boswijk, G. and Fowler, A. (2005a). An update of modern Northland Kauri (*Agathis australis*) tree-ring chronologies 1: Puketi State Forest. New Zealand tree-ring Site Report No.19, School of Geography and Environmental Science Working Paper 29, University of Auckland, New Zealand.

Gergis, J., Boswijk, G. and Fowler, A. (2005b). An update of modern Northland Kauri (*Agathis australis*) tree-ring chronologies 2: Trounson Kauri Park. New Zealand tree-ring Site Report No.20, School of Geography and Environmental Science Working Paper 30, University of Auckland, New Zealand.

Gergis, J., Fowler, A., Braganza, K., Mooney, S. and Risbey, J. (2005c). El Niño-Southern Oscillation (ENSO) since A.D. 1525: integrating evidence from tree-ring, coral, ice core and documentary archives. *PAGES 2nd Open Science Meeting: Palaeoclimate, Environmental Sustainability and Our Future*, August 10-12, Beijing, China.

Gergis, J., Fowler, A., Braganza, K., Risbey, J. and Mooney, S. (2005d). Multiproxy approaches to El Niño-Southern Oscillation (ENSO) reconstruction; integrating evidence from

tree-ring, coral, ice and documentary archives, A.D. 1525-2002. *Reconstructing Past Climates for Future Prediction: Integrating High-Resolution Palaeo Data for Meaningful Prediction in the Australasian Region*, June 27-28, Canberra, Australia.

Gergis, J., Fowler, A. and Mooney, S. (2004). A Multiproxy Analysis of El Niño Southern Oscillation (ENSO) Variability. *1st International CLIVAR Science Conference: Understanding and Predicting Our Climate System*, June 21-25, 2004, Baltimore, Maryland, USA.

Gergis, J., Fowler, A. and Mooney, S. (2005e). A Multiproxy Analysis of El Niño-Southern Oscillation Variability. *1st Alexander Von Humboldt International Conference on the El Niño Phenomenon and its Global Impact*, 16-20 May, 2005, Guayaquil, Ecuador, European Geophysical Union pp 35-36.

Holmes, R., Adams, R. and Fritts, H. (1986). Users manual for program ARSTAN. *Tree-ring chronologies of western North America: California, eastern Oregon and northern Great Basin*. Tucson, University of Arizona: 50-65.

Jones, P. and Mann, M. (2004). Climate over past millennia. *Review of Geophysics* **42**: 1-42.

La Marche Jr, V., Holmes, R., Dunwiddie, P. and Drew, L. (1979). Tree-ring chronologies of the Southern Hemisphere: 3. New Zealand., Laboratory of Tree-Ring Research, University of Arizona, Tucson, USA.

Lara, A. and Villalba, R. (1993). A 3620 year temperature record from Fitzroya cupressoides tree rings in southern South America. *Science* **260**: 1104-1106.

Lorrey, A. (2004). Tree-ring analysis of Kauri (Agathis australis) from Waitakere Reservoir, Waitakere Ranges, Auckland. New Zealand tree-ring Site Report No.15, School of Geography and Environmental Science Working Paper 23, University of Auckland, New Zealand.: 1-12.

Ogden, J., Wilson, A., Hendy, C. and Newnham, R. (1992). The Late Quaternary history of Kauri (Agathis australis) in New Zealand and its climatic significance. *Journal of Biogeography* **19**: 611-622.

Palmer, J. (1982). A dendrochronological study of Kauri (*Agathis australis*). MSc. thesis, University of Auckland, Auckland, New Zealand.

Salmon, J. (1980). *The Native Trees of New Zealand.* Wellington, New Zealand, Reed Methuen.

Stahle, D., D'Arrigo, R., Krusic, P., Cleaveland, M., Cook, E., Allan, R., Cole, J., Dunbar, R., Therrell, M., Gay, D., Moore, M., Stokes, M., Burns, B., Villanueva-Diaz, J. and

Thompson, L. (1998). Experimental dendroclimatic reconstruction of the Southern Oscillation. *Bulletin of the American Meteorological Society* **79** (10): 2137-2152.

Stokes, M. and Smiley, T. (1968). *An introduction to tree-ring dating.* Chicago., University of Chicago Press.

Trenberth, K. and Hoar, T. (1997). El Niño and climate change. *Geophysical Research Letters* **24** (23): 3057-3060.

Tyers, I. (1999). Dendro for Windows Program Guide, 2nd Edition. ARCUS Report 500.

CHAPTER 5.
DISCRETE ENSO EVENT ANALYSIS

5.1 Introduction

ENSO events create a far-reaching system of climate anomalies that operate on a range of time scales that are important to society (Glantz, 1996). ENSO influences extreme climate events such as drought, flooding, bushfires and tropical cyclone activity across vast areas of the Earth. In monsoonal areas across Australasia, Africa and the Americas, these episodes can adversely impact agricultural productivity and the livelihood of hundreds of millions of people (Bouma *et al.*, 1997; Dunbar and Cole, 1999; Caviedes, 2001; Chen *et al.*, 2001). Yet, despite being the dominant source of global inter-annual climate variability, many characteristics of individual ENSO episodes including long-term changes in their frequency, duration and magnitude, remain largely unknown (Crowley, 2000; Grove and Chappell, 2000).

It is well known that the late 20th century contained a number of extreme and prolonged ENSO episodes (Trenberth and Hoar, 1996), including the two most intense El Niño (1982-83 and 1997-98) and La Niña (1988-89, 1973-74) events of the instrumental periods (see Chapter 2). However, the long-term context of apparently anomalous ENSO behaviour witnessed in recent decades has received little attention (Crowley, 2000; Folland *et al.*, 2001; Mann, 2003) Consequently, multi-century palaeoclimate reconstructions derived from long proxy records, such as annually resolved tree ring, coral, ice or documentary records can be used to assess the significance of recent ENSO variability within a multi-century context (Folland *et al.*, 2001).

The intention of this chapter is to provide an overview of previous approaches to discrete ENSO event reconstruction. Issues associated with proxy calibration, ENSO event magnitude classification, reconstruction skill quantification and verification are detailed. This chapter also introduces novel methodology for the development of a discrete ENSO event chronology using tree-ring, coral, ice and documentary data for

the A.D. 1525-2002 period, allowing late 20th century ENSO extremes to be assessed from a long-term, multiproxy perspective.

5.2 Previous ENSO Event Chronologies

5.2.1 'Quinn' records of historical El Niño events

A key paper for the historical chronology of El Niño events was that of Quinn *et al.* (1987). Following on from exploratory work on the association between ENSO and Indonesian droughts (Quinn *et al.*, 1978), Quinn *et al.* (1987) established a magnitude scale of the El Niño events that has been generally adopted by the ENSO scientific community (see for example, Mann *et al.* (2000), Stahle *et al.* (1998), Rodbell *et al.* (1999), Diaz and Markgraf (2000)). Quinn's list of past El Niño events recorded in the eastern Pacific during the past four and a half centuries has been viewed as the major reference for any long-term analysis of ENSO (Ortlieb, 2000). Quinn (1987) proposed an ordinal scale of event intensity ranging from weak, moderate, strong and very strong. The scale was compiled from documentary data based on reports of anomalous rainfall and storm events on the coast of Peru, travel time of ships in the eastern Pacific, or anomalous SST and air-temperature episodes in western South America (Quinn *et al.*, 1987). Importantly, however, the record only documents El Niño, excluding the occurrence of La Niña episodes.

In the early 1990s, Quinn and Neal (1992) refined this chronology by adding documentary data, from countries adjacent to Peru including Chile, Bolivia and Brazil. This became the major reference for proxy calibrations and for most studies on climate variability related to ENSO during historical and pre-instrumental times (Ortlieb, 2000). In fact, Ortlieb (2000) noted that practically all the decadal-centennial ENSO studies during the 1990s that used dendroclimatology, coral records, tropical ice cores or other proxy sequences were compared to and calibrated with Quinn's El Niño chronologies. In addition, the chronology of historical ENSO events was expanded to incorporate the Nile River flood data from Egypt (Quinn, 1992).

Two chronological records of climatic anomalies were established (Ortlieb, 2000). One was considered to be of global relevance, based on all available data from East Africa and the Pacific Oceans and was referred to as the 'ENSO Chronology' (Quinn, 1992).

The other, referred to as the 'regional El Niño chronology', was based on eastern Pacific and western South American data (Quinn and Neal, 1992). With respect to the original work of Quinn *et al.* (1987), the regional El Niño chronology (Quinn and Neal, 1992) differed by several years or showed discrepancies in the timing or magnitude of some episodes (Ortlieb, 2000).

Subsequently, researchers such as Ortlieb and Machare (1993) questioned the occurrence, magnitude and reliability of some events recorded in the South American regional El Niño indices given by Quinn and Neal (1992). Some authors questioned the occurrence of some of the reconstructed events (A.D. 1525-1900), or the inferred intensity of some other events (Ortlieb, 2000). More recently, Ortlieb (2000) updated Quinn's chronology, by revising all available documentary sources dealing with climatic anomalies between the 16th-19th centuries in Peru and southern Ecuador (Ortlieb, 2000). These studies highlighted the problem validating El Niño proxies, in terms of the geographical distribution of the impacts and the palaeo-intensity of the events (Ortlieb, 2000).

5.2.2 Eastern Hemisphere teleconnection chronology

Using data covering the A.D. 1525-1994 period, an attempt was made to extend the record of climatic extremes affecting the Eastern Hemisphere related to ENSO (Whetton and Rutherfurd, 1994). Whetton and Rutherford (1994) used an annual flood height time series of the Nile at Cairo, a rainfall index from northern China based on historical records and tree-ring widths based on Teak growing in Java, Indonesia. In addition, two historical event chronologies of an Indian drought and famine chronology, and the El Niño chronology assembled by Quinn and Neal (1992) were also analysed.

Significantly, Whetton and Rutherford (1994) were the first to attempt to document both phases of the ENSO phenomenon and to date, no other similar chronology of La Niña events has been compiled (Whetton and Rutherfurd, 1994; Allan and D'Arrigo, 1999; Ortlieb, 2000). In fact, the ENSO chronology of Eastern Hemisphere teleconnections compiled by Whetton and Rutherford (1994) has been considered to be the most complete attempt to document both phases of ENSO for pre-instrumental times (Allan and D'Arrigo, 1999; Ortlieb, 2000). As such, the chronology is an

important source for determining the presence of ENSO conditions for the historical period.

Whetton and Rutherford (1994) used a variety of statistical techniques to assess whether, or over which periods, the data sets demonstrated ENSO-related teleconnections. Originally, particular emphasis was placed on how well the selected data series correlated with the regional El Niño chronology of Quinn and Neal (1992). ENSO-related teleconnections could be traced in the data back to about A.D. 1750, and a chronology of teleconnection years characteristic of ENSO events was prepared for the A.D. 1701-1979 period (Whetton and Rutherford, 1994).

Due to inadequate long-term data coverage, the ENSO chronology and analysis of teleconnection stability analysis were restricted to A.D. 1701-1979 period (Whetton and Rutherfurd, 1994). It is, however, important to note that the study only provided a list of the occurrence of extreme ENSO events as defined using a (0.5) standard deviation departure from the long term mean of each record analysed, rather than the range of magnitude classes detailed by the 'Quinn' chronologies. Furthermore, the La Niña aspect of the chronology is only based on three records (Java, Nile, and China), two of which originate from teleconnection regions outside of the tropical core ENSO zone.

Revision of the Whetton and Rutherford (1994) chronology was undertaken using the revised 'global' Quinn (1992) chronology, which modified the regional South American El Niño chronology through the addition of Nile River flood data to provide a broader scale ENSO event chronology (Whetton *et al.*, 1996). The updated Quinn (1992) El Niño record considerably improved the statistical relationships of the proxies used by Whetton and Rutherford (1994), highlighting the importance of wide spatial representation of high quality proxy records for the reliable interpretation global ENSO anomalies (Whetton *et al.*, 1996).

5.2.3 Protracted ENSO event chronology

Using the proxy data set provided by Stahle *et al.* (1998) (see Chapter 6), Allan and D'Arrigo (1999) derived a multiple regression reconstruction of the Southern Oscillation Index (SOI) for the A.D. 1706-1875 period. Allan and D'Arrigo (1999) discussed how recent El Niño sequence/climatic anomalies, such as the protracted ENSO event of 1990-1995, have only been considered with regard to contemporary

data and events (Trenberth and Hoar, 1996; Trenberth and Hoar, 1997). Since the presence of such signals in records of relatively short length may be of limited statistical significance, other instrumental, documentary and palaeoclimatic data is critical to investigate longer-term, natural (non-anthropogenic) variability of the ENSO system (Allan and D'Arrigo, 1999).

Allan and D'Arrigo (1999) demonstrated that features indicative of protracted event sequences have occurred prior to the period of instrumentally based indices. They concluded that persistent events have occurred over the past 100-120 years (although the 1990-1995 was the longest in duration), and that persistent warm and cold event sequences noted in documentary evidence from other ENSO-sensitive regions across the Indo-Pacific basin (Quinn and Neal, 1992; Whetton *et al.*, 1996), have occurred with similar frequency and magnitude in the observed record (Allan and D'Arrigo, 1999).

Allan and D'Arrigo (1999) concluded that ENSO sequences of three years duration or longer are not rare or unusual, and estimated that El Niño events of this nature have occurred around four or five times per century when matched against the historical documentary evidence of Whetton *et al.* (1996). This estimate compared favourably with the instrumentally based data which revealed a frequency of about six protracted events per century, supporting evidence that decadal signals are present in the ENSO record (Allan and D'Arrigo, 1999). Once again, the merits of integrating complementary and well-dated, high-resolution records into multiproxy reconstructions for comparison with instrumental trends was clearly demonstrated (Allan and D'Arrigo, 1999).

5.3 Multiproxy ENSO Event Analysis

5.3.1 Issues with reconstructing ENSO events

The dynamic nature of ENSO makes any reconstruction using proxy archives problematic. Although ENSO is phase-locked to the annual cycle and peaks in amplitude of ENSO anomalies are generally observed during the austral summer (DJF), episodes are known to differ in terms of their relative strengths, seasons of onset, maturity, overall duration and the spatial extent of maximum Sea Surface Temperature

(SST) anomalies in the tropical Pacific (Rasmusson and Carpenter, 1982; Trenberth and Stepaniak, 2001; Lyon and Barnston, 2005). Rainfall, SST and wind field anomalies associated with ENSO events differ considerably from event to event, as 'centres of action' shift (Allan *et al.*, 1996; Fedorov and Philander, 2000). Since any major redistribution of equatorial rainfall regimes are communicated into extra-tropical regions via 'teleconnections', ENSO exerts a near-global influence on climate variability (Allan *et al.*, 1996; Kumar and Hoerling, 1997).

To illustrate this complexity, the recent 2004-05 El Niño was a characteristic example of a decoupled ENSO event. SST anomalies exceeded 0.5°C in the western-central Pacific (Niño 4, Niño 3.4 and Niño 3 regions), while warming exceeding 1°C did not expand eastward of 140°W, resulting in near zero anomalies along the 'classical' El Niño region off the west coast of South America (Niño 1+2 SST region) (Lyon and Barnston, 2005). The atmosphere failed to couple with SST conditions until late in the austral summer when in February 2005, the SOI reached its lowest level since the 1982-83 event (Lyon and Barnston, 2005). Interestingly, this weak El Niño was detected by the Niño 3.4 SST index for at least six months, while the Niño 3 SST index (commonly used to calibrate ENSO proxy records) only indicated anomalous conditions for 1-2 months (Lyon and Barnston, 2005).

The consequences of the non-stationarity behaviour of ENSO have profound implications for the reconstruction of past ENSO events. Climate proxies derived from a number of ENSO influenced locations result in considerable differences in the seasonality of response signatures. This means a variety of regions are needed to adequately capture the spatial variability of ENSO through time (Fairbanks *et al.*, 1997). Thus, representation of ENSO signals from a number of widely-spaced regional proxies is more likely to be representative of large-scale ocean-atmosphere processes than is possible from single proxy analysis (Baumgartner *et al.*, 1989; D'Arrigo *et al.*, 1994; Diaz and Pulwarty, 1994; Gedalof and Mantua, 2002).

The limitations and bias of various proxies are well understood (Jones and Mann, 2004). These include differences in temporal resolution (seasonal versus annual) and limitations in temporal coverage. This ranges from a few centuries for corals and historical documentary sources to thousands of years for tree-ring and ice core sequences (Jones and Mann, 2004). Moreover, a proxy record is typically only sensitive to a specific seasonal window, rarely captures more than 50% of instrumental variance and is

commonly unable to register variance equally well across a number of frequency domains (Bradley, 1996). Thus, each proxy represents unique signals from different regions of the globe (tropics versus extra tropics) and environmental contexts (terrestrial versus marine environments) allowing complementary information about the widespread nature of ENSO event signatures to be investigated (Jones and Mann, 2004).

Common statistical approaches to calibrating proxies are based on linear regression against instrumental climate data. The statistical relationship of proxy data and instrumental climate time series is characterised by imposing a line of best fit which implicitly disregards statistical outliers, potentially resulting in a loss of variance (Von Storch *et al.*, 2004; Moberg *et al.*, 2005). Thus, anomalously high or low values recorded in proxies may not be accounted for in commonly generated transfer functions. Consequently, it is possible that important teleconnection information may be lost about a given proxy's response to the range of ENSO magnitudes.

Alternatives to the continuous, multivariate regression approaches to ENSO reconstruction (see Chapter 6) include a number of discrete event analyses detailed in Section 5.2. These records provide a year-by-year chronology of unusual meteorological and hydrological phenomena characteristic of ENSO events conditions such as the failure of anchovy fisheries, extreme flooding or drought conditions (Quinn *et al.*, 1987; Whetton and Rutherfurd, 1994). To determine the intensity of events, years are subjectively classified from very strong to weak based on the apparent extent of destruction and societal cost detailed in these historical documents (Quinn *et al.*, 1987).

Here, a 'multiproxy' approach, which capitalises on the complementary strengths of several records from various ENSO influenced locations, provides a more comprehensive technique for assessing global signatures of past ENSO events. The intention of Chapter 5 is to improve the spatial and temporal replication of the extreme ENSO event chronology assembled by Whetton and Rutherfurd (1994) back to A.D. 1525 for a range of ENSO event magnitudes. This is established using novel applications of percentile analysis to ENSO reconstruction, providing a new methodology for the reliable identification of ENSO events and assessment of magnitude and reconstruction quality through time. ENSO stationarity is examined in regards to the frequency, duration and magnitude of events on decadal timescales,

allowing the long-term nature of late 20th century events in the context of an ENSO reconstruction spanning the past 478 years.

5.4 Data Sources

5.4.1 Instrumental indices

The Coupled ENSO Index (CEI) of Gergis and Fowler (2005) was used for proxy calibration. As detailed in Chapter 2, the CEI is a composite index for the identification of both atmospheric (Southern Oscillation Index) and oceanic (Niño 3.4 region SST) anomalies. To recap, the CEI time series was developed by adding monthly SOI values to monthly Niño 3.4 SST anomalies (multiplied by –1 to allow warm SST values to directionally correspond to low SOI values, indicative of El Niño conditions). Thus, anomalies expressed in only one of the two composite indices (indicative of decoupled and/or lead/lag ENSO characteristics) are maintained in the CEI, while coupled ocean-atmospheric anomalies results in the amplification of ENSO conditions indicated by the CEI.

Since the CEI maintains information about both ENSO components, the examination of decoupled events (i.e. ENSO anomalies expressed in either atmospheric or oceanic indices only), and/or the presence of lead/lag event signatures from proxy records is permitted. Using the CEI, an ENSO event is defined as at least six months of simultaneous oceanic and atmospheric anomalies, with no more than two consecutive neutral months interrupting ENSO conditions, consistent with approaches found in the literature (Trenberth, 1997; Allan and D'Arrigo, 1999; Hanley *et al.*, 2003).

5.4.2 Proxy selection and standardisation

Proxies used in this study (Figure 5.1) are previously published records from core ENSO or key teleconnection areas identified as containing an 'ENSO signal' from both eastern and western Pacific locations back to A.D. 1525 (see Chapter 3, Table 3.1, and Appendix 2). Coral sequences were limited to those with sufficient, continuous record length and to those given a positive assessment by Lough (2004). As a result, a number of shorter and/or discontinuous coral records were excluded from this analysis (Cole *et al.*, 2000; Urban *et al.*, 2000; Cobb *et al.*, 2003).

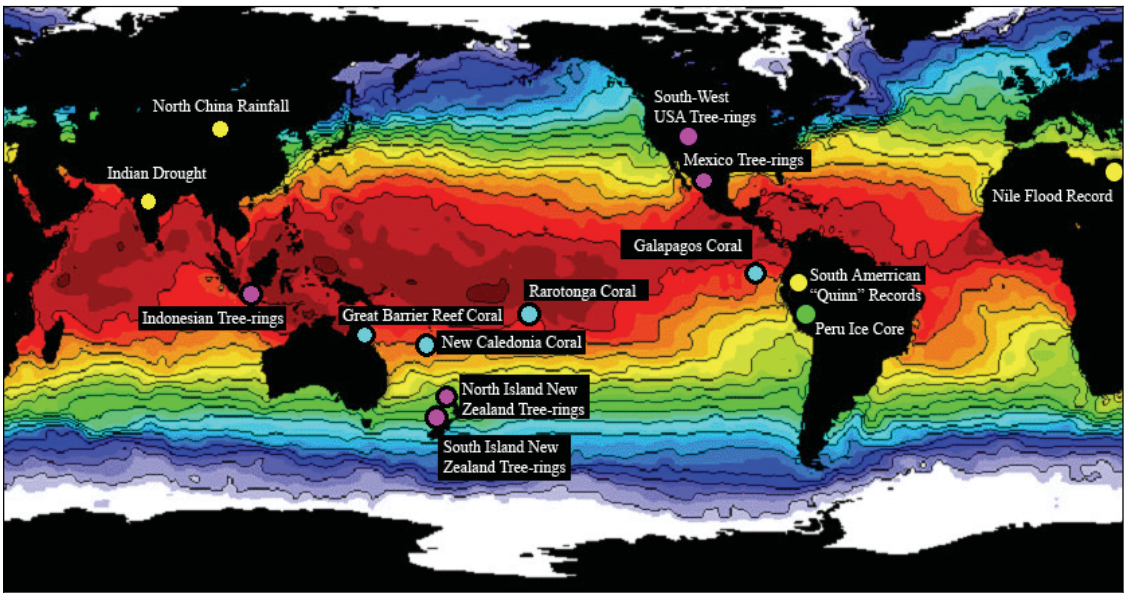

Figure 5.1. Location of tree-ring (purple), coral (blue), historical (yellow) and ice (green) records used in this study. Details of each record are listed in Chapter 3, Table 3.1 and Appendix 2. Regional differences associated with absolute SSTs of the 1997-98 El Niño event are clearly seen, emphasising the merits of using a multiproxy approach to ENSO reconstruction. **Source:** NCEP SST analysis modified from Bureau of Meteorology Research Centre (http://www.bom.gov.au/bmrc/ocean/results/pastanal.htm).

Although a number of the records listed in Table 3.1 extend earlier than A.D. 1525 (e.g. the Quelccaya ice core data and all tree-ring records except for the Indonesian Teak) the lack of long-term coral data from tropical regions makes it difficult to establish evidence of global teleconnections associated with ENSO events (Whetton and Rutherfurd, 1994; Grove and Chappell, 2000). Accordingly, the analysis is limited to the A.D. 1525-2002 period.

With the exception of the Kauri, Pink Pine, and Teak raw tree-ring data was obtained from NOAA's World Data Centre-A for Palaeoclimatology. Aside from the Kauri record, Pink Pine and Berlage Teak records were sourced via personal communication (Whetton and Rutherfurd, 1994; Fenwick, 2003). In addition, the Great Barrier Reef coral master luminescence record was also accessed via personal communication (Hendy *et al.*, 2003).

All tree-ring sequences (except the Berlage Teak record) were standardised using the program ARSTAN (Holmes *et al.*, 1986) to remove the effects of biological growth for climate analysis. Tree-ring data was filtered using a smoothing spline with 50% variance cut off at 20 years, suitable for high-frequency ENSO analysis, precluding the analysis

of low frequency trends (Fowler and Boswijk, 2003). To overcome site specific biases inherent to individual localities, all standardised series available for a given species were combined into tree means and then averaged to produce a regional master chronology using the tree-ring chronology development software of Fowler and Boswijk (2003).

To circumvent the biases noted by Whetton *et al.* (1996) of using a more global ENSO chronology when a regional signal is required, an El Niño chronology derived purely from South American sources was used in this study. The record assembled by Ortlieb (2000) was used until A.D. 1900 (inclusive). From A.D. 1901 onward, classification reverted back to the Quinn and Neal (1992), continuing on from where the update by Ortlieb (2000) terminates.

The Berlage Teak record used in this study is a version modified by Murphy and Whetton (1989). Biological trends in the tree-ring series were removed using a linear-logarithmic approximation to produce a tree-ring index series with approximately zero mean (Murphy and Whetton, 1989). The tree-ring index was then filtered to remove long-period fluctuations using a 10-year Gaussian filter, as was done for the Nile and Northern Chinese Rainfall records (also supplied by Whetton and Rutherfurd, *pers comm.*).

Consistent filtering of each proxy record was not possible, primarily because Whetton and Rutherfurd (*pers comm.*) provided proxy records in a standardised format designed to maximise high frequency variability associated with ENSO analysis. However, care was taken to be consistent with approaches designed for high frequency ENSO analysis noted elsewhere in the relevant proxy literature (Whetton and Rutherfurd, 1994; Diaz and Markgraf, 2000; Linsley *et al.*, 2004; Lough, 2004; D'Arrigo *et al.*, 2005).

To emphasise inter-annual variability, all coral and ice records were high-pass filtered using a three-year high-pass Gaussian filter (which excludes frequencies greater than 3 years from the data) to remove longer period fluctuations in the data that would obscure annual fluctuations. Consequently, this excludes the analysis of low frequency (multi-decadal to centennial) ENSO trends. Historical Indian drought and Quinn chronologies required no further treatment due the event-based nature of the data.

5.5 Reconstruction Calibration

5.5.1 Quantifying proxy quality for ENSO reconstruction

Ideally, precisely dated and climatically sensitive proxies from the equatorial Pacific centres of action of ENSO would be used to reconstruct the core characteristics of ENSO. This way all remaining annual resolution proxies could then be used to map the spatial anomaly patterns of tropical and extra-tropical teleconnections associated with each reconstructed ENSO event (Stahle *et al.*, 1998). Unfortunately, this ideal approach of reconstructing tropical ENSO variability and associated extra-tropical anomalies is barely possible for the 20th century due to the limited spatial coverage of instrumental data and the restricted network of precisely dated annually resolved proxies currently available (Stahle *et al.*, 1998).

ENSO reconstruction is further complicated by the fact that proxies are not uniformly accurate in recording their local climate or oceanographic environment, and sometimes the narrow seasonal response of climate-sensitive proxies may not perfectly coincide with the seasonality of the local ENSO teleconnection (Stahle *et al.*, 1998). Hypothetically, a 'perfect' proxy would have a constant relationship with local climate that has remained stable through time, allowing each ENSO event to be systematically expressed as a function of tree-ring/coral growth and/or ice accumulation rates. In reality, non-stationarities in ENSO behaviour, proxy-dating issues and inconsistencies in El Niño/La Niño phase sensitivity influences the number of accurately detected ENSO events relative to misidentified event years ('false positive' cases).

Similar to the approach of Mann *et al.* (2000), no *a priori* seasonal window for calibration purposes is used here, in recognition that proxy indicators vary considerably in the registration of climate-related anomalies. Thus, each of the seasonal ENSO classifications of Gergis and Fowler (2005), which maintain information about separate SST and SOI conditions, were used to identify the season which expressed the strongest ENSO signal within a given proxy record. This allowed decoupled events (i.e. events only registered by the atmosphere or ocean but not experienced simultaneously by both) to be featured in the analysis, maintaining important evolutive information from proxy reconstructions (Gergis and Fowler, 2005). As Allan *et al.* (2003) recently asserted, resolving more of the ENSO life cycle is critical if greater modeling precision is be achieved.

To assess the nature of any ENSO signal contained within a proxy, each record was calibrated against the instrumental ENSO record using a percentile-based approach. Percentile analysis primarily differs from commonly used regression techniques in that outliers are not excluded from the calibration process, so there is no loss of variance as a result of statistical treatment. The analysis then allows threshold responses of teleconnection patterns associated with both ENSO phases to be evaluated. Since increasing or decreasing a percentile threshold was found to alter the relative proportion of correct/incorrect event detection, the calibration process was designed to optimise the signal to noise ratio to approximate a 2:1 level of accuracy (detailed further in Section 5.5.2.

5.5.2 Single proxy calibration

The veracity of event identification was quantified using a 'phase-score' whereby a score of 1 was assigned each time a proxy response accurately corresponded to instrumental ENSO conditions (Figure 5.2). Since ENSO exhibits periodic decoupling of synchronous SOI and SST anomalies, half weight scores were applied when the proxy agreed with only one ENSO index (atmospheric or SST conditions). The phase-score was optimised separately for each phase by iteratively adjusting percentile thresholds until the best agreement between a proxy and the instrumental overlap of each CEI season (i.e. DJF, MAM, JJA, SON) was achieved (see Figure 5.3).

In an effort to quantify the degree of uncertainty associated with event detection for each proxy, misidentified cases or 'false positives' were similarly quantified to further assess proxy skill. False positives are defined here as a proxy exhibiting a response conflicting with instrumental conditions, for example, a CEI El Niño corresponding to an apparent La Niña proxy response, or vice versa. In this case, a score of –1 was assigned.

Finally, the phase score and false positive score were added to provide an overall measure of 'proxy skill' (Figure 5.2). The calibration process was designed to achieve a high signal (phase score) to noise (false positive score) ratio by not allowing the proportion of false positive cases to exceed ~33%. This corresponds to a skill score of approximately 0.66, indicating a 2/3 chance of accurate event detection by a proxy. This was considered to be a more conservative target than a 50/50 split of event 'hits and misses'.

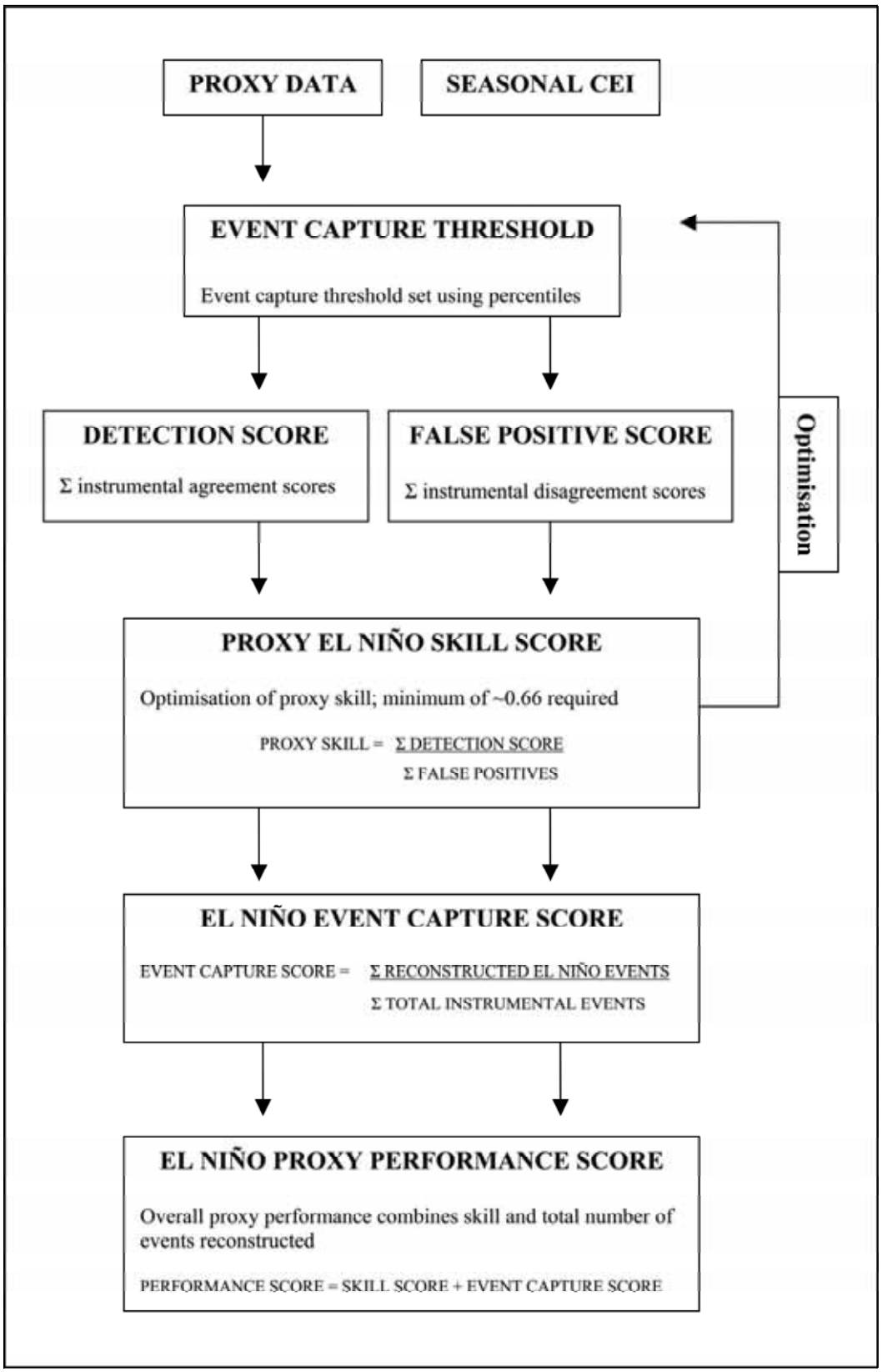

Figure 5.2. Method for calibrating single proxy records to instrumental ENSO for independent phase reconstruction. Instrumental ENSO conditions in this study are represented by seasonal CEI event classification (Gergis and Fowler, 2005).

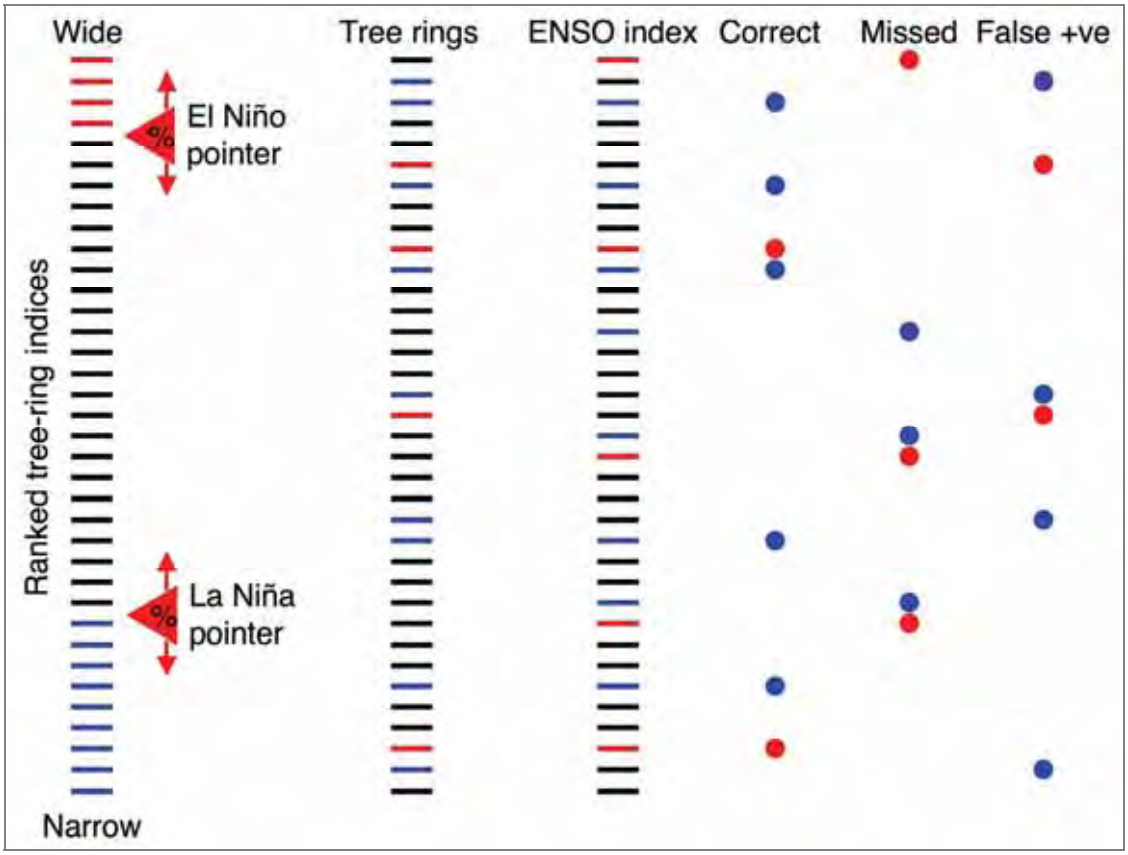

Figure 5.3. A schematic example of percentile based calibration of the Kauri tree-ring record with the CEI instrumental record outlined in Figure 5.2. The El Niño/La Niña 'pointer' refers to the optimal percentile threshold value used for proxy calibration. **Source:** Fowler *pers comm.*

After selecting the most optimal seasonal window and percentile thresholds for each proxy (see Figure 5.3), for each ENSO phase, all records were ranked in terms of their usefulness for El Niño, La Niña or both phases of the reconstruction. The percentile thresholds identified as producing the optimal skill score in the instrumental period (Figure 5.3) were then applied to the remainder of the proxy data to identify pre-instrumental ENSO signatures. To facilitate a more complete indication of each proxy's overall reconstruction potential, CEI event capture values (%) were next converted into a decimal and added to the proxy skill values to produce an overall 'proxy performance score' (Figure 5.2).

To further illustrate this process, Table 5.1 displays the steps involved in the calibration of the Great Barrier Reef coral record for ENSO analysis. Clearly, a threshold is reached beyond which no improvement in event capture is achieved for each phase. Indeed, there is a decline in the overall proxy skill as the proportion of false positives

increases suggesting a compromise between the number of events captured and the accuracy (or 'skill' with which they are detected) is required. Very high skill of 0.81 is possible using the 0.1 threshold for the El Niño calibration, however, relatively few events are registered. From Table 5.1, it is apparent that a general target of a skill score of least ~0.66 appears to be a reasonable target that allows sufficient sensitivity to event capture. Due to the inherent replication implicated by multiproxy analysis, maximising the event capture at the single proxy level was desired, as false positives are likely to be 'lost' from the larger multiproxy environment as the likelihood of false positives occurring simultaneously in many locations is likely to be low.

Table 5.1. Impact of skill score optimisation process on the Great Barrier Reef coral record aimed at maximising event capture while maintaining a high degree of skill, determined from the period of instrumental overlap, 1871-1985. Note the greater La Niña phase sensitivity. In this instance, an overall proxy performance score of 1.06 for the El Niño and 1.27 for La Niña reconstructions were selected.

Percentile Threshold	Instrumental Event Capture (%)	Phase Score	False Positives Score	Skill Score	Overall Proxy Performance
El Niño					
0.10	18.5	5.5	1.0	0.81	0.99
0.15	29.6	9.0	2.0	0.77	1.06
0.20	33.3	10.5	3.5	0.67	1.00
0.25	37.1	12.0	6.0	0.50	0.87
0.30	44.4	14.0	8.5	0.39	0.83
0.35	48.2	16.5	9.0	0.45	0.80
La Niña					
0.65	61.7	23.0	8.0	0.65	1.27
0.70	52.9	20.0	7.0	0.65	1.18
0.75	41.2	15.5	6.5	0.58	0.99
0.80	35.3	13.0	6.0	0.53	0.88
0.85	32.4	11.5	4.0	0.65	0.97
0.90	20.6	7.5	3.0	0.60	0.80

Finally, to identify fluctuations in the strength and stability of the ENSO signal present in each regional proxy, the frequency of reconstructed events for each phase were calculated in 25-year periods and compared and non-stationarities identified.

5.6 Assessment of Reconstruction Quality

5.6.1 Impact of fluctuating sample depth on reconstruction quality

Only a few proxy records have the ability to extend back more than a few centuries due to fewer samples available in individual proxies (i.e. age-growth relationships) and the overall loss of proxies available back in time. As a result, there is an inevitable degradation of the quality of any reconstruction back through time as replication diminishes. This is especially the case in the context of the wider multiproxy network, as the representation of long records decreases back in time (Figure 5.4). Thus, most confidence can be placed on the period containing the most records. Nevertheless, eight (six) El Niño (La Niña) proxies are present in the reconstruction back to A.D. 1525.

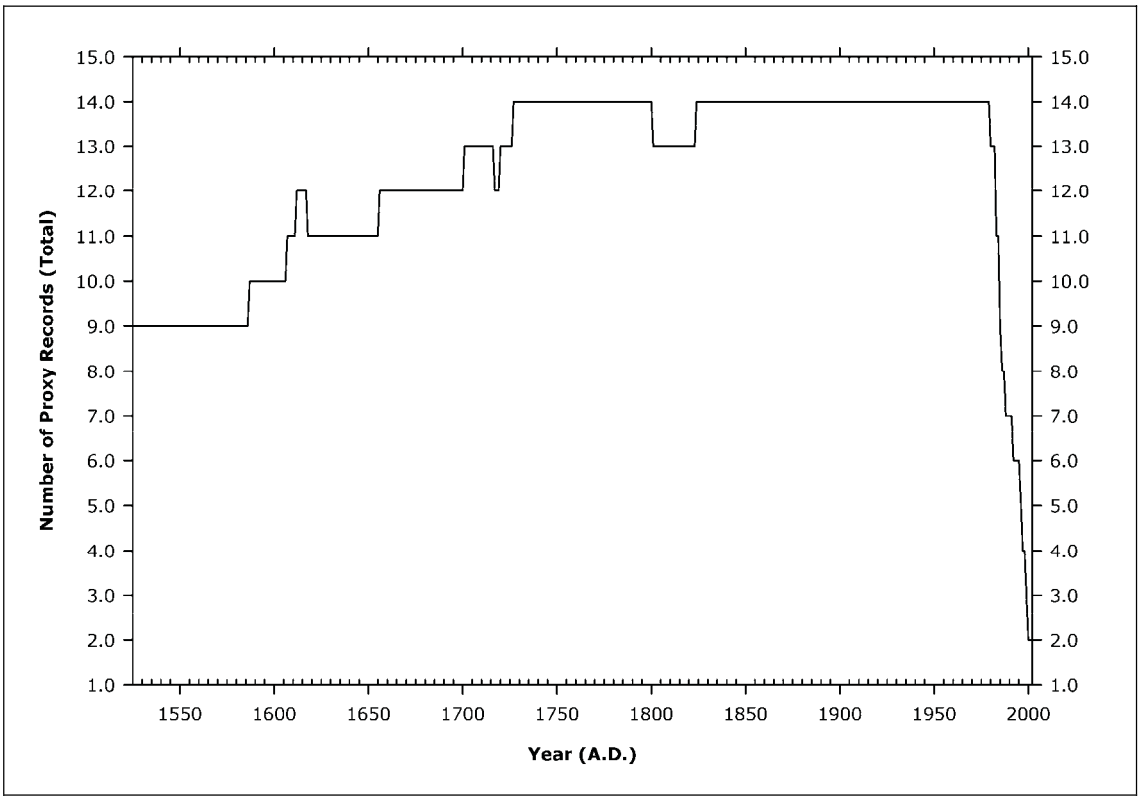

Figure 5.4. Temporal coverage of proxy data used in this study. Prominent sample depth (number of available proxies) fluctuations are due to a) various gaps in the Nile flood data, b) loss of temporal coverage of coral sequences, c) post-1900 gaps in the Galapagos coral record and d) only six records covering the 1990s.

5.6.2 Sub-sample sensitivity analysis

To assess the implication of loss of sample depth through time, a sensitivity analysis was undertaken on a sub-sample of El Niño and La Niña proxies (Figure 5.5). This was done by calculating differences in event capture, magnitude and reconstruction quality from ENSO reconstructions based on the lowest number of proxies continuously present back to A.D 1525, compared to reconstructions based on the fluctuating total of records available. Correlations between the reconstruction quality and event magnitude were then compared to allow the minimum threshold of replication needed to compensate for loss of records back through time (Figure 5.4). This allowed the robustness of the reconstruction with diminishing replication to be quantified.

5.7 Multiproxy Event Definition

5.7.1 Proxy-threshold sensitivity

Following the calibration of single proxy records with instrumental ENSO indices outlined in Figure 5.2, a sensitivity analysis was undertaken to explore the number of proxies needed to maximise ENSO event capture (while minimising false positive cases) in a multiproxy context during the instrumental period (1871-2002). This was carried out on subsets of El Niño and La Niña sensitive proxies with skill scores exceeding 0.66. This allowed the degree of uncertainty associated with defining an ENSO event based on a minimum requirement of three proxies to over seven proxies in terms of correct event capture, false positive cases, decoupled and missed events to be quantified. This provided a basis for assessing the potential of over/under reconstruction of ENSO events in the pre-instrumental period. Unlike Whetton and Rutherfurd (1994), no criteria were imposed that a particular proxy must indicate an ENSO response for event definition since teleconnection non-stationarities are known to exist (Stahle *et al.*, 1998; Mann *et al.*, 2000; Hendy *et al.*, 2003).

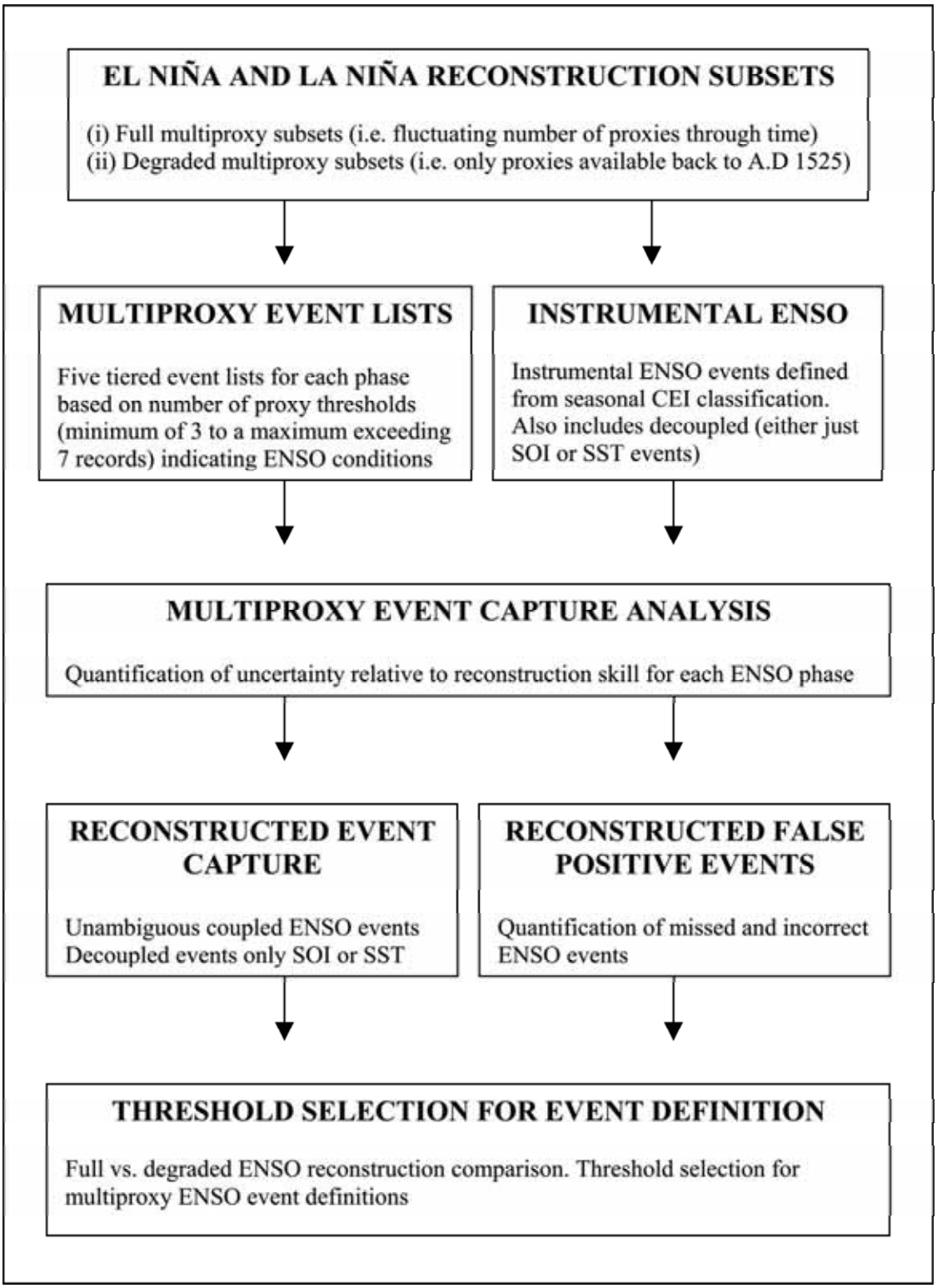

Figure 5.5. Event capture sensitivity analysis based on a three to seven proxy-thresholds for full and degraded proxy subsets. Separate proxy subsets used to reconstruct separate El Niño and La Niña conditions and compared to instrumental ENSO conditions to assess under/over reconstruction issues associated with various proxy-thresholds.

5.7.2 Quality adjusted magnitude scoring (MQ)

As the number of proxies analysed through time fluctuates there may be inflation (under-estimation) in the occurrence of an event due to higher (lower) relative numbers of available proxy records (Figure 5.4). Furthermore, the reconstruction quality is likely to reflect the overall skill of the subset of proxies contributing to the reconstruction for each year.

Thus, to allow the skill of the proxy to be incorporated into the quantification of event magnitude, a quality adjusted magnitude (MQ) time series was devised (Figure 5.6). Firstly, the mean reconstruction quality score (MS) was developed to indicate the general quality of the subset of proxies contributing to the reconstruction at a given point in time. The relative *proportion* (rather than total number) of ENSO responsive records was then multiplied by the MS score for each year to allow the weight of the best proxies to be inherently recognised in the MQ score. This addresses the issue of a loss of records through time.

To define the intensity and quality of reconstructed events, a percentile analysis on the quality adjusted magnitude time series was performed to isolate extreme, very strong, strong, moderate and weak El Niño (La Niña) conditions (Figure 5.6). This was achieved by selecting five percentile classes based on calibrating the multiproxy network response to match historical strong-extreme events identified by Trenberth (1997) and Gergis and Fowler (2005) during the instrumental (1871-2002) period.

Five event classes ranging from extreme (>90th percentile) very strong (70th - 90th percentile), strong (50th - 70th), moderate (50th - 30th) and weak events (<30th) identified from the instrumental period were then applied to the quality adjusted magnitude time series back to A.D. 1525. To further examine the nature of past ENSO events, changes in the frequency, duration and magnitude of events per decade and per century were calculated.

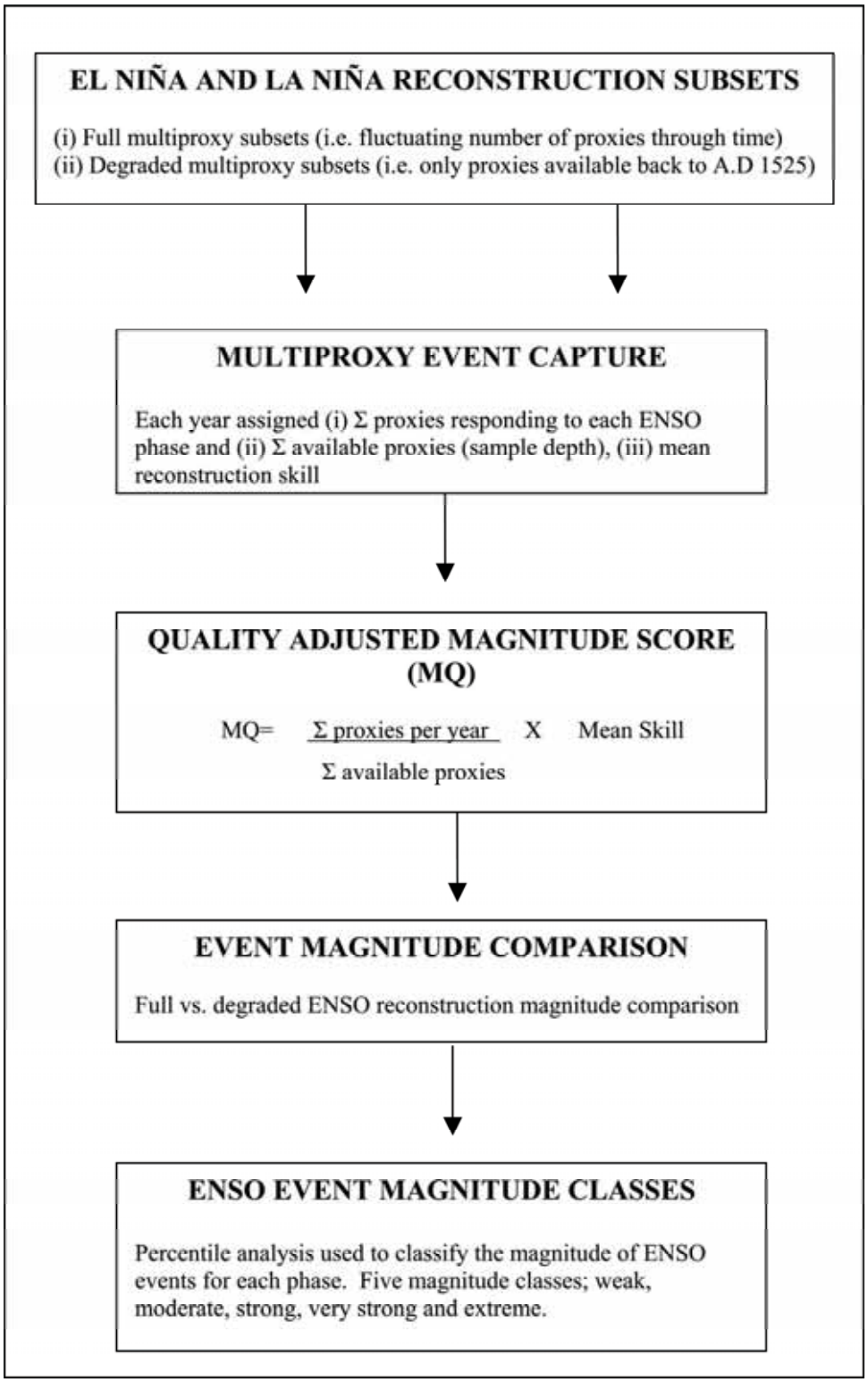

Figure 5.6. Outline of ENSO event quality-adjusted magnitude (MQ) index. Amplitude of ENSO events are relative to the corresponding number of proxy records available for each phase.

5.8 Results

5.8.1 Single proxy calibration results

Results of the proxy calibration analysis are shown in Table 5.2. Of the 15 records analysed, 12 (9) records achieved an El Niño (La Niña) skill score of ≥0.66. However for La Niña this rose to twelve if the skill score criterion was relaxed to a minimum skill of 0.6. In an attempt to address this bias, this slightly lower threshold was adopted for three La Niña proxies (D'Arrigo Teak (0.6), Great Barrier Reef (0.65) and New Caledonia (0.64)) to allow a similar number of records into the each ENSO phase reconstruction. The bias towards El Niño sensitivity of proxy records is reflected in the overall skill and proxy performance scores shown in Table 5.2.

El Niño skill scores ranged from 0.56 for New Caledonia coral to a high 0.96 for the Indian drought chronology. When considering overall proxy performance, Mexico, Berlage Teak and Kauri are the most useful tree-ring records, while the Quinn record and Indian drought chronology also rank second and third in terms of reconstruction importance. Rarotonga coral record appears in the top ten El Niño proxies, with the Quelccaya ice core performing better than any of the coral records. Clearly, the Nile, China and New Caledonian coral records are not strong overall performers for El Niño reconstruction.

The Chinese record had the lowest La Niña skill score of 0.46 and the Galapagos coral sequence the highest (0.82). The Berlage Teak sequence from Indonesia is the overall best performing tree-ring record, followed by the southwest USA, and Mexican tree-ring chronologies. The Great Barrier Reef record was the best performer of the coral sequences. With the exception of the Great Barrier Reef record, the other coral sequences do not seem to rank highly in terms of their La Niña event sensitivity, as was the case for the Quelccaya ice record from Peru.

Single-phase sensitivity was noted for a number of proxies. La Niña sensitivity was observed for proxies from New Caledonia, southwest USA and the Galapagos, while single El Niño-phase sensitivity was noted in the Chinese rainfall, Quinn record, and Indian drought records. Dual-phase sensitivity was noted for all the tree-ring records (with the lesser La Niña sensitivity of D'Arrigo Teak record noted above), the two coral records from Rarotonga and Great Barrier Reef and the Quelccaya ice core.

Table 5.2. Proxy calibration results for El Niño (above) and La Niña (below) phase reconstruction ranked in relation to overall proxy performance score outlined in Figure 5.2. In this study, the record length available for calibration with instrumental data is an important factor in determining the quality of a given proxy. Thus, to capitalise on the length of each record, the analysis was calculated on the full period of instrumental overlap for each ENSO proxy to allow records with a longer record length to be completely utilised and contribute to overall proxy skill. Note that a lower skill score of ~0.6 was need for three La Niña proxies (D'Arrigo Teak (0.6), Great Barrier Reef (0.65) and New Caledonia (0.64)) to allow a similar number of records into each ENSO phase reconstruction.

	Record Type	CEI Event Capture (%)	Percentile Threshold	Phase Score	False Positive Score	Proxy Skill Score	Proxy Performance Score (Skill & Event Capture)
El Niño							
Mexico	Tree-ring	81.25%	59th	31.00	-7.50	0.76	1.57
Quinn	Documentary	74.07%	65th	24.50	-6.00	0.76	1.50
India	Documentary	48.15%	65th	14.00	-0.50	0.96	1.45
Berlage Teak	Tree-ring	60.00%	30th	8.00	-1.50	0.81	1.41
Kauri	Tree-ring	60.61%	74th	23.00	-6.00	0.74	1.36
Quelccaya	Ice Core	62.96%	70th	19.50	-6.00	0.69	1.32
SW USA	Tree-ring	59.38%	63rd	24.50	-9.50	0.61	1.21
Rarotonga	Coral	45.16%	74th	16.50	-4.50	0.73	1.18
D'Arrigo Teak	Tree-ring	48.39%	29th	15.00	-5.00	0.67	1.15
Pink Pine	Tree-ring	44.12%	27th	18.50	-6.00	0.68	1.12
Galapagos	Coral	50.00%	25th	12.50	-5.00	0.60	1.10
Nile	Rainfall	32.14%	20th	11.50	-3.50	0.70	1.02
Great Barrier Reef	Coral	33.33%	16th	10.00	-2.00	0.67	1.00
China	Rainfall	19.23%	90th	5.50	-1.50	0.73	0.92
New Caledonia	Coral	10.34%	93rd	4.50	-2.00	0.56	0.66

	Record Type	CEI Event Capture (%)	Percentile Threshold	Phase Score	False Positive Score	Proxy Skill Score	Proxy Performance Score (Skill & Event Capture)
La Niña							
Berlage Teak	Tree-ring	69.23%	59th	12.50	-3.50	0.72	1.41
SW USA	Tree-ring	63.16%	38th	27.50	-7.50	0.73	1.36
Mexico	Tree-ring	63.89%	42nd	28.00	-8.00	0.71	1.35
Great Barrier Reef	Coral	61.76%	65th	23.00	-8.00	0.65	1.27
Nile	Rainfall	50.00%	86th	9.50	-2.50	0.74	1.24
Pink Pine	Tree-ring	54.17%	27th	20.50	-7.00	0.66	1.20
Kauri	Tree-ring	52.50%	37th	23.50	-7.50	0.68	1.20
D'Arrigo Teak	Tree-ring	58.33%	29th	22.50	-9.00	0.60	1.18
New Caledonia	Coral	51.43%	93rd	22.50	-8.00	0.64	1.16
Galapagos	Coral	31.82%	25th	5.50	-1.00	0.82	1.14
Rarotonga	Coral	38.89%	74th	15.50	-4.50	0.71	1.10
Quelccaya	Ice Core	38.24%	70th	15.00	-4.50	0.70	1.08
China	Rainfall	34.29%	29th	14.00	-7.50	0.46	0.81

5.8.2 Proxy stationarity analysis

To identify trends in the stability of the ENSO signal present in each regional proxy record, the frequency of reconstructed events for each phase was calculated in 25-year periods and compared. Table 5.3 indicates some notable fluctuations in event capture characteristics for both phases, particularly in regards to the coral sequences. With the exception of the Rarotonga record, El Niño event registration appears to have fluctuated considerably especially during the 17th century. The New Caledonia (Galapagos) coral record appears to have the most inconsistent El Niño (La Niña) event capture with sensitivity, a result also confirmed in Table 5.3, suggesting significant non-stationarities or dating issues. The Nile and Chinese rainfall record are also noteworthy for their non-

stationary relationships to El Niño conditions. By contrast, all the tree-ring chronologies and the ice record appear to be robust indicators of both ENSO phases.

Table 5.3. Frequency of reconstructed ENSO event years per 25-year periods to assess the stability of proxy-ENSO sensitivity and/or dating issues. A dash (-) indicates no temporal coverage.

	Quinn	India	Nile	China	Indonesia	Pink Pine	Kauri	Mexico	SW USA	Peru	New Caledonia	Great Barrier Reef	Galapagos	Rarotonga
El Niño														
1975-2000	3	2	0	0	5	3	4	9	9	2	0	2	2	2
1950-1975	6	5	1	2	4	4	6	6	7	2	0	3	2	3
1925-1950	4	3	2	3	5	6	6	7	6	3	1	3	1	5
1900-1925	7	8	1	1	4	5	5	6	5	5	2	2	2	6
1875-1900	7	3	0	2	4	4	5	6	5	4	1	3	2	5
1850-1875	10	5	0	1	7	3	3	7	5	2	3	2	4	3
1825-1850	5	3	0	0	4	6	7	6	6	5	3	1	4	5
1800-1825	8	4	0	1	5	5	3	6	6	1	2	1	1	2
1775-1800	4	2	2	3	3	5	6	5	6	2	1	3	4	2
1750-1775	6	2	0	0	3	3	4	5	4	0	0	3	3	4
1725-1750	5	4	0	0	3	5	6	4	8	4	4	5	5	0
1700-1725	8	3	1	1	6	6	5	8	6	3	1	2	4	0
1675-1700	6	2	0	2	3	5	3	7	8	3	3	1	0	0
1650-1675	5	2	0	0	4	5	7	5	6	3	2	0	4	0
1625-1650	5	3	0	1	6	5	2	4	6	2	-	0	1	0
1600-1625	7	2	0	2	5	4	5	6	4	2	-	0	3	0
1575-1600	5	3	0	1	1	4	1	5	6	2	-	-	-	-
1550-1575	5	1	0	0	4	7	3	8	2	2	-	-	-	-
1525-1550	6	1	0	1	2	3	0	6	6	3	-	-	-	-

	Quinn	India	Nile	China	Indonesia	Pink Pine	Kauri	Mexico	SW USA	Peru	New Caledonia	Great Barrier Reef	Galapagos	Rarotonga
La Niña														
1975-2000	N/A	N/A	0	0	5	3	5	7	6	1	4	2	0	3
1950-1975	N/A	N/A	0	4	5	6	8	9	9	3	4	8	4	4
1925-1950	N/A	N/A	0	3	4	5	7	7	5	1	5	4	2	3
1900-1925	N/A	N/A	0	5	7	5	6	6	6	3	2	4	2	3
1875-1900	N/A	N/A	1	5	5	5	6	4	5	2	1	5	3	4
1850-1875	N/A	N/A	1	5	6	4	4	6	5	6	3	7	0	3
1825-1850	N/A	N/A	1	5	6	4	8	8	6	3	0	5	3	5
1800-1825	N/A	N/A	0	5	3	6	8	6	8	5	2	6	2	3
1775-1800	N/A	N/A	0	2	3	4	8	6	8	5	3	3	0	5
1750-1775	N/A	N/A	0	5	5	5	7	5	8	4	4	4	0	2
1725-1750	N/A	N/A	1	7	6	3	5	4	6	3	1	5	0	2
1700-1725	N/A	N/A	0	5	3	4	4	5	6	3	4	3	1	0
1675-1700	N/A	N/A	0	4	5	5	6	7	6	7	2	3	2	0
1650-1675	N/A	N/A	0	4	5	6	5	5	7	7	1	1	0	0
1625-1650	N/A	N/A	0	3	5	5	5	5	5	3	-	5	7	0
1600-1625	N/A	N/A	0	4	3	3	7	5	4	4	-	2	3	0
1575-1600	N/A	N/A	0	3	3	4	11	8	4	3	-	-	-	-
1550-1575	N/A	N/A	0	4	2	3	11	5	7	6	-	-	-	-
1525-1550	N/A	N/A	0	1	2	5	14	7	6	4	-	-	-	-

5.8.3 Multiproxy event capture threshold sensitivity analysis

To investigate the impact of proxy-threshold definition on ENSO event reconstruction, an analysis of the frequency and duration characteristics based on replication is presented in Table 5.4. Raising the proxy-threshold from three to seven proxies reduced

both the overall event capture and false positive 'misfires'. Generally, as more stringent proxy-thresholds of replication are imposed, event capture decreases discernibly as does mean event duration. Furthermore, it was evident that increasing the number of proxies used to define an ENSO event was indicative of the magnitude of an event. Logically, highest confidence in the reconstruction was found to be associated with events of a stronger magnitude when there is a high degree of replication of the climate signal in various proxies.

For the El Niño reconstruction, there are minor differences in the frequency of events using a three proxy-threshold for the instrumental period, ranging from 22-27 reconstructed events (Table 5.4). However, in the pre-instrumental period where sample depth decreases (see Figure 5.5), the implications of using higher thresholds for event definition become apparent. For example, there is a discrepancy of 47 events between using three and five proxy records in the pre-instrumental period.

Table 5.4. Event frequency and duration characteristics for reconstructed instrumental and pre-instrumental periods.

Number of Proxy Records	Instrumental Frequency (1871-2002)	Mean/Maximum Duration (Years)	Pre-Instrumental Frequency (1525-1870)	Mean/Maximum Duration (Years)	Total Events (1525-2002)
El Niño					
≥3	27	2.4/8.0	65	1.9/7.0	92
≥4	22	2.0/5.0	40	1.3/3.0	62
≥5	20	1.5/4.0	18	1.1/2.0	38
≥6	8	1.6/4	5	1.0/1.0	13
≥7	3	1.3/2	1	1.0/1.0	4
La Niña					
≥3	26	3.1/11.0	56	3.3/36.0 (2.8/11.0)	82
≥4	21	2.4/6.0	60	2.0/9.0	81
≥5	16	2.3/5.0	36	1.8/8.0	52
≥6	15	1.5/3.0	18	1.3/2.0	33
≥7	8	1.0/1.0	10	1.0/1.0	18

Post-1870, mean event duration declines from 2.4 to 1.3 years using the three (seven) proxy event definition thresholds. Notably, the three-proxy threshold maintains the most consistency in mean and maximum event characteristics in both the observed and pre-instrumental period, in addition to a high event capture. In fact, 28 El Niño events are noted by Gergis and Fowler (2005) from the instrumental CEI record, suggesting good compatibility with instrumentally observed frequency of events.

For the La Niña reconstruction, three and four-proxy thresholds for event definition yield comparable frequency results for the instrumental and pre-instrumental periods. Raising the threshold to five proxies reduces instrumental event capture by up to 10 (30) events compared to the three-proxy threshold for the calibration (pre-instrumental) period. Event duration appears over-sensitive for the lowest three-proxy threshold, resulting in a maximum duration of 36 consecutive years between A.D. 1738-1773, which is unlikely. Excluding this protracted event results in a mean (maximum) duration of 2.8 (11) years, which is similar to the three proxy-threshold duration characteristics noted for the observational period (Table 5.4).

The four-proxy La Niña threshold appears to maintain consistent mean duration characteristics in both the post-1870 (2.4 years) and pre-instrumental (2.0 years) periods, while maintaining a reasonable overall event capture. The 21 events captured in the observational period compares well to the 26 La Niñas identified in the instrumental CEI record (Gergis and Fowler, 2005). The similarities of the La Niña event capture noted in the pre-instrumental period for the three and four proxy thresholds is a result of the prolonged cool event from A.D. 1863-1875 being split into three separate events (A.D. 1863-1864, 1866-1868, 1870-1875) using the four proxy threshold.

The impact of lowering the proxy event capture threshold is further examined in Table 5.5. Clearly, lowering the minimum proxy threshold for ENSO event definition increases the probability of including false positives in the reconstruction, reflected in lower confidence scores listed in Table 5.5. For example, there is a notable increase in the number of missed events from a minimum of four to a maximum of 20 events using the three and seven proxy minimum for the El Niño reconstruction. This implies that adopting a lower threshold may be more appropriate in the interest of maintaining reconstruction potential from the multiproxy assemblage.

There is an increase in the capture of decoupled events as a lower threshold is adopted. This increase is more pronounced for the La Niña analysis where lower proxy thresholds result in the reconstruction of a maximum of eight decoupled SOI events (e.g. 1929, 1960, 1981). Importantly, none of the reconstructions for either phase are able to faithfully reproduce the instrumentally observed CEI, although considerable skill is still achieved, as seen in Table 5.2.

Table 5.5. Reconstruction quality characteristics associated with each multiproxy threshold. False positives are defined here as a proxy exhibiting a response conflicting with instrumental conditions, decoupled events refer to events only registered by the atmosphere or ocean but not experienced simultaneously by both and an event unresolved by a reconstruction subset. Reconstruction confidence level refers to the proportion of false positives relative to accurate instrumental event capture (%) as represented by the CEI of Gergis and Fowler (2005).

Number of Proxy Records	Instrumental Event Capture (1871-2002)	Total False Positives (Events)	Decoupled Events (Total)	Missed Events (Total)	Reconstruction Confidence Level (%)
El Niño proxies					
3+	27	5	4	4	81.5
4+	22	1	3	6	95.5
5+	20	1	2	6	95.0
6+	8	0	1	15	100.0
7+	3	0	0	21	100.0
La Niña proxies					
3+	26	7	8	1	73.1
4+	21	5	4	4	76.2
5+	16	3	0	7	81.3
6+	15	2	0	8	86.7
7+	9	1	0	14	87.5

The maximum confidence level for the La Niña reconstruction is 87.5% for the seven-proxy threshold. The sole false positive case relates to 1953 where an exceptional nine proxies indicate La Niña conditions. That year does not correspond to the six-month instrumentally observed El Niño that achieved a maximum SST anomaly of 1.13°C. However, La Niña conditions began developing in the SOI by June 1954, culminating in a coupled event spanning August 1954 to March 1955 (not shown). This highlights the potential weaknesses inherent in palaeoclimate reconstruction, and may suggest that proxies were responding to factors other than ENSO at this time.

Since there were minor differences in the event capture characteristics of the three and four-proxy event lists, using four proxies for La Niña event definition was considered to be slightly more conservative than a criteria based on a three-proxy threshold. Thus, three (four) proxy threshold was adapted for El Niño (La Niña) event definition using our multiproxy assemblage to resolve the highest degree of events possible from the reconstruction.

5.9 Reconstruction Quality Results

5.9.1 Degraded subset event capture analysis

As noted in Section 5.6, the number of proxy records replicating an ENSO signal fluctuates through time which may bias the apparent trends seen in the occurrence and magnitude of reconstructed ENSO events. Thus, to investigate the implications of the inevitable loss of records, event capture statistics for the full data set (Table 5.6) were compared with those for a 'degraded' data set of the proxy subsets available back to A.D. 1525. The 1871-2002 period was used as it is the only interval that can be cross verified with observational ENSO data, represented in this study by the CEI.

Table 5.6. Comparison of the A.D. 1525 (degraded) subset and the full reconstruction event capture characteristics as per Table 5.5) for the instrumental (A.D. 1871-2002) and pre-instrumental (A.D. 1525-1870) periods. False positives are defined here as a proxy exhibiting a response conflicting with instrumental conditions, decoupled events refer to events only registered by the atmosphere or ocean but not experienced simultaneously by both and an event unresolved by a reconstruction subset. 'Proportion of Instrumentally observed events' refers to the proportion of false positives relative to accurate instrumental event capture (%) as represented by the CEI of Gergis and Fowler (2005).

Proxy Record subsets present at A.D. 1525	Instrumental Event Capture (1871-2002)	Total False Positives (Events)	Decoupled Events (Total)	Missed Events (Total)	Proportion of Full Set Events (1871-2002) (%)	Pre-Instrumental Event Capture (1525-1870)	Total Event Capture (1525-2002)
El Niño proxies							
≥3	26	4	4	4	92.8	66	92
≥4	20	1	1	6	90.1	33	53
≥5	11	0	1	13	55.0	12	23
≥6	1	0	0	22	10.0	2	3
La Niña proxies							
≥3	25	3	4	3	96.2	74	99
≥4	17	2	1	7	80.9	47	64
≥5	6	1	0	16	37.5	13	19
≥6	1	0	0	19	6.0	1	2

Table 5.6 indicates the event capture obtained using the three-proxy thresholds between the full and 1525 proxy subsets of the reconstruction for each phase. For the El Niño (La Niña) phase 93% (96%) of events noted in the full reconstruction are present in the subset back to A.D. 1525. This suggests loss of sample depth is not detrimental in event capture using a three-proxy threshold for event definition in the multiproxy environment.

Raising the threshold to four-proxies, there is still good agreement for the El Niño phase (90%), however, the La Niña reconstruction suffers from a loss of replication,

falling to 81% agreement. Beyond a four-proxy threshold, there is substantial loss in reconstruction potential which is most marked for La Niña phase reconstruction, reflecting the lower overall proxy sensitivity noted in Table 5.1.

The apparent increase in La Niña event capture numbers at lower thresholds, as seen in Table 5.6, is a result of 'event splitting' resulting from the stricter criteria for event definition. This is most noticeable for pre-instrumental event capture using the three-proxy threshold. In this instance, there is a discrepancy of eighteen events between the full (56 events seen in Table 5.4) and the degraded 1525 subset (74 events). This is a result of apparently protracted events (A.D. 1622-1632, 1675-1679, 1738-1773, 1857-1875) splitting into a maximum of ten events for the highly unusual A.D. 1738-1773 period.

A comparison of the mean skill (MS) time series calculated for the degraded and full reconstruction revealed considerable similarity. Correlations between mean El Niño (La Niña) skill for the 1525 subset and full reconstruction was 0.97 (0.83), suggesting sufficient high quality proxies exist at the early end of the reconstruction to overcome quality issues associated with loss of sample depth. Similarly, correlations between the magnitude time series for the 1525 subset and full reconstructions for El Niño (La Niña) were 0.91 (0.87). The near-identical quality of the degraded and full El Niño reconstructions reiterates the relatively lower sensitivity of proxies to La Niña conditions noted in Section 5.8.1.

5.9.2 ENSO event verification results

To assist the selection of thresholds for the multiproxy event definition, the three and four proxy-threshold events were compared to past ENSO event lists published for the instrumental period (Rasmusson and Carpenter, 1983; Kiladis and Diaz, 1989; Quinn and Neal, 1992; Whetton and Rutherfurd, 1994; Mullan, 1995; Trenberth, 1997; Ortlieb, 2000; Allan *et al.*, 2003). For the pre-instrumental period, two lists provided by the 'Quinn record' (Ortlieb (2000) pre-1901 and Quinn and Neal (1992) for the post-1900 period) and Whetton and Rutherford (1994) were used. These chronologies are hereafter referred to as 'QO00' and 'WR94', respectively. Table 5.7 shows the event capture characteristics of the two primary long-term ENSO event lists of QO00 and WR94 and the multiproxy event lists from the analysis presented here.

There is a high degree of similarity between the QO00 record and the use of three proxies for event definition. The additional 16 events not included in the multiproxy event lists may indicate El Niño conditions that may have only been regional in nature (e.g. A.D. 1531-1532, 1604, 1624, 1761, 1819). Events from the multiproxy reconstructions have a longer duration than a number of the events indicated in QO00 (not shown), which may reflect the impact of calibrating proxies using the CEI which allowed lead/lag signatures associated with decoupled events to be resolved. Consequently, the results may be a sign of larger-scale patterns of ENSO events, rather than the response of one (East Pacific) teleconnection region.

Table 5.7. Comparison of multiproxy event lists with published events for verification.

ENSO Event Lists	Instrumental Event Capture (1871-2002)	Pre-Instrumental Event Capture (1525-1870)	Total Event Capture (1525-2002)
El Niño			
3+ Multiproxy events	27	65	92
4+ Multiproxy events	22	40	62
Quinn & Ortlieb	29	80	109
Whetton and Rutherfurd	16	23	39
La Niña			
3+ Multiproxy events	26	59	85
4+ Multiproxy events	21	61	82
Quinn and Ortlieb	-	-	-
Whetton and Rutherfurd	4	6	10

Verification of La Niña events was substantially more difficult due to the lack of coverage in the QO00 and a total of ten events noted by WR94. The year A.D. 1906 is the only La Niña event not present in the three or four proxy La Niña chronologies, however, the 1826 La Niña noted by WR94 is only detectable using the three-proxy threshold. Since there were minor differences in the event capture characteristics of the three and four-proxy event lists (see Section 5.6), using four proxies for La Niña event was considered to be slightly more conservative than a criteria based on a three-proxy threshold. Thus, three (four) proxy threshold was adapted for El Niño (La Niña) event definition using our multiproxy assemblage to resolve the highest degree of events possible from the reconstruction (Table 5.8).

5.9.3 Multiproxy ENSO event definition

For the El Niño (La Niña) reconstruction, a quality adjusted magnitude score (MQ) value associated with the three (four) proxy threshold was used to define an event. This provided a minimum quality threshold, allowing events based on fewer, but higher quality proxy records, to be included in the analysis. This was most crucial for the beginning and end of the reconstruction when fewer proxies were available.

The appropriate MQ minimum thresholds were then applied to the remainder of the time series to identify years where reconstruction quality standards were met, regardless of the total number of proxies replicating an ENSO signal. This allowed the quality and level of replication to be used as a basis for event identification (ranging from weak to extreme events), to compensate for lower magnitude decoupled, lead or lag event characteristics (Table 5.8).

Table 5.8. *presented overleaf* El Niño and La Niña multiproxy event lists based 3(4) proxy threshold replication for El Niño (La Niña) event definition, A.D. 1525-2002. Quality adjusted magnitude score (MQ) class scores were assigned using the percentile analyses detailed in Section 5.7.2. Note that various seasonal windows are represented in the reconstruction (see Table 5.1 and Table 5.2) with DJF reflect the year in which the month of January falls. 'PR' refers to proxy ratio i.e. the number of records indicating an ENSO signal relative to total number of proxies available, 'MS' mean skill, 'and 'MC' magnitude classification. A percentile analysis of the MQ time series was used to classify extreme (>90th percentile) very strong (70th - 90th percentile), strong (50th - 70th), moderate (50th - 30th) and weak events (<30th).

El Niño Year	PR	MS	MQ	MC	La Niña Year	PR	MS	MQ	MC
2002	1/1,	0.74,	0.74,	E	2000	1/2,	0.73,	0.37,	S
1997	1/3,	0.76,	0.25,	W	1998	3/4,	0.68,	0.51,	E
1992	3/5,	0.73,	0.44,	VS	1996	2/5,	0.72,	0.29,	M
1991	3/5,	0.70,	0.42,	VS	1995	3/6,	0.72,	0.33,	S
					1990	4/7,	0.69,	0.39,	VS
1987	3/6,	0.73,	0.37,	VS	1989	5/7,	0.69,	0.49,	VS
1985	2/7,	0.78,	0.22,	W	1988	3/7,	0.67,	0.29,	M
1983	6/9,	0.72,	0.48,	E	1986	3/7,	0.68,	0.29,	M
1982	6/10,	0.78,	0.46,	E	1985	3/8,	0.63,	0.24,	W
1980	4/10,	0.70,	0.28,	M	1984	4/10,	0.67,	0.27,	M
1979	4/11,	0.79,	0.29,	M	1975	5/9,	0.66,	0.36,	S
1977	3/11,	0.74,	0.20;	W	1974	9/11,	0.68,	0.56,	E
1976	5/11,	0.71,	0.32,	M	1973	4/11,	0.67,	0.24,	W
1973	3/11,	0.74,	0.20,	W	1972	4/11,	0.68,	0.25,	W
1972	5/11,	0.76,	0.35,	M	1971	7/11,	0.67,	0.43,	VS
					1970	5/11,	0.65,	0.30,	M
1969	5/11,	0.73,	0.33,	S	1968	4/11,	0.67,	0.24,	W
1968	5/11,	0.76,	0.34,	S	1963	4/11,	0.68,	0.25,	W
1967	3/11,	0.70,	0.19,	W	1962	4/11,	0.67,	0.25,	W
1966	4/11,	0.80,	0.29,	M	1960	4/11,	0.67,	0.25,	W
1965	5/11,	0.76,	0.35,	S					
1964	5/11,	0.71,	0.32,	S					
1959	3/11,	0.75,	0.20,	W	1959	4/11,	0.69,	0.25,	W
1958	4/11,	0.74,	0.27,	M	1958	5/11,	0.66,	0.30,	M
1957	5/11,	0.71,	0.32,	S	1957	4/11,	0.70,	0.25,	W
1952	3/11,	0.80,	0.22,	W	1956	7/11,	0.68,	0.43,	VS
1951	4/11,	0.79,	0.29,	M	1955	6/11,	0.67,	0.36,	S
					1953	9/11,	0.68,	0.56,	E
					1951	5/11,	0.68,	0.31,	M
					1950	8/11,	0.69,	0.50,	E
1949	3/11,	0.75,	0.20,	W	1946	6/11,	0.69,	0.38,	S
1947	3/11,	0.71,	0.19,	W	1945	4/11,	0.69,	0.25,	W
1944	5/11,	0.72,	0.33,	S	1943	4/11,	0.66,	0.24,	W
1942	7/11,	0.72,	0.46,	E					
1941	7/11,	0.76,	0.48,	E					
1940	6/11,	0.72,	0.39,	VS					
1939	4/11,	0.77,	0.28,	M	1934	3/11,	0.69,	0.25,	W
1938	4/11,	0.72,	0.26,	M	1932	4/11,	0.67,	0.24,	W
1937	3/11,	0.70,	0.19,	W					
1935	3/11,	0.72,	0.26,	W					
1933	3/11,	0.73,	0.20,	W					
1931	5/11,	0.75,	0.34,	S					
1930	4/11,	0.74,	0.27,	M					
1926	8/11,	0.74,	0.54,	E	1923	5/11,	0.68,	0.31,	W
1925	5/11,	0.78,	0.35,	S	1922	6/11,	0.69,	0.38,	S
1924	3/11,	0.73,	0.20,	W	1921	4/11,	0.70,	0.25,	W
1920	3/11,	0.82,	0.22,	W					
1919	5/11,	0.75,	0.34,	S	1918	6/11,	0.69,	0.38,	S
1918	5/11,	0.79,	0.36,	VS	1917	7/11,	0.67,	0.43,	VS
1915	6/11,	0.80,	0.43,	VS	1916	6/11,	0.68,	0.32,	S
1914	6/11,	0.74,	0.40,	VS					
1913	6/11,	0.79,	0.43,	VS					
1912	6/11,	0.74,	0.40,	VS					
1911	4/11,	0.79,	0.29,	M					
1906	3/11,	0.73,	0.20,	W	1910	8/11,	0.68,	0.44,	VS
1905	7/11,	0.76,	0.48,	E	1909	6/11,	0.70,	0.38,	VS
1904	3/11,	0.83,	0.22,	W	1908	6/11,	0.68,	0.32,	S
1903	3/11,	0.70,	0.19,	W	1907	5/11,	0.67,	0.31,	M
1902	6/11,	0.76,	0.41,	VS	1904	5/11,	0.68,	0.26,	W
1901	4/11,	0.82,	0.30,	S					
1900	6/11,	0.75,	0.41,	VS					
1899	4/11,	0.82,	0.30,	S	1896	4/11,	0.70,	0.25,	W
1897	5/11,	0.77,	0.30,	S	1894	8/11,	0.70,	0.51,	E
1896	4/11,	0.76,	0.27,	M	1893	7/11,	0.69,	0.39,	VS
1891	6/11,	0.77,	0.42,	VS	1892	7/11,	0.68,	0.38,	S
					1891	4/11,	0.69,	0.25,	W
					1890	6/11,	0.67,	0.36,	S
1889	3/11,	0.77,	0.21,	W	1887	7/11,	0.68,	0.38,	VS
1888	6/11,	0.73,	0.40,	VS	1886	5/11,	0.67,	0.30,	M
1885	5/11,	0.77,	0.35,	S	1880	7/11,	0.69,	0.38,	VS
1884	3/11,	0.73,	0.20,	W					
1881	4/11,	0.74,	0.27,	M					
1878	4/11,	0.72,	0.26,	M	1879	9/11,	0.69,	0.51,	E
1877	5/11,	0.80,	0.37,	VS	1878	4/11,	0.67,	0.24,	W
1876	3/11,	0.79,	0.21,	W	1875	6/11,	0.68,	0.32,	S
1874	3/11,	0.73,	0.20,	W	1874	5/11,	0.71,	0.32,	S
					1873	6/11,	0.70,	0.38,	VS
					1872	5/11,	0.69,	0.31,	M
					1871	6/11,	0.72,	0.39,	VS
					1870	7/11,	0.69,	0.39,	VS
1868	5/11,	0.79,	0.36,	VS	1868	5/11,	0.70,	0.32,	S
1866	5/11,	0.79,	0.36,	VS	1867	6/11,	0.69,	0.38,	S
1865	4/11,	0.80,	0.29,	M	1866	5/11,	0.67,	0.31,	M
1864	3/11,	0.83,	0.22,	W	1864	4/11,	0.71,	0.26,	W
1860	3/11,	0.84,	0.23,	W	1863	7/11,	0.68,	0.44,	VS
					1862	5/11,	0.69,	0.31,	M
					1861	8/11,	0.69,	0.50,	VS
					1860	6/11,	0.70,	0.38,	VS

El Niño Year	PR	MS	MQ	MC	La Niña Year	PR	MS	MQ	MC
1858	4/11,	0.73,	0.27,	M	1857	4/11,	0.70,	0.25,	W
1857	4/11,	0.71,	0.26,	M	1851	5/11,	0.69,	0.31,	M
1856	4/11,	0.74,	0.27,	M	1850	4/11,	0.67,	0.24,	W
1853	5/11,	0.82,	0.37,	VS					
1852	3/11,	0.76,	0.21,	W					
1848	3/11,	0.74,	0.20,	W	1849	5/11,	0.68,	0.31,	M
1847	3/11,	0.74,	0.20,	W	1848	4/11,	0.69,	0.25,	W
1846	3/11,	0.75,	0.20,	W	1847	6/11,	0.69,	0.38,	S
1845	6/11,	0.75,	0.41,	VS	1843	5/11,	0.70,	0.26,	W
1844	4/11,	0.79,	0.29,	M	1841	4/11,	0.68,	0.25,	W
					1840	4/11,	0.70,	0.25,	W
1838	3/11,	0.80,	0.22,	W	-				
1837	4/11,	0.82,	0.30,	S					
1833	5/11,	0.78,	0.35,	S					
1832	3/11,	0.80,	0.22,	W					
1829	3/11,	0.74,	0.20,	W	1825	5/11,	0.68,	0.31,	M
1824	4/11,	0.79,	0.29,	M	1823	4/10,	0.71,	0.28,	M
					1820	5/10,	0.70,	0.35,	S
1817	4/10,	0.75,	0.30,	S	1819	5/10,	0.69,	0.35,	S
1816	3/10,	0.78,	0.23,	W	1813	4/10,	0.71,	0.29,	M
1815	3/10,	0.77,	0.23,	W	1811	5/10,	0.69,	0.34,	S
1814	3/10,	0.78,	0.23,	W	1810	5/10,	0.69,	0.34,	S
1812	4/10,	0.82,	0.33,	S					
1807	4/10,	0.75,	0.30,	S	1809	5/10,	0.72,	0.36,	S
1806	5/10,	0.79,	0.40,	VS	1808	7/10,	0.69,	0.48,	VS
1804	3/10,	0.78,	0.23,	W	1805	7/20,	0.69,	0.49,	VS
1803	4/10,	0.82,	0.33,	S	1802	7/10,	0.68,	0.48,	VS
					1801	6/10,	0.69,	0.42,	VS
1799	5/11,	0.76,	0.34,	S	1798	4/11,	0.70,	0.25,	W
1798	3/11,	0.74,	0.20,	W	1797	5/11,	0.69,	0.31,	M
1794	4/11,	0.74,	0.27,	M	1795	4/11,	0.69,	0.25,	W
1793	4/11,	0.74,	0.27,	M	1790	5/11,	0.70,	0.32,	S
1792	3/11,	0.72,	0.20,	W					
1791	6/11,	0.78,	0.42,	VS					
1784	3/11,	0.72,	0.20,	W	1789	4/11,	0.71,	0.26,	W
1783	4/11,	0.80,	0.29,	M	1788	6/11,	0.70,	0.38,	VS
1782	3/11,	0.80,	0.22,	W	1787	6/11,	0.69,	0.37,	S
					1786	5/11,	0.70,	0.32,	S
					1785	4/11,	0.72,	0.26,	W
					1782	4/11,	0.70,	0.25,	W
					1780	5/11,	0.71,	0.32,	S
1777	3/11,	0.76,	0.21,	W	1779	5/11,	0.70,	0.32,	S
1770	5/11,	0.79,	0.36,	VS	1778	4/11,	0.70,	0.26,	W
					1776	4/11,	0.72,	0.26,	W
					1773	4/11,	0.71,	0.26,	W
					1772	5/11,	0.69,	0.31,	M
1769	4/11,	0.79,	0.29,	M	1765	6/11,	0.69,	0.37,	S
1768	3/11,	0.75,	0.20,	W	1763	5/11,	0.70,	0.32,	S
1766	3/11,	0.76,	0.21,	W	1761	5/11,	0.69,	0.32,	M
1754	3/11,	0.75,	0.20,	W	1758	4/11,	0.68,	0.25,	W
					1757	6/11,	0.69,	0.37,	M
					1756	5/11,	0.69,	0.31,	M
					1755	5/11,	0.70,	0.32,	S
					1754	5/11,	0.69,	0.31,	M
					1753	6/11,	0.69,	0.38,	S
					1752	7/11.	0.69,	0.44,	VS
					1751	5/11,	0.69,	0.31,	M
					1750	5/11,	0.70,	0.32,	S
1748	4/11,	0.77,	0.28,	M	1748	4/11,	0.70,	0.26,	W
1747	4/11,	0.81,	0.29,	M	1747	4/11,	0.72,	0.26,	W
1746	3/11,	0.83,	0.22,	W	1745	5/11,	0.71,	0.32,	S
1744	3/11,	0.83,	0.22,	W	1743	6/11,	0.70,	0.38,	VS
					1742	8/11,	0.70,	0.51,	E
					1741	5/11,	0.70,	0.32,	S
					1740	7/11,	0.70,	0.45,	VS
1738	3/11,	0.71,	0.19,	W	1739	6/11,	0.70,	0.38,	VS
1737	7/11,	0.79,	0.50,	E	1736	4/11,	0.72,	0.26,	W
1734	3/11,	0.78,	0.21,	W	1735	4/11,	0.72,	0.26,	W
					1733	6/11,	0.70,	0.38,	VS
					1732	5/11,	0.69,	0.31,	M
					1731	5/11,	0.68,	0.31,	M
					1730	4/11,	0.70,	0.25,	W
1729	3/11,	0.73,	0.20,	W	1725	4/10,	0.68,	0.27,	M
1728	5/11,	0.78,	0.35,	S	1724	4/10,	0.69,	0.28,	M
1726	3/10,	0.75,	0.23,	W					
1724	3/10,	0.77,	0.23,	W					
1723	6/10,	0.76,	0.46,	E					
1722	4/10,	0.73,	0.29,	M					
1721	3/10,	0.76,	0.23,	W					
1720	3/10,	0.77,	0.23,	W					
1719	4/9,	0.75,	0.33,	S	1716	5/10,	0.70,	0.35,	S
1718	5/9,	0.79,	0.44,	E	1715	5/10,	0.69,	0.35,	S
1714	3/10,	0.74,	0.22,	W					
1713	4/10,	0.74,	0.30,	M					
1712	3/10,	0.76,	0.23,	W					
1710	3/10,	0.75,	0.23,	W	1709	4/10,	0.69,	0.28,	M
1709	3/10,	0.80,	0.24,	W	1708	5/10,	0.68,	0.34,	S
1707	3/10,	0.78,	0.23,	W	1702	4/10,	0.69,	0.28,	M
1700	3/9,	0.75,	0.25,	W	1701	4/10,	0.70,	0.28.	M

El Niño Year	PR	MS	MQ	MC	La Niña Year	PR	MS	MQ	MC
1695	3/9,	0.73,	0.24,	W	1696	5/9,	0.71,	0.39,	VS
1694	4/9,	0.72,	0.32,	S	1690	4/9,	0.69,	0.31,	M
1692	3/9,	0.73,	0.24,	W					
1687	5/9,	0.79,	0.43,	VS	1686	4/9,	0.70,	0.31,	M
1684	3/9,	0.75,	0.25,	W	1685	4/9,	0.72,	0.32,	S
					1678	4/9,	0.70,	0.31,	M
					1676	4/9,	0.72,	0.32,	S
					1675	4/9,	0.69,	0.30,	M
					1668	4/9,	0.69,	0.31,	M
1669	3/9,	0.75,	0.25,	W	1663	5/9,	0.69,	0.39,	VS
1665	3/9,	0.75,	0.25,	W					
1661	4/9,	0.79,	0.35,	S					
1660	5/9,	0.79,	0.44,	VS					
1659	3/9,	0.84,	0.28,	M	1658	4/9,	0.70,	0.31,	M
1652	3/9,	0.75,	0.25,	W	1654	5/8,	0.71,	0.44,	VS
1651	3/9,	0.75,	0.25,	W					
1650	6/9,	0.79,	0.52,	E					
1648	3/9,	0.82,	0.27,	M	1649	3/8,	0.70,	0.26,	W
1646	3/9,	0.75,	0.25,	W	1648	3/8,	0.72,	0.27,	W
1642	3/9,	0.74,	0.24,	W	1645	6/8,	0.69,	0.52,	E
1641	3/9,	0.75,	0.25,	W	1644	4/8,	0.69,	0.34,	S
					1642	4/8,	0.70,	0.35,	S
					1641	5/8,	0.70,	0.44,	VS
1639	3/9,	0.72,	0.24,	W	1639	3/8,	0.71,	0.27,	M
1638	3/9,	0.77,	0.26,	W	1638	3/8,	0.72,	0.27,	M
1635	4/9,	0.72,	0.32,	M	1637	4/8,	0.71,	0.35,	S
1630	3/9,	0.83,	0.28,	M	1635	3/8,	0.70,	0.27,	W
					1632	7/8,	0.69,	0.61,	E
					1631	5/8,	0.70,	0.44,	VS
					1630	4/8,	0.68,	0.34,	S
1621	3/9,	0.76,	0.25,	W	1629	4/8,	0.69,	0.35,	S
1620	3/9,	0.73,	0.24,	W	1628	3/8,	0.69,	0.26,	W
					1627	3/8,	0.69,	0.26,	W
					1626	5/8,	0.69,	0.43,	VS
					1625	3/8,	0.72,	0.27,	M
					1624	5/8,	0.71,	0.45,	VS
					1623	5/8,	0.71,	0.44,	VS
					1622	4/8,	0.69,	0.34,	S
1619	4/9,	0.77,	0.34,	S	1612	4/9,	0.70,	0.31,	M
1618	5/9,	0.79,	0.44,	VS	1611	4/9,	0.70,	0.35,	S
1614	3/10,	0.83,	0.25,	W					
1609	3/9,	0.75,	0.25,	W	1605	3/7,	0.69,	0.30,	M
1608	5/9,	0.76,	0.42,	VS	1604	3/7,	0.69,	0.30,	M
1607	5/9,	0.73,	0.41,	VS	1603	3/7,	0.68,	0.29,	M
1601	3/9,	0.78,	0.26,	M	1602	3/7,	0.68,	0.29,	M
					1601	3/7,	0.70,	0.30,	M
					1600	4/7,	0.70,	0.40,	VS
1597	3/9,	0.80,	0.27,	M	1597	3/7,	0.71,	0.30,	M
1596	5/9,	0.77,	0.34,	S	1593	3/7,	0.72,	0.41,	VS
1594	4/9,	0.77,	0.34,	S	1592	4/7,	0.71,	0.40,	VS
1591	4/9,	0.74,	0.33,	S	1590	3/7,	0.72,	0.31,	M
1585	4/8,	0.74,	0.37,	VS	1584	4/6,	0.71,	0.47,	VS
1584	3/8,	0.70,	0.26,	M	1583	3/6,	0.71,	0.36,	S
1583	3/8,	0.72,	0.27,	M	1581	3/6,	0.69,	0.35,	S
					1580	3/6,	0.69,	0.35,	S
1574	4/8,	0.74,	0.37,	VS	1579	3/6,	0.71,	0.36,	S
					1578	3/6,	0.71,	0.36,	S
					1577	3/6,	0.70,	0.35,	S
					1576	3/6,	0.71,	0.36,	S
					1573	4/6,	0.70,	0.58,	E
					1572	5/6,	0.70,	0.58,	E
					1571	3/6,	0.69,	0.35,	S
1567	3/8,	0.78,	0.28,	M	1566	3/6,	0.70,	0.35,	S
1565	4/8,	0.75,	0.38,	VS	1561	3/6,	0.71,	0.35,	S
1563	3/8,	0.75,	0.28,	M	1560	4/6,	0.70,	0.23,	VS
1559	4/8,	0.75,	0.38,	VS					
1558	3/8,	0.78,	0.29,	M					
1556	4/8,	0.75,	0.40,	VS					
1554	4/8,	0.79,	0.30,	S					
1544	4/8,	0.75,	0.38,	VS	1549	3/6,	0.69,	0.35,	S
1540	3/8,	0.83,	0.31,	S	1548	3/6,	0.71,	0.47,	VS
					1546	3/6,	0.70,	0.35,	S
					1544	3/6,	0.70,	0.35,	S
					1542	3/6,	0.72,	0.36,	S
					1541	3/6,	0.71,	0.36,	VS
					1540	3/6,	0.69,	0.34,	S
1539	3/8,	0.74,	0.28,	M	1538	3/6,	0.72,	0.36,	S
					1535	3/6,	0.70,	0.35,	S
					1533	5/6,	0.70,	0.70,	E
					1532	4/6,	0.70,	0.47,	VS
					1531	4/6,	0.70,	0.47,	VS
1527	3/8,	0.73,	0.27,	M	1528	5/6,	0.70,	0.58,	E
1526	4/8,	0.72,	0.36,	VS					
1525	4/8,	0.72,	0.36,	VS					

5.10 Event Magnitude Analysis Results

5.10.1 ENSO events since A.D. 1525

Having verified the accuracy of the reconstruction, changes in the relative frequency, duration and magnitude of ENSO events suggested by the data were examined. Five categorisations of the magnitude time series (outlined in Section 5.7.2) for each phase were analysed to reveal changes in the proportions of ENSO years per decade (per century) are displayed in Figure 5.7 (Figure 5.8).

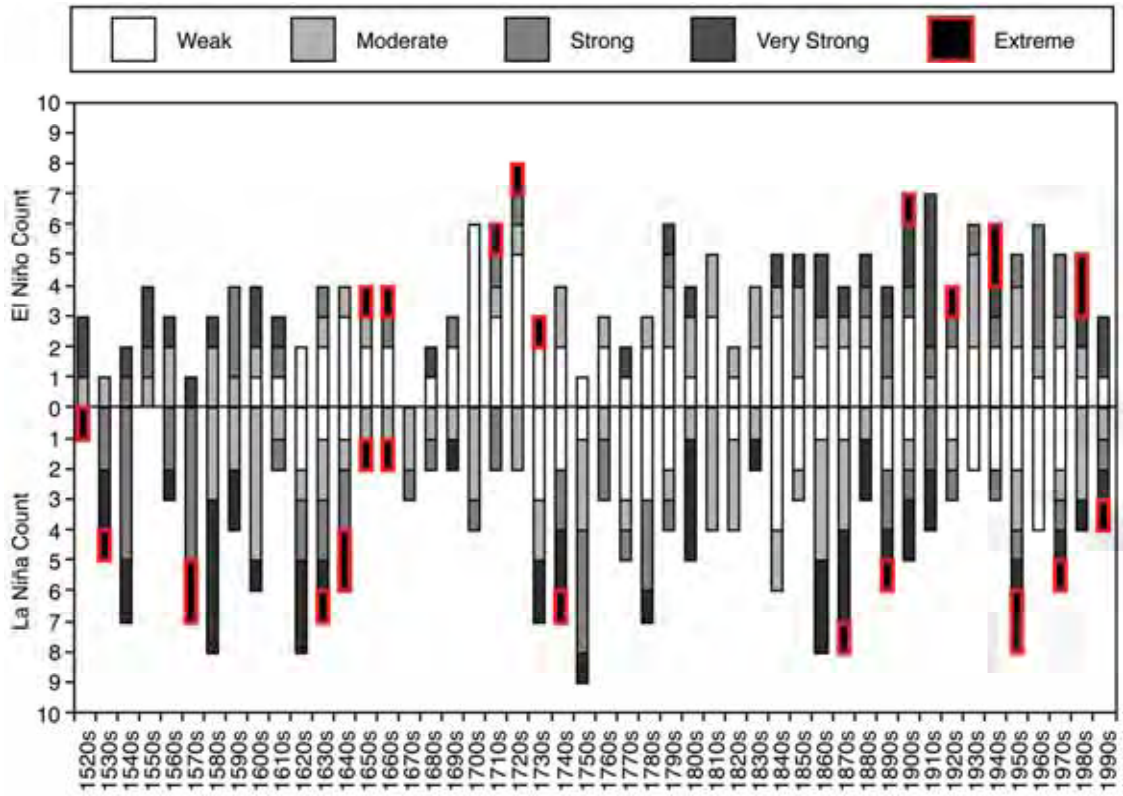

Figure 5.7. Decadal trends in reconstructed El Niño and La Niña event magnitude characteristics, A.D. 1525-2000. Five percentile classes were used to classify ENSO magnitude into extreme (>90th percentile) very strong (70th - 90th percentile), strong (50th - 70th), moderate (50th - 30th) and weak events (<30th).

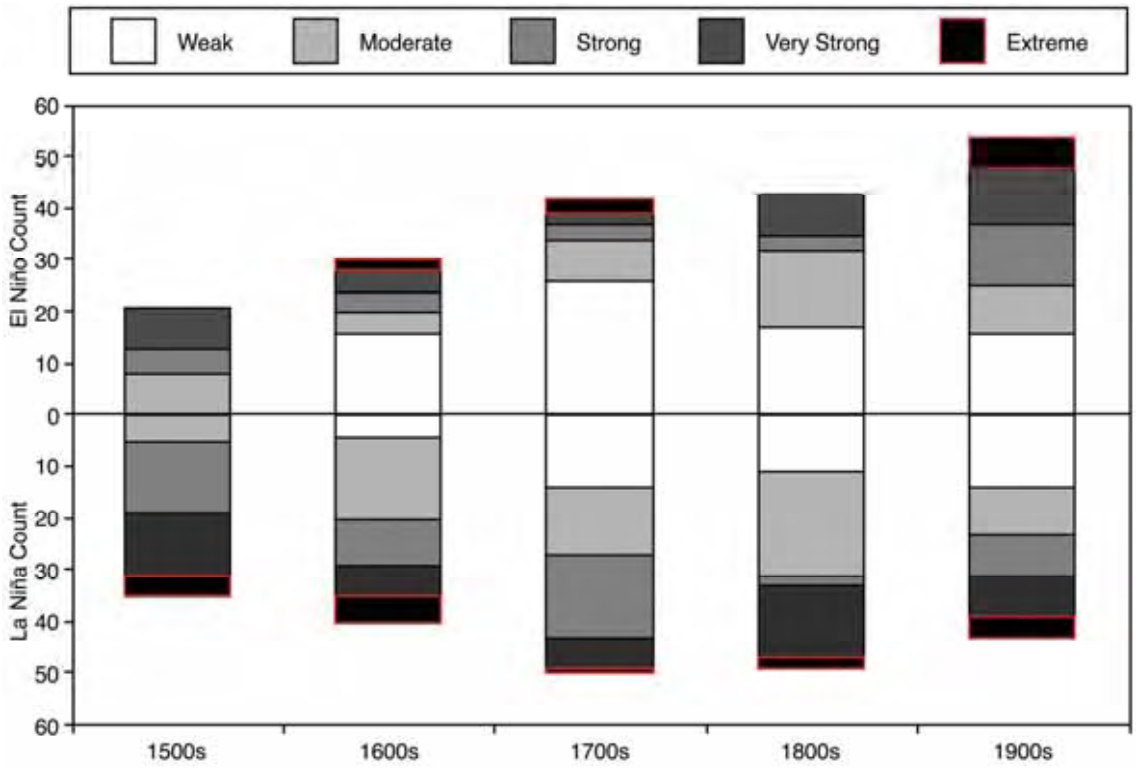

Figure 5.8. Centennial trends in ENSO episodes reconstructed for A.D. 1525-2002. Five percentile classes were used to classify ENSO magnitude into extreme (>90th percentile) very strong (70th - 90th percentile), strong (50th - 70th), moderate (50th - 30th) and weak events (<30th).

A period of relative El Niño inactivity is observed from the 1670s to 1780s, including one decade (1670s) where no El Niño years were reconstructed. From the 1700s to the 1720s, events appear to have generally lasted longer than events in the instrumental period but were mostly weak to moderate in strength (see Table 5.8). An exception to this general trend occurred during the 1720s when 80% of the decade experienced persistent El Niño conditions. El Niño occurrence and duration is notably reduced from the 1730s to 1780s event, with the exception of the extreme event noted during the 1730s.

The number of strong, very strong and extreme El Niños increased in the mid 19th century. Interestingly, approximately 42% of all very strong event years in the 478-year reconstruction occur within the instrumental (post-1870) period. The highest proportion of reconstructed El Niño years outside of the 18th century is reached during the 1900s and 1910s when 70% of each of these decades appear to have been characterised by persistent El Niño conditions; 57% and 86% of which fell within strong-extreme magnitude categories, respectively. Two decades, the 1940s and 1980s,

have the highest proportion of extreme event years in the reconstruction, where at least 50% of the El Niño years were extreme. Overall, 55% of extreme El Niños reconstructed since A.D. 1525 occur within the 20th century (1900s, 1920s, 1940s, 1980s). In addition, 43% (32%) of the El Niño events reconstructed for the 20th century are classed as strong-very strong (very strong-extreme), underscoring enhanced El Niño activity during the 20th century (Figure 5.8).

The 16th to mid 17th centuries stands out as the most sustained period of La Niña activity, with the exception of the 1550s for which no reconstructed La Niña conditions were reconstructed (Figure 5.7). During the 1520s, 1530s, 1570s and 1630s-1660s, nine extreme La Niña event years occur, representing 56% of all extreme event years in the entire La Niña reconstruction. Notably, from the 1650s to the 1720s, there is a general reduction of La Niña activity, with three decades (1650s, 1660s, 1690s) displaying extreme or strong event years, suggesting a low frequency but relatively high magnitude of events during this period. From the 1720s, a period of increased La Niña activity is observed through to the 20th century. The majority of these event years are, however, weak-moderate in nature. The maximum proportion of La Niña conditions for the entire record is noted during the 1750s when an overwhelming 90% of the decade was dominated by La Niña conditions.

A period of notable La Niña activity was reached during the 19th century when 53% of the century was characterised by La Niña conditions. The 1860s and 1870s are the only two decades that persistently expressed La Niña conditions consecutively 80% of the time. Similarly, for six consecutive decades (1860s-1910s), very strong-extreme La Niñas are noted. The late 19th century to the end of 20th century is characterised by an increase in the proportion of strong, very strong and, notably, extreme La Niña events (1870s, 1890s, 1950s, 1970s, 1990s), a trend also observed in the El Niño reconstruction. In fact, 26% of the 19th and 30% of the 20th centuries were classed as very strong-extreme (Figure 5.8).

However, between the 1920s-1960s, there is an overall reduction in the frequency of La Niñas, associated with a period of less frequent, but extreme El Niño events. The notable exception is the 1950s, when very strong or extreme event years were observed. Following weak conditions during the 1960s (a period dominated by strong El Niño conditions), the period spanning the 1970s-1990s, represents three consecutive decades when very strong to extreme events La Niña years were observed.

Overall there has been a general increase in the number of ENSO years reconstructed from this multiproxy study. For example, during the 1500s, a total of 21 El Niño years were reconstructed compared to over 54 during the 20th century. Peak La Niña frequency is observed during the 18th and 19th centuries when approximately 50 La Niña years were reconstructed, falling to 43 by the 20th century. Strikingly, 43% of all extreme ENSO events reconstructed since A.D. 1525 occurred post-1900.

5.10.2 Protracted ENSO episodes

To investigate the frequency of protracted ENSO episodes through time, all events listed in Table 5.8 exceeding three years were listed in Table 5.9. A total of 24 (26) protracted El Niño (La Niña) events since A.D. 1525 are noted from the reconstruction presented here. Of all protracted ENSO events, 28% occur in the 20th century, recognised as a period characterised by a high number of extreme events. The longest La Niña spanned 11 years occurs between A.D. 1622-1632, while a maximum duration of seven years is seen twice in the El Niño reconstruction (A.D. 1900-1906 and A.D. 1718-1724).

Interestingly, more events are reconstructed here than the 23 (17) protracted El Niño (La Niña) events identified between A.D. 1706-1977 by Allan and D'Arrigo (1999). This may reflect the shorter length of the time series, decoupled and lead or lag signatures maintained in the calibration process (detailed in Section 5.5), or indeed, over-reconstruction. Nevertheless, there is good agreement of the timing of the events shared by Table 5.9 and Allan and D'Arrigo (1999) in both instrumental and pre-instrumental times. This may suggest that the results also represent true differences between SOI event signatures compared to the combined ocean-atmosphere ENSO signals captured by the CEI.

Table 5.9. Protracted CEI ENSO events since A.D. 1525, Following Allan and D'Arrigo (1999), a protracted event is defined as persisting for three years or more.

Reconstructed Protracted events	***Duration (Years)***	***Reconstructed Protracted events***	***Duration (Years)***
El Niño events			
1964-1969	6	1791-1794	4
1957-1959	3	1782-1784	3
1937-1942	6	1768-1771	4
1924-1926	3	1746-1748	3
1918-1920	3	1718-1724	7
1911-1915	5	1712-1714	3
1900-1906	7	1659-1661	3
1876-1878	3	1650-1652	3
1864-1866	3	1618-1621	4
1856-1858	3	1607-1609	3
1844-1848	5	1585-1583	3
1814-1817	4	1525-1527	3
		Total	24
La Niña events			
1988-1990	3	1808-1811	4
1984-1986	3	1785-1790	6
1970-1975	6	1778-1780	3
1955-1960	6	1750-1758	9
1921-1923	3	1739-1743	5
1916-1918	3	1730-1733	4
1907-1910	4	1637-1639	3
1890-1894	5	1622-1632	11
1878-1880	3	1600-1605	6
1870-1875	6	1576-1581	6
1866-1868	3	1571-1573	3
1860-1864	5	1540-1542	3
1847-1851	5	1531-1533	3
		Total	26

5.11 Discussion

To calibrate single proxy records to instrumental ENSO conditions, the signal to noise ratio used to assess proxy skill was essentially arbitrary. Due to the replication inherent in multiproxy analysis, maximising the event capture at the single proxy level was desired, as false positives are likely to be 'lost' from the larger multiproxy environment as the likelihood of false positives occurring simultaneously in many locations is expected to be low.

The lower confidence levels noted for the La Niña phase reconstruction may be related to the overall lower number of highly La Niña sensitive proxies listed in Table 5.2. To compensate for the scarcity of La Niña proxies available for ENSO reconstruction, three slightly less skilful La Niña proxies were used (D'Arrigo Teak (0.6), Great Barrier Reef (0.65) and New Caledonia (0.64) to match the number of records used for the El Niño phase reconstruction. This inclusion may explain the higher number of false positive cases noted in Table 5.4 for the La Niña reconstruction.

Interestingly, the tree-ring records appear to have stronger ENSO sensitivity than the other proxy records used in this study. For example, the Mexican Douglas Fir and the Berlage Teak tree-ring records appear in the top five of both ENSO sensitivity tables, suggesting their importance in reconstructive work. This may reflect the exact dating of tree-ring chronologies which results from rigorous replication inherent to crossmatching and chronology development that helps enhance any climate signal and minimise noise.

For the purpose of this multiproxy analysis, the dating of coral records were sourced from the primary literature describing the data. As such, no attempt was made to adjust age models provided by the scientists who contributed the proxy data. It is possible that the weaker sensitivities found in coral sequences is a consequence of dating issues and/or non-stationary trends reported elsewhere (Gagan *et al.*, 2000; Hendy *et al.*, 2003; Linsley *et al.*, 2004; Lough, 2004). Until improved replication within each regional coral record becomes commonplace (e.g. Hendy *et al.*, 2003), perhaps more emphasis should be placed on the more exactly dated tree-ring proxy records using a non-equally weighted scheme when reconstructing ENSO in a multiproxy context.

The high overall proxy performance observed for the Quelccaya ice record (Table 5.2) suggests dating and/or stationarity issues are not as problematic as noted for coral.

These results support the favourable assessment of the Quelccaya record for use in annual and decadal climate analysis undertaken by Bradley (1996), suggesting that imposing strict seasonal windows for reconstruction (e.g. Stahle *et al.*, 1998) may exclude important proxy records. This result suggests other available, high quality tropical ice cores should be examined for any ENSO-sensitivity and incorporated into future multiproxy analyses (Thompson, 2000; Thompson *et al.*, 2000; Thompson *et al.*, 2002). The high performance noted for the Quinn and Indian documentary records may reflect their listing of fewer, discrete events rather than being a continuous time series, which probably accounts for the low false positive cases listed in Table 5.2.

To address the lack of precisely dated, equatorial proxies and a diminishing number of proxy records through time, no geographical equal weighting was applied to proxies from core/teleconnection and east/west Pacific proxies. As previously stated, ideally climatically sensitive proxies from the equatorial Pacific centres of action of ENSO would be used to reconstruct core characteristics of ENSO, and all remaining annual resolution proxies could then be used to map the spatial anomaly patterns of tropical and extra-tropical teleconnections associated with each reconstructed ENSO event (Stahle *et al.*, 1998). However the lack of long, proxy data availability from the tropics currently precludes this.

Since ENSO teleconnection patterns can fluctuate considerably, it must be acknowledged that reconstructions based on more peripheral teleconnection sites may not be as stable through time, as observed in Section 5.8.2. Nevertheless, the degraded subset analysis importantly reflects the internal robustness of the multiproxy chronology analysed here. This supports the conclusion of Bradley (1996:617) that "it is clear that excellent reconstructions of the global mean (temperature) series can be obtained with only a limited number of judiciously selected data points". Indeed, this may also be true of proxies used for ENSO reconstruction, again supporting the use of a multiproxy approach to ENSO reconstruction.

Interestingly, the subsets of records present at A.D. 1525 were based on proxies from teleconnection (e.g. New Zealand, Mexico and the USA) rather than core ENSO localities. This suggests that *in lieu* of well-replicated, exactly dated equatorial proxies, robust chronologies from key teleconnections still remain our strongest evidence of past ENSO behaviour (Stahle *et al.*, 1998). It is acknowledged that further investigation into the differences in eastern/western Pacific teleconnection stationarities and event

propagation characteristics is warranted, however this was beyond the scope of the primary intention of developing multiproxy event lists for both ENSO phases.

Verification consistent with the approaches of Whetton and Rutherfurd (1994) and Allan and D'Arrigo (1999) revealed that a three-proxy minimum for event definition compared well with the two primary long-term ENSO event lists of QO00 and WR94. This study provides substantial replication of the events reported by previous research and introduces the first substantial La Niña event lists back to A.D. 1525.

Although there is more uncertainty associated with the reconstruction due to fewer La Niña sensitive proxies, considerable skill is still achieved as noted in Section 5.9. Notably, the duration of La Niña events in the reconstructions were found to be greater than their El Niño counterparts. This is most conspicuous in the case of the mid to late 18th century when eight La Niñas are recorded by the reconstruction, including a nine-year episode spanning A.D. 1750-1758. This compares to a maximum duration of an eight-year El Niño event spanning A.D. 1899-1906. Indeed if the trends reported here are considered to be reliable, it may signify important differences in the nature of El Niño and La Niña events.

The results presented here are in general agreement with the conclusion of Allan and D'Arrigo (1999) that 'persistent' ENSO event sequences have occurred prior to the period of instrumentally based indices, and that the 1990-1995 El Niño event is not unprecedented from the context of the past 478 years. It is, however, noteworthy that 28% of all protracted ENSO events also occur in 20th century. Allan (2000) suggested that the existence of protracted ENSO events may be due to the phasing of high frequency (quasi-biennial) ~2 year activity with the 'classical' 3-7 year (lower frequency) ENSO variability. An investigation of the long-term changes in the periodicities of ENSO activity since A.D. 1525 is provided in Chapter 6.

Quinn and Neal (1992) identified periods of apparently anomalous long-term El Niño behaviour from their South American reconstruction. These near-decadal or longer periods include A.D. 1539-1578, 1600-1624, 1701-1728, 1792-1802, 1812-1832, 1864-1891, 1897-1919, 1925-1932 and 1976-1987. Jones and Bradley (1992) recommended that these intervals should be the focus of future research to determine the larger scale significance of periods with above or below average ENSO frequency. Accordingly, these intervals were examined from our reconstruction to reveal similar

periods of high El Niño activity during 1525-1565, 1596-1635, 1712-1738, 1768-1807, 1812-1853, 1864-1891, 1896-1931, 1957-1976 and 1982-2002 where there is a considerable frequency of high magnitude episodes.

ENSO behaviour appears to have fluctuated significantly since A.D. 1525. A notable period of relative inactivity was identified between A.D. 1650-1780 when ENSO events were largely weak or moderate, coincident with the broadly defined Little Ice Age (~A.D. 1550-1850) (Lamb, 1982), but more specifically, the Maunder Minimum period of low solar variability (~A.D. 1645-1715) (Eddy, 1977; Reid, 1997). Whetton and Rutherfurd (1994) tentatively concluded that ENSO teleconnections were less active during the broadly defined LIA compared to the middle of the 19th century. They were, however, not confident that the data used in the early part of the record was sufficiently reliable. They stated, "until we have better evidence to the contrary, (El Niño and La Niña) events may be assumed to have occurred over recent centuries at something like the frequency and intensity observed over the instrumental period" (Whetton and Rutherfurd, 1994:249).

Having presented further evidence for the early period, this study suggests that ENSO has displayed considerably variability over the past five centuries. A prominent decrease (increase) in ENSO activity, is indeed coincident with the duration (termination) of the LIA. This finding is further supported by D'Arrigo *et al.* (2005) who presented evidence from North American of lowest ENSO variability over the past six centuries during this time.

The apparent height of extreme La Niña activity is noted during the 16th to mid 17th centuries, when 56% of all extreme La Niña years noted in the reconstruction occur. These trends, however, may reflect loss of sample depth for the early part of the record when only six La Niña sensitive records (compared to the eight El Niño proxies) are present. Since there is a reduction in the relative proportions of responsive proxies to available sample depth, there may be a slight amplification of magnitude noted here. Nonetheless, if the results noted here are representative of real trends in La Niña event magnitude, it may suggest that periods of more extreme La Niña events than have currently been witnessed could be expected in the future (Timmermann *et al.*, 1999).

Interestingly, the 20th century contains over 43% of all the extreme ENSO events noted in the multiple proxy reconstruction. Indeed, the post-1940 period alone accounts for

30% of these exceptional climate events. Despite efforts to adjust for proxy skill, it is acknowledged that event magnitude may be relatively underestimated at the tail ends of the time series due to the inevitable reduction in sample depth. However, it is worth noting that there are still eight (six) El Niño (La Niña) proxies used present in the reconstruction back to A.D. 1525.

Lack of proxy coverage noted late in the observational period (largely post-1990) is not as problematic, as higher quality, instrumental data becomes available for comparison in the content of the long-term proxy reconstruction. Of the extreme events noted by Gergis and Fowler (2005) in the instrumental CEI, 50% of all extreme ENSO events are observed post-1970, suggesting real climatic trends in the reconstruction rather than an artifactual construct of the methodology employed.

5.12 Summary

A number of ENSO-sensitive proxy records (tree-ring, coral, ice and documentary) were examined to isolate ENSO signals associated with both phases of the phenomenon. Regional signals were compared, revealing large-scale trends in the frequency, magnitude and duration of pre-instrumental ENSO using novel applications of percentile analysis. A number of threshold dependent ENSO reconstructions allowed late 20th century ENSO variability to be assessed from a multi-centennial perspective with various degrees of certainty. Clearly, multiproxy ENSO reconstruction is still in its infancy, and abundant potential remains to characterise teleconnection patterns, propagation signatures and non-stationarities of large-scale ENSO behaviour.

This study has expanded upon the ENSO event chronologies provided by previous researchers (e.g. Quinn and Neal (1992), Ortlieb (2000) and Whetton and Rutherfurd, 1994; 1996). Importantly there has been the addition of an extensive chronology of La Niña events, the identification of a variety of ENSO event magnitude classes and the introduction of multiple proxies from widespread geographical coverage spanning the West and East Pacific locations. This allowed the large-scale (rather than regional) spatial patterns for a variety of ENSO event magnitudes to be examined over the past five centuries. The chronology of pre-instrumental ENSO events provides an alternative to the Quinn records commonly used for calibration/verification chronology of past ENSO conditions for palaeo-environmental studies.

Analysis of the multiproxy reconstruction revealed considerable ENSO variability through time. Importantly, this study is consistent with the conclusions of D'Arrigo *et al.* (2005) concerning solar/temperature related modification of ENSO behaviour. Periods of inactivity were identified throughout the record. Most notably, during the 1600s ENSO appears to have weakened, coincident with the height of the commonly defined Little Ice Age and Maunder Minimum epochs.

The clearly anomalous nature of late 20th century ENSO is evident. The height of La Niña activity occurred during the 16th and 19th centuries, while the 20th century is identified as the peak period of El Niño activity. Although extreme ENSO events are seen throughout the 478-year ENSO reconstruction, approximately 43% of extreme, 20% of very strong and 28% of all protracted ENSO events reconstructed occur in the 20th century, suggesting the frequency with which they occurred during this period is anomalous in the context of the past five centuries. Of particular note, the post-1940 period alone accounts for 30% of extreme ENSO years noted since A.D. 1525. Given the considerable large-scale socio-economic impacts of ENSO events, future investigation into the implications of an increasingly anthropogenically-warmed world may have on ENSO behaviour is vital.

5.13 References

Allan, R. (2000). ENSO and climatic variability in the past 150 years. *El Niño and the Southern Oscillation: Multiscale Variability and Global and Regional Impacts.* H. Diaz and V. Markgraf. Cambridge, Cambridge University Press: 3-35.

Allan, R. and D'Arrigo, R. (1999). 'Persistent' ENSO sequences: how unusual was the 1990-1995 El Niño ? *The Holocene* **9** (1): 101-118.

Allan, R., Lindsay, J. and Parker, D. (1996). *El Niño Southern Oscillation and climate variability.* Melbourne, Australia, CSIRO.

Allan, R., Reason, C., Lindesay, J. and Ansell, T. (2003). Protracted ENSO episodes and their impacts in the Indian Ocean region. *Deep Sea Research Part II* **50** (12-13): 2331–2347.

Baumgartner, T., Michaelsen, J., Thompson, L., Shen, G., Soutar, A. and Casey, R. (1989). The recording of interannual climatic change by high-resolution natural systems: tree rings, coral bands, glacial ice layers and marine varves. *Aspects of Climate Variability in*

the Pacific and Western Americas. Geophysical Monograph. D. Peterson. Washington, American Geophysical Union. **55:** 1-14.

Bouma, M., Kovats, R., Goubet, S., Cox, J. and Haines, A. (1997). Global assessment of El Niño's disaster burden. *The Lancet* **350**: 1435-1438.

Bradley, R. (1996). Are there optimum sites for global paleotemperature reconstruction? *Climate Variations and Forcing Mechanisms of the Last 2000 years.* P. Jones, R. Bradley and J. Jouzel. Berlin, Springer-Verlag**:** 603-624.

Caviedes, C. (2001). *El Niño In History: Storming Throughout the Ages.* Gainesville, USA, University Press of Florida.

Chen, C., Mc Carl, B. and Adams, R. (2001). Economic Implications of Potential ENSO Frequency and Strength Shifts. *Climatic Change* **49**: 147–159,.

Cobb, K., Charles, C., Cheng, H. and Edwards, L. (2003). El Niño/Southern Oscillation and tropical Pacific climate during the last millennium. *Nature* **424**: 271-276.

Cole, J., Dunbar, R., Mc Clanahan, T. and Muthiga, N. (2000). Tropical Pacific forcing of decadal SST variability in the Western Indian Ocean over the past two centuries. *Science* **287** (5453): 617-619.

Crowley, T. (2000). Causes of Climate Change over the Past 1,000 years. *Science* **289**: 270-277.

D'Arrigo, R., Cook, E., Wilson, R., Allan, R. and Mann, M. (2005). On the variability of ENSO over the past six centuries. *Geophysical Research Letters* **32** (L03711): 1-4.

D'Arrigo, R., Jacoby, G. and Krusic, P. (1994). Progress in Dendroclimatic Studies in Indonesia. *Terrestrial, Atmospheric and Oceanographic Sciences* **5**: 349-363.

Deser, C. and Wallace, J. (1987). El Niño Events and Their Relation to the Southern Oscillation: 1925-1986. *Journal of Geophysical Research* **92** (C13): 14,189-14,196.

Diaz, H. and Markgraf, V. (2000). *El Niño and the Southern Oscillation; Multiscale Variability and Global and Regional Impacts.* Cambridge, Cambridge University Press.

Diaz, H. and Pulwarty, R. (1994). An analysis of the time scales of variability in centuries-long ENSO-sensitive records in the last 1000 years. *Climatic Change* **26**: 317–342.

Dunbar, R. and Cole, J. (1999). *Annual Records of Tropical Systems (ARTS); Recommendations for Research.* Geneva, Switzerland, IGBP Science Series.

Eddy, J. (1977). Climate and the changing sun. *Climatic Change* **1**: 173-190.

Fairbanks, R., Evans, M., Rubenstone, J., Mortlock, R., Broad, K., Moore, M. and Charles, C. (1997). Evaluation of climate indices and their geochemical proxies measured in corals. *Coral Reefs* **16** (Supplement): S93-S100.

Fedorov, A. and Philander, G. (2000). Is El Niño changing? *Science* **288**: 1997-2002.

Fenwick, P. (2003). Reconstruction of past climates using Pink Pine (*Halocarpus biformus*) tree-ring chronologies. Christchurch, New Zealand, Soil Plant and Ecological Sciences, Linclon University.

Folland, C., Karl, T., Christy, J., Clarke, R., Gruza, G., Jouzel, J., Mann, M., Oerlemans, J., Salinger, M. and Wang, S. (2001). Observed Climate Variability and Change. *Climate Change 2001: The Scientific Basis. Contribution of Working Group 1 to the Third Assessment Report of the Intergovernmental Panel on Climate Change.* J. Houghton, Y. Ding, D. Griggs *et al.* United Kingdom and New York, Cambridge University Press.

Fowler, A. and Boswijk, G. (2003). Chronology stripping as a tool for enhancing the statistical quality of tree-ring chronologies. *Tree Ring Research* **59** (2): 53-62.

Fowler, A., Boswijk, G. and Ogden, J. (2004). Tree-ring studies on Agathis australis (Kauri): a synthesis of development work on Late Holocene chronologies. *Tree Ring Research* **60** (1): 15-29.

Gagan, M., Ayliffe, L., Beck, J., Cole, J., Druffel, E., Dunbar, R. and Schrag, D. (2000). New views of tropical palaeoclimates from corals. *Quaternary Science Reviews* **19**: 45-64.

Gedalof, Z. and Mantua, N. (2002). A multi-century perspective of variability in the Pacific Decadal Oscillation: new insights from tree rings and coral. *Geophysical Research Letters* **29** (24): 57/1-57/3.

Gergis, J. and Fowler, A. (2005). Classification of synchronous oceanic and atmospheric El Niño-Southern Oscillation (ENSO) events for palaeoclimate reconstruction. *International Journal of Climatology* **25**: 1541–1565.

Glantz, M. (1996). *Currents of Change: El Niño's Impact on Climate and Society.* Cambridge University Press,

Grove, R. and Chappell, J. (2000). El Niño chronology and the history of global crises during the Little Ice Age. *El Niño- History and Crisis*. R. Grove and J. Chappell. Cambridge, The White Horse Press: 5-34.

Hanley, D., Bourassa, M., O'Brian, J., Smith, S. and Spade, E. (2003). A Quantitative Evaluation of ENSO Indices. *Journal of Climate* **16**: 1249-1258.

Hendy, E., Gagan, M. and Lough, J. (2003). Chronological control of coral records using luminescent lines and evidence for non-stationarity ENSO teleconnections in north-eastern Australia. *The Holocene* **13** (2): 187-199.

Jones, P. and Mann, M. (2004). Climate over past millennia. *Review of Geophysics* **42**: 1-42.

Kiladis, G. and Diaz, H. (1989). Global climatic anomalies associated with extremes in the Southern Oscillation. *Journal of Climate* **2**: 1069-1090.

Kumar, A. and Hoerling, M. (1997). Interpretation and Implications of the Observed Inter-El Niño Variability. *Journal of Climate* **10**: 83-91.

Lamb, S. (1982). *Climate, History and the Modern World.* London, Routledge.

Linsley, B., Wellington, G., Schrag, D., Ren, L., Salinger, J. and Tudhope, A. (2004). Geochemical evidence from corals for changes in the amplitude and spatial pattern of South Pacific interdecadal climate variability over the last 300 years. *Climate Dynamics* **22**: 1-11.

Lough, J. (2004). A strategy to improve the contribution of coral data to high-resolution palaeoclimatology. *Palaeogeography, Palaeoclimatology, Palaeoecology* **204**: 115-143.

Lyon, B. and Barnston, A. (2005). The evolution of the weak El Niño of 2004-2005. *US CLIVAR Variations* **3** (2): 1-4.

Mann, M. (2003). On Past Temperatures and Anomalous Late-20th Century Warmth. *Eos* **84** (27): 1-3.

Mann, M., Bradley, R. and Hughes, M. (2000). Long-term variability in the El Niño/Southern Oscillation and associated teleconnections. *El Niño and the Southern Oscillation; Multiscale Variability and Global and Regional Impacts.* H. Diaz, and Markgraf, V. Cambridge, Cambridge University Press: 327-372.

Moberg, A., Sonechkin, D., Holmgren, K., Datsenko, N. and Karlen, W. (2005). Highly variable Northern Hemisphere temperature reconstructed from low and high resolution proxy data. *Nature* **433**: 613-617.

Mullan, A. (1995). On the linearity and stability of Southern Oscillation-climate relationships for New Zealand. *International Journal of Climatology* **15**: 1365-1386.

Murphy, J. and Whetton, P. (1989). A re-analysis of a tree-ring chronology from Java. *Proceedings of the Koninklijke Nederlandse Akademie van Wetenschappen (Dendrochronology)* **Proceedings B 92** (3): 241-257.

Ortlieb, L. (2000). The documentary historical record of El Niño events in Peru: An update of the Quinn record (sixteenth through nineteenth centuries). *El Niño and the Southern Oscillation: Variability, Global and Regional Impacts.* H. Diaz and V. Markgraf. Cambridge, Cambridge University Press: 207-295.

Ortlieb, L. and Macharé, J. (1993). Former El Niño events: records from western South America. *Global and Planetary Change* **7**: 181–202.

Quinn, W. (1992). A study of Southern Oscillation-related climate activity for A.D. 622-1900 incorporating Nile River flood data. *El Niño: Historical and Palaeoclimatic Aspects of the Southern Oscillation.* H. Diaz, and Markgraf, V. Cambridge, Cambridge University Press.: 119-149.

Quinn, W. and Neal, V. (1992). The historical record of El Niño events. *Climate Since A.D. 1500.* R. Bradley and P. Jones. London, Routledge.: 623–648.

Quinn, W., Neal, V. and Antunez de Mayola, S. (1987). El Niño occurrences over the past four and a half centuries. *Journal of Geophysical Research* **92** (C13): 14449–14461.

Quinn, W., Zopf, D., Short, K. and Yang, R. (1978). Historical trends and statistics of the southern oscillation, El Niño and Indonesian droughts. *Fishery Bulletin* **76** (3): 663-678.

Rasmusson, E. and Carpenter, T. (1982). Variations in tropical sea surface temperature and surface wind fields associated with the Southern Oscillation/El Niño. *Monthly Weather Review* **110**: 354-384.

Rasmusson, E. and Carpenter, T. (1983). The relationship between eastern equatorial Pacific sea surface temperatures and rainfall over India and Sri Lanka. *Monthly Weather Review* **111**: 517-528.

Reid, G. (1997). Solar forcing of global climate change since the mid 17th century. *Climatic Change* **37**: 391-405.

Stahle, D., D'Arrigo, R., Krusic, P., Cleaveland, M., Cook, E., Allan, R., Cole, J., Dunbar, R., Therrell, M., Gay, D., Moore, M., Stokes, M., Burns, B., Villanueva-Diaz, J. and Thompson, L. (1998). Experimental dendroclimatic reconstruction of the Southern Oscillation. *Bulletin of the American Meteorological Society* **79** (10): 2137-2152.

Thompson, L. (2000). Ice core evidence for climate change in the Tropics: Implications for our future. *Quaternary Science Reviews* **19**: 19-35.

Thompson, L., Mosley-Thompson, E., Davis, M., Henderson, K., Brecher, H., Zagorodnov, V., Mashiotta, T., Lin, P., Mikhalenko, V., Hardy, D. and Beer, J. (2002). Kilimanjaro

ice core records: evidence of Holocene climate change in tropical Africa. *Science* **298**: 589-593.

Thompson, L., Mosley-Thompson, E. and Henderson, K. (2000). Ice-core palaeoclimate records in tropical South America since the Last Glacial Maximum. *Journal of Quaternary Science* **15** (4): 377-394.

Timmermann, A., Oberhuber, J., Bacher, A., Esch, M., Latif, M. and Roeckner, E. (1999). Increased El Niño frequency in a climate model forced by future greenhouse warming. *Nature* **398**: 694-697.

Trenberth, K. (1997). The Definition of El Niño. *Bulletin of the American Meteorological Society* **78** (12): 2771-2777.

Trenberth, K. and Hoar, T. (1996). The 1990-1995 El Niño Southern Oscillation event: Longest on Record. *Geophysical Research Letters* **23** (1): 57-60.

Trenberth, K. and Hoar, T. (1997). El Niño and climate change. *Geophysical Research Letters* **24** (23): 3057-3060.

Trenberth, K. and Stepaniak, D. (2001). Indices of El Niño evolution. *Journal of Climate* **14**: 1697-1701.

Urban, F., Cole, J. and Overpeck, J. (2000). Influence of mean climate change on climate variability from a 155-year tropical Pacific coral record. *Nature* **407**: 989-993.

Von Storch, H., Zorita, E., Jones, J., Dimitriev, Y., Gonzalez-Rouco, F. and Tett, S. (2004). Reconstructing Past Climate from Noisy Data. *Nature* **306**: 679-682.

Whetton, P., Allan, R. and Rutherfurd, I. (1996). Historical ENSO teleconnections in the Eastern Hemisphere: comparisons with latest El Niño series of Quinn. *Climatic Change* **32**: 103-109.

Whetton, P. and Rutherfurd, I. (1994). Historical ENSO teleconnections in the Eastern Hemisphere. *Climatic Change* **28**: 221-253.

CHAPTER 6. RECONSTRUCTING ENSO INDICES

6.1 Introduction

Reconstructions of past climate are unique in their ability to provide a long-term, historical context for evaluating the nature of 20th century climate change. Chapter 1 highlighted the significant advances that have been made in the reconstruction of mean hemispheric and global temperatures of the past five centuries (Mann *et al.*, 1998; Crowley, 2000; Folland *et al.*, 2001; Jones and Mann, 2004; Moberg *et al.*, 2005). Surprisingly, however, despite being the primary mode of global climate variability operating in 2-7 year time scales (Folland *et al.*, 2001), the long-term context of apparently anomalous ENSO behaviour witnessed in recent decades has received relatively little attention (Trenberth and Hoar, 1996; Trenberth and Hoar, 1997; Crowley, 2000; Mann *et al.*, 2000a; Folland *et al.*, 2001; Mann, 2003).

High quality ENSO reconstructions would enable extremes such as the 1982-83, 1997-98 and 1990-95 El Niño events to be placed within a longer-term perspective (Allan and D'Arrigo, 1999; Mann *et al.*, 2000a;Allan *et al.*, 2003). From such a position, climate scientists should be better able to assess whether or not these seemingly anomalous events represent significant and potentially anthropogenic-forced climate change (Trenberth and Hoar, 1996; Trenberth and Hoar, 1997; Mann *et al.*, 2000a; Folland *et al.*, 2001).

Such reconstructions are based on various proxy indicators with an identified sensitivity to atmospheric and/or oceanic teleconnections of ENSO variability. A common approach to the reconstruction of past climates involves Principal Component Analysis (PCA), or the equivalent Empirical Orthogonal Function (EOF) techniques (Jolliffe, 1986; Von Storch and Zwiers, 1999). PCA is a multivariate analysis method used to derive the dominant modes of variability contained within a set of proxy data (Jolliffe, 1986; Stahle *et al.*, 1998; Mann *et al.*, 2000a). This technique makes it possible to represent very large fields of data in just a few spatial patterns and their time varying

amplitudes. More formally, it is a linear transformation that chooses a new coordinate system for the data set such that the greatest variance by any projection of the data set comes to lie on the first axis (then called the first principal component), the second greatest variance on the second axis, and so on (Jolliffe, 1986; Von Storch and Zwiers, 1999).

Principal components are the uncorrelated, linear combinations of a set of variables that represent the largest fraction of the variance of the data for any combination of these variables, with the dominant modes represented by the leading principal components (Jolliffe, 1986; Von Storch and Zwiers, 1999). Since PCA is concerned with identifying patterns of simultaneous variation, it is of interest to know how each of the elements varies in time in relation to every other element. This is achieved by calculating a correlation matrix or the covariance matrix (Jolliffe, 1986; Von Storch and Zwiers, 1999). Correlation-based PCA represents the variations of the normalised data and are useful for showing relationships between variables with very different variances, while covariance-based PCA represent the dominant modes of the actual data (Jolliffe, 1986; Von Storch and Zwiers, 1999).

The amount of variance explained by each principal component (or mode of variability) is represented as a fraction of one. In addition it is possible to calculate a PC score or amplitude of the principal component at each time, allowing the strength of the coherent pattern of variability at each point in time to be investigated (Jolliffe, 1986; Von Storch and Zwiers, 1999). Finally, the pattern and amplitude of variability can potentially be related to physical process such as those associated with ENSO.

Effectively, the use of PCA reduces the noise associated with various proxies, minimising differences associated with the seasonality and duration of regional ENSO teleconnection signatures (Stahle *et al.*, 1998; Mann *et al.*, 2000a). Variables used to reconstruct ENSO are produced from the multiproxy data by first decomposing the data into principle components (PC). The associated time series (PC scores) is a simple, least squares multiple linear regression model that relates variability in the palaeoclimate data with instrumental ENSO indices (Von Storch and Zwiers, 1999).

To date, only a limited number of multiproxy reconstructions of ENSO for the past few centuries have been attempted. The intention of this Chapter is to provide an overview of the PCA-based ENSO reconstructions currently available and some background into

the problems associated with the reconstruction of palaeo ENSO. A number of new reconstructions of seasonal SOI, Niño 3.4 SST and CEI are also presented for comparison against existing global and regional multiproxy ENSO reconstructions.

Unlike previous studies, this Chapter seeks to reconstruct all seasons using three ENSO indices (SOI, Niño 3.4 SST, CEI) calibrated to an expanded set of proxy indicators from the western Pacific locations. Increasing the spatial coverage of high quality ENSO proxies is vital to reduce uncertainties associated with reconstruction. Comparisons of reconstructions calibrated to the coupled ocean-atmosphere ENSO index of Gergis and Fowler (2005) are made with previous studies based on one seasonal window of the SOI or SSTs alone. In an analysis of instrumental ENSO, Gergis and Fowler (2005) demonstrated that the identification of ENSO events was dependent upon the index employed, with Niño 3.4 SSTs recording more episodes than the SOI alone, regardless of the threshold that was imposed on the SOI. Consequently, differences in atmospheric, oceanic and coupled reconstructions of ENSO are discussed. Finally, assessments of changes in the nature of ENSO variability and the stability of regional ENSO teleconnections since A.D. 1525 are presented.

6.1.1 SOI reconstruction

Expanding on early studies demonstrating the potential of tree-rings for resolving ENSO (Lough and Fritts, 1985; D'Arrigo and Jacoby, 1991; Cleaveland *et al.*, 1992; D'Arrigo *et al.*, 1994) Stahle *et al.* (1998) were the first to use extensive tree-ring data from south-western USA, Mexico and Indonesia to experimentally reconstruct the Southern Oscillation (hereafter referred to as 'ST98'). Currently, these exactly dated tree-ring chronologies from ENSO-sensitive regions in subtropical North America and Indonesia are considered to register the strongest ENSO signal yet detected in tree-ring data worldwide (Stahle *et al.*, 1998).

Selected annual-resolution coral and ice core records available from the equatorial Pacific were also used to develop reconstructions of the December-February SOI (Stahle *et al.*, 1998). However, the coral and ice core data available for the analysis were found to be either relatively short (< 130 years) or were not well correlated with the particular seasonal index of the SO that was most consistent with the tree-ring data (Stahle *et al.*, 1998). As a result, Stahle *et al.* (1998) based their experimental reconstruction of December-January-February (DJF) SOI from A.D. 1706-1977, solely

on the tree-ring data and reserved the coral and ice core proxies for comparison with the tree-ring estimates of past ENSO variability.

Seasonalised DJF SOI data was chosen to represent the season in which ENSO events are typically mature in the equatorial Pacific (Rasmusson and Carpenter, 1982; Kiladis and Diaz, 1989; Allan *et al.*, 1996; Stahle *et al.*, 1998). The reconstruction explained 53% of the variance in the instrumental DJF SOI and was verified by comparisons with independent instrumental SOI and SST data (Stahle *et al.*, 1998). The results tentatively suggested that the ENSO variance might have increased from the 19th to 20th century. The analysis also indicated a small increase in the atmospheric pressure gradient across the Pacific during the period A.D. 1879-1977, suggestive of more positive DJF SOI and more frequent La Niñas, compared with the A.D. 1706–1878 time period (Stahle *et al.*, 1998).

Importantly, Stahle *et al.* (1998) highlighted the fact that the network of ENSO-sensitive proxies is indeed still in its infancy, hindering substantial advancements in ENSO reconstruction. For example, they recognised that longer coral records from the tropical Pacific and additional tree-ring chronologies from the western tropical Pacific would substantially improve on tree-ring reconstructions of the SOI (Stahle *et al.*, 1998). They proposed that ideally, exactly dated and climatically sensitive proxies from the equatorial Pacific centres of action of ENSO should be used to reconstruct the characteristics of ENSO, and all remaining annual resolution proxies could then be used to map the spatial anomaly patterns of tropical and extra tropical climate associated with each reconstructed ENSO events (Stahle *et al.*, 1998).

Clearly, this ideal approach is hardly possible even for the 20th century due to the poor spatial coverage of instrumental data, particularly over the oceans, and the limited network of exactly dated annually resolved palaeoclimate proxies currently available (see Chapter 3) (Stahle *et al.*, 1998). The reconstruction of tropical ENSO variability and the associated extra tropical climate impact is further complicated by the fact that climate proxies are not uniformly accurate in recording their local climate or oceanographic environment, and the sometimes brief seasonal response of even the most sensitive proxies may not perfectly coincide with the seasonality of the local ENSO teleconnection.

Nevertheless, Stahle *et al.* (1998) stressed that the available tree-ring data from sub-tropical North America and Java demonstrated a temporal and spatial ENSO signal and strongly justified the further development of annual palaeoclimatic proxies of the ENSO system (Stahle *et al.*, 1998). They concluded that if these reconstructed 19-20th century changes in reconstructed DJF SOI are substantiated by further studies, they will have important implications to the long-term dynamics of ENSO and its associated climate teleconnections (Stahle *et al.*, 1998).

6.1.2 Niño 3 SST reconstruction

Using a 'tropical' subset of the Mann *et al.* (1998) multiproxy database, a reconstruction of October to March Niño 3 SSTs for the period A.D. 1650-1980 was developed by Mann *et al.* (2000a) and Mann *et al.* (2000b). Approximately 20 distinct tropical or subtropical sites were used to reconstruct the specific tropical Pacific El Niño signal (Mann *et al.*, 2000a; Mann *et al.*, 2000b). This is hereafter referred to as the'MBH00' reconstruction.

Unlike the ST98 reconstruction, descriptions of low-frequency changes in the mean state were maintained. Additionally, changes in the amplitude of inter-annual variability, ENSO extremes and trends in the global pattern of ENSO variability were reported (Mann *et al.*, 2000a; Mann *et al.*, 2000b). Certain ENSO-related patterns such as enhanced inter-decadal variance appear to have exhibited significant trends during the 20th century, however, Mann *et al.* (2000a; 2000b) suggest that typical ENSO indices show only modest warming trends in comparison with the dramatic warming trend in hemispheric and global temperature during the past century (Mann *et al.*, 2000a). Nonetheless, some indication of a pattern associated with negative tropical feedbacks dampening an El Niño-like warming trend in the tropical Pacific were identified (Mann *et al.*, 2000a).

Mann *et al.* (2000a; 2000b) also found evidence of changes in the amplitude of inter-annual ENSO variability, global teleconnections of ENSO and the amplitude and frequency of extreme events (Mann *et al.*, 2000b). As is apparent from Figure 6.1, the incidence of large warm and cold events appears to have increased during the past century (Mann *et al.*, 2000a). The apparent breakdown of inter-annual ENSO variability during the 19th century appears to have had significant impact on the

incidence of extremes and on global teleconnection patterns of ENSO during that period (Mann *et al.*, 2000a).

MBH00 provides evidence supporting the hypothesis that this breakdown may have been associated with the same external forcing that led to generally cold global temperatures during the 19th century. This period may thus provide an analogue for the behaviour of ENSO and the possible breakdown of typical mechanisms of ENSO variability under the impacts of external and anthropogenic forcing of climate (Mann *et al.*, 2000a). Once again, they recognised that as increasingly rich networks of high quality, seasonally resolved proxy data become available, both global temperature and ENSO reconstructions should be possible with considerably reduced uncertainties (Mann *et al.*, 2000a). In particular, the increased availability of well-dated coral isotopic indicators in the tropical Pacific were identified as being especially useful for ENSO-scale reconstruction in the future.

Most recently, using an expanded and updated version of the Stahle *et al.* (1998) data, D'Arrigo *et al.* (2005) reconstructed December to February Niño 3 SSTs . Following the protocol of D'Arrigo *et al.* (2005), it is hereafter referred to as the 'Cook05' reconstruction. A total of 175 chronologies from the south-western USA and Mexico were screened as potential predictors (lags t-1; t+1) of the instrumental Niño-3 data in principal component regression (D'Arrigo *et al.*, 2005). Both the tree-ring and instrumental data were prewhitened using autoregressive modeling, with instrumental persistence added back in to the reconstruction.

Essentially, prewhitening removes all annual periodicities (such as biological growth factors) that may otherwise dominate the spectrum and impair its fidelity at other frequencies (Gilman *et al.*, 1963). This is by fitting Autoregressive-moving average (ARMA) techniques which are mathematical models designed to identify persistence, or autocorrelation, in a time series (Chatfield, 1975). A subset of ARMA models is the autoregressive or AR models which express a time series as a linear function of its past values plus a noise term (Chatfield, 1975). The order of the AR model indicates how many lagged past values are included (see Section 6.4.1).

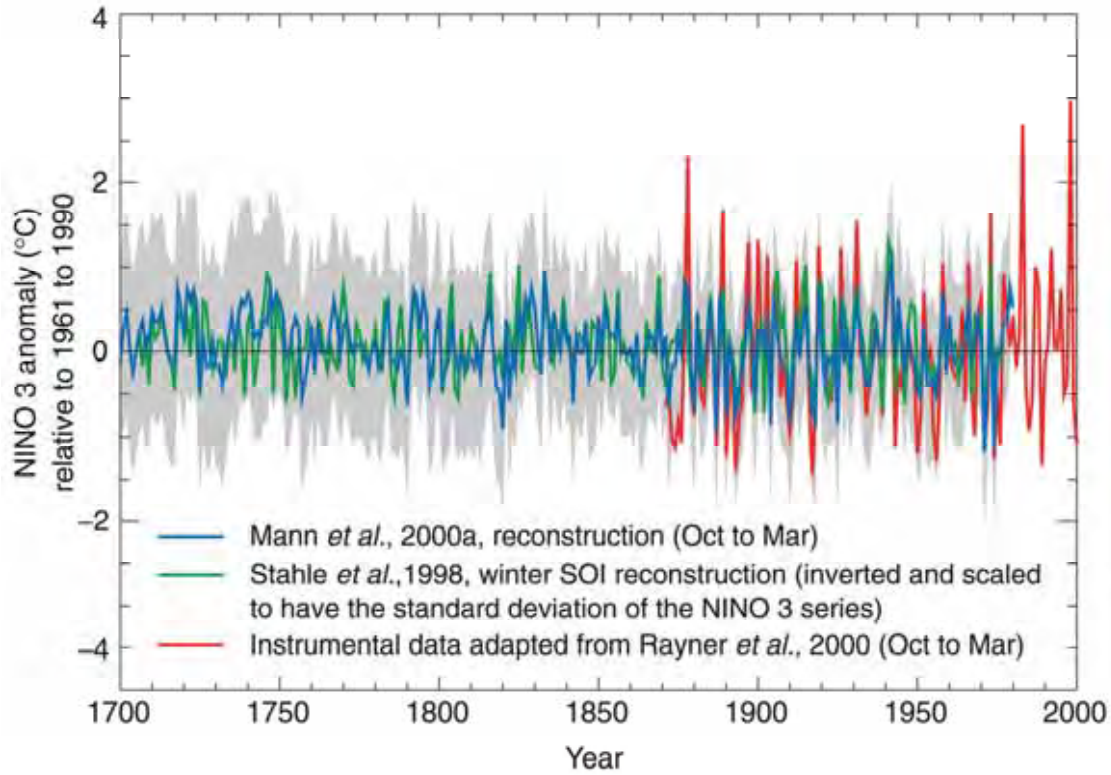

Figure 6.1. Reconstructions since A.D. 1700 of proxy-based ENSO indices. Shown are the October-March mean Niño 3 SST index of Mann *et al.* (2000) and the December-February SOI index of Stahle *et al.* (1998). An instrumental Niño 3 index from 1871 to 2000 is shown for comparison (Rayner *et al.*, 2000) with two standard error limits (grey shading) of the proxy Niño 3 SST reconstruction. Note the occurrence of extreme ENSO events during the 20th century appears outside variance reconstructed over the past three centuries. While the ST98 series (due to autoregressive modeling) generally lacks decadal and longer-term information on ENSO, the MBH00 series exhibits more lower-frequency variability. **Source:** Folland *et al.* (2001).

Tree-ring series that were significantly correlated with the instrumental record were then used to reconstruct Niño 3 SSTs using a nested procedure (in which the number of chronologies declined back in time) in order to develop the longest possible reconstruction, with iterative nests beginning in A.D. 1408, 1507, 1608 and 1709 (D'Arrigo *et al.*, 2005). The final reconstruction was developed by averaging early and late calibration reconstructions within each nest, and splicing these series together after their variance and mean had been adjusted to that of the A.D. 1709-1978 nest. All chronologies were compiled from indices of tree growth (primarily ring width) detrended to remove biological trends (Cook and Peters, 1981). Consequently, the reconstructions best reflects the high frequency 2-7 year band of ENSO variability.

D'Arrigo *et al.* (2005) concluded that ENSO variability appears to be somewhat modulated by external solar forcing. Generally, higher ENSO variability reflected in the Niño 3 SST tree-ring reconstruction coincided with decreased radiative forcing in line with recent coral and modeling results (Cobb *et al.*, 2003; Mann *et al.*, 2005). However, a notable exception occurred during the Maunder Minimum period of low solar activity when the lowest ENSO variability of the reconstruction was observed.

It is, however, prudent to acknowledge that a thorough assessment of the response of ENSO to solar forcing would require complementary reconstructions of historic synoptic conditions associated with apparent changes in reconstructed indices. In this manner, proxy reconstructions could be better employed to constrain the variety of numerical experiments that are required to understand the dynamics of changes in this coupled phenomenon. Here, no attempt is made to address such issues, as it is beyond the primary objective of this analysis which is to develop long-term, multiproxy reconstructions of ENSO indices. As such, in line with previous research (Mann *et al.*, 2000a; D'Arrigo *et al.*, 2005), we comment on apparent changes in reconstructed ENSO behaviour and the known timings of changes in solar activity.

6.2 Reconstructing ENSO Indices; CEI, SOI and Niño 3 SSTs

6.2.1 Issues with ENSO reconstruction

The limitations and/or potential biases that are specific to each type of proxy are well understood (Jones and Mann, 2004). For example, temporal coverage varies from a few centuries, in the case of coral records and historical documentary sources, to thousands of years in the case of tree-ring and ice core sequences (Jones and Mann, 2004). Limitations also exist in the temporal resolving power of proxy indicators, generally in the range of seasonal to inter-annual timescales. Commonly, a proxy record is specific to one particular season and rarely captures more than 50% of instrumental variance, and is unable to register variance equally well across a number of frequency domains (Bradley, 1996).

ENSO episodes are known to differ in terms of their relative strengths, season of onset and maturity. As detailed in Chapter 2, how best to define and monitor ENSO is a

question that has been posed for some time (Rasmusson and Carpenter, 1982; Allan *et al.*, 1996; Trenberth, 1997; Gergis and Fowler, 2005; Lyon and Barnston, 2005). This is largely due to the fact that although ENSO is a dynamic, generally coupled ocean-atmosphere phenomenon, the system periodically exhibits a 'decoupling' of atmospheric and oceanic anomalies. An instructive example of a decoupled ENSO event was the most recent 2004-2005 El Niño, when both Pacific SSTs and the SOI indicated at various times, but never synchronously, conditions characteristic of an El Niño (Lyon and Barnston, 2005). In an analysis of instrumental ENSO Gergis and Fowler (2005) demonstrated that the identification of ENSO events was dependent upon the index employed, with Niño 3.4 SSTs recording more episodes than the SOI alone, regardless of the threshold that was used to define an ENSO event.

Of further relevance to ENSO reconstructions calibrated from single (uncoupled) indices is the fact that ocean and atmosphere components of the system need not be synchronous in their timing or amplitude. Events that register strongly in some indices may be absent in others, which has obvious implications for reconstructions based on single atmospheric or oceanic indices alone (Gergis and Fowler, 2005). Unfortunately, palaeo-ENSO researchers rarely incorporate indices from both components of ENSO into the calibration process, which may fail to adequately represent large-scale dynamics of the coupled ocean-atmosphere system.

As previously outlined, reconstructive efforts to date have tended to focus on only one aspect of the ENSO phenomenon, commonly the Southern Oscillation Index (Stahle *et al.*, 1998) in the atmosphere or oceanic Niño 3 SST region (Mann *et al.*, 1998; 2000a; D'Arrigo *et al.*, 2005). While it may be argued that an SST or atmospheric pressure index alone may characterise ENSO effectively enough for the purpose of short term climate forecasting, it is not clear whether reconstructions of such indices using proxy indicators fully characterise the magnitude or timing of ENSO perturbations.

In an effort to describe more of the nature and evolution of ENSO conditions, Gergis and Fowler (2005) devised a Coupled ENSO Index (CEI), which simultaneously registers oceanic (Niño 3.4 SST) and atmospheric (SOI) anomalies for the instrumental period (1871-2003) (Chapter 2). Anomalies expressed in either Niño 3.4 SSTs or SOI alone (and therefore perhaps indicative of decoupled or out of phase behaviour) are maintained in the CEI, while fully coupled ocean-atmospheric anomalies result in an

amplification of the index. The potential advantage of this for ENSO reconstruction is highlighted in Section 6.8.1.

Having both atmospheric and oceanic components of ENSO represented in the calibration process is likely to help resolve seasonal and spatial (teleconnection) characteristics of both decoupled and coupled ENSO episodes using existing palaeoarchives. In this Chapter, a number of reconstructions of ENSO indices (CEI, SOI, Niño 3.4 SSTs) are presented to investigate whether proxy-climate data can be better characterised using a coupled ocean-atmosphere index. There is little researchers can do about the problems of temporal non-stationarity in ENSO other than to accept this as a caveat to the interpretation of results.

Fluctuations in ENSO climate teleconnections from event to event are also likely to confound reconstruction attempts, particularly if proxy data is limited to isolated (single) regions where the response to ENSO may vary in strength and persistence. To date, the coverage of proxy data has been limited to predominately Eastern Pacific teleconnection regions (Stahle *et al.*, 1998; D'Arrigo *et al.*, 2005) with little to no representation of sites influenced by the west Pacific warm pool. Thus, differences in site specific response signatures make it necessary to include proxy indicators from a variety of regions to adequately capture the spatial variability of ENSO through time (Fairbanks *et al.*, 1997).

In this Chapter, sets of ENSO-sensitive proxies representing climate signals from a range of different Pacific basin regions (tropics versus extra tropics, terrestrial versus marine environments) are employed. These locations were chosen because of their past documented responses to ENSO forcing (see Appendix 2). This approach was taken with the aim of providing complementary information from widespread ENSO climate teleconnections. Uncertainty due to complications in the proxy records themselves, such as temporal resolving power and filtering are largely neglected here. The proxy chronologies used here have been described in Chapter 3.

Importantly, three new western Pacific proxies are introduced into the ENSO reconstructions presented here, including two high quality tree-ring records from New Zealand (Fowler *et al.*, 2000; Fenwick, 2003), and a well replicated Australian coral record from the Great Barrier Reef (Hendy *et al.*, 2002; Hendy *et al.*, 2003). Significantly, these records provide an important counterpart to the chronologies

developed from eastern Pacific locations (Dunbar *et al.*, 1994; Stahle *et al.*, 1998; D'Arrigo *et al.*, 2005). This allows for the nature of past ENSO to be assessed from both east and west Pacific proxy indicators, providing insight on Pacific basin-wide changes associated with ENSO over the past five centuries.

6.3 Data

6.3.1 Data sources and proxy sub-selection

To ensure the use of high quality data, proxies used in this study are predominately published records from core ENSO or key teleconnection areas previously identified as containing an 'ENSO signal' from both eastern and western Pacific locations (e.g. Stahle *et al*,.1998; Fowler *et al.*, 2004; Hendy *et al.*, 2003) detailed in Chapter 3. Furthermore, the analysis was limited to continuous proxies with long overlap with instrumental calibration indices from core, rather than more peripheral, ENSO regions. Consequently, the Berlage Teak sequence (terminates A.D. 1929), the 'Quinn' El Niño chronology, north Chinese rainfall index and the Nile flood records featured in Chapter 5, were omitted from the analysis presented here.

A subset of the multiproxy set of climate indicators listed in Chapter 3, Table 3.1 was used for this analysis presented in this chapter. The five tree ring data sets, four coral records and one ice core record are listed in Table 6.1. Two of the tree-ring records, the Kauri (Fowler *et al.*, 2004) and Pink Pine (Fenwick, 2003), come from locations in New Zealand. A further two records, the Mexican Douglas Fir and South-west USA Pinyon Pine (Stahle *et al.*, 1998; Cleaveland *et al.*, 2003) come from Eastern Pacific locations and one record, the Indonesian Teak (D'Arrigo *et al.*, 1994), from the Western Pacific.

The coral records are similarly geographically widespread, coming from locations in the area influenced by the western Pacific warm pool (Great Barrier Reef, New Caledonia), the central Pacific (Rarotonga) and the far eastern Pacific (the Galapagos Islands). Coral sequences were limited to those with sufficient, continuous record length and to those given a positive assessment by Lough (2004). This resulted in the exclusion of shorter and/or discontinuous coral records from this analysis (e.g. Cole *et al.*, 2000; Urban *et al.*, 2000; Cobb *et al.*, 2003).The only ice core record used is from the Quelccaya ice cap in Peru, in the eastern Pacific (Thompson *et al.*, 1984; 2000).

With the exception of the Kauri, Pink Pine and the Great Barrier Reef coral record, data was obtained from NOAA's World Data Centre-A for Palaeoclimatology (see Chapter 3). The Kauri, Pink Pine and Great Barrier Reef chronologies were sourced via personal communication (Fenwick, 2003; Hendy *et al.*, 2003; Fowler *et al.*, 2004; Gergis *et al.*, 2005b; 2005a). Although a number of the records listed in Table 6.1 extend well beyond A.D. 1525 (e.g. the Quelccaya ice core data and all tree-ring records except for the Indonesian Teak) the lack of long-term coral data from tropical regions makes it difficult to establish evidence of global teleconnections associated with ENSO events (Whetton and Rutherfurd, 1994; Grove and Chappell, 2000). Accordingly, the analysis was limited to the A.D. 1525-1982 period.

As well as the Coupled ENSO Index (CEI), we also use both the Southern Oscillation Index (SOI) and Niño 3.4 SST indices to represent observational ENSO over the 20th century, detailed in Chapter 2.

Table 6.1. Subset of proxy data indicators used for principal component regression analysis. Specific details of each proxy can be found in Chapter 3, Table 3.1.

Proxy Record	*Dates (A.D.)*	*Latitude/Longitude*	*Data Smoothing*	*ENSO Zone*	*Proxy Variable*
Tree-rings					
New Zealand Kauri [a]	1525-2002	35°-37° S, 173°-175° E	20-year Spline	West Pacific	Total Ring Widths
New Zealand Pink Pine [b]	1525-1998	42°-47° S, 167°-174° E	20-year Spline	West Pacific	Total Ring Widths
Mexican Douglas Fir [c]	1525-1998	19°-30° S, 97°–108° W	20-year Spline	East Pacific	Total Ring Widths
SW USA Pinyon Pine [d]	1525-2000	33°-37° S, 106°-112° W	20-year Spline	East Pacific	Total Ring Widths
Indonesian Teak [e]	1841-1995	8° S, 113° E	20-year Spline	West Pacific	Total Ring Widths
Coral					
Great Barrier Reef [f]	1612-1985	20° S, 147° E	3-year Gaussian	West Pacific	Luminescence SSS
New Caledonia [g]	1658-1992	22° S, 166° E	3-year Gaussian	West Pacific	δO^{18} SST
Raratonga [i]	1727-1997	21° S, 159° W	3-year Gaussian	Central Pacific	Sr/Ca SST
Galapagos Islands [h]	1607-1982	1° S, 91° W	3-year Gaussian	East Pacific	δO^{18} SST
Ice					
Quelccaya Ice Core [j]	1525-1984	14° S, 71° W	3-year Gaussian	East Pacific	Net accumulation

6.4 Methodology

6.4.1 Isolating the ENSO signal

Prior to inclusion in a regression model, it is important to ensure that the predictors (independent proxy data) have a high association with the predictand (dependent ENSO index) under reconstruction. Any relationship real or artificial, between predictor and predictand that is not associated with ENSO is likely to degrade the quality of the reconstruction. To some degree, the isolation of ENSO signals should be achieved by taking the ENSO-related PC time series alone, since this process filters the data into orthogonal modes of variability. However, it is prudent to filter the individual chronologies prior to this step to remove the effects of red noise or persistence (Stahle *et al.*, 1998). Red noise in proxy data may be associated with biological processes in the proxies themselves or to low frequency climate influences (Fisher, 2002).

Since a definitive method could not be sourced from the literature, several approaches to assess the sensitivity of filtering before calibrating the proxies to instrumental indices were undertaken in this study. Three approaches (their combinations thereof) were explored;

1. Prewhitening of the proxy chronologies and ENSO indices using a low order auto-regressive (AR) model. The order of the model was chosen based on the autocorrelation structure of the ENSO indices and proxy data and the calibration was performed using PC scores from pre-whitened data. The auto-correlation structure of the relevant ENSO index (AR-3) was then added back to the resultant reconstruction.

2. Appropriately filtering the data to isolate ENSO timescales. Tree-ring sequences were high-pass filtered using a smoothing cubic spline with 50% variance cut off at 20 years using ARSTAN (Holmes *et al.*, 1986). The use of a 20-year smoothing spline has been shown previously to effectively remove the effect of biological growth from tree ring sequences (Cook and Peters, 1981; Holmes *et al.*, 1986; Fowler *et al.*, 2004; D'Arrigo *et al.*, 2005). The coral and ice records were filtered using a 3-year Gaussian filter, as used in previous palaeo-climate studies (Diaz

and Markgraf, 2000; Goodwin *et al.*, 2004; Linsley *et al.*, 2004; Lough, 2004). Furthermore, this filter was chosen to provide the highest ratio of correctly/incorrectly identified ENSO events, as defined using instrumental indices using a given proxy record (Gergis *et al.*, 2004; 2005c; 2005d; 2005e).

3. Linear detrending of the data by removing a fourth order (quartic) polynomial fitted to the timeseries over the calibration period. This method has been shown previously to effectively detrend climate data while preserving high amplitude (<10 year) variability (Braganza *et al.*, 2003; 2004).

In general, the results were insensitive to the different methods applied, with marginal differences in the resultant reconstructions (Braganza *et al.*, 2005). Prewhitening of tree-ring proxies to account for auto-correlation due to biological growth is an approach that has been applied by Stahle *et al.* (1998). That study found that prewhitening of the predictor and predictand (the SOI) produced a reconstruction that was more coherent in the ENSO frequency domain. However, in this analysis it was found that the prewhitening approach produced the least desirable results in terms of verification statistics (Braganza *et al.*, 2005). In addition, since the auto-correlation within the ENSO indices themselves was small, it is unclear whether removal of this persistence was meaningful (Braganza *et al.*, 2005).

The best results were achieved by both filtering and detrending the normalised (unit standard deviation) proxy anomalies (using the methods described above) and calibrating against normalised anomalies of the ENSO indices (Braganza *et al.*, 2005). Results of the comparison of statistical techniques used to isolate ENSO signals are not presented here to avoid detracting from the primary scope of the Chapter. Further detail can be found in Braganza *et al.* (2005). Here, the high-pass filtered, detrended proxy time series and the resultant PC scores were found to exhibit very little low-order autocorrelation and low frequency variability during the calibration period, while retaining the 3-7 year ENSO signal. As such, all subsequent results are based on filtered, detrended proxy reconstructions, consistent with the approach taken in Chapter 3.

6.4.2 Principal component analysis (PCA)

Following the approach of previous researchers (Stahle *et al.*, 1998; Mann *et al.*, 2000a; D'Arrigo *et al.*, 2005) ENSO indices were reconstructed from the multiproxy data by first decomposing the data into principle components (PC) and using the associated time series (PC scores) in a multiple regression model that relates variability in the proxy data with variability in the ENSO indices. To allow for differences in the seasonal and physical development of ENSO, annually resolved multiproxy data are calibrated against the seasonal (DJF, MAM, JJA, SON) ENSO indices of the SOI, Niño 3.4 SSTs and CEI.

The master chronologies of proxy climate data were divided into three sets, each grouped according to the criteria of having the same length of continuous records. Hence, three multiproxy data sets at annual resolution were defined beginning from A.D. 1525, 1727 and 1871 and ending in 1982. The A.D. 1871 set (R10) contains all the proxy records (10 chronologies) listed in Table 6.1. This full set overlaps entirely with the instrumental record and provides a 'base period' reconstruction against which the suitability of the methodology and extended reconstructions can be compared.

The A.D. 1727 subset (R9) (which contains all the coral sequences) contains one less record due to the exclusion of Indonesian Teak on the grounds of record length and data inhomogeneity (see Chapter 3). Note that in this thesis, Sr/Ca values used from the Rarotonga coral record (Linsley *et al.*, 2000) were used starting from A.D. 1727, as data is only available for one season (SON) of the year A.D. 1726. The Teak record was maintained in the 1871 set to assess regional sensitivity represented by the record. The A.D. 1525 reconstruction (R5) contains only five chronologies, the two New Zealand and two Eastern Pacific tree-ring records and the Quelccaya ice core sequence, still maintaining a Pacific Basin wide distribution of proxies.

PCA was used to reduce each of the three sets of annual proxy data into three potential predictors of each ENSO index (SOI, CEI, Niño 3.4 SSTs) for each season (MAM, JJA, SON, DJF). These were derived for each proxy by leading (t-1), synchronising (t) and lagging (t+1) the proxy time series. The resultant PC scores time series were then used in a simple, least squares multiple linear regression model to calibrate the palaeoclimate proxies with the instrumental ENSO indices. This involves fitting a line of 'best fit' to a set of data in an attempt to minimise the sum of the squares of the

ordinate differences (called residuals) between the fitted function and the data (Chatfield, 1975). This has the inherent limitation of truncating outliers that could influence the accurate reconstruction of the full range of ENSO magnitude, as addressed in Chapter 5.

Nevertheless, using three proxy subsets present at A.D. 1525 (R5), 1727 (R9) and 1871 (R10), predictors of each ENSO index (SOI, CEI, Niño 3.4) for each season (MAM, JJA, SON, DJF) were developed. The use of PC-based regression reduces noise associated with differences in the seasonal climate responses of each proxy and the differences associated with the seasonality and persistence of regional ENSO teleconnections (Stahle *et al.*, 1998).

6.4.3 Proxy model calibration

Table 6.2 shows the variance explained by the first four PCs for the R10, R9, and R5 multiproxy data sets. While the total variance of the chronologies is evenly spread through the four leading modes of variability, only the first two were well correlated with any of the ENSO indices. This uniform distribution of the variance may reflect the degree of noise on inter-annual to multi-decadal timescales that exists within the palaeo data.

The prediction model was defined by regressing the leading two principal components of the covariance matrix from each proxy data subset against the instrumental record for each index and in each season over the period of overlap (A.D. 1871-1982). The leading two PCs (PC1 and PC2) were found to represent up to 50% of the total variability in each of the master chronology sets (Table 6.2). While the inclusion of more than two PCs improves the regression model over the 20th century, this was considered to be a result of fitting additional 20th century noise in the data and thus was not expected to realistically contribute to the reconstruction prior to this period. This differs from previous approaches that use more PCs in the case of ST98 for ENSO reconstruction, who used four PCs regardless of their correlation with ENSO.

All three multiproxy reconstructions have been calibrated against the instrumental record for the A.D. 1871-1982 period. Following previous studies, the quality of the calibration method was first tested by training the data using smaller subsets of the instrumental data to predict the whole overlap period for each index in each season (Stahle *et al.*, 1998). Following this, the full instrumental period (1871-1982) was used

to train the regression model and reconstruct the ENSO indices back in time to A.D. 1525. While it is impossible to verify the accuracy of these reconstructions from the observations alone, the split calibrations provide an assessment of how accurately the palaeo record subsets are at reproducing 20th century ENSO. To further investigate this, a comparison of spectral power was made for all ENSO indices back in time using the spectral analysis method detailed in Section 6.8.

Table 6.2. Variance Explained (%) of first four principal components (PCs) of multiproxy data. Note that the covariance matrix was used to calculate PCs.

Multiproxy Subset	PC1	PC2	PC3	PC4
Start Date (A.D.)				
1871 (R10)	21	16	12	10
1727 (R9)	20	15	12	11
1525 (R5)	30	21	20	16

6.4.4 Proxy covariability

As previously suggested, the geographic distribution of proxies is an important component in accurately capturing ENSO-related variability. Table 6.3 shows the relative loading (eigenvectors) of each proxy chronology and their lead/lag correlation with the associated PC time series calculated using the covariance matrix. The loadings represent a measure of coherent variability associated with the direction of the first two PCs and hence indicate which sites contribute most to the overall variance within these modes and the subsequent reconstruction.

The variance associated with the leading mode (PC1) is dominated by co-variability in the Mexican Douglas Fir, South-Western USA Pinyon Pine, New Zealand Pink Pine and all of the coral records. The Quelccaya ice-core, while providing a small fraction of the variance in this mode, is strongly correlated with PC1 temporal variability (e.g. for t, r=0.60). Generally speaking, PC1 appears to have a stronger association with proxies from the eastern Pacific, with the exceptions of the New Zealand Pink Pine and to a lesser degree the Great Barrier Reef coral record. PC2 meanwhile, has a greater association with western Pacific sites and is dominated by variability in the New Zealand Kauri, Indonesian Teak and Great Barrier Reef corals record, the exception in this case being the south-western USA Pinyon Pine.

Table 6.3. PC Loadings and annual Pearson's correlation (r) between proxy chronologies and the PC1 and PC2 shown with lead and lag time of one year. Note that the covariance matrix was used to calculate PCs.

Individual Proxy records represented in the 1871 Multiproxy Subset	PC Loading	t-1	t	t+1
PC 1				
Kauri tree-rings	0.03	0.14	0.04	-0.32
Pink Pine tree-rings	0.36	-0.03	0.49	0.13
Mexican tree-rings	-0.48	0.07	-0.66	0.03
SW USA tree-rings	-0.40	-0.02	-0.56	0.26
Indonesian tree-rings	-0.04	-0.09	-0.06	0.16
Rarotonga coral	-0.44	-0.16	-0.55	-0.10
Great Barrier Reef coral	0.28	0.19	0.38	-0.09
Galapagos coral	-0.40	-0.05	0.13	0.15
New Caledonia coral	-0.20	-0.07	-0.28	-0.28
Quelccaya ice core	0.09	-0.21	-0.60	-0.45
PC2				
Kauri tree-rings	0.61	0.03	0.72	0.05
Pink Pine tree-rings	-0.23	-0.28	-0.27	0.04
Mexican tree-rings	0.11	0.41	0.13	-0.19
SW USA tree-rings	-0.39	0.19	-0.46	-0.11
Indonesian tree-rings	-0.50	-0.01	-0.59	-0.11
Rarotonga coral	0.19	0.22	0.04	0.05
Great Barrier Reef coral	0.28	-0.15	0.33	0.12
Galapagos coral	0.03	-0.04	-0.16	0.09
New Caledonia coral	0.16	0.26	0.19	0.00
Quelccaya ice core	-0.13	0.27	0.23	0.23

6.4.5 Proxy ENSO regression model

To investigate the potential seasonality of relationships between each proxy and instrumental time-series, correlations between the annual PC score time series and the ENSO indices for each of the seasons over the A.D. 1871-1982 calibration period were calculated (Table 6.4). The transfer function used to estimate each seasonal ENSO index was based on a simple, least squares regression model using the observed ENSO indices as the dependent variable and the leading two PCs from the multiproxy sets as independent variables.

Table 6.4. Pearson's correlations (r) with 1-year lead (t-1), synchronous (t) and lag (t+1) relationships between the annual PC score time series and SOI, Niño 3 SSTs and CEI ENSO indices of the for each season (DJF, MAM, JJA, SON) during the 1871 reference period. Optimum lead, synchronous, and lag correlations indicated per season for each ENSO index. Note that the DJF season represents the year in which the month of January falls.

ENSO Index & Seasonal Window	Correlation & Timing	Correlation & Timing
DJF	***PC1 (t)***	***PC2 (t-1)***
CEI	0.73	-0.57
SOI	0.68	-0.56
Niño 3.4 SST	-0.65	0.51
MAM	***PC1 (t)***	***PC2 (t-1)***
CEI	0.63	-0.51
SOI	0.55	-0.48
Niño 3.4 SST	-0.71	0.54
JJA	***PC1 (t+1)***	***PC2 (t)***
CEI	0.55	-0.46
SOI	0.52	-0.44
JJA	***PC1 (t)***	***PC2 (t-1)***
Niño 3.4 SST	-0.61	0.45
SON	***PC1 (t+1)***	***PC2 (t)***
CEI	0.67	-0.54
SOI	0.62	-0.54
Niño 3.4 SST	-0.50	0.41

From the relationships identified in Table 6.4, the following linear relationships between the proxy data and each of the ENSO indices were derived;

1. DJF (CEI, SOI, SST) = B1*PC1(0) + B2*PC2(-1)
2. MAM (CEI, SOI, SST) = B1*PC1(0) + B2*PC2(-1)
3. JJA (SST) = B1*PC(0) + B2*PC2(-1)
4. JJA (SOI, CEI) = B1*PC1(+1) + B2*PC2(0)
5. SON (CEI, SOI, SST) = B1*PC1(+1) + B2*PC2(0)

It is worthy of note that the growth season of many proxies often straddles two calendar years, as does the timing of peak maturity of ENSO events. This is reflected in lead and lag associations reflected in Table 6.4. For DJF and MAM in each of the ENSO indices (CEI, SOI, and Niño 3.4 SST), the best relationship with PC1 is found in the same year and with PC2 of the previous year. For JJA, the best relationships in SST are found in the same year for PC1 and in the previous year for PC2, while for CEI and SOI the best relationship is found with PC1 of the next year and with PC2 in the concurrent year. Generally, on inter-annual timescales it would appear that the proxies are simultaneously associated with JJA SST but with the JJA pressure signal from the following year. For SON, PC2 is associated with ENSO of the same year while PC1 is associated with the SON ENSO signal of the following year (Table 6.4).

Table 6.4 indicates the high statistical agreement between the proxy network and instrumental ENSO indices. Overall, the best agreement of the full R10 data set with PC1 over the instrumental period was noted from DJF CEI (r = 0.73). Good results for PC1 were also seen with MAM SST (r = -0.71) and DJF SOI (r = 0.68). The variability represented by proxy PC2, was somewhat lower with a maximum correlation of –0.57 observed with DJF CEI. Results for the R5, R9 and R10 proxy subsets were found to be similar.

6.5 Model Verification

6.5.1 Split calibration

To verify the robustness of the regression model, a series of statistical cross-validation or verification experiments was performed. In these experiments, the R10 reconstructions were compared against direct instrumental data over the 1871-1982 period. A number of these partial, or 'split' period calibration analyses were undertaken based on a number of calibration intervals. Correlations with ENSO indices are shown for reconstructions based on 5, 10, 30 and 50-year calibration periods from different start dates during the 20th century, as seen in Table 6.5.

Table 6.5. Verification of reconstruction model using 5, 10, 30 and 50-year sub-sample calibrations. Pearson correlations (r) are shown for the reconstruction over the full overlap period 1871-1982. Results are shown for 1727 set of proxies and the CEI only. Results for other proxy data sets and ENSO indices are quantitatively similar.

Calibration Period		Correlation with CEI			
Length	*Sub-Sample*	*MAM*	*JJA*	*SON*	*DJF*
5	1975-1980	-0.65	-0.20	-0.30	-0.01
10	1970-1980	0.66	0.56	0.67	0.75
10	1910-1920	0.66	0.54	0.69	0.75
30	1940-1970	0.59	0.57	0.70	0.73
50	1871-1930	0.66	0.57	0.70	0.75
113	1871-1982	0.66	0.57	0.70	0.75

Calibration Period		CEI % Variance Explained			
Length	*Sub-Sample*	*MAM*	*JJA*	*SON*	*DJF*
5	1975-1980	0.42	0.04	0.09	0.00
10	1970-1980	0.44	0.31	0.45	0.56
10	1910-1920	0.44	0.29	0.48	0.56
30	1940-1970	0.35	0.32	0.49	0.53
50	1871-1930	0.44	0.32	0.49	0.56
113	1871-1982	0.44	0.32	0.49	0.56

In general, the results of Table 6.5 support the validity of this method of ENSO index reconstruction. Indeed, the consistencies of the correlations show that periods as small as 10 years contain enough information to represent 20th century ENSO. While one may expect non-stationarity of the late 19th to early 20th century SOI and Niño 3.4 SSTs as noted by previous researchers (Stahle *et al.*, 1998; Allan, 2000; Trenberth and Caron, 2000), to have an effect on the reconstruction, calibrations using different periods of the 20th century time series show that this may have little impact.

Residuals from the reconstructions were shown to be normally distributed and free of significant auto-correlation (Figure 6.2). Furthermore, the analysis of the root mean square (RMS) error presented in Table 6.6 indicates that the errors are fairly consistent using different proxy subsets and indices. Since the errors are unbiased, this distribution may be used to calculate confidence intervals for the reconstructions. Alternatively, uncertainty estimates can also be derived from the variance of the regression coefficients used in the transfer function which, by definition, are also normally distributed.

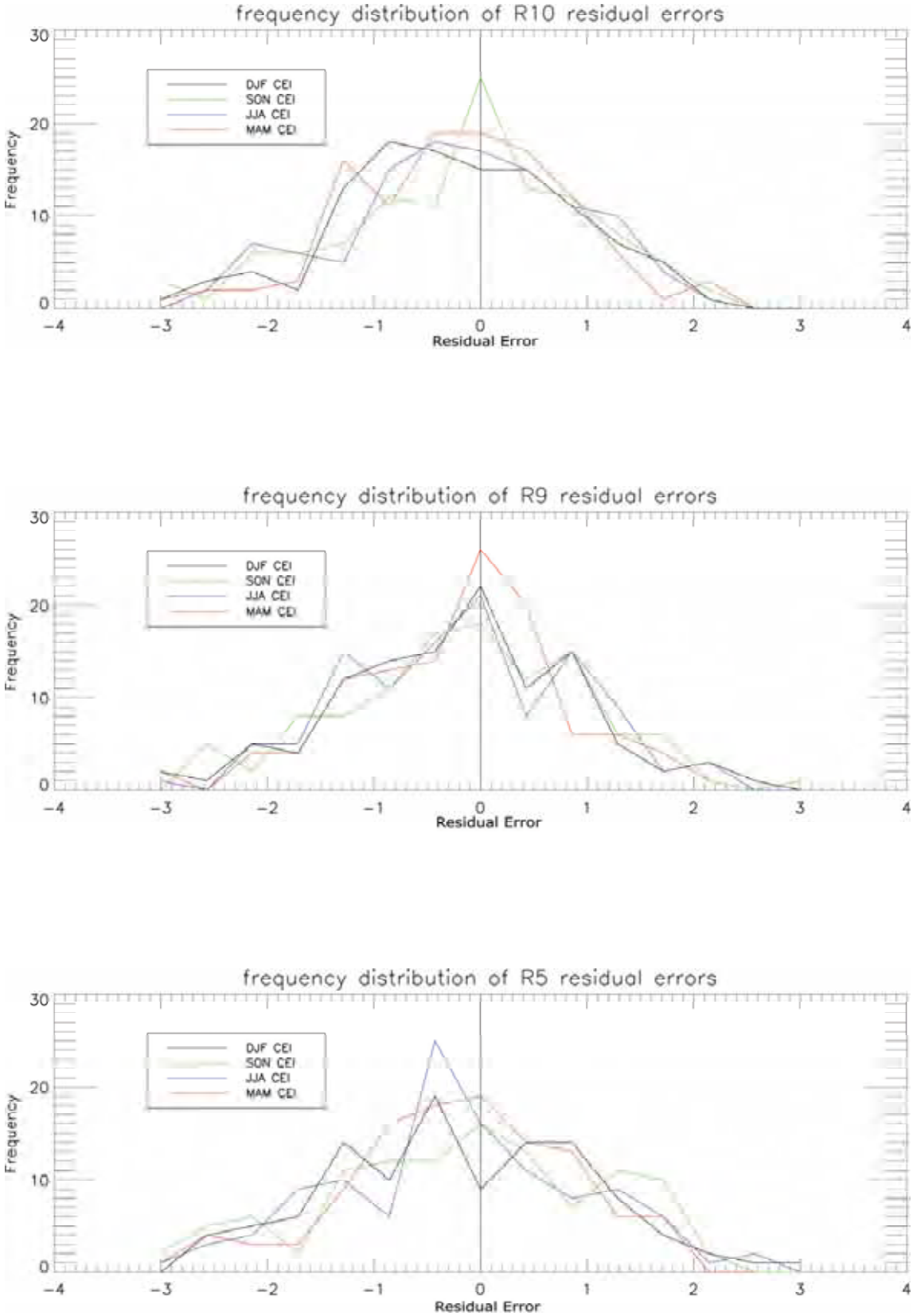

Figure 6.2. Distribution of residual errors for (a) R10, (b) R9 and (c) R5 CEI reconstructions.

Table 6.6. Root mean square (RMS) error for reconstructions over the A.D. 1871-1982 calibration period for R5, R9 and R10 proxy reconstructions.

ENSO Index & Seasonal Window	RMS Error for R10 Multiproxy Subset	RMS Error for R9 Multiproxy Subset	RMS Error for R5 Multiproxy Subset
CEI			
MAM	0.99	1.00	1.04
JJA	1.09	1.11	1.20
SON	1.22	1.25	1.38
DJF	1.08	1.11	1.24
SOI			
MAM	0.53	0.53	0.54
JJA	0.60	0.61	0.66
SON	0.59	0.61	0.66
DJF	0.47	0.48	0.53
Niño 3.4 SST			
MAM	0.73	0.74	0.82
JJA	0.60	0.61	0.63
SON	0.62	0.63	0.66
DJF	0.74	0.75	0.82

6.5.2 Replication and seasonal sensitivity

The effect of the degree of replication in the reconstruction is apparent from the high correlations seen in Table 6.7. Despite showing quite good correlation statistics, the 1525 (R5) reconstruction, shows the least coherent results. Differences between the 1727 (R9) and 1871 (R10) data sets are extremely small, indicating that the inclusion of the Indonesian Teak record is not crucial to the quality of the reconstruction. This may be due to the inclusion of other proxies from the western Pacific.

In terms of seasonality, the highest associations were found between the proxies and ENSO indices from December through to May. This result is consistent with previous studies (Rasmusson and Carpenter, 1982; Stahle *et al.*, 1998; Allan, 2000) that show that links between ENSO indices and proxy records are greatest at this time, and is indicative of peak ENSO maturity. The seasonal dependence of accuracy in the reconstructions seems unaffected by seasonal differences in the variability of the indices, and this is reflected by in the uniform standard deviations of each index throughout the year (Table 6.8).

As seen in Table 6.7, the 1871 and 1727 data sets were found to have near identical skill in reproducing instrumental DJF CEI, DJF SOI and MAM Niño 3.4 SST. The results

for the R9 reconstruction are shown in Figure 6.3. Note that despite having good statistical agreement, the magnitude of instrumental ENSO is not precisely captured. This becomes more evident with a loss of replication back in time, reflected in the R5 (1525) reconstruction statistics listed in Table 6.6. Nevertheless, both reconstructions appear to track mean state changes in ENSO behaviour very well, as seen in Figure 6.4.

Table 6.7. Correlation of reconstructions over the calibration period 1871-1982 shown for SOI, Niño 3.4 SSTs and CEI ENSO indices for each season.

ENSO Index & Seasonal Window	*1871(R10) Multiproxy Subset Full Period Calibration Correlations*	*1727 (R9) Multiproxy Subset Full Period Calibration Correlations*	*1525 (R5) Multiproxy Subset Full Period Calibration Correlations*
CEI			
MAM	0.67	0.66	0.62
JJA	0.59	0.57	0.46
SON	0.71	0.70	0.61
DJF	0.77	0.75	0.67
SOI			
MAM	0.60	0.60	0.56
JJA	0.56	0.53	0.41
SON	0.68	0.66	0.56
DJF	0.73	0.71	0.62
Niño 3.4 SST			
MAM	0.74	0.73	0.65
JJA	0.64	0.63	0.59
SON	0.53	0.52	0.44
DJF	0.68	0.67	0.59

Table 6.8. Comparison of variability (standard deviation) between the R5, R9 and R10 reconstructions, as well as instrumental indices for overlap periods 1871-1982 and 1727-1871.

Data Set	CEI	SOI	Niño 3.4 SST
1871-1982			
Instrumental	1.67	0.68	1.08
R5	1.06	0.39	0.68
R9	1.20	0.44	0.77
R10	1.22	0.45	0.77
1727-1870			
R5	0.86	0.31	0.56
R9	0.97	0.35	0.62

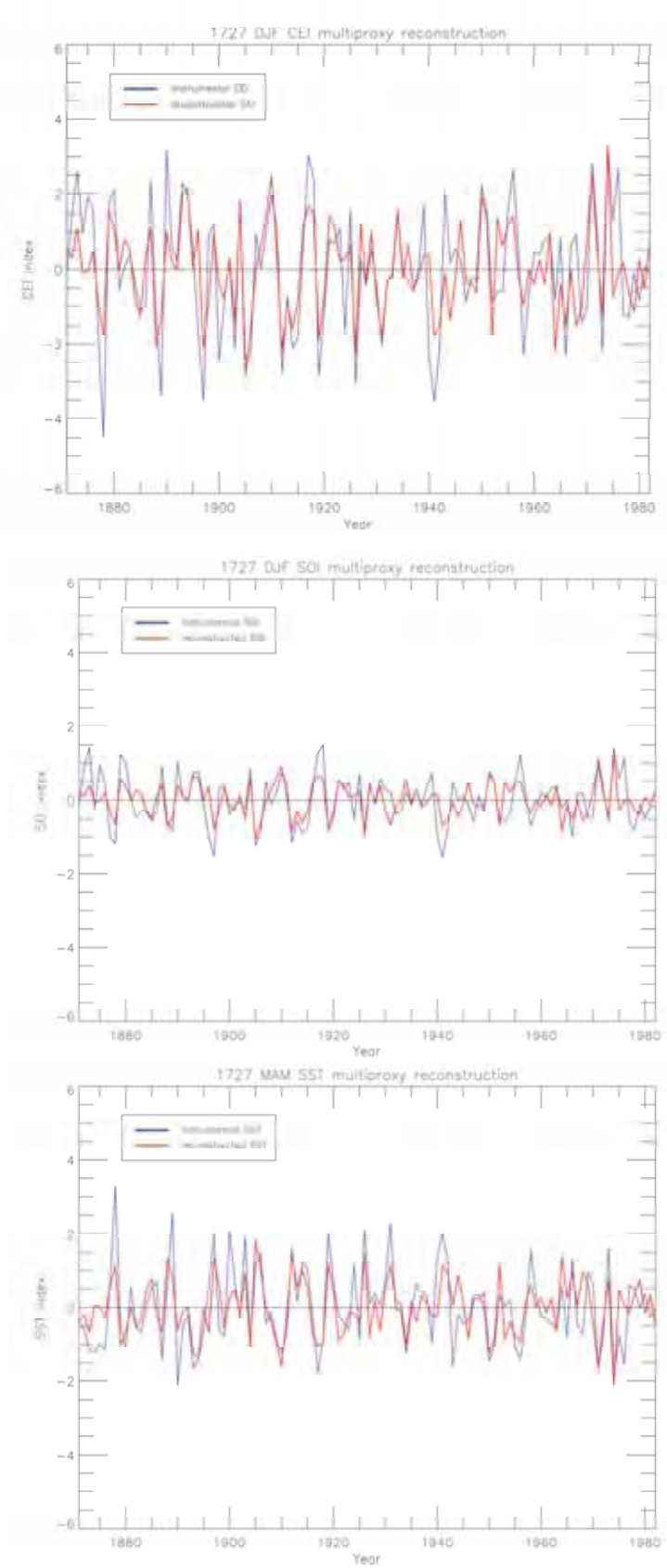

Figure 6.3. Reconstructed (red) and instrumental (blue) (a) CEI DJF (b) SOI DJF (c) MAM Niño 3.4 SST using R9 proxy subset.

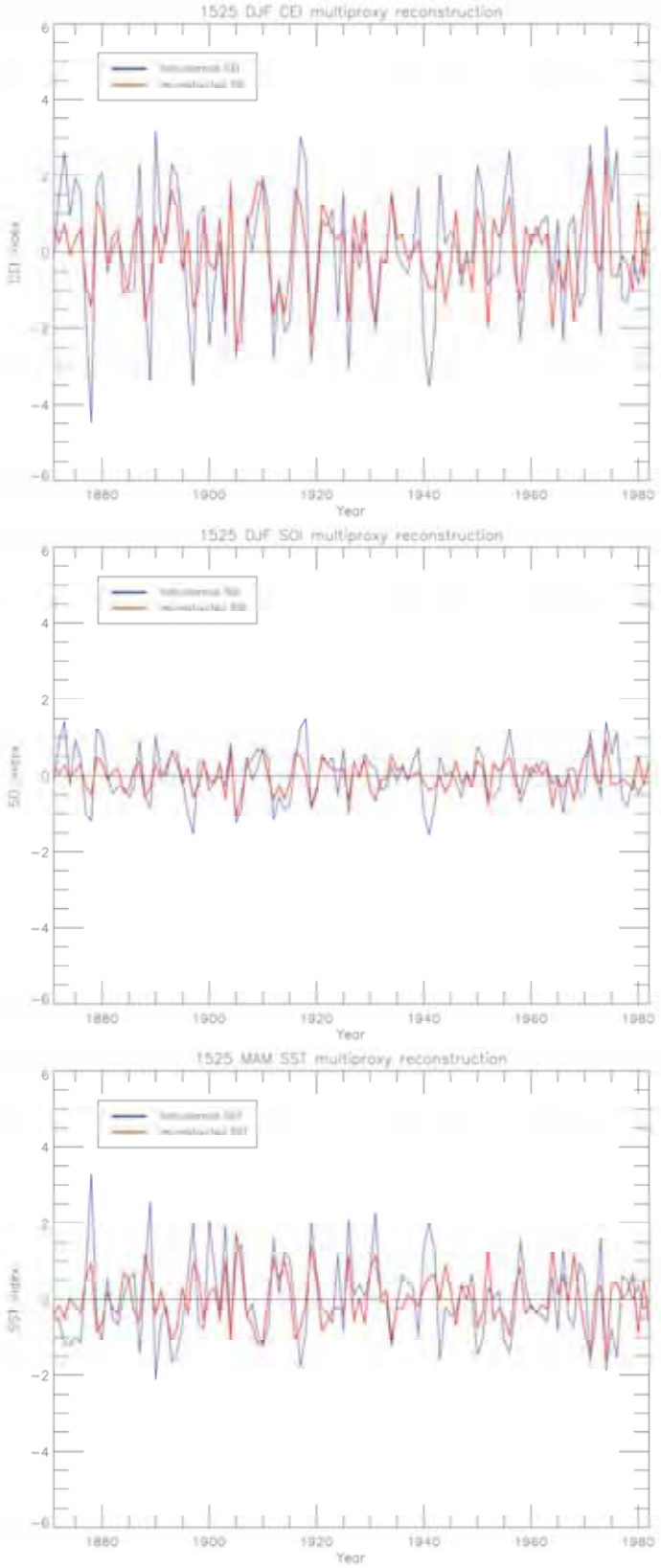

Figure 6.4. Reconstructed (red) and instrumental (blue) (a) CEI DJF (b) SOI DJF (c) MAM Niño 3.4 SST using R5 proxy subset.

6.6 Pre-Instrumental ENSO Reconstructions

A PC linear regression model calibrated over the full reference period (1871-1982), allowed reconstructions for the CEI, SOI, and Niño 3.4 SSTs from A.D. 1525. As shown in Figure 6.5, this was done for the most optimum season for each ENSO index. Of the three ENSO indices, greatest skill was achieved in reproducing the CEI combined ocean-atmosphere index. It is apparent from each reconstruction presented in Figure 6.5 that ENSO variability has fluctuated considerably through time. The CEI shows the most amplitude variability of the three indices reconstructed, and the SOI the least, mirroring the results presented in Table 6.8.

6.7 Capturing instrumental variance

A further measure of a reconstruction's skill is revealed through the calculation of the proportion of common variance (r^2) shared between a given proxy reconstruction and its corresponding instrumental index. Essentially, this provides a simple measure of how well a set of proxy indicators are reproducing climate variability contained within the instrumental data. Using the three dominant eigenvectors, Mann *et al.* (2000) report that they were able to resolve 34-42% of October to March Niño 3 SST. Using the four leading PCs, the Stahle *et al.* (1998) SOI reconstruction explains a maximum 53% of December-February SOI variance. Most recently, the Cook05 reconstruction detailed by D'Arrigo *et al.* (2005) resolved between 43-52% of Niño 3 DJF SST.

The proportion of common variance shared between the 1871 (R10) 1727 (R9) and 1525 (R5) subset reconstructions and each seasonal ENSO index is shown in Table 6.9. Compared to previous reconstructions, similar degrees of skill are achieved, however, some marked improvements were also noted. For example, using the Niño 3.4 SST index, the strongest relationship for December-May is best represented by MAM, when a maximum of 55% of is explained using the R10 Niño 3.4 SST subset. The Niño 3.4 SST index appears to suffer the most from loss of replication, perhaps as a reflection of the loss of coral records available back in time, and has reduced skill in predicting JJA SST conditions (Table 6.9). Significantly, these results indicate the greater suitability of the CEI for proxy calibration than either of the component indices.

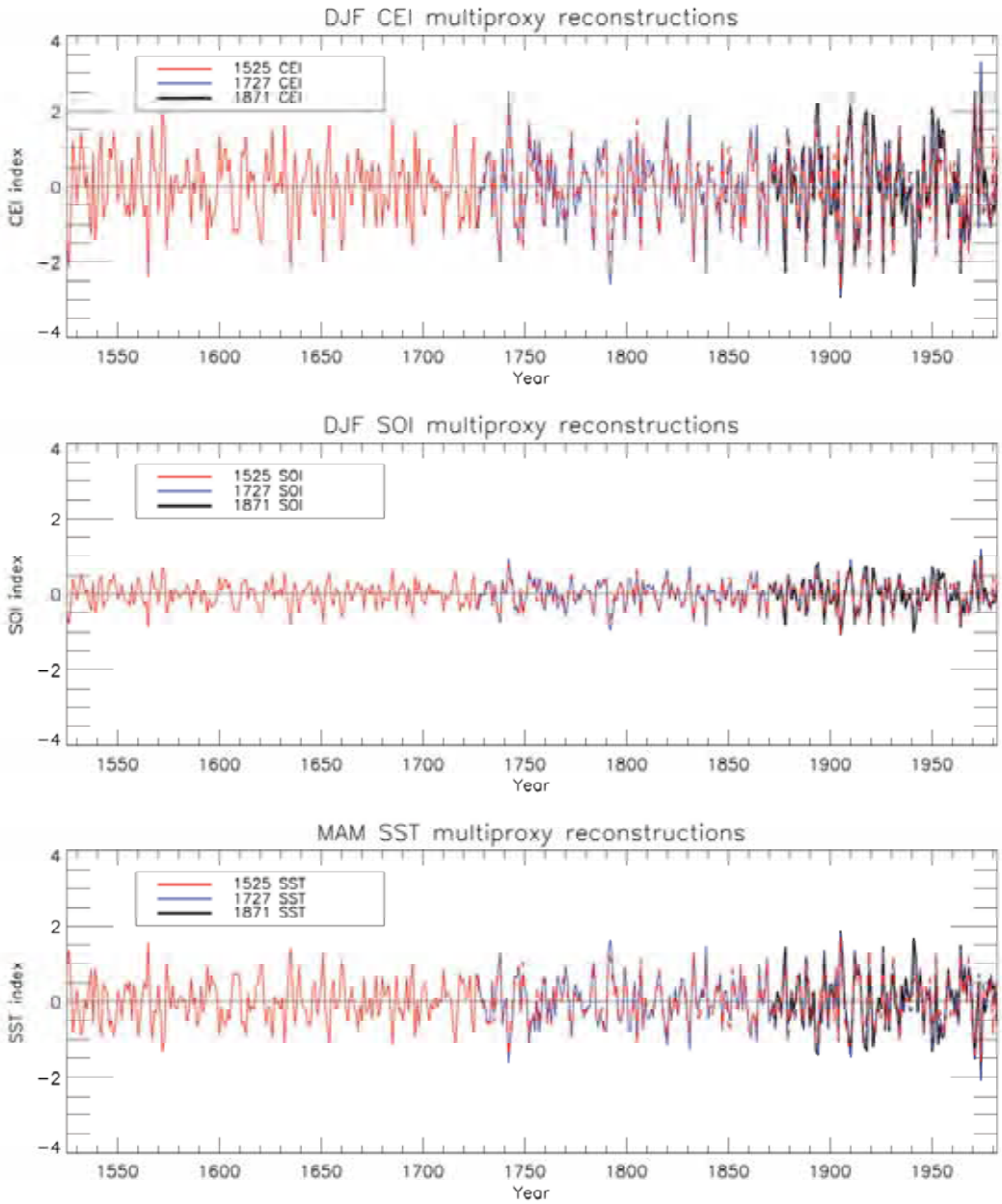

Figure 6.5. Reconstructions of A.D. 1525-1982 ENSO using (i) DJF CEI (ii) DJF SOI and (iii) MAM Niño 3.4 SSTs.

The results indicate comparable (and somewhat improved) predictive skill using only the first two PCs of the multiproxy data set, suggesting a more refined ENSO model may be possible with further analysis. Significantly, CEI reconstructions were often found to be the best predictors of ENSO (for all seasons) compared with the SOI or SST-based ENSO reconstructions. Approximately 59% (45%) of variance in instrumental DJF CEI was explained by the R10 (R5) subset, representing the strongest relationships observed for any index or season, with the exceptions of MAM and JJA

Niño 3.4 SSTs. Importantly, these results suggest that a relatively good estimate of ENSO behaviour is available using the CEI back to A.D. 1525.

Table 6.9. Proportion of common variance (R^2) shared by each proxy reconstructions and seasonal instrumental ENSO index.

Multiproxy Subset & Seasonal Window	Coupled ENSO Index (CEI)	Southern Oscillation Index (SOI)	Niño 3.4 SST Index
R10 Proxy Subset			
MAM	0.45	0.36	0.55
JJA	0.35	0.31	0.41
SON	0.50	0.46	0.28
DJF	0.59	0.53	0.46
R9 Proxy Subset			
MAM	0.44	0.36	0.53
JJA	0.32	0.28	0.40
SON	0.49	0.44	0.27
DJF	0.56	0.50	0.45
R5 Proxy Subset			
MAM	0.38	0.31	0.42
JJA	0.21	0.17	0.35
SON	0.37	0.31	0.19
DJF	0.45	0.38	0.35

6.8 Spectral Analysis

6.8.1 Instrumental analysis

The spectrum of a time series is the distribution of variance of the series as a function of frequency (Ghil and Yiou, 1996). Spectral analysis is designed to extract information from short and noisy time series to provide potential insight into the dynamics of the underlying system that generated the series (Ghil and Yiou, 1996). In this study, the spectral properties of the CEI reconstructions were compared to those of the instrumental calibrating period (1871-1982) using a Fast Fourier Transform (FFT) with the mean removed (Brigham, 1988). Smoothing was applied across the frequency domain using multiple passes of a centrally weighted, three-point moving window (1-2-1). The background noise spectrum was estimated from the theoretical AR1 or Markov process noise (Gilman, 1963; Torrence e*t al.*, 1998), with AR1 autocorrelation calculated by taking the inverse transform of the power spectrum (Bath, 1974). The

degrees of freedom used for confidence interval estimation is dependent on the size of the effective bandwidth after smoothing. Thus, the significance of spectral peaks relative to the 90% confidence interval for background noise was estimated from the AR1 noise spectrum and the Chi Squared distribution to the 90-95% significance level (Bath, 1974).

The spectral density of a signal is a way of measuring the strength of the different frequencies that form the signal (Ghil *et al.*, 2002). The power spectral density (PSD) describes how the power (or variance) of a time series is distributed with frequency (Ghil *et al.*, 2002). The spectral density of the signal is the square of the magnitude of the continuous Fourier transformation of the signal (Ghil *et al.*, 2002). Generally, a Fourier transformation decomposes a function into a continuous spectrum of the frequencies that comprise that function (Ghil *et al.*, 2002).

'White' noise in a time series refers to an even distribution of variance across all frequencies, that is, the signal's power spectral density has equal power in any band and frequency (Gilman *et al.*, 1962). On the other hand, 'red 'noise' is due to autocorrelation between successive measurements characterised by a general suppression of variance at higher frequencies with inflation at lower frequency (Gilman *et al.*, 1962).

A comparison of PSD characteristics of instrumental CEI, SOI and Niño 3.4 SST indices are shown in Figure 6.6. The dominant frequencies centred between 2-7years are seen across all indices but appear more subdued in the individual atmospheric and oceanic signals. Clearly, the CEI has more spectral power variability across all frequencies than either of the component indices. This may reflect an enhanced signal to noise ratio, probably because of the amplification of the synchronous ocean-atmospheric events. The SOI has the weakest spectral power of the ENSO indices, registering PSD variability approximately three times less than the CEI. It is important to note however, that the results presented in Figure 6.6 are un-normalised to demonstrate that the CEI has greater overall variability than its component indices.

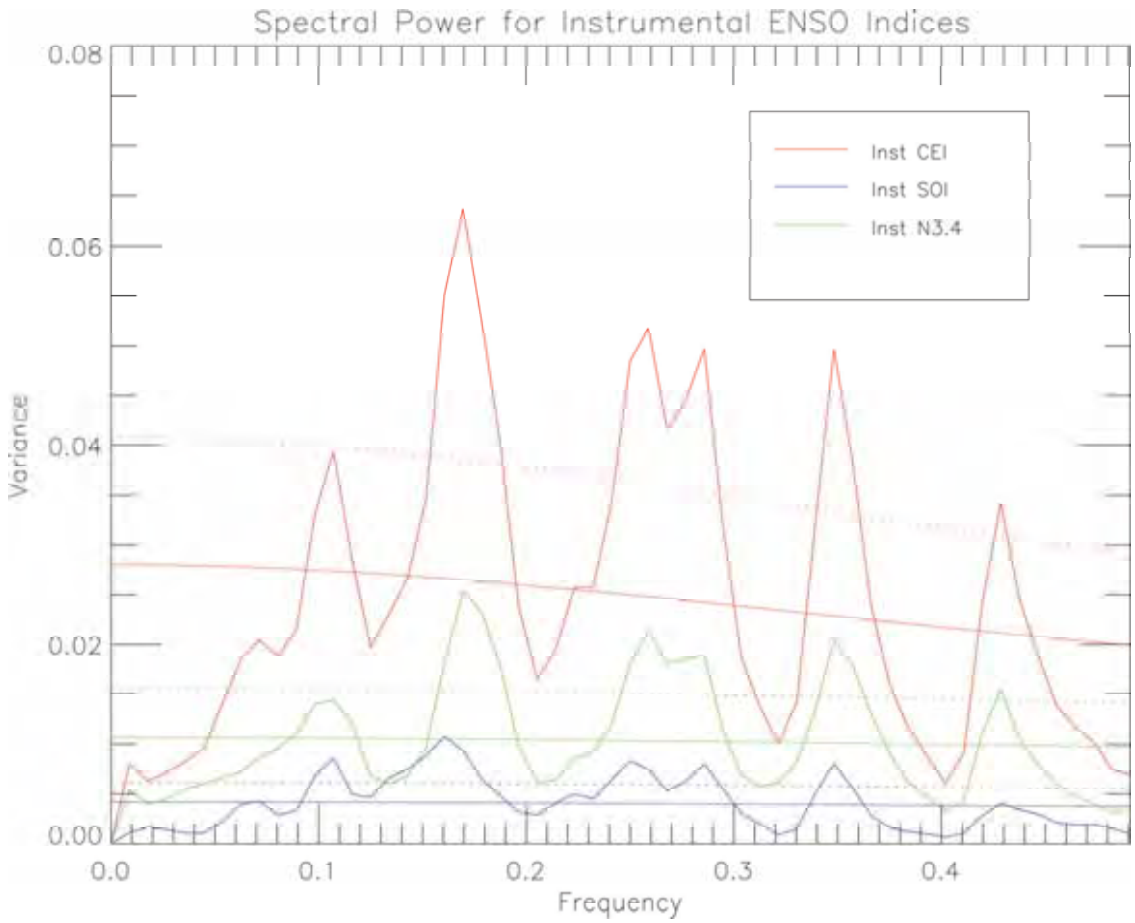

Figure 6.6. A comparison of un-normalised Power spectrum (un-normalised variance). characteristics of instrumental CEI (red), Niño 3.4 SST (black) and SOI (blue) indices. A.D. 1871-1982. Dashed lines indicate 90% (solid lines) and 95% significance level (dotted line) is estimated relative to background AR1 red noise for each index.

As seen from Figure 6.7, both PCs display spectral peaks at inter-annual and near decadal timescales. The most prominent peaks in both PC1 and PC 2 occur at 3.5- 4 year and 5.5–7 year bands. These peaks correspond well to the 'classic' 2-7 year ENSO frequencies noted in the literature (Allan, 2000), suggesting the reconstructions are capable of reproducing the main spectral features of the instrumental record. Furthermore, a prominent decadal peak in both PCs is centred around ~10 years which is also consistent with identification of lower-frequency modes in the instrumental record (Allan, 2000; D'Arrigo *et al.*, 2005).

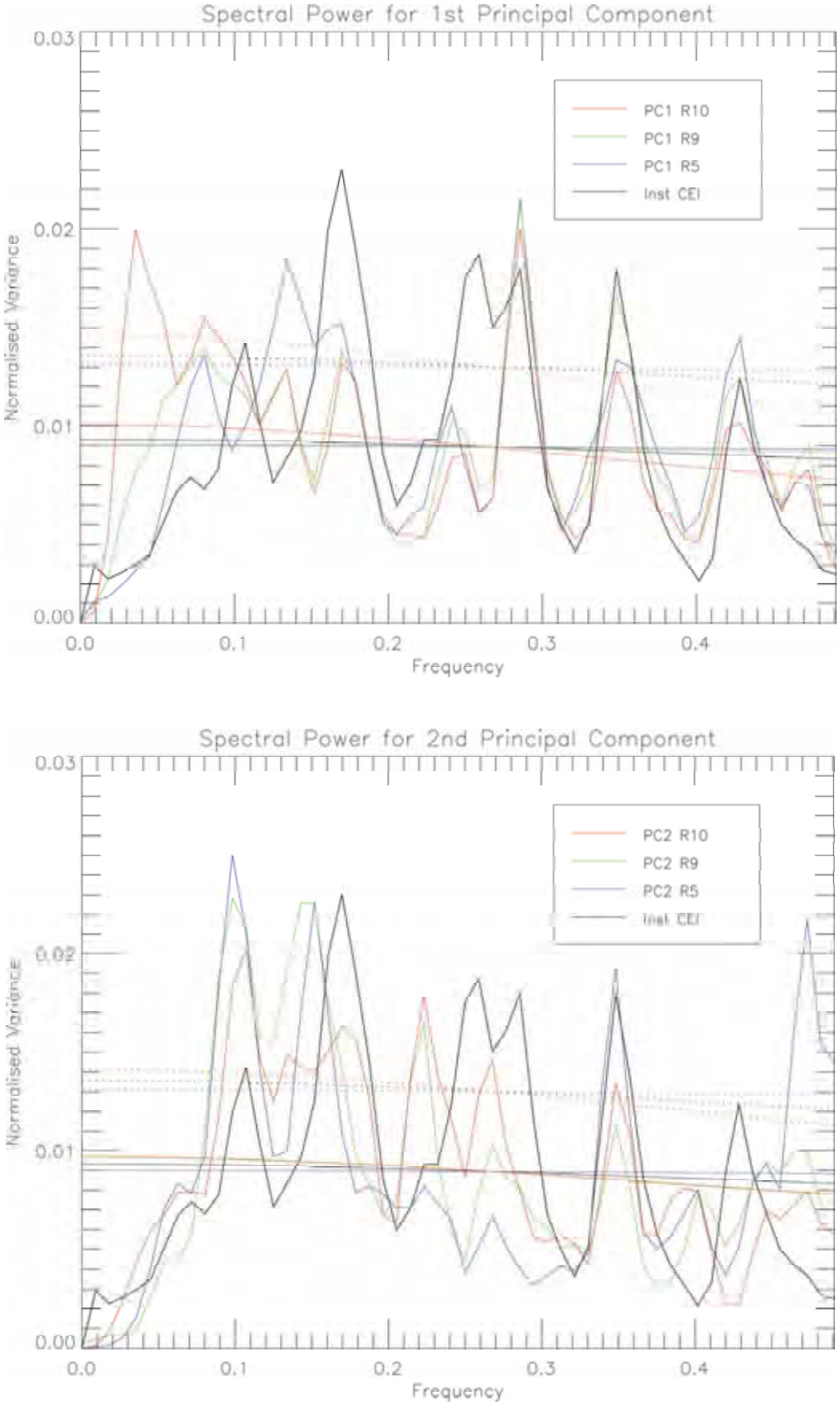

Figure 6.7. Spectral characteristics of normalised instrumental CEI (black) and PC 1 (top) PC 2 (bottom) derived from reconstructed 1871 (R10- green), 1727 (R9-blue) and 1525 (R5-red) datasets. Dashed (solid) lines indicate significance at the 90 (99) % confidence level.

Having established the ability of the reconstructions to capture dominant ENSO signals observed from the instrumental record, further analysis was undertaken on each of the reconstructed CEI, SST and Niño 3 SST indices. Hovmoller or evolutive power spectral density (PSD) plots, indicating temporal fluctuations in the spectral power across the frequency domain, were plotted to highlight changes in ENSO variance since A.D. 1525 (Figure 6.8). This analysis revealed that the March-July period in Niño 3.4 SST PSD plot indicates periods of intensification in spectral power around the early 17th century and mid 18th century, indicated by dark shading in Figure 6.8, a trend not as marked in the SOI and CEI reconstructions.

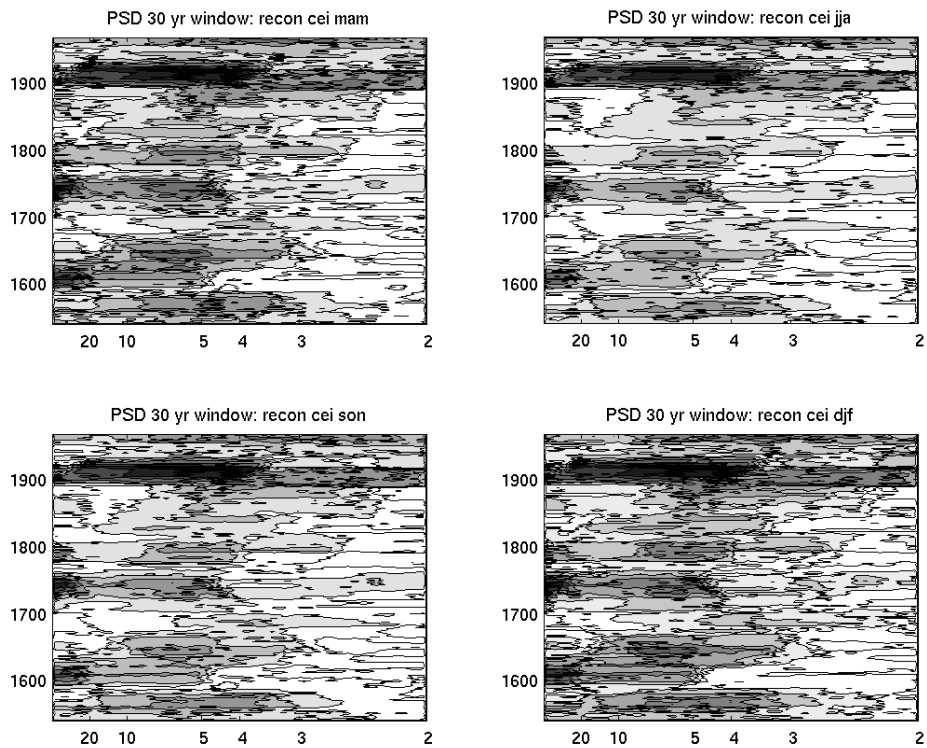

Figure 6.8. Spectral Density (PSD) characteristics using 1525 data sets for CEI, Dark (light) shading indicates intensified (weakened) PSD features in the reconstruction. *Continued overleaf*

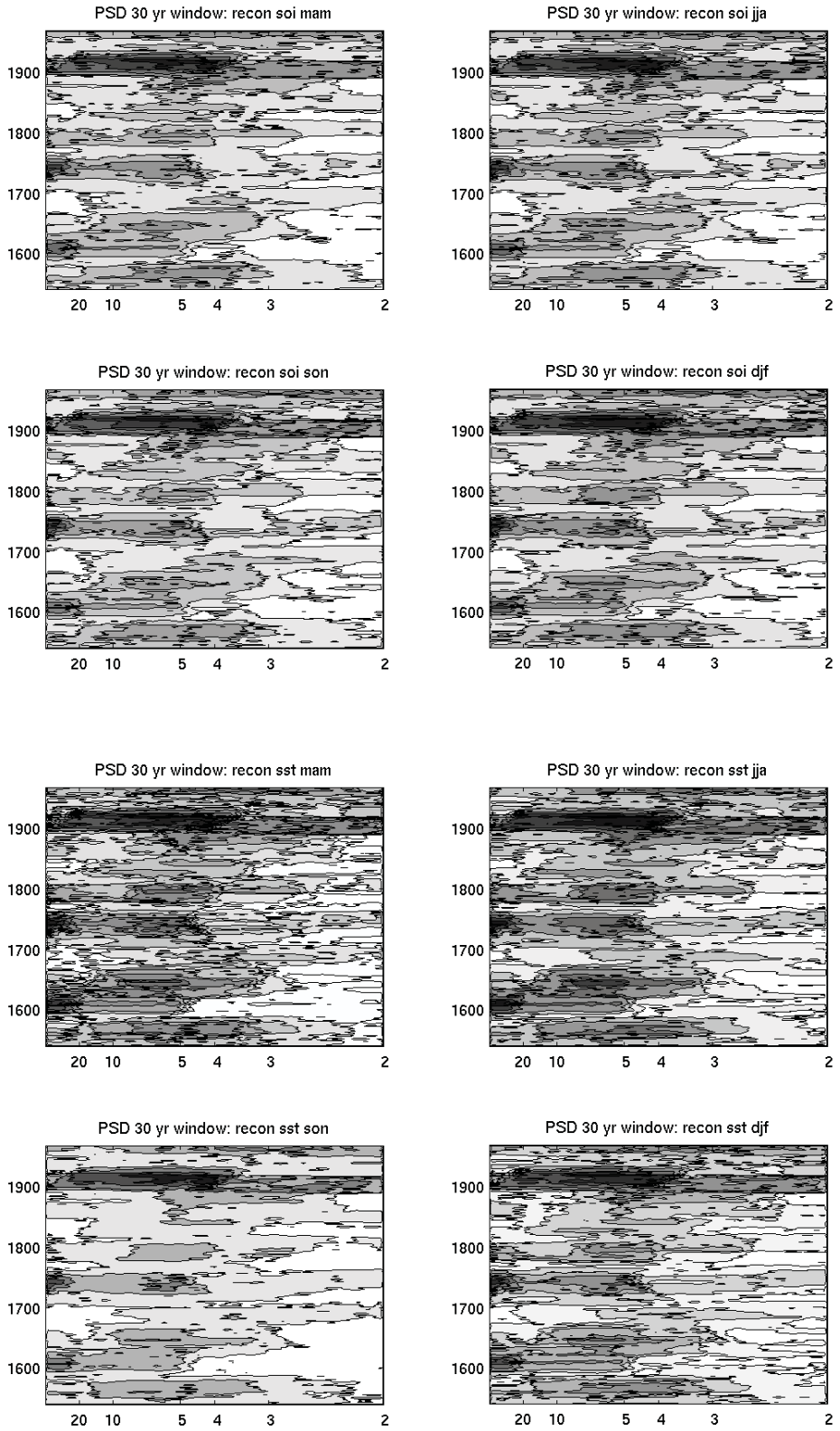

Figure 6.8. *continued* Seasonal comparison of Power Spectral Density (PSD) characteristics using 1525 data sets for (a) SOI (upper panel) and (b) Niño 3.4 SSTs (lower panel). Dark (light) shading indicates intensified (weakened) PSD features in the reconstruction.

The results present in Figure 6.8 are consistent with instrumental spectral peaks identified in Figure 6.6, and indicate considerable variability within 'classical' ENSO bandwidths over the past five centuries. The variability appears to be grouped in three frequency bands, defined here as 2-4 years, 4-8 years and 8-20 years. To further examine these changes, a 30-year sliding window of mean PSD was plotted for these three bands for the CEI reconstruction Figure 6.9. It is important to note that the frequency bands do not represent discrete modes of variability; but rather they were selected on the grounds of apparent changes in PSD structure shown in Figure 6.8.

The considerable enhancement of spectral power at all frequencies in the early 20th century, representing concurrent increases in power of signals across all three frequencies is immediately apparent from Figure 6.9. The magnitude of all frequency bands begins to rise sharply from A.D. 1830, culminating in a late 19th to early 20th century peak when a very prominent enhancement in mean power across the defined frequency bands occurs. In addition, this interval corresponds to some of the most extreme events registered over the entire record (see section 6.10, and Chapter 5).

Figure 6.9 suggests considerable amplitude and frequency modulation of the ENSO signal since A.D. 1525. Interestingly, the interval follows the termination of the Maunder Minimum period of low solar activity (A.D. 1645-1715) (Eddy, 1977) characterised by lows in the mean PSD trends shown in Figure 6.9. Following this weakening, a period of enhanced ENSO activity occurs between A.D. 1740-1770, particularly in the form of intense La Niña events (also identified in Chapter 5), and is characterized here by increased 8-20 year variability. For the 4-8 year frequency band, two prominent peaks are observed in the ~A.D. 1650 and early 20th century. Relatively minor fluctuations in variance are seen between ~A.D. 1680-1820, before the very prominent increase in variance culminates in the early 20th century peak.

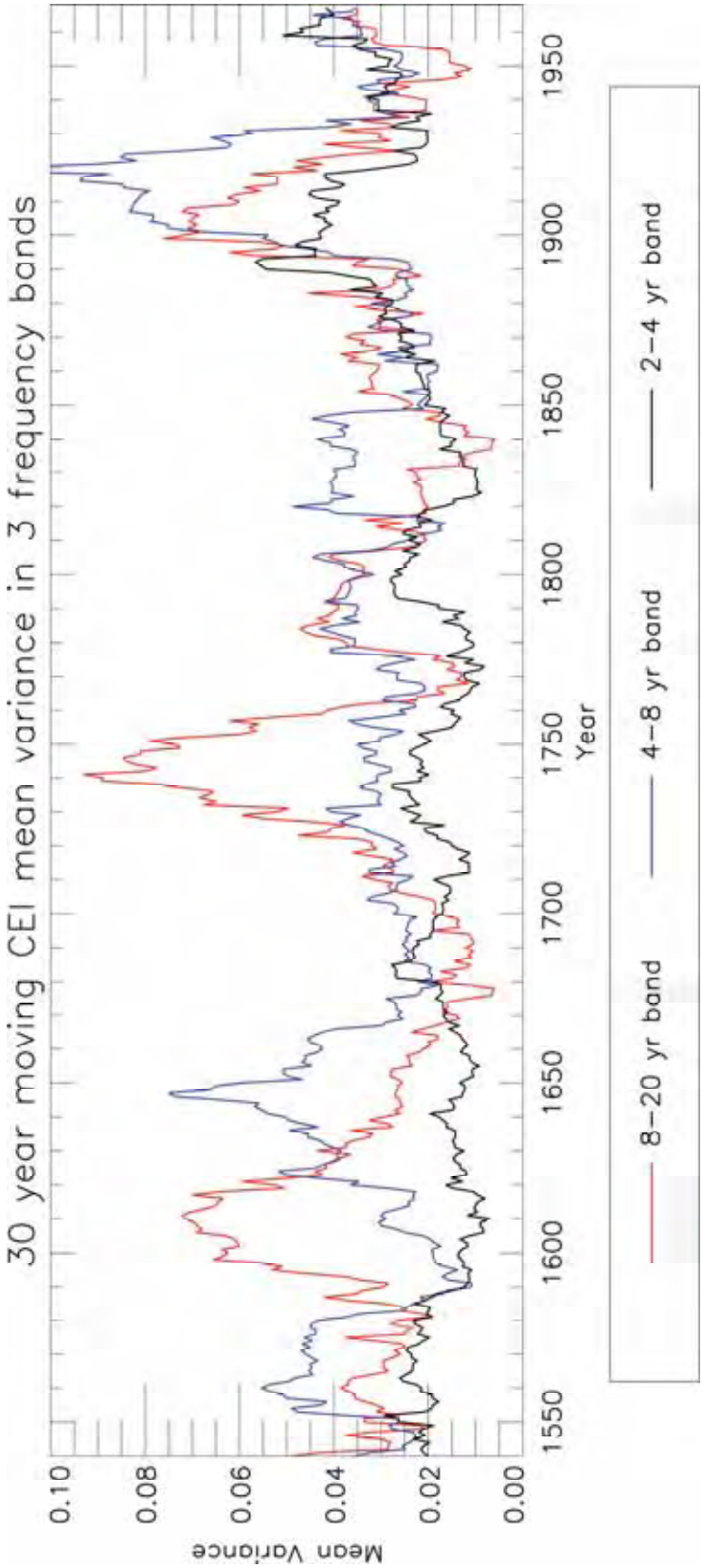

Figure 6.9. A 30-year sliding window of mean power spectral density (PSD) variance for DJF CEI plotted for three distinct frequency bands of 2–4 years (black), 4–8 years (blue) and 8–20 years (red).

By inspecting Figure 6.10, two main periods of PSD enhancement are identified as occurring between A.D. 1900-1920, and to a lesser degree between1940-1960. The first intensification took place between 1900-1920, when spectral power is enhanced across a several frequencies in the 3-10 year domain. A second more subdued peak around 1960 is more closely centred on low frequency (~10 year) variance. These periods are consistent with findings noted elsewhere in the literature (Allan, 2000). Section 6.9, which addresses the issue of discrete event capture, further discusses the phase trends noted during these periods.

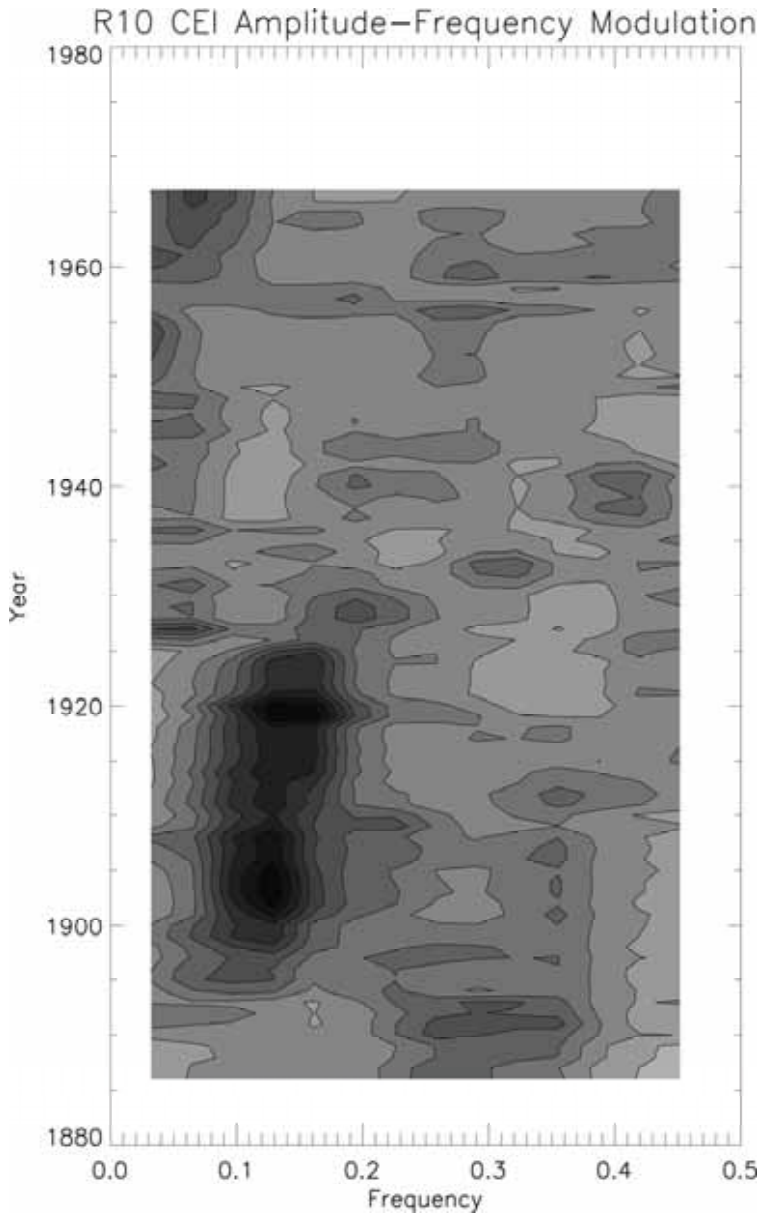

Figure 6.10. Trends in 20th century amplitude-frequency characteristics for the DJF CEI reconstructions using A.D. 1871 (R10) data.

6.8.2 Long-term changes in variance

To examine long-term changes in mean ENSO magnitude over time, sliding variance plots were applied to both instrumental and reconstructed ENSO indices. First, changes in ENSO variability during the calibration period (A.D. 1871-1982) were first examined using 10-year sliding variance plots for each of the R5, R9 and R10 DJF CEI reconstructions shown in Figure 6.11. The most striking feature is that none of the reconstructions are able to reproduce the variance exhibited by the instrumental record with fidelity. This is seen most clearly around A.D. 1890, 1920 and 1940. Encouragingly, however, all three CEI reconstructions perform similarly over the calibration period.

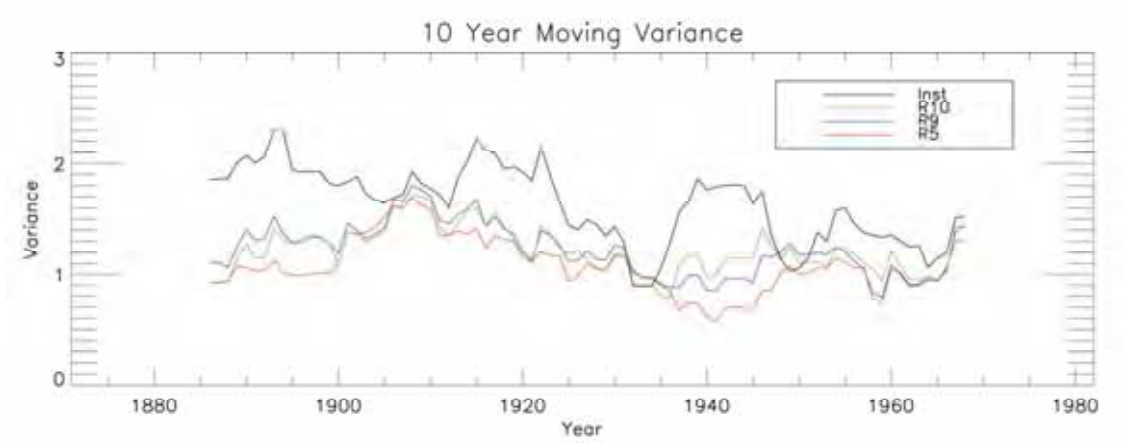

Figure 6.11. Comparison of instrumental (black) and reconstructed variance for DJF CEI 1871 (R10), 1727 (R9), and 1525 (R5) reconstructions. Note that the reconstructions are unable to reproduce variance exhibited in the instrumental data.

To compare long terms changes in ENSO magnitude, sliding variance plots with a 10-year window were applied to the long-term ENSO SST reconstructions of MBH00 and Cook05 (Figure 6.12). Notably, the Niño 3.4 SST reconstructions exhibit the same overall trends seen by previous reconstructions. However, some differences in the magnitude of variance are noted in the mid 18th century and at the beginning of the 20th century.

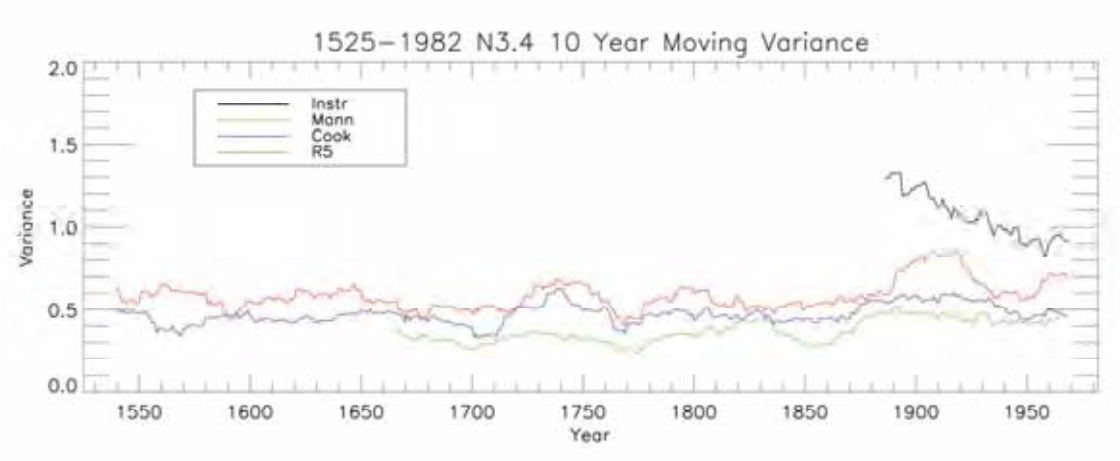

Figure 6.12. Comparison of sliding 10 year variance of DJF CEI (red), Mann Niño 3 SST (green) and Cook Niño 3 SST (blue) ENSO reconstructions with instrumental variance plotted (black) for comparison. Note that the reconstructions are unable to reproduce variance exhibited in the instrumental data.

6.9 ENSO Event Capture

6.9.1 Methodology

To quantify the degree of discrete ENSO event capture for each reconstruction a standard deviation definition of ENSO events was used, following the approach of Stahle *et al.* (1998). For the definition of an El Niño (La Niña) event, the reconstruction value had to fall below (exceed) one standard deviation relative to the long-term mean of each reconstruction. To be classified as an extreme event, the threshold was raised to two standard deviations. The reconstruction skill for each reconstruction derived herein (R5, R9 and R10), and previous attempts were assessed for the A.D. 1871-1982 calibration period (Table 6.10). Events were defined as periods with greater than one standard deviation defined from reconstructions and instrumental indices over the 1871-1982 base period. Event *years* were defined as the total number of years above a given standard deviation threshold, while discrete *events* were defined as the occurrence of each discrete episode. As an example, three event years collectively make up one event.

A 'percentage success' diagnostic was calculated to represent the ratio of correctly reconstructed events compared to events defined using direct instrumental indices. A 'percentage failure' ratio was also used to represent the number of falsely identified

events (false positives) relative to the total number of reconstructed events. In this analysis, reconstruction 'skill' scores were then calculated by subtracting the % failure from % success, with a maximum score of 1 (-1) indicative of the detection of all accurate (false positive) events. To verify the accuracy of the trends indicated by our reconstructions, comparison with previous PCA and discrete ENSO event reconstructions were made.

6.9.2 ENSO event capture

The R10 reconstruction set showed close agreement with instrumental event capture for each corresponding ENSO index shown in Table 6.10. Interestingly, however, the well-replicated R9 data set (which includes all coral records) shows the highest degree of event capture for both ENSO phases in all instances. The close agreement of event capture statistics for the instrumental period across all indices noted for the R9 and R5 reconstructions may reflect the internal quality of the constituent proxy records used for reconstructing ENSO.

During the instrumental period, the R9 DJF CEI reconstruction has the greatest skill in accurate El Niño event capture (0.58), while the R9 MAM Niño 3.4 SST reconstruction displayed the best skill in accurate La Niña event detection (0.53). Despite showing very good El Niño skill (0.42-0.65), the SOI-based reconstructions were found to have virtually no skill in discerning La Niña events. The CEI reconstructions have greater skill in La Niña event detection (maximum skill of 0.33 for the R9 reconstruction) than the SOI, but comparatively less La Niña skill compared to the SST reconstructions.

Of the previous reconstructions listed in Table 6.11, the Cook05 reconstruction was found to have the highest El Niño event skill (0.68). Based on the criteria proposed here, the ST98 reconstruction showed virtually no skill in detecting El Niño events (0.03), in line with the other SOI reconstructions shown in Table 6.10. The MBH00 reconstruction performed well in both event phases during the instrumental period, however, the total number of events captured during the pre-instrumental period is lower than other reconstructions seen in Table 6.11. Generally, these results may suggest that El Niño events are better captured using a SOI or CEI based reconstruction, while SST based indices may be more appropriate for La Niña prediction.

Table 6.10. Reconstruction skill assessment for each reconstruction R5, R9 and R10, as well as previous reconstructions for 1871-1982 for DJF CEI, DJF SOI and MAM N3.4 SST. Note that for the Niño 3 SST reconstructions, event comparison was assessed relative to instrumental Niño 3.4 SST anomalies.

Data set	Event Years	Total Events	False Positives	Missed Events	Success (%)	Failure (%)	Skill Score
CEI El Niños							
Instrumental	21	16	-	-	-	-	-
R10	15	11	2	5	0.69	0.15	0.53
R9	20	13	4	3	0.81	0.24	0.58
R5	18	11	5	5	0.69	0.31	0.38
CEI La Niñas							
Instrumental	19	15	-	-	-	-	-
R10	18	8	5	7	0.53	0.38	0.15
R9	20	10	5	5	0.67	0.33	0.33
R5	16	8	4	7	0.53	0.33	0.20
SOI El Niños							
Instrument	18	12	-	-	-	-	-
R10	17	11	4	1	0.92	0.27	0.65
R9	20	10	7	2	0.83	0.41	0.42
R5	18	10	6	2	0.83	0.38	0.46
Stahle SOI	24	9	8	3	0.75	0.47	0.28
SOI La Niñas							
Instrumental	18	15	-	-	-	-	-
R10	18	8	5	7	0.53	0.38	0.15
R9	22	10	7	5	0.67	0.41	0.25
R5	16	7	6	8	0.47	0.46	0.01
Stahle SOI	17	8	8	7	0.53	0.50	0.03
SST El Niños							
Instrumental	18	14	-		-	-	-
R10	18	10	3	4	0.71	0.23	0.48
R9	19	8	4	6	0.57	0.33	0.24
R5	19	10	4	4	0.71	0.29	0.43
Mann Niño 3	19	12	4	4	0.75	0.25	0.50
Cook Niño 3	22	13	2	3	0.81	0.13	0.68
SST La Niñas							
Instrumental	19	16	-	-	-	-	-
R10	16	11	2	5	0.69	0.15	0.53
R9	21	13	5	3	0.81	0.28	0.53
R5	18	11	5	5	0.69	0.31	0.38
Mann Niño 3	16	11	3	4	0.73	0.21	0.52
Cook Niño 3	18	9	9	6	0.60	0.50	0.10

Table 6.11. El Niño event identification of reconstructions R5, R9 and R10, as well as previous reconstructions of ST98, MBH00, Cook05 for 1525-1871 using DJF CEI, DJF SOI and MAM Niño 3.4 SST. Events were defined as periods with greater than one standard deviation from reconstructions and instrumental indices over the entire period of the reconstruction. Event years were defined as the total number of years above the threshold, while discrete events were defined as single continuous periods above the threshold. Comparison is made with the R9 reconstruction for the instrumental period 1871-1982.

CEI DJF El Niño events				
Data	**Period**	**Event Years**	**Events**	**Event/10 years**
R5	1525-1726	31	25	1.23
R5	1727-1870	22	19	1.32
R9	1727-1870	23	17	1.18
R9	1871-1982	21	18	1.61

SOI DJF El Niño events				
Data	**Period**	**Event Years**	**Events**	**Event/10 years**
R5	1525-1726	34	27	1.33
R5	1727-1870	22	19	1.32
R9	1727-1870	23	18	1.25
ST98	1727-1870	27	16	1.11
R9	1871-1982	21	17	1.52

SST MAM El Niño events				
Data	**Period**	**Event Years**	**Events**	**Event/10 years**
R5	1525-1649	18	16	1.28
Cook05	1525-1649	13	12	
R5	1650-1726	9	7	0.91
Cook05	1650-1726	8	7	0.91
MBH00	1650-1726	2	2	0.26
R5	1727-1870	18	14	0.97
R9	1727-1870	17	13	0.90
Cook05	1727-1870	14	10	0.69
MBH00	1727-1870	10	8	0.56
R9	1871-1982	25	18	1.61

6.9.3 Comparison with CEI events

To provide a common basis for event capture comparison, all records were compared to instrumental events identified by Gergis and Fowler (2005) (Table 6.12). In line with the approach of Stahle *et al.* (1998), event definition thresholds were based on the long term mean and standard deviation of each reconstruction rather than the characteristics of the instrumental base period. Table 6.12 indicates a high degree of consistency with instrumental event capture across all indices and sub intervals. Of all the reconstructions the R9 data set indicated the highest degree of event capture, with La Niña phase events suffering most from a loss of replication (also noted in Chapter 5). Nevertheless, it is encouraging to observe that the pre-instrumental frequencies are similar across all indices and the loss of sample depth appears to have virtually no impact on overall event capture. However, the frequency of extreme events appears to be underestimated by all reconstructions when compared to instrumental event capture.

Although the MBH00 shows good event accuracy during the instrumental period (Table 6.9), only 29 La Niña events (12 of which classed as extreme events) were reconstructed back to A.D. 1650 (Table 6.13). This is in contrast to the total number of reconstructed events seen in other reconstructions. In fact, the shorter ST98 reconstruction indicates eight more events than the MBH00 reconstruction; although the skill of these reconstructed events is substantially lower (see Table 6.11). Furthermore, during the instrumental period, 11 extreme events are noted from MBH00, nearly twice the number registered from the observational CEI record.

Careful inspection of the number ENSO events reconstructed from the Cook05 relative to instrumentally observed events (1871-1982) indicates a potential for over (under) reconstruction of La Niña (El Niño) episodes, consistent with the findings of Hanley *et al.* (2003). The tendency to over reconstruct La Niña events is also noted from the CEI and ST98 reconstructions, but to a lesser degree. It is possible that these results reflect the fact that the instrumental list of ENSO events defined by the CEI only relate to coupled ENSO episodes, thus some decoupled (i.e. exclusively atmospheric or oceanic anomalies) events may not be accounted for.

Interestingly, the highest total number of El Niño events were reconstructed using the two discrete event approaches, the 'Quinn' records (Quinn and Neal, 1992; Ortlieb, 2000) and the event chronology presented in Chapter 5. This may result from the

regression-based approach which truncates statistical outliers, potentially resulting in a loss of variance (Von Storch *et al.*, 2004; Moberg *et al.*, 2005).

Table 6.12. Sensitivity of discrete CEI defined ENSO event capture due to a loss of replication back using the 1871, 1727, and 1525 data used to reconstruct ENSO indices for the season exhibiting the strongest signal for both the instrumental (1871-1982) and pre-instrumental (1870-1727) periods. Note that the relative frequency of extreme event years shown in brackets.

ENSO Reconstruction	1871-1982 El Niño events (extremes)	1871-1982 La Niña events (extremes)	1727-1870 El Niño events (extremes)	1727-1870 La Niña events (extremes)
CEI DJF				
Instrumental	20 (7)	18 (6)	-	-
1871	13 (3)	13 (2)	-	-
1727	17 (1)	15 (3)	20 (3)	18 (2)
1525	16 (2)	12 (2)	18 (5)	18 (2)
SOI DJF				
1871	15 (3)	13 (2)	-	-
1727	17 (2)	17 (2)	20 (3)	18 (2)
1525	17 (5)	12 (1)	20 (5)	19 (2)
Niño 3.4 MAM SST				
1871	13 (3)	13 (2)	-	-
1727	18 (1)	14 (3)	20 (3)	17 (2)
1525	16 (2)	14 (2)	18 (5)	17 (2)

6.9.4 Extreme event analysis

It is noteworthy that all the reconstructions listed in Table 6.13 underestimate the frequency of extreme ENSO events noted in the instrumental CEI record. With the exception of the 1525 DJF SOI reconstruction all the reconstructions reconstruct between 15-50% of the extreme ENSO events (for both phases) noted in the instrumental period. The tendency for the observed underestimation of La Niña extremes may reflect the relatively weaker event magnitudes noted from instrumental data (Gergis and Fowler, 2005). This may be of significance to proxy records which are likely to be expressed as anomalously high or low values, hence may not be accounted for in commonly generated transfer functions. Hence, higher values may reflect decoupled event signatures noted above.

Table 6.13. Comparison of instrumental and reconstructed discrete ENSO events, A.D. 1525-1982. Note that the use of the A.D. 1707 (1525) sub-period cut-off date corresponds to the termination of the ST98 (CEI) reconstruction. For the definition of an El Niño (La Niña) event, the reconstruction value had to fall below (exceed) 1 standard deviation relative to the long-term mean of each reconstruction. To be classified as an extreme event, the threshold was raised to 2 standard deviations. Note that the relative frequency of extreme event years shown in brackets and that very-strong 'Quinn' events were used to represent extreme El Niño conditions for the purpose of this analysis. The 'Gergis and Fowler' reconstruction refers to the ENSO event chronology presented in Chapter 5.

ENSO Reconstruction		El Niño events (extremes)	La Niña Events (extremes)
Instrumental CEI			
1871-1982		20 (7)	18 (6)
CEI DJF			
1871-1982		18 (7)	19 (4)
1707-1870		23 (3)	19 (2)
1525-1706		20 (4)	17 (0)
	Total	61 (14)	55 (6)
SOI DJF			
1871-1982		18 (8)	20 (5)
1707-1870		24 (3)	20 (2)
1525-1706		19 (4)	17 (0)
	Total	61 (15)	57 (7)
Niño 3.4 MAM SST			
1871-1982		19 (6)	19 (4)
1707-1870		23 (3)	18 (2)
1525-1706		19 (4)	20 (1)
	Total	61 (13)	57 (7)
Cook Niño 3 SST			
1871-1982		13 (4)	22 (4)
1707-1870		20 (5)	19 (3)
1525-1706		22 (2)	23 (4)
	Total	55 (11)	64 (11)
Stahle SOI			
1871-1982		15 (5)	19 (4)
1707-1870		17 (3)	18 (0)
1525-1706		-	-
	Total	32 (8)	37 (4)
Mann Niño 3 SST			
1871-1982		14 (1)	16 (11)
1707-1870		16 (1)	11 (1)
1525-1706		8 (1)	2 (0)
	Total	38 (3)	29 (12)
Quinn and Ortlieb			
1871-1982		28 (6)	-
1707-1870		43 (4)	-
1525-1706		39 (2)	-
	Total	110 (12)	-
Gergis and Fowler			
1871-1982		25 (5)	18 (5)
1707-1870		31 (3)	34 (1)
1525-1706		34 (1)	26 (6)
	Total	90 (9)	78 (12)

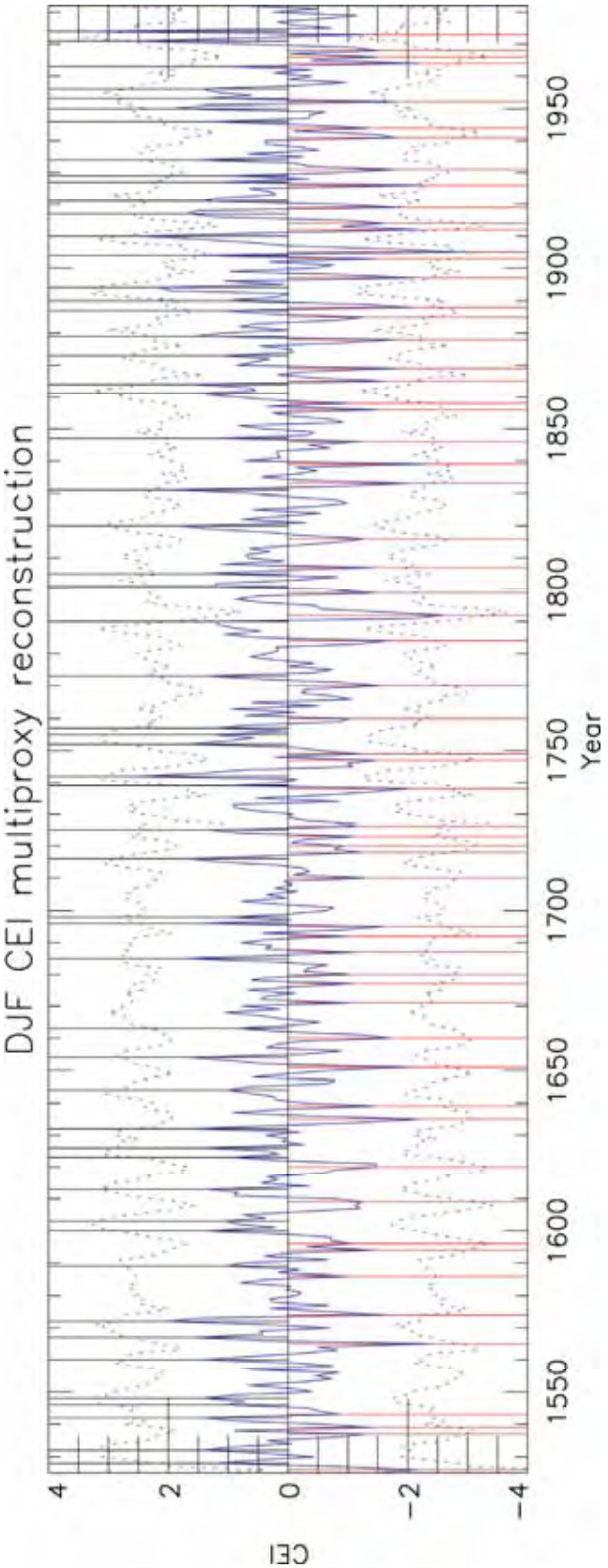

Figure 6.13. Summer (DJF) CEI reconstruction with El Niño (red) and La Niña (black) events annotated. ENSO events are defined as exceeding 1 standard deviation threshold relative to the mean and standard deviation of the A.D. 1871-1982 calibration period. Dashed line indicated 2 standard deviation uncertainty estimates. Combined reconstructions R5 and R9 DJF CEI for 1525-1982.

It is clear that the instrumental period (1871-1982) contains the highest frequency of extreme events of all the reconstructions analysed (Figure 6.13), despite being the shortest interval of the sub-periods examined (Table 6.13). Of the 10 extreme La Niña events reconstructed from each of the ENSO indices, 40% occur within the 20th century, with 1974, 1971 and 1910 identified as the most extreme years reconstructed since A.D. 1525 from each index. The extreme La Niña event years of 1917 and 1950 are also common across all indices.

Similar trends were also observed from each of the El Niño phase reconstructions. Significantly, 40% of the 10 most extreme El Niños observed from the R5 CEI and Niño 3.4 SST reconstructions, along with 50% of the 10 most extreme SOI, all occur within the 20th century. The three most extreme years common to all indices are the years of 1905, 1964 and 1912, while the El Niño years of 1919, 1916 and 1941 were also identified within the top 10 extreme El Niño years since A.D. 1525.

When assessing the results from the R9 reconstructions the trend is slightly more pronounced. From the CEI, 60 (50) % of the ten most extreme El Niños (La Niñas) occur in the 20th century. From the SOI (SST) record 60 (50) % of the 10 most extreme El Niño events and 40(50)% of the 10 most extreme La Niña events are contained within the post 1900 period. The fact that the extreme ENSO events years are verified independently in each of the atmospheric and oceanic indices and by the CEI, reinforces that coupled anomalies produce the highest ENSO event magnitudes. Finally, the results confirm that greater potential predictability for extreme warm events exists compared to extreme cold events, a likely consequence of the stronger seasonal mean signal exhibited during extreme El Niño conditions (Hoerling, 2001).

6.10 Teleconnection Analysis

The strength of the regional teleconnection patterns associated with ENSO events are known to have varied during the observational and pre-instrumental periods (Stahle *et al.*, 1998; Allan, 2000; Mann *et al.*, 2000a; Hendy *et al.*, 2003). While co-variability over the whole analysis period may be strong between individual proxy sites, these relationships may not hold for certain periods of the record. This is similar to the variability of the strength of co-variability (represented in the eigenvectors) projected onto the PC time series.

To identify non-stationarities in the stability of the ENSO signal identified, 21-year running correlations between individual regional records and DJF CEI multiproxy reconstructions were calculated (Figure 6.14 and Figure 6.15). Fluctuating correlations here reflect the strength of a regional response to large-scale ENSO forcing represented by the multiproxy CEI reconstructions.

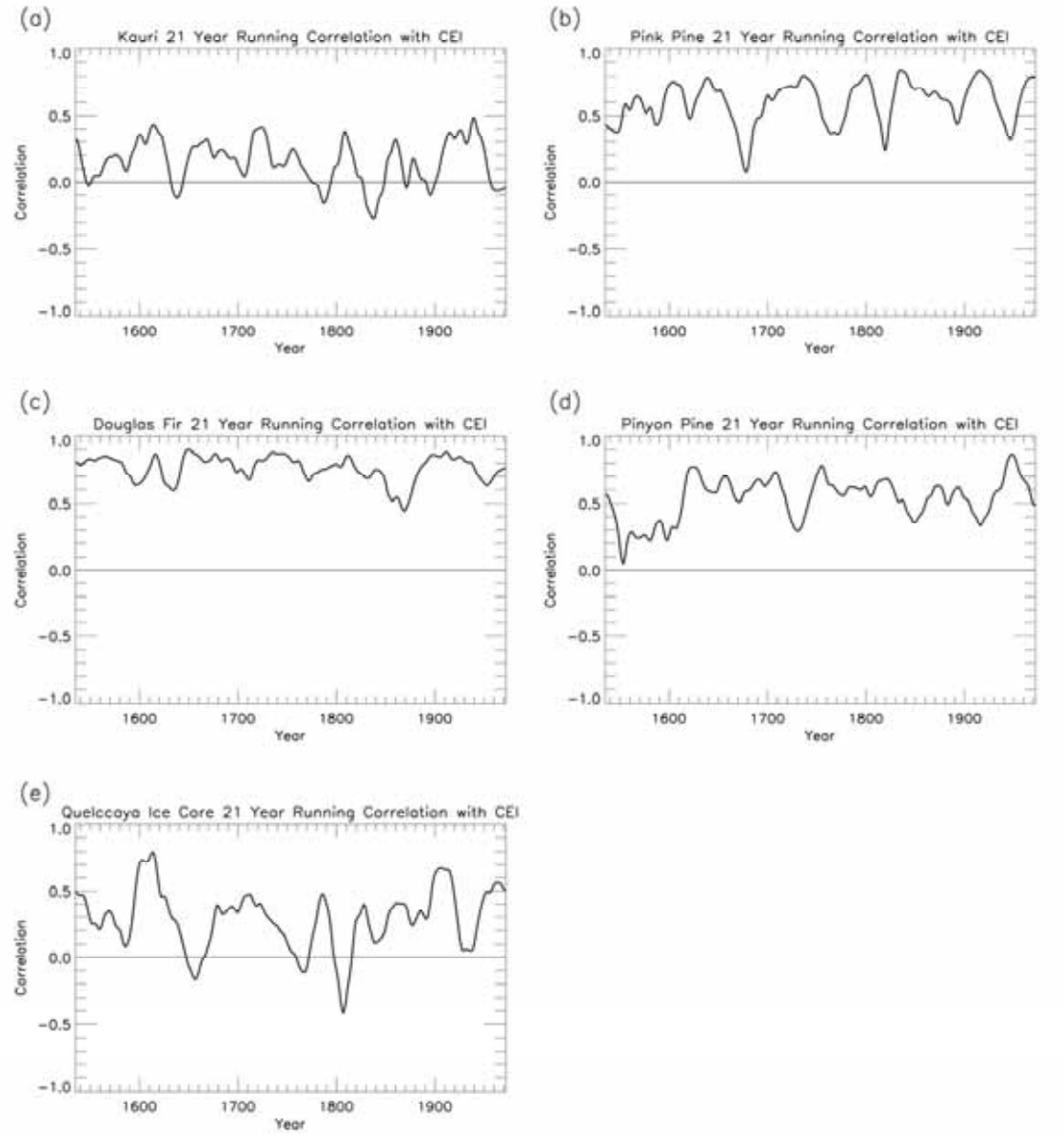

Figure 6.14. 21-year running correlations between regional tree-ring and ice records and R5 DJF CEI reconstructions.

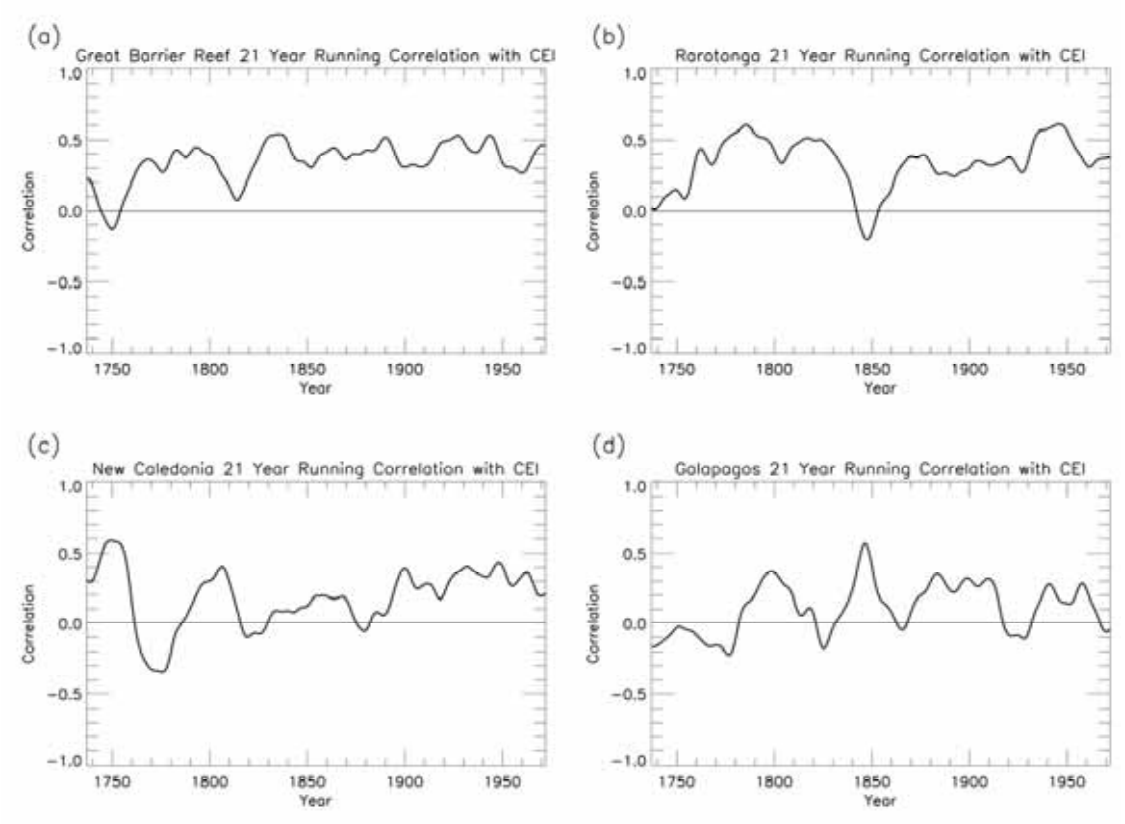

Figure 6.15. 21-year running correlations between regional coral records and R9 DJF CEI reconstruction.

It is evident from Figure 6.14 and Figure 6.15 that ENSO sensitivity in each regional record has not remained stationary over the past five centuries. The region showing the highest degree of stability is the Mexican Douglas Fir tree-ring record, while the coral sequences display the highest degree of variability.

The Kauri record not only contributes the highest loading in PC2 (0.61), but the record also exhibits a high degree of variability. The south-western USA tree-ring chronology which has a high loading for both PC 1 (-0.40) and PC2 (-0.39) also displays considerable variability as seen in Figure 6.14. These results imply that fluctuations in correlations between individual proxy records and the multiproxy reconstruction may reflect real changes in teleconnection strength. Hence, simultaneous peaks may represent periods when all sites are well correlated with the loading (temporal fluctuation) of the dominant common mode of variability defined by the given PC.

There are number of periods when the reconstructions exhibit synchronous periods of strong ENSO teleconnection. This occurs in early 17th century in all the tree-ring records (Figure 6.14) and mid-20th century in the coral proxies (Figure 6.15). There are

also some weakening in the relationship, most notably in the mid 19th and mid 17th centuries as seen in several records in both Figure 6.14 and Figure 6.15.

It is also possible to examine shifts in correlations between regional signals with respect to the large-scale ENSO multiproxy reconstruction. Figure 6.14 and Figure 6.15 indicate inconsistencies in teleconnection characteristics, particularly in regards to the coral sequences. Indeed, there are periods when the weakening of teleconnection patterns are characterised by a reversal in sign of the correlations. This is seen most clearly during the mid-18th to mid-19th centuries in the New Caledonia, Galapagos, Kauri and Quelccaya records. In other proxies such as the South-western USA, Mexico and Pink Pine chronologies, the response during this period is dampened, indicated by a decline rather than a reversal in correlations. This may be indicative of proximities to ENSO centres of action, stronger relational teleconnection or dating issues noted for the coral and ice sequences (discussed in Chapter 3). Significantly, this analysis highlights that regional ENSO signals have indeed fluctuated considerably through time, thus, one proxy alone cannot be considered to be representative of large-scale ENSO behaviour.

6.11 ENSO Since A.D. 1525

It is clear that considerable improvements in ENSO reconstruction are possible using a data set which expands upon records available from the Western Pacific. This was also raised by Stahle *et al.* (1998), who reported that the Indonesian Teak record had the single highest beta weight (PC loading) of the 21 tree-ring chronologies used in the development of their SOI reconstruction.

Indeed, the results shown in Table 6.3 further confirm the recognised importance of data from this region for the purpose of ENSO reconstruction (D'Arrigo *et al.*, 1994; Stahle *et al.*, 1998). This is most obvious in the case of the Kauri tree-ring record which contributes the highest loading of PC2 and the considerable influence the Pink Pine and Great Barrier Reef chronologies have in the two leading modes of co variability (PCs) analysed here. This supports the findings of Mann *et al.* (2000) who recognised that a more skilful Niño 3 SST reconstruction was achieved using a limited 'tropical' subset of proxies (from approximately 20 distinct sites) than was possible from the entire proxy network used for the global reconstructions. The merit of a multiproxy approach

to ENSO reconstruction data from both east and west Pacific centres of action has been further confirmed by this study.

Considered collectively, the set of proxy data resolves two orthogonal modes of co-variability that are clearly dominated by ENSO. These modes provide robust reconstructions of CEI, SOI and N3.4 SST over the 20th century (R10) as well as extended reconstructions R5 and R9. While the full set of proxies provides the best results in terms of 20th century verification, the smaller subsets of R5 and R9 do not provide greatly degraded reconstructions. Significantly, of the three indices used here, greatest correspondence/skill was found in CEI reconstructions, indicating that the proxy response is best suited to capture indices that attempt to account for both ocean and atmosphere components of ENSO variability.

The extended ENSO reconstructions presented in this Chapter confirm considerable fluctuations in ENSO variability over the past five centuries. In particular, evidence of low frequency changes in the amplitude and frequency of ENSO variability suggested by previous modeling and proxy reconstruction studies (Mann *et al.*, 2000a; Mann *et al.*, 2000b; D'Arrigo *et al.*, 2005) is generally found here. A notable period of relative inactivity was identified between A.D. 1650-1780 when ENSO appears to have been weakened, when ENSO events were largely weak or moderate, coincident with the broadly defined 'Little Ice Age' (LIA) (~A.D. 1550-1850), but more specifically, the Maunder Minimum period of low solar irradiance (~A.D. 1645-1715). The results derived from the multiproxy CEI reconstructions indicate low variance from ~A.D. 1650-1720, consistent with timing of the coolest conditions of the LIA which occur between ~A.D. 1570-1730 (Bradley and Jones, 1993; Bradley *et al.*, 2003). These results are also reflected in the Cook05 reconstruction (A.D. 1408-1978), which indicates the lowest variability of the entire reconstruction during the LIA and the Maunder Minimum periods.

These trends were further confirmed by revisiting spectral power density characteristics presented in Figure 6.9. Following the termination of the cool Maunder Minimum period (~A.D. 1720), a marked increase in variance in the 8-20 year frequency band occurred, before another reduction in ENSO variance is observed, consistent with the timing of the Dalton solar minimum (~A.D. 1790-1820) (Reid, 1997). By A.D. 1850 (the termination of the LIA cool interval), there is a prominent increase in ENSO variance in both high and low frequency bands. Thus, it appears that a prominent

decrease (increase) in ENSO activity is indeed coincident with the duration (termination) of the LIA. This finding is further supported by D'Arrigo *et al.* (2005) who presented evidence from North America of lowest ENSO variability over the past six centuries during this time.

D'Arrigo (2005) concluded that ENSO variability appears to be somewhat modulated by external solar forcing. Generally, higher ENSO variability reflected in the Cook 05 tree-ring reconstruction coincided with decreased solar variability in line with recent coral and modeling results (Cobb *et al.*, 2003; Mann *et al.*, 2005). However, a notable exception occurs during the Maunder Minimum when the lowest ENSO variability of the Cook 05 reconstruction was observed. The results presented here show low ENSO variability during the Maunder and Dalton minimums, with pronounced ENSO variability observed during the Damon (A.D. 1870-1930) period of low solar activity.

From the CEI-based reconstruction presented, A.D. 1870-1930 is the only period where enhanced ENSO variability appears to be associated with low solar variability (Damon minimum, A.D. 1880-1930). Furthermore, this period represents the most sustained interval of reconstructed ENSO activity observed since A.D. 1525. Intriguingly, Reid (1997) suggested that the observed temperature increase of around 0.5°C between 1900 and 1955 is only explained when both solar, volcanic and greenhouse forcing are included in the temperature model, suggesting that greenhouse-gas forcing may have been somewhat instrumental in offsetting cooling expected under reduced solar forcing. However, it may also indicate an absence of recent volcanic activity compared to the preceding period.

While it is difficult to determine the reality of past changes inferred from palaeo-reconstructions, it is unclear what mechanisms may have forced such changes. Dynamical studies have suggested that solar, volcanic and anthropogenic radiative forcing have influenced past ENSO variability, particularly a tendency toward El Niño like conditions during periods of radiative cooling (Clement *et al.*, 2000; Cane, 2004; Mann *et al.*, 2005), although the complexity of the atmosphere-ocean feedbacks involved and inconsistency in current ENSO models increase the uncertainty of such conclusions (Collins 2005).

The 20th century period is of special interest in that the frequency of peak spectral power converges in all three bands during this time (Figure 6.9). This feature is accompanied

by an increase in mean variance and increased noise in the frequency domain, particularly at higher frequencies, which may reflect improved resolution over the calibration period. Nonetheless, the 20th century was found to contain a very high proportion of all the extreme events reconstructed since A.D. 1525. The appearance of these apparently unusual changes may be amplified by the fact that trends contained within the calibration period may not be adequately resolved by the pre-instrumental reconstructions, or may be diagnostic of a period of increased warming due to both anthropogenic and natural forcing (Tett *et al.*, 1999; Stott *et al.*, 2001; Karoly *et al.*, 2003; Braganza *et al.*, 2004). While equal power at all frequencies can be associated with monotonic trends, no significant trend in the CEI is found during this time.

Using the data set of Mann *et al.* (1998), a recent study by Damon and Peristykh (2005) revealed that modeled solar irradiance only accounts for about 18% of 20th century global warming to 1997. They concluded that this demonstrates that solar forcing was not a dominant cause of 20th century Northern Hemisphere warming, and that solar forcing was likely to have played a very significant role in the forcing of pre-industrial climate (Damon and Peristykh, 2005). The implication such warming may have on ENSO activity in a greenhouse-gas warmed future is as yet unknown (Collins, 2005; Mann *et al.*, 2005). However, recently Barnett *et al.* (2005) reported that 84% of the total heating of the Earth system over the past 40 years has gone into warming the oceans, which may signal unforeseen influences on ENSO behaviour in the coming decades.

6.12 Summary

The results presented in this Chapter demonstrate that the nature and frequency of ENSO variability and its associated teleconnections have fluctuated considerably over the past five centuries. Expanded representation of western Pacific sites appears to be of importance to large-scale ENSO reconstruction. Importantly, the CEI results suggest a Pacific basin wide representation of ENSO behaviour back to A.D. 1525 is achievable. The results suggest that ENSO may be more effectively characterised using a coupled ocean-atmosphere index, particularly for December-May periods.

Significantly, of the three indices reconstructed here, greatest skill was found in CEI reconstructions, indicating that the proxy response is best suited to capture indices that account for oceanic and atmospheric components. The CEI reconstructions were largely found to be the best predictors of ENSO (for all seasons) compared with the SOI or SST-based ENSO reconstructions. Approximately 59% (45%) of variance in instrumental DJF CEI was explained by the R10 (R5) subset, representing the strongest relationships observed for any index or season, with the exceptions of MAM and JJA Niño 3.4 SSTs.

Discrete chronology and continuous (PCA) based techniques reveal marked differences in ENSO event capture. PCA reconstructions display less sensitivity, reflecting a loss of variance required by the statistical treatment of the data. Generally, the results suggest that El Niño events are better captured using a CEI or SOI based reconstruction, while SST based indices may be more appropriate for La Niña prediction.

A clear trend toward increased ENSO variability over the past 150 years was identified in this study. Compared to the pre-instrumental period, the late 19th and early 20th century period shows increased spectral power at all frequencies. In particular, high frequency variability (~3 years or less) is enhanced during this period, corresponding to a period of extreme ENSO events in recent decades. From the CEI, a maximum of 60 (50)% of the 10 most extreme El Niños (La Niñas) occur in the 20th century. In this study, recent ENSO variability appears unprecedented in the context of the past five centuries, and may reflect the influence of anthropogenic global warming.

6.13 References

Allan, R. (2000). ENSO and climatic variability in the past 150 years. *El Niño and the Southern Oscillation: Multiscale Variability and Global and Regional Impacts.* H. Diaz and V. Markgraf. Cambridge, Cambridge University Press: 3-35.

Allan, R. and D'Arrigo, R. (1999). 'Persistent' ENSO sequences: how unusual was the 1990-1995 El Niño ? *The Holocene* **9** (1): 101-118.

Allan, R., Lindsay, J. and Parker, D. (1996). *El Niño Southern Oscillation and climate variability.* Melbourne, Australia, CSIRO.

Allan, R., Reason, C., Lindesay, J. and Ansell, T. (2003). Protracted ENSO episodes and their impacts in the Indian Ocean region. *Deep Sea Research Part II* **50** (12-13): 2331–2347.

Barnett, T., Pierce, D., AchutaRao, K., Gleckler, P., Santer, B., Gregory, J. and Washington, W. (2005). Penetration of Human-Induced Warming into the World's Oceans. *Science* **309**: 204-287.

Bath, M. (1974). *Spectral Analysis in Geophysics*, Amsterdam, Elsevier Scientific Publishing.

Baumgartner, T., Michaelsen, J., Thompson, L., Shen, G., Soutar, A. and Casey, R. (1989). The recording of interannual climatic change by high-resolution natural systems: tree rings, coral bands, glacial ice layers and marine varves. *Aspects of Climate Variability in the Pacific and Western Americas. Geophysical Monograph*. D. Peterson. Washington, American Geophysical Union. **55:** 1-14.

Bradley, R. (1996). Are there optimum sites for global palaeotemperature reconstruction? *Climate Variations and Forcing Mechanisms of the Last 2000 years.* P. Jones, R. Bradley and J. Jouzel. Berlin, Springer-Verlag**:** 603-624.

Bradley, R., Briffa, K., Cole, J., Hughes, M. and Osborn, T. (2003). The climate of the last millennium. *Palaeoclimate, Global Change and the Future*. K. Alverson, Bradley, R. and Pedersen, T. Berlin, Springer Verlag**:** 105-141.

Bradley, R. and Jones, P. (1993). 'Little Ice Age' summer temperature variations: Their nature and relevance to recent global warming trends. *The Holocene* **3**: 367–376.

Braganza, K., Karoly, D., Hirst, A., Mann, M., Stott, P., Stouffer, R. and Tett, S. (2003). Simple indices of global climate variability and change: Part I: variability and correlation structure. *Climate Dynamics* **20**: 491-502.

Braganza, K., Karoly, D., Hirst, A., Stott, P., Stouffer, R. and Tett, S. (2004). Simple indices of global climate variability and change Part II: attribution of climate change during the twentieth century. *Climate Dynamics* **22**: 823-838.

Braganza, K., Gergis, J., Risbey, J., Fowler, A. and Mooney, S. (2005). El Niño-Southern Oscillation (ENSO) since A.D. 1525 *in prep*.

Brigham, E.O. (1988). *The Fast Fourier Transform and its Application*, Englewood Cliffs, New Jersey, Prentice-Hall.

Cane, M. (2004). The evolution of El Niño, past and future. *Earth and Planetary Science Letters* **164**: 1-14.

Chatfield, C. (1975). *The analysis of time series: theory and practice*. London, Chapman and Hall.

Cleaveland, M., Cook, E. and Stahle, D. (1992). Secular variability of the Southern Oscillation detected in tree-ring data from Mexico and the southern United States. *El Niño:*

Historical and Palaeoclimatic Aspects of the Southern Oscillation. H. Diaz and V. Markgraf. Cambridge, Cambridge University Press: 271–291.

Cleaveland, M., Stahle, D., Therrell, M., Villanueva-Diaz, J. and Burns, B. (2003). Tree-ring Reconstructed Winter Precipitation and Tropical Teleconnections in Durango, Mexico. *Climatic Change* **59**: 369–388.

Clement, A., Seager, R. and Cane, M. (2000). Suppression of El Niño during the mid-Holocene by changes in the Earth's orbit. *Palaeoceanography* **15** (6): 731-737.

Cobb, K., Charles, C., Cheng, H. and Edwards, L. (2003). El Niño/Southern Oscillation and tropical Pacific climate during the last millennium. *Nature* **424**: 271-276.

Cole, J., Dunbar, R., Mc Clanahan, T. and Muthiga, N. (2000). Tropical Pacific forcing of decadal SST variability in the Western Indian Ocean over the past two centuries. *Science* **287** (5453): 617-619.

Collins, M. (2005). El Niño or La Niña-like climate change? *Climate Dynamics* **24**: 89-104.

Cook, E. and Peters, K. (1981). The smoothing spline: a new approach to standardizing forest interior tree-ring width series for dendroclimatic studies. *Tree Ring Bulletin* **41**: 45-53.

Crowley, T. (2000). Causes of Climate Change over the Past 1,000 years. *Science* **289**: 270-277.

Damon P., Peristykh A. (2005). Solar Forcing of Global Temperature Change Since AD 1400. *Climatic Change* **68**(1-2): 101.

D'Arrigo, R., Cook, E., Wilson, R., Allan, R. and Mann, M. (2005). On the variability of ENSO over the past six centuries. *Geophysical Research Letters* **32** (L03711): 1-4.

D'Arrigo, R. and Jacoby, G. (1991). A thousand year record of north-western New Mexico winter precipitation reconstructed from tree rings and its relation to El Niño and the Southern Oscillation. *The Holocene* **1/2**: 95–101.

D'Arrigo, R., Jacoby, G. and Krusic, P. (1994). Progress in Dendroclimatic Studies in Indonesia. *Terrestrial, Atmospheric and Oceanographic Sciences* **5**: 349-363.

D'Arrigo, R., Jacoby, G. and Krusic, P. (1994). Progress in Dendroclimatic Studies in Indonesia. *Terrestrial, Atmospheric and Oceanographic Sciences* **5**: 349-363.

Diaz, H. and Markgraf, V. (2000). *El Niño and the Southern Oscillation; Multiscale Variability and Global and Regional Impacts.* Cambridge, Cambridge University Press.

Diaz, H. and Pulwarty, R. (1994). An analysis of the time scales of variability in centuries-long ENSO-sensitive records in the last 1000 years. *Climatic Change* **26**: 317–342.

Dunbar, R., Wellington, G., Colgan, M. and Glynn, P. (1994). Eastern Pacific sea surface temperature since 1600 A.D. the $\delta^{18}O$ record of climate variability in Galapagos corals. *Palaeoceanography* **9**: 291–316.

Eddy, J. (1977). Climate and the changing sun. *Climatic Change* **1**: 173-190.

Fairbanks, R., Evans, M., Rubenstone, J., Mortlock, R., Broad, K., Moore, M. and Charles, C. (1997). Evaluation of climate indices and their geochemical proxies measured in corals. *Coral Reefs* **16** (Supplement): S93-S100.

Fenwick, P. (2003). Reconstruction of past climates using Pink Pine (*Halocarpus biformus*) tree-ring chronologies. Christchurch, New Zealand, Soil Plant and Ecological Sciences, Linclon University.

Fisher, D. (2002). High-resolution multiproxy climatic records from ice cores, tree-rings, corals and documentary sources using eigenvector techniques and maps: assessment of recovered signal and errors. *The Holocene* **12** (4): 401-419.

Folland, C., Karl, T., Christy, J., Clarke, R., Gruza, G., Jouzel, J., Mann, M., Oerlemans, J., Salinger, M. and Wang, S. (2001). Observed Climate Variability and Change. *Climate Change 2001: The Scientific Basis. Contribution of Working Group 1 to the Third Assessment Report of the Intergovernmental Panel on Climate Change.* J. Houghton, Y. Ding, D. Griggs *et al.* United Kingdom and New York, Cambridge University Press.

Fowler, A., Boswijk, G. and Ogden, J. (2004). Tree-ring studies on Agathis australis (Kauri): a synthesis of development work on Late Holocene chronologies. *Tree Ring Research* **60** (1): 15-29.

Fowler, A., Palmer, J., Salinger, J. and Ogden, J. (2000). Dendroclimatic interpretation of tree-rings in Agathis australis (Kauri) 2; Evidence of a significant relationship with ENSO. *Journal of Royal Society of New Zealand* **30** (3): 277-292.

Gedalof, Z. and Mantua, N. (2002). A multi-century perspective of variability in the Pacific Decadal Oscillation: new insights from tree rings and coral. *Geophysical Research Letters* **29** (24): 57/1-57/3.

Gergis, J., Boswijk, G. and Fowler, A. (2005a). An update of modern Northland Kauri (*Agathis australis*) tree-ring chronologies 1: Puketi State Forest. New Zealand tree-ring Site Report No.19, School of Geography and Environmental Science Working Paper 29, University of Auckland, New Zealand.

Gergis, J., Boswijk, G. and Fowler, A. (2005b). An update of modern Northland Kauri (*Agathis australis*) tree-ring chronologies 2: Trounson Kauri Park. New Zealand tree-ring Site

Report No.20, School of Geography and Environmental Science Working Paper 30, University of Auckland, New Zealand.

Gergis, J. and Fowler, A. (2005). Classification of synchronous oceanic and atmospheric El Niño-Southern Oscillation (ENSO) events for palaeoclimate reconstruction. *International Journal of Climatology* **25**: 1541–1565.

Gergis, J., Fowler, A., Braganza, K., Mooney, S. and Risbey, J. (2005c). El Niño-Southern Oscillation (ENSO) since A.D. 1525: integrating evidence from tree-ring, coral, ice core and documentary archives. *PAGES 2nd Open Science Meeting: Palaeoclimate, Environmental Sustainability and Our Future*, August 10-12, Beijing, China.

Gergis, J., Fowler, A., Braganza, K., Risbey, J. and Mooney, S. (2005d). Multiproxy approaches to El Niño-Southern Oscillation (ENSO) reconstruction; integrating evidence from tree-ring, coral, ice and documentary archives, A.D. 1525-2002. *Reconstructing Past Climates for Future Prediction: Integrating High-Resolution Palaeo Data for Meaningful Prediction in the Australasian Region*, June 27-28, Canberra, Australia.

Gergis, J., Fowler, A. and Mooney, S. (2004). A Multiproxy Analysis of El Niño Southern Oscillation (ENSO) Variability. *1st International CLIVAR Science Conference: Understanding and Predicting Our Climate System*, June 21-25, 2004, Baltimore, Maryland, USA.

Gergis, J., Fowler, A. and Mooney, S. (2005e). A Multiproxy Analysis of El Niño-Southern Oscillation Variability. *1st Alexander Von Humboldt International Conference on the El Niño Phenomenon and its Global Impact*, 16-20 May, 2005, Guayaquil, Ecuador, European Geophysical Union pp 35-36.

Ghil, M., Allen, M., Dettinger, M., Ide, K., Kondrashov, D., Mann, M., Robertson, A., Saunders, A., Tian, Y., Varadi, F. and Yiou, P. (2002). Advanced Spectral Methods for Climatic Time Series. *Review of Geophysics* **40** (1): 1-41.

Ghil, M. and Yiou, P. (1996). Spectral Methods: what they can and cannot do for climatic time series. *Decadal Climate Variability: Dynamics and Predictability.* D. Anderson and J. Willebrand. Berlin, Elsevier: 1-31.

Gilman, D., Fuglister, F. and Mitchell, J. (1964). On the Power Spectrum of 'Red Noise'. Journal of Atmospheric Sciences **20**:182-184.

Goodwin, I., van Ommen, T., Curran, M. and Mayeweski, P. (2004). Mid latitude winter climate variability in the South Indian and southwest Pacific regions since 1300 A.D.. *Climate Dynamics* **22**: 783-794.

Grove, R. and Chappell, J. (2000). El Niño chronology and the history of global crises during the Little Ice Age. *El Niño- History and Crisis*. R. Grove and J. Chappell. Cambridge, The White Horse Press: 5-34.

Hanley, D., Bourassa, M., O'Brian, J., Smith, S. and Spade, E. (2003). A Quantitative Evaluation of ENSO Indices. *Journal of Climate* **16**: 1249-1258.

Hendy, E., Gagan, M., Alibert, C., Mc Culloch, M., Lough, J. and Isdale, P. (2002). Abrupt Decrease in Tropical Pacific Sea Surface Salinity at End of Little Ice Age. *Science* **295** (5559): 1511-1514.

Hendy, E., Gagan, M. and Lough, J. (2003). Chronological control of coral records using luminescent lines and evidence for non-stationarity ENSO teleconnections in north-eastern Australia. *The Holocene* **13** (2): 187-199.

Hoerling, M., Kumar, A., and Xu, T. (2001). Robustness of the Nonlinear Climate Response to ENSO's Extreme Phases. *Journal of Climate* **14**: 1277-1293.

Holmes, R., Adams, R. and Fritts, H. (1986). Users manual for program ARSTAN. *Tree-ring chronologies of western North America: California, eastern Oregon and northern Great Basin*. Tucson, University of Arizona: 50-65.

Jolliffe, I. T. (1986). *Principal Component Analysis.* New-York, Springer Verlag.

Jones, P. and Mann, M. (2004). Climate over past millennia. *Review of Geophysics* **42**: 1-42.

Karoly, D., Braganza, K., Stott, P., Arblaster, J., Meehl, G., Broccoli, A. and Dixon, K. (2003). Detection of human influence on North American climate. *Science* **302**: 1200-1203.

Kiladis, G. and Diaz, H. (1989). Global climatic anomalies associated with extremes in the Southern Oscillation. *Journal of Climate* **2**: 1069-1090.

Linsley, B., Wellington, G. and Schrag, D. (2000). Decadal Sea Surface Temperature Variability in the Subtropical South Pacific from 1726 to 1997 A.D. *Science* **290**: 1145-1149.

Linsley, B., Wellington, G., Schrag, D., Ren, L., Salinger, J. and Tudhope, A. (2004). Geochemical evidence from corals for changes in the amplitude and spatial pattern of South Pacific interdecadal climate variability over the last 300 years. *Climate Dynamics* **22**: 1-11.

Lough, J. (2004). A strategy to improve the contribution of coral data to high-resolution palaeoclimatology. *Palaeogeography, Palaeoclimatology, Palaeoecology* **204**: 115-143.

Lough, J. and Fritts, H. (1985). The Southern Oscillation and tree rings: 1600–1961. *Journal of Climate and Applied Meteorology* **24**: 952–966.

Lyon, B. and Barnston, A. (2005). The evolution of the weak El Niño of 2004-2005. *US CLIVAR Variations* **3** (2): 1-4.

Mann, M. (2003). On Past Temperatures and Anomalous Late-20th Century Warmth. *Eos* **84** (27): 1-3.

Mann, M., Bradley, R. and Hughes, M. (1998). Global-scale temperature patterns and climate forcing over the past six centuries. *Nature* **392**: 779-787.

Mann, M., Bradley, R. and Hughes, M. (2000a). Long-term variability in the El Niño/Southern Oscillation and associated teleconnections. *El Niño and the Southern Oscillation; Multiscale Variability and Global and Regional Impacts.* H. Diaz, and Markgraf, V. Cambridge, Cambridge University Press: 327-372.

Mann, M., Cane, M., Zebiak, S. and Clement, A. (2005). Volcanic and Solar Forcing of the Tropical Pacific over the Past 1000 Years. *Journal of Climate* **18**: 447-456.

Mann, M., Gille, E., Bradley, R., Hughes, M., Overpeck, J., Keimig, F. and Gross, W. (2000b). Global temperature patterns in past centuries: an interactive presentation. *Earth Interactions* **4** (4): 1-29.

Moberg, A., Sonechkin, D., Holmgren, K., Datsenko, N. and Karlen, W. (2005). Highly variable Northern Hemisphere temperature reconstructed from low and high resolution proxy data. *Nature* **433**: 613-617.

Ortlieb, L. (2000). The documentary historical record of El Niño events in Peru: An update of the Quinn record (sixteenth through nineteenth centuries). *El Niño and the Southern Oscillation: Variability, Global and Regional Impacts.* H. Diaz and V. Markgraf. Cambridge, Cambridge University Press: 207-295.

Osborn, T. and Briffa, K. (2004). The Real Colour of Climate Change? *Science* **306**: 621-622.

Quinn, W. and Neal, V. (1992). The historical record of El Niño events. *Climate Since A.D. 1500*. R. Bradley and P. Jones. London, Routledge.: 623–648.

Rasmusson, E. and Carpenter, T. (1982). Variations in tropical sea surface temperature and surface wind fields associated with the Southern Oscillation/El Niño. *Monthly Weather Review* **110**: 354-384.

Rayner, N., Parker, D., Frich, P., Horton, E., Folland, C. and Alexander, L. (2000). SST and sea-ice fields for ERA40. *Proceedings of the Second International WCRP Conference On Reanalyses*, Wokefield Park, Reading, UK, 23-27 August 1999.

Reid, G. (1997). Solar forcing of global climate change since the mid 17th century. *Climatic Change* **37**: 391-405.

Stahle, D., D'Arrigo, R., Krusic, P., Cleaveland, M., Cook, E., Allan, R., Cole, J., Dunbar, R., Therrell, M., Gay, D., Moore, M., Stokes, M., Burns, B., Villanueva-Diaz, J. and Thompson, L. (1998). Experimental dendroclimatic reconstruction of the Southern Oscillation. *Bulletin of the American Meteorological Society* **79** (10): 2137-2152.

Stott, P., Tett, S., Jones, G., Allen, M., Ingram, W. and Mitchell, J. (2001). Attribution of twentieth century temperature change to natural and anthropogenic causes. *Climate Dynamics* **17**: 1-22.

Tett, S., Stott, P., Allen, M. and Ingram, M., J. (1999). Causes of twentieth-century temperature change near the Earth's surface. *Nature* **399**: 569-572.

Thompson, L., Henderson, K., Mosley-Thompson, E. and Lin, P. (2000). The Tropical Ice Core Record of ENSO. *El Niño and the Southern Oscillation: Multiscale Variability and Global and Regional Impacts.* H. Diaz and V. Markgraf. Cambridge, Cambridge University Press.

Thompson, L., Mosley-Thompson, E. and Morales Arnao, B. (1984). El Niño-Southern Oscillation events recorded in stratigraphy of the tropical Quelccaya Ice Cap. *Science* **276**: 50-52.

Torrence C. and Compo, G. (1998). A Practical Guide to Wavelet Analysis, *Bulletin of the American Meteorological Society* **79:** 61-78.

Trenberth, K. (1997). The Definition of El Niño. *Bulletin of the American Meteorological Society* **78** (12): 2771-2777.

Trenberth, K. and Caron, J. (2000). The Southern Oscillation revisited: sea level pressures, surface temperatures, and precipitation. *Journal of Climate* **13**: 4358-4365.

Trenberth, K. and Hoar, T. (1996). The 1990-1995 El Niño Southern Oscillation event: Longest on Record. *Geophysical Research Letters* **23** (1): 57-60.

Trenberth, K. and Hoar, T. (1997). El Niño and climate change. *Geophysical Research Letters* **24** (23): 3057-3060.

Urban, F., Cole, J. and Overpeck, J. (2000). Influence of mean climate change on climate variability from a 155-year tropical Pacific coral record. *Nature* **407**: 989-993.

Von Storch, H., Zorita, E., Jones, J., Dimitriev, Y., Gonzalez-Rouco, F. and Tett, S. (2004). Reconstructing Past Climate from Noisy Data. *Nature* **306**: 679-682.

Von Storch, H. and Zwiers, F. (1999). *Statistical Analysis in Climate Research*. Cambridge, Cambridge University Press.

Whetton, P. and Rutherfurd, I. (1994). Historical ENSO teleconnections in the Eastern Hemisphere. *Climatic Change* **28**: 221-253.

CHAPTER 7. CONCLUSIONS

7.1 Outcomes of Research Objectives

The primary intention of this thesis was to develop long-term multiproxy reconstructions of ENSO back to A.D. 1525, providing a long-term context for the assessment of recent ENSO variability. This was undertaken through four key research objectives proposed in Chapter 1. They are reviewed here with a brief discussion of the major results generated from each focus area.

7.1.1 Objective 1

Investigate the use of appropriate ENSO definitions and indices used for proxy calibration for ENSO reconstruction.

Chapter 2 addressed issues associated with the complexity of ENSO characterisation through comparing the event capture ability of currently used indices of ENSO. It was shown that the use of a sole ENSO index may be undesirable. This is because a single component index can only indicate one physical aspect of the phenomenon, and as such is unlikely to represent the wider interactions that exist within the coupled ocean-atmospheric system. Analysis of the nature of instrumental ENSO events from the CEI suggests that the frequency and intensity of post-1970 ENSO events (when 50% of all extreme events identified occur) are the most anomalous in the context of the past century.

In an effort to describe more of the nature and evolution of ENSO events, the Coupled ENSO Index (CEI) was devised to identify synchronous oceanic (Niño 3.4 SST) and atmospheric (Southern Oscillation Index) anomalies associated with ENSO for the instrumental period (A.D. 1871-2003). Anomalies expressed in either Niño 3.4 SSTs or SOI alone (and therefore perhaps indicative of decoupled or out of phase behaviour) are

maintained in the CEI, while coupled ocean-atmospheric anomalies result in an amplification of the index. The representation of both atmospheric and oceanic components of ENSO in the calibration process was found to improve the resolution of seasonal and spatial (teleconnection) characteristics of decoupled and coupled ENSO episodes analysed in the palaeoarchives of Chapters 5 and 6.

This study highlighted the significant implications of appropriate threshold selection on ENSO event sensitivity for subsequent palaeoclimate applications. The need to apply appropriate thresholds to instrumental records is vital if ENSO reconstructions are to maintain magnitude resolution. This is turn reinforces the need for 'amplitude preservation' in proxy calibration to refine the details essential for subsequent applications such as the validation of palaeoclimate model variability (Hegerl *et al.*, 2004).

The CEI is of practical relevance to the ENSO community as it provides an amplitude preserving instrumental baseline for the calibration of proxy records to reconstruct both components of the ENSO system. The need for palaeoclimatic disciplines to collaborate to establish standard protocols, such as the consistent statistical treatment of proxy records suggested by Lough (2004) to facilitate ready intercomparison of proxy records, is advocated by this study. It is hoped that the CEI will facilitate palaeo-ENSO research to systematically resolve the long-term context of past ENSO behaviour to further assess whether the apparently anomalous nature of late 20th century variability is unprecedented within existing palaeoclimate archives.

Encouragingly, Chapter 6 indicated the CEI has more (un-normalised) spectral power across all frequencies than either of the component indices. This may reflect an enhanced signal to noise ratio, probably because of the amplification of the synchronous ocean-atmospheric events. Of the three ENSO indices, the SOI has the weakest spectral power, registering PSD values approximately three orders of magnitude less than the CEI.

The analysis presented in Chapter 6 provides the first long-term, simultaneous reconstruction of the coupled atmosphere-ocean system for comparison with previous reconstructions of individual components of ENSO. Notably, of the three indices analysed in Chapter 6, greatest skill was found in CEI reconstructions, indicating that the proxy response is best suited to capture indices that attempt to account for both

ocean and atmosphere components of ENSO variability. Thus, incorporation of CEI-based reconstructions signifies a potentially significant contribution to existing palaeo-ENSO research.

7.1.2 Objective 2

Contribute to the development of a regional West Pacific ENSO proxy using the New Zealand Kauri tree-ring record.

Chapter 4 introduced the New Zealand Kauri tree-ring record as an important, well-replicated high-resolution record from the Southern Hemisphere. More than 20 years of research on Kauri in New Zealand has resulted in a quality tree-ring master chronology that is now available for high-resolution palaeoclimate applications. Chapter 3 presented a revision of the modern Kauri database for the purpose of, in this instance, multiproxy ENSO reconstruction.

The value of updating proxies to improve the period of overlap with meteorological data to refine proxy calibration is well recognised (Bradley, 1996). The use of Kauri records in this study has provided expanded spatial representation and sample replication of late 20th century variability to be applied to the 1990s - a decade recognised for its extreme and prolonged ENSO episodes (Trenberth and Hoar, 1997; Allan and D'Arrigo, 1999). Thus, a period seen as climatically anomalous could be examined from a multi-centennial perspective.

In particular, the post A.D. 1982 and pre A.D. 1600 low sample depth periods were targeted. Samples from living Kauri trees from Puketi State Forest, Trounson Kauri Park, Hidden Valley and Waitakere Dam were incorporated into updated versions of the modern Kauri master chronologies (AGAUm05a and AGAUm05b) for climate analysis. Prior to the update, 149 trees (344 series) from 15 sites were used to develop the modern Kauri master chronology. Following revision, the modern Kauri master chronology is now derived from 426 series from 191 trees from 17 sites from Kauri's entire geographic range. Significantly, there has been a mean increase of 25% in the number of trees replication the pre A.D1600 period, and a doubling of post A.D. 1982 replication.

Importantly, the incorporation of material from the update sites has improved overall replication of the late 20th century and the spatial representation of material from the west (TROU, WTDM), north (PUKF) and east (HIDV). Previously, the significance of any climatic interpretation of the post A.D. 1998 period from AGAU03d may have been geographically biased due to lack of spatial replication. As it now stands, the Kauri modern master can be confidently interpreted to represent the large-scale, regional climate forcing suggested by Fowler *et al.* (2004). The Kauri record shows a prominent 50-70 year cycle in variance, with a marked prominent increase ~A.D. 1870, coinciding with the end of the Little Ice Age (~A.D. 1550-1850) and increases in global industrialisation.

From the ENSO analysis presented in Chapter 5, it can be concluded that Kauri shows sensitivity to both ENSO phases, but is a stronger proxy for El Niño rather than La Niña. Similarly, the Kauri record has displayed a considerable degree of nonstationarity since A.D. 1525, suggesting that, like all proxies, Kauri derives its broadest utility in a multiproxy context. This is clearly demonstrated in Chapter 6, where the Kauri tree-ring record contributes the highest loading of PC2 for the reconstructions of ENSO indices introduced in this study.

Long tree-ring records from the Southern Hemisphere have long been sought after by the palaeoclimate community to allow recent ENSO variability to be placed into long-term context from a key teleconnection area (Stahle *et al.*, 1998; Briffa, 2000; Jones and Mann, 2004). Significantly, Kauri now joins the handful of tree species in the world which contains an identified ENSO signal in its growth ring patterns, introducing an important long-term counterpart to the eastern Pacific tree-ring chronologies currently available (Stahle *et al.*, 1998; Cook *et al.*, 2000; D'Arrigo *et al.*, 2005). The Kauri chronology is now the longest tree-ring proxy record of past ENSO variability available from the western Pacific. Indeed, it is now the longest tree-ring record of past ENSO variability in the world.

7.1.3 Objective 3

Develop a chronology of discrete ENSO events using tree-ring, coral, ice core and documentary records spanning both the east and west Pacific centres of action, and to examine trends in the frequency and magnitude of pre-instrumental ENSO episodes on decadal-centennial timescales.

Chapter 5 detailed the development of an extensive 478-year chronology of ENSO events using a variety of regional ENSO signals derived from selected tree-ring, coral, ice and documentary records spanning the both the east and west Pacific back to A.D. 1525. Importantly, for the first time, there was improved proxy representation from the western Pacific sites, allowing both key ENSO 'centres of action' to be adequately assessed over the past four and a half centuries

Using novel applications of percentile analysis, a number of replication-based ENSO reconstructions were compared to reveal large-scale trends in the frequency, magnitude and duration of pre-instrumental ENSO. The use of percentile analysis is advocated for proxy-ENSO calibration as there is no loss of variance or information gained from statistical outliers which are truncated from standard regression based approaches. This may be of significance to proxy records that may display anomalously high or low values in response to ENSO conditions, hence may not be accounted for in commonly generated transfer functions. As a result, it is possible that important teleconnection information may be lost about a given proxy's response to the range of ENSO magnitudes.

Interestingly, the tree-ring records appear to have stronger ENSO sensitivity than the other proxy records used in this study. For example, the Mexican Douglas Fir and the Berlage Teak tree-ring records appear in the top five of both of the ENSO sensitivity tables, suggesting these records are of considerable importance to reconstructive efforts. This may reflect the exact dating of tree-ring chronologies as a result of rigorous replication inherent to cross matching and chronology development, detailed in Chapters 3 and 4.

For the purpose of this multiproxy analysis the dating of coral records were sourced from the primary literature describing the data. As such, no attempt was made to adjust

age models provided for proxy data by the scientists who contributed the data. Thus, it is recognised that the weaker sensitivities generally noted for the coral sequences may reflect the dating issues outlined in Chapter 3 and/or non-stationarities trends reported elsewhere (Gagan *et al.*, 2000; Hendy *et al.*, 2003; Linsley *et al.*, 2004; Lough, 2004). Until improved replication within each regional coral record becomes commonplace (e.g. Hendy *et al.*, 2003), perhaps more emphasis should be placed upon the more exactly dated tree-ring proxy records available through the application of a non-equally weighted scheme when reconstructing ENSO in a multiproxy context.

Importantly, methods for the quantification of event magnitude and reconstruction uncertainty were provided for both ENSO phases. This chronology expands upon the discrete ENSO event chronologies such as those provided by previous researchers (e.g. Quinn and Neal (1992), Ortlieb (2000) and Whetton and Rutherfurd (1994)), providing an alternative to the 'Quinn records' commonly used for the calibration and verification past ENSO conditions from palaeoarchives. Significantly, the most comprehensive La Niña event chronology compiled to date is presented here for the A.D. 1525-2002 period.

Analysis of the ENSO event chronology revealed considerable decadal-centennial scale ENSO variability over the A.D. 1525-2002 period. Having presented further supporting lines of evidence for the early period using a wider range of proxy data, this study supports the conclusion of Whetton and Rutherfurd (1994) that ENSO teleconnections were less active during the commonly defined Little Ice Age (~A.D. 1550-1850) than since the middle of the 19th century. Periods of inactivity were identified throughout the reconstructions, most notably between A.D. 1650-1780. Indeed, during the 16th century approximately 80% of ENSO events were weak or moderate, coincident with the broadly defined LIA. Furthermore, this reduction in ENSO activity coincides with the timing of the Maunder Minimum period of low solar activity (A.D. 1645-1715), a trend also noted from the sub-tropical USA tree-ring data presented by D'Arrigo *et al.* (2005).

The clearly anomalous nature of the 20th century ENSO is evident from the reconstructions presented in Chapter 5. Although extreme ENSO events are seen throughout the 478-year ENSO reconstruction, 43% of extreme, 20% of very strong, and 28% of all protracted ENSO reconstructed events since A.D. 1525 occur in the 20th century, suggesting the frequency with which they occurred during this period is

anomalous in the context of the past five centuries. Notably, the post-1940 period alone accounts for 30% of extreme ENSO years noted since A.D. 1525.

The height of La Niña activity occurred during the 16th and 19th Centuries, while the 20th century is identified as the peak period of El Niño activity. In particular, the duration of La Niñas in the reconstructions were found to be greater than their El Niño counterparts. This is most conspicuous in the case of an eleven-year episode spanning A.D. 1622-1632, compared to a maximum duration of seven years for an El Niño event (A.D. 1718-1724 and A.D. 1900-1006).

Indeed if the trends reported here are considered to be reliable, it may signify important differences in the nature of El Niño and La Niña events, and may suggest that more extreme La Niña events could be expected in the 21st century (Timmermann *et al.*, 1999). Given the considerable large-scale socio-economic impacts of ENSO events, future investigation into the possible implications of an increasingly anthropogenically-warmed world may have on ENSO behaviour is critical.

7.1.4 Objective 4

Analyse past changes in (i) the frequency and amplitude in oceanic, atmospheric and coupled elements of ENSO, and (ii) the relative stability of regional teleconnections using spectral analysis and principal component regression techniques.

Chapter 6 introduced long-term, multiproxy reconstructions of atmospheric (SOI) oceanic (Niño 3.4 SST) and coupled (CEI) indices of ENSO. A variety of analyses revealed that the set of palaeo-climate chronologies considered here are shown to be suitable proxy indicators of ENSO variability over the 20th century. The data showed good correspondence with ENSO in the frequency domain and with temporal changes over the 20th century. Considered collectively, the set of proxy data resolves two orthogonal modes of co-variability that are clearly dominated by ENSO. These modes provide robust reconstructions of CEI, SOI and N3.4 SST over the 20th century (R10) as well as extended reconstructions 1525 (R5) and 1727 (R9), signifying a considerable 347-year extension of the instrumental record.

Comparison with previous ENSO reconstructions (Stahle *et al.*, 1998; Mann *et al.*, 2000; D'Arrigo *et al.*, 2005) shows considerable improvement using a data set which

expands upon records available from the Western Pacific. The results presented in Chapter 6 further confirm the importance of data from this region for ENSO reconstructions (D'Arrigo *et al.*, 1994; Stahle *et al.*, 1998). This is most obvious in the case of the Kauri tree-ring record that contributes the highest loading of PC2 and the considerable influence the Pink Pine and Great Barrier Reef chronologies exhibit to the two leading modes of co variability analysed here.

In comparison to other reconstructions over the 20th century, those represented here rank highly in terms of temporal correspondence/ common variance and event capture. While the full set of proxies provides the best results in terms of 20th century verification, split calibration analysis on the smaller subsets of R5 and R9 do not provide greatly degraded reconstructions. The inclusion of a variety of sites for proxy source data, especially multiple sites from the western Pacific centre of action, has led to improved stability in the reconstruction, since the regional teleconnections have clearly been shown to be non-stationary.

It is evident that the ENSO sensitivity of each regional proxy record has not remained stationary over the past five centuries. The region that shows the highest degree of stability is the Mexican Douglas Fir tree-ring record, while the coral sequences display the highest degree of variability. Since each proxy is being compared to PC-based CEI reconstructions, it would be reasonable to suggest that the strength of proxy correlations may be influenced by the PC loading a particular record contributes to the multiproxy reconstruction (see Figure 6.3).

However, on closer inspection, it appears that this may not be the case. For example, although the Kauri record contributes the highest loading in PC2 (0.61) used in the reconstructions, the record still exhibits a high degree of variability. Similarly, the south-western USA tree-ring chronology which has a high loading for both PC 1 (-0.40) and PC2 (-0.39) still displays considerable variability, as seen in Figure 6.13. These results may imply that fluctuations seen in the correlations between individual proxy records and the multiproxy reconstruction may be more reflective of real changes in teleconnection strength rather than an artefact of the methodology applied here.

Significantly, none of the reconstructions presented in Chapter 6 or by other researchers are able to completely reproduce the variance exhibited by the instrumental record. Nevertheless, the CEI reconstructions show good correspondence with the instrumental

record, capturing a maximum of 59% of instrumental variability. Spectral analysis of reconstructed ENSO since 1525 shows significant variability in spectral power in the 3-10 year frequency range on multi-decadal timescales.

Compared to the pre-instrumental period, the late 19th and early 20th century period shows increased spectral power at all frequencies. In particular, high frequency variability (~3 years or less) is enhanced during this period, though maximum power still lies in the 3-10 year band. As well as changes in frequency, the reconstructed ENSO indices also show significant temporal changes in the magnitude of variability, with a trend toward increased variability in the past 150 years.

It is noteworthy that all of the reconstructions underestimate the frequency of extreme ENSO events noted from the instrumental CEI record by 15-50% for both phases. Nonetheless, it is clear that the instrumental period (A.D. 1871-1982) contains the highest frequency of extreme events. Of the 10 extreme La Niñas reconstructed from each of the ENSO indices, 40% occur within the 20th century, with 1974, 1971 and 1910 identified as the three most extreme years reconstructed since A.D. 1525 from each index. Also common across all indices are the extreme La Niña event years of 1917 and 1950.

Similar trends were also observed from each of the El Niño phase reconstructions. Strikingly, 40% of the 10 most extreme El Niños observed from the R5 CEI and Niño 3.4 SST reconstructions along with 50% of the 10 most extreme SOI all occur within the 20th century. The three most extreme years common to all indices are the years of 1905, 1964 and 1912, while the El Niño years of 1919, 1916 and 1941 were also identified within the top 10 extreme El Niño years since A.D. 1525.

When assessing the results from the R9 reconstructions, the trend is slightly more pronounced. From the CEI, 60 (50)% of the 10 most extreme El Niños (La Niñas) occur in the 20th century. From the SOI (SST) record 60 (50)% of the 10 most extreme El Niños and 40 (50)% of the 10 most extreme La Niñas are contained within the post-1900 period. The fact that extreme ENSO events years are verified independently in each of the atmospheric and oceanic indices, and indeed by the CEI, suggests that coupled anomalies produce the highest ENSO event magnitudes. Finally, the results confirm that greater potential for the predictability of El Niños exists compared to La

Niña events, a likely consequence of the stronger seasonal mean signal exhibited during extreme El Niño conditions (Hoerling *et al.*, 2001).

Interestingly, the highest total numbers of El Niño events are reconstructed using the two discrete event approaches, the 'Quinn' records (Quinn and Neal, 1992; Ortlieb, 2000) and the event chronology presented in Chapter 5. This may be due to linear regression techniques which implicitly disregard statistical outliers, potentially resulting in a loss of variance (Von Storch *et al.*, 2004; Moberg *et al.*, 2005). This may be of significance to proxy records which are likely to be expressed as anomalously high or low values, hence may not be accounted for in commonly generated transfer functions. Hence, higher values may reflect decoupled event signatures discussed in Chapter 5.

Comparison of trends in ENSO activity appears to have a coincidental relationship with periods of low solar activity. This is supported by trends seen in the spectral power density characteristics of the ENSO reconstructions presented in Chapter 6. Following the termination of the very cool Maunder Minimum period (~A.D. 1720), there indicate a marked increase in variance in the 8-20 year frequency band, before another reduction in ENSO variance is observed, consistent with the timing of the Dalton solar minimum (~A.D. 1790-1820) (Reid, 1997). By A.D. 1850 (the termination of the LIA cool interval), there is a prominent increase in ENSO variance in both high and low frequency bands, in line with findings suggested from the discrete ENSO event chronology of Chapter 5. Thus, it appears that a prominent decrease (increase) in ENSO activity is indeed coincident with the duration (termination) of the LIA.

This finding is supported by D'Arrigo *et al.* (2005) who presented evidence from North America of lowest ENSO variability over the past six centuries during the LIA. D'Arrigo (2005) concluded that ENSO variability appears to be somewhat modulated by external solar forcing. Generally, higher ENSO variability reflected in the Cook05 tree-ring reconstruction coincided with decreased radiative forcing in line with recent coral and modeling results (Cobb *et al.*, 2003; Mann *et al.*, 2005). However, a notable exception occurs during the Maunder Minimum when the lowest ENSO variability of the Cook05 reconstruction was observed. The results presented here show low ENSO variability during the Maunder and Dalton minimums, with pronounced ENSO variability observed during the Damon (A.D. 1870-1930) period of low solar activity.

From the CEI-based reconstructions presented, A.D. 1870-1930 is the only period where enhanced ENSO variability appears to be associated with low solar variability (Damon minimum, A.D. 1880-1930). Furthermore, this period represents the most sustained interval of reconstructed ENSO activity observed since A.D. 1525. Intriguingly, Reid (1997) suggested that the observed temperature increase of around 0.5°C between 1900 and 1955 is only explained when both solar and greenhouse forcing are included in the temperature model, suggesting that greenhouse-gas forcing may have been instrumental in offsetting the cooling expected under reduced solar forcing.

Using the data set of Mann *et al.* (1998), a recent study by Damon and Peristykh (2005) revealed that modeled solar irradiance only accounts for about 18% of 20th century global warming to 1997. They concluded that this demonstrates that solar forcing was not a dominant cause of 20th century Northern Hemisphere warming, and that solar forcing was likely to have played a very significant role in the forcing of pre-industrial climate (Damon and Peristykh, 2005). The implication such warming may have on ENSO activity in a greenhouse-gas warmed future is as yet unknown (Collins, 2005; Mann *et al.*, 2005). However, recently Barnett *et al.* (2005) report that 84% of the total heating of the Earth system over the past 40 years has gone into warming the oceans, which may signal unforeseen influences on ENSO behaviour in the coming decades.

However, it is apparent that reconstructions of simple ENSO indices such as CEI, SOI and Niño 3.4 SST are insufficient to clearly characterise ENSO behaviour. While the apparent amplitude and frequency modulations shown here are suggestive of some interesting changes in past ENSO behaviour and are in generally consistent with previous studies, they tell us little about the forcings of these changes. Furthermore, such analysis is reasonably sensitive to the statistical techniques employed, which on top of uncertainties inherent in reconstruction processes, make the results less definitive. If low frequency (decadal and greater) intrinsic variability of ENSO and the response of ENSO to external radiative forcing is to be thoroughly assessed, then attempts must be made to reconstruct the larger historic synoptic conditions associated with changes in reconstructed indices. In this way, reconstructions can be better used to constrain the variety of numerical experiments that are required to understand the dynamics of ENSO. Once again, the need for expanding of high quality proxies from key ENSO affected regions, particularly from the western Pacific sites, is apparent.

7.2 Summary

Clearly, multiproxy ENSO reconstruction is still in its infancy, and abundant potential remains to characterise teleconnection patterns, propagation signatures and non-stationarities of large-scale ENSO behaviour. As the spatial and temporal details of ENSO dynamics are increasingly resolved, high resolution reconstructions of the recent past may be readily used as quality templates for calibrating networks of longer, lower resolution proxies and palaeoclimate models (Jones and Mann, 2004). Cane (2004:10) recently concluded "if we are to trust a model to predict ENSO in the greenhouse world, it is necessary that it reproduces the changes in prior centuries". Currently, climate models have great difficulty in realistically simulating ENSO as they often fail to adequately integrate both oceanic and atmospheric aspects of the phenomenon (Latif *et al.*, 2001; Cane, 2004).

In conclusion, this study asserts that recent ENSO variability appears anomalous in the context of the past five centuries. Significantly, a marked change in the frequency and intensity of ENSO begins ~A.D. 1850, coinciding with the end of the Little Ice Age and the boom in global industrialisation. Given the considerable socio-economic impacts of ENSO events, future investigation into the implications an increasingly anthropogenically-warmed world may have on ENSO is vital. It is hoped that the multi-centennial reconstructions presented here will contribute to the crucial development of ENSO simulations for the 21st century.

7.3 References

Allan, R. and D'Arrigo, R. (1999). 'Persistent' ENSO sequences: how unusual was the 1990-1995 El Niño ? *The Holocene* **9** (1): 101-118.

Barnett, T., Pierce, D., AchutaRao, K., Gleckler, P., Santer, B., Gregory, J. and Washington, W. (2005). Penetration of Human-Induced Warming into the World's Oceans. *Science* **309**: 204-287.

Bradley, R. (1996). Are there optimum sites for global palaeotemperature reconstruction? *Climate Variations and Forcing Mechanisms of the Last 2000 years.* P. Jones, R. Bradley and J. Jouzel. Berlin, Springer-Verlag: 603-624.

Briffa, K. (2000). Annual climate variability in the Holocene: interpreting the message of ancient trees. *Quaternary Science Reviews* **19**: 87-105.

Cane, M. (2004). The evolution of El Niño, past and future. *Earth and Planetary Science Letters* **164**: 1-14.

Cobb, K., Charles, C., Cheng, H. and Edwards, L. (2003). El Niño/Southern Oscillation and tropical Pacific climate during the last millennium. *Nature* **424**: 271-276.

Collins, M. (2005). El Niño or La Niña-like climate change? *Climate Dynamics* **24**: 89-104.

Cook, E., D'Arrigo, R., Cole, J., Stahle, D. and Villalba, R. (2000). Tree-ring records of past ENSO variability and forcing. *El Niño and the Southern Oscillation; Multiscale Variability and Global and Regional Impact*. H. Diaz, and Markgraf, V. New York, Cambridge University Press: 297-323.

Damon P., Peristykh A. (2005). Solar Forcing of Global Temperature Change Since AD 1400. *Climatic Change* **68**(1-2): 101.

D'Arrigo, R., Cook, E., Wilson, R., Allan, R. and Mann, M. (2005). On the variability of ENSO over the past six centuries. *Geophysical Research Letters* **32** (L03711): 1-4.

D'Arrigo, R., Jacoby, G. and Krusic, P. (1994). Progress in Dendroclimatic Studies in Indonesia. *Terrestrial, Atmospheric and Oceanographic Sciences* **5**: 349-363.

Gagan, M., Ayliffe, L., Beck, J., Cole, J., Druffel, E., Dunbar, R. and Schrag, D. (2000). New views of tropical palaeoclimates from corals. *Quaternary Science Reviews* **19**: 45-64.

Hegerl, G., Karl, T., Allan, M., Bindoff, N., Karoly, D., Gillet, N. and Zwiers, F. (2004). Climate change detection and attribution: Beyond mean temperature signals. *1st International CLIVAR Science Conference: Understanding and Predicting Our Climate System*, June 21-25, 2004, Baltimore, Maryland, USA.

Hendy, E., Gagan, M. and Lough, J. (2003). Chronological control of coral records using luminescent lines and evidence for non-stationarity ENSO teleconnections in north-eastern Australia. *The Holocene* **13** (2): 187-199.

Hoerling, M., Kumar, A., and Xu, T. (2001). Robustness of the Nonlinear Climate Response to ENSO's Extreme Phases. *Journal of Climate* **14**: 1277-1293.

Jones, P. and Mann, M. (2004). Climate over past millennia. *Review of Geophysics* **42**: 1-42.

Latif, M., Sperber, L., Arblaster, J., Braconnot, P., Chen, D., Colman, A., Cubasch, U., Cooper, C., Delecluse, P., De Witt, D., Fairhead, L., Flato, G., Hogan, T., Ji, M., Kimoto, M., Kitoh, A., Knutson, T., Le Treut, H., Li, T., Manabe, S., Marti, O., Mechoso, C., Meehl, G., Power, S., Roeckner, E., Sirven, J., Terray, L., Vintzileos, A., Voss, R., Wang, B., Washington, W., Yoshikawa, I., Yu, J. and Zebiak, S. (2001).

ENSIP: the El Niño simulation intercomparison project. *Climate Dynamics* **18**: 255-276.

Linsley, B., Wellington, G., Schrag, D., Ren, L., Salinger, J. and Tudhope, A. (2004). Geochemical evidence from corals for changes in the amplitude and spatial pattern of South Pacific interdecadal climate variability over the last 300 years. *Climate Dynamics* **22**: 1-11.

Lough, J. (2004). A strategy to improve the contribution of coral data to high-resolution palaeoclimatology. *Palaeogeography, Palaeoclimatology, Palaeoecology* **204**: 115-143.

Mann, M., Bradley, R. and Hughes, M. (1998). Global-scale temperature patterns and climate forcing over the past six centuries. *Nature* **392**: 779-787.

Mann, M., Bradley, R. and Hughes, M. (2000). Long-term variability in the El Niño/Southern Oscillation and associated teleconnections. *El Niño and the Southern Oscillation; Multiscale Variability and Global and Regional Impacts.* H. Diaz, and Markgraf, V. Cambridge, Cambridge University Press: 327-372.

Mann, M., Cane, M., Zebiak, S. and Clement, A. (2005). Volcanic and Solar Forcing of the Tropical Pacific over the Past 1000 Years. *Journal of Climate* **18**: 447-456.

Moberg, A., Sonechkin, D., Holmgren, K., Datsenko, N. and Karlen, W. (2005). Highly variable Northern Hemisphere temperature reconstructed from low and high resolution proxy data. *Nature* **433**: 613-617.

Ortlieb, L. (2000). The documentary historical record of El Niño events in Peru: An update of the Quinn record (sixteenth through nineteenth centuries). *El Niño and the Southern Oscillation: Variability, Global and Regional Impacts.* H. Diaz and V. Markgraf. Cambridge, Cambridge University Press: 207-295.

Quinn, W. and Neal, V. (1992). The historical record of El Niño events. *Climate Since A.D. 1500.* R. Bradley and P. Jones. London, Routledge.: 623–648.

Reid, G. (1997). Solar forcing of global climate change since the mid 17th century. *Climatic Change* **37**: 391-405.

Stahle, D., D'Arrigo, R., Krusic, P., Cleaveland, M., Cook, E., Allan, R., Cole, J., Dunbar, R., Therrell, M., Gay, D., Moore, M., Stokes, M., Burns, B., Villanueva-Diaz, J. and Thompson, L. (1998). Experimental dendroclimatic reconstruction of the Southern Oscillation. *Bulletin of the American Meteorological Society* **79** (10): 2137-2152.

Timmermann, A., Oberhuber, J., Bacher, A., Esch, M., Latif, M. and Roeckner, E. (1999). Increased El Niño frequency in a climate model forced by future greenhouse warming. *Nature* **398**: 694-697.

Trenberth, K. and Hoar, T. (1997). El Niño and climate change. *Geophysical Research Letters* **24** (23): 3057-3060.

Von Storch, H., Zorita, E., Jones, J., Dimitriev, Y., Gonzalez-Rouco, F. and Tett, S. (2004). Reconstructing Past Climate from Noisy Data. *Nature* **306**: 679-682.

NOTES